Control of EGR and VGT for Emission Control and Pumping Work Minimization in Diesel Engines

Johan Wahlström

Division of Vehicular Systems
Department of Electrical Engineering
Linköping University, SE–581 83 Linköping, Sweden

Linköping 2009

**Control of EGR and VGT for
Emission Control and
Pumping Work Minimization in
Diesel Engines**

johwa@isy.liu.se
http://www.vehicular.isy.liu.se
Department of Electrical Engineering,
Linköping University,
SE–581 83 Linköping,
Sweden.

Abstract

Legislators steadily increase the demands on lowered emissions from heavy duty vehicles. To meet these demands it is necessary to integrate technologies like Exhaust Gas Recirculation (EGR) and Variable Geometry Turbochargers (VGT) together with advanced control systems. Control structures are proposed and investigated for coordinated control of EGR valve and VGT position in heavy duty diesel engines. Main control goals are to fulfill the legislated emission levels, to reduce the fuel consumption, and to fulfill safe operation of the turbocharger. These goals are achieved through regulation of normalized oxygen/fuel ratio and intake manifold EGR-fraction. These are chosen as main performance variables since they are strongly coupled to the emissions.

To design successful control structures, a mean value model of a diesel engine is developed and validated. The intended applications of the model are system analysis, simulation, and development of model-based control systems. Dynamic validations show that the proposed model captures the essential system properties, i.e. non-minimum phase behaviors and sign reversals.

A first control structure consisting of PID controllers and min/max-selectors is developed based on a system analysis of the model. A key characteristic behind this structure is that oxygen/fuel ratio is controlled by the EGR-valve and EGR-fraction by the VGT-position, in order to handle a sign reversal in the system from VGT to oxygen/fuel ratio. This structure also minimizes the pumping work by opening the EGR-valve and the VGT as much as possible while achieving the control objectives for oxygen/fuel ratio and EGR-fraction. For efficient calibration an automatic controller tuning method is developed. The controller objectives are captured by a cost function, that is evaluated utilizing a method choosing representative transients. Experiments in an engine test cell show that the controller achieves all the control objectives and that the current production controller has at least 26% higher pumping losses compared to the proposed controller.

In a second control structure, a non-linear compensator is used in an inner loop for handling non-linear effects. This compensator is a non-linear state dependent input transformation. PID controllers and selectors are used in an outer loop similar to the first control structure. Experimental validations of the second control structure show that it handles nonlinear effects, and that it reduces EGR-errors but increases the pumping losses compared to the first control structure.

Substantial experimental evaluations in engine test cells show that both these structures are good controller candidates. In conclusion, validated modeling, system analysis, tuning methodology, experimental evaluation of transient response, and complete ETC-cycles give a firm foundation for deployment of these controllers in the important area of coordinated EGR and VGT control.

Sammanfattning

Lagkrav på emissioner för tunga fordon blir allt hårdare samtidigt som man vill ha låg bränsleförbrukning. För att kunna möta dessa krav införs nya teknologier såsom återcirkulering av avgaser (EGR) och variabel geometri-turbin (VGT) i dieselmotorer. I EGR-systemet finns ett spjäll som gör att man kan påverka EGR-flödet och i VGT:n finns ett ställdon som gör att man kan påverka turbinflödet. De primära mekanismerna som används för att minska emissioner är att kväveoxider kan minskas genom att öka andelen EGR-gaser i insugsröret, och att partiklar kan minskas genom att öka syre/bränsle-förhållandet i cylindrarna. Därför väljes EGR-andel och syre/bränsle-förhållande som prestandavariabler. Dessa prestandavariabler beror på ett komplicerat sätt av positionerna i EGR-spjället och i VGT:n, och det är därför nödvändigt att ha samtidig reglering av EGR och VGT för att uppnå lagkraven på emissioner.

För att designa framgångsrika reglerstrukturer, utvecklas och valideras en matematisk modell av en dieselmotor. Modellen används för systemanalys, simulering och utveckling av modellbaserade reglersystem. Dynamiska valideringar visar att den föreslagna modellen fångar de väsentliga systemegenskaperna, vilka är icke-minfasbeteenden och teckenväxlingar.

En första reglerstruktur som består av PID-regulatorer och min/max-väljare är utvecklad baserat på en systemanalys av modellen. Huvudlooparna i strukturen väljes så att syre/bränsle-förhållandet regleras av EGR-spjället och EGR-andelen regleras av VGT-positionen för att hantera en teckenväxling i systemet från VGT till syre/bränsle-förhållande. Denna struktur minimerar också bränsleförbrukningen genom att minimera pumpförluster, där pumpförluster orsakas av att trycket på avgassidan är större än trycket på insugssidan i en stor del av arbetsområdet. Principen i denna minimering är att öppna EGR-spjället och VGT:n så mycket som möjligt under tiden som reglermålen för syre/bränsle-förhållande och EGR-andel är uppfyllda. För att få en effektiv kalibrering av reglerstrukturen utvecklas en automatisk inställningsmetod av regulatorparametrarna. Reglermålen fångas av en kostnadsfunktion, som utvärderas genom att använda en metod för att välja ut representativa transienter. Experiment i en motortestcell visar att regulatorn klarar av alla reglermål och att den nuvarande regulatorn som finns i produktion har minst 26% högre pumpförluster jämfört med den föreslagna regulatorn.

I en andra reglerstruktur används en olinjär kompensator i en inre loop för att hantera olinjära effekter. Denna kompensator är en olinjär tillståndsberoende transformation av insignaler. PID-regulatorer och väljare används i en yttre loop på liknande sätt som för den första reglerstrukturen. Experiment med den andra reglerstrukturen visar att den hanterar olinjära effekter, och att den minskar EGR-fel men ökar pumpförlusterna jämfört med den första reglerstrukturen.

Omfattande experimentella utvärderingar i motortestceller visar att båda dessa regulatorstrukturer är goda kandidater. Sammanfattningsvis ger modellering, systemanalys, inställningsmetodik, experimentella utvärderingar av transientsvar och fullständiga europeiska transientcykler en stabil grund för användning av dessa regulatorer vid samtidig reglering av EGR och VGT.

Acknowledgments

This work has been performed at the department of Electrical Engineering, division of Vehicular Systems, Linköping University, Sweden. I am grateful to my professor and supervisor Lars Nielsen for letting me join this group, for all the discussions we have had, and for proofreading my work.

I would like to thank my second supervisor Lars Eriksson for many interesting discussions, for giving valuable feedback on the work, and for telling me how to improve my research. Thanks go to Erik Frisk for the discussions regarding my research and the help regarding LaTeX. Carolina Fröberg, Susana Högne, and Karin Bogg are acknowledged for all their administrative help and the staff at Vehicular Systems for creating a nice working atmosphere.

I also thank Magnus Pettersson, Mats Jennische, David Elfvik, David Vestgöte, and Yones Strand at Scania CV AB for the valuable meetings, for showing great interest, and for the measurement supply. Also the Swedish Energy Agency are gratefully acknowledged for their financial support.

A special thank goes to Johan Sjöberg for being a nice friend, for getting me interested in automatic control and vehicular systems during the undergraduate studies, and for giving me a tip of a master's thesis project at Vehicular Systems

Finally, I would like to express my gratitude to my parents, my sister, my brother, and Kristin for always being there and giving me support and encouragement.

<div align="right">

Linköping, April 2009

Johan Wahlström

</div>

Contents

ix

Part I

Introduction

1

Introduction

Legislated emission limits for heavy duty trucks are constantly reduced while at the same time there is a significant drive for good fuel economy. To fulfill the requirements, technologies like Exhaust Gas Recirculation (EGR) systems and Variable Geometry Turbochargers (VGT) have been introduced in diesel engines, see Fig. 1.1. The primary emission reduction mechanisms utilized are that NO_x can be reduced by increasing the intake manifold EGR-fraction and smoke can be reduced by increasing the air/fuel ratio [5]. However the EGR fraction and air/fuel ratio depend in complicated ways on the EGR and VGT actuation and it is therefore necessary to have coordinated control of the EGR and VGT to reach the legislated emission limits. Various approaches have been published, and an overview of different control aspects of diesel engines with EGR and VGT is given in [4]. A non-linear multi-variable controller based on a Lyapunov function is presented in [6], some approaches that differ in the selection of performance variables are compared in [12], and in [15] decoupling control is investigated. Other control approaches are rank one PI control [16], PI control [12], model predictive control [14], multivariable H_∞ control [11, 8], non-linear control [1], control using exhaust gas oxygen sensor [2], motion planning with model inversion [3], and feedback linearization [13].

Three structures for coordinated EGR and VGT control are here developed and investigated in an academic and industrial collaboration. The structures provide a convenient way for handling emission requirements, and the first two structures introduce a novel and straightforward approach for optimizing the engine efficiency by minimizing pumping work. Further, a non-linear compensator with PI controllers is investigated in the second structure and a non-linear control design is investigated in the third structure for handling non-linear effects. Added to that,

EGR actuator

VGT actuator

x_{egr}

λ_O

VGT actuator
u_{vgt}

EGR actuator
u_{egr}
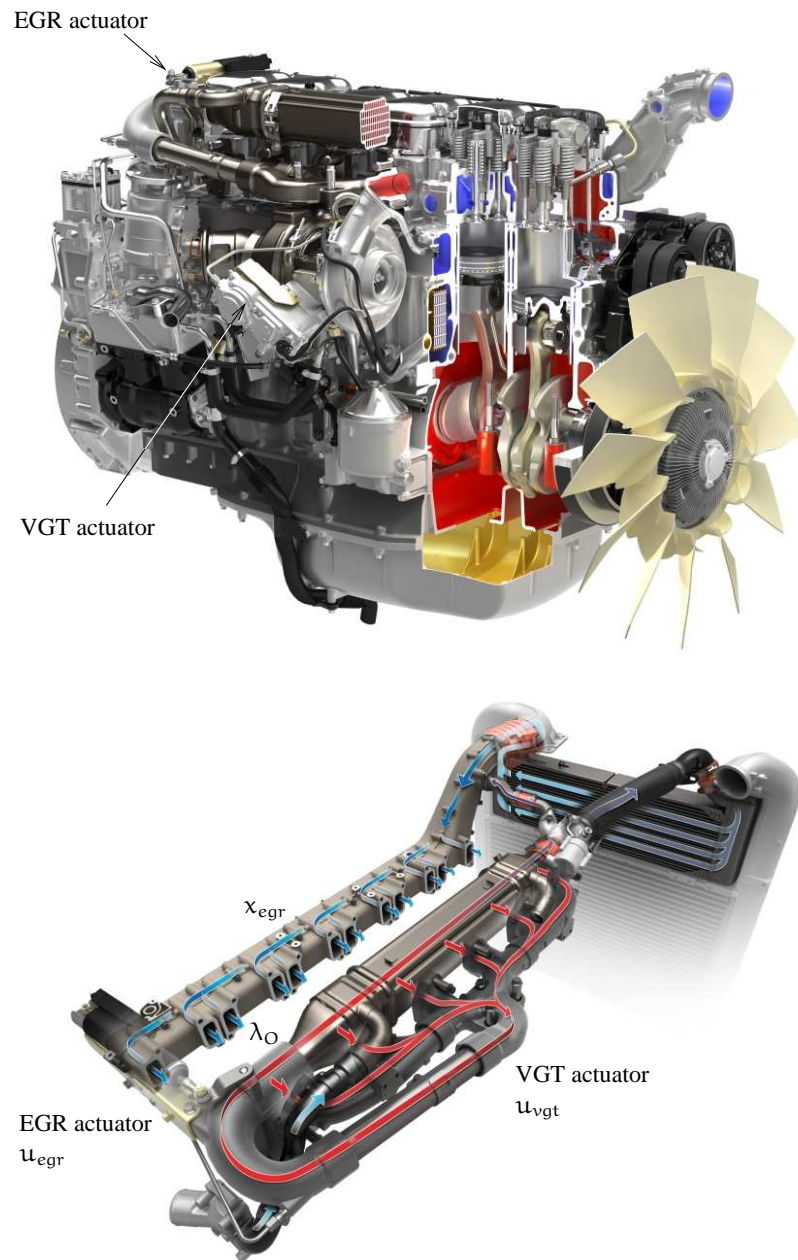
Figure 1.1 Top: *Illustration of the Scania six cylinder engine with EGR and VGT used in this thesis.* **Bottom:** *Illustration of the EGR-system and the performance variables oxygen/fuel ratio λ_O and EGR-fraction x_{egr} used in this thesis.*

the thesis covers requirements regarding additional control objectives, interfaces between inner and outer loops, and calibration that have been important for industrial validation and application.

The selection of performance variables is an important first step [19], and for emission control it should be noted that exhaust gases, present in the intake from EGR, also contain oxygen. This makes it more suitable to define and use the oxygen/fuel ratio instead of the traditional air/fuel ratio. The main motive is that it is the oxygen content that is crucial for smoke generation, and the idea is to use the oxygen content of the cylinder instead of air mass flow, see e.g. [10]. Thus, intake manifold EGR-fraction x_{egr} and oxygen/fuel ratio λ_O in the cylinder (see Fig. 1.1) are a natural selection for performance variables as they are directly related to the emissions. These performance variables are equivalent to cylinder air/fuel ratio and burned gas ratio which are a frequent choice for performance variables [6, 12, 13, 16].

The main goal of this thesis is to design control structures that regulate the performance variables x_{egr} and λ_O by using the EGR and VGT actuators.

The publications related to this thesis will be described in Sec. 1.1. Sec. 1.2 will give an overview and describe the contributions of the six publications presented in this thesis.

1.1   List of Publications

This thesis is based on the following publications

- Publication 1 is also available as the technical report "Modeling of a Diesel Engine with VGT and EGR capturing sign reversal and non-minimum phase behaviors" by Johan Wahlström and Lars Eriksson. An earlier version of this material was presented in the technical report "Modeling of a diesel engine with VGT and EGR including oxygen mass fraction" by Johan Wahlström and Lars Eriksson, and in the Licentiate thesis "Control of EGR and VGT for emission control and pumping work minimization in diesel engines" by Johan Wahlström.

- Publication 2 is also available as the technical report "System analysis of a Diesel Engine with VGT and EGR" by Johan Wahlström, Lars Eriksson, and Lars Nielsen. An earlier version of this material was presented in the Licentiate thesis "Control of EGR and VGT for emission control and pumping work minimization in diesel engines" by Johan Wahlström".

- Publication 3 has been submitted for publication. Parts of this material were presented in the Licentiate thesis "Control of EGR and VGT for emission control and pumping work minimization in diesel engines" by Johan Wahlström". Related to this publication is the conference paper "PID controllers and their tuning for EGR and VGT control in diesel engines" by Johan Wahlström, Lars Eriksson, Lars Nielsen, and Magnus Pettersson, 16th

IFAC World Congress, 2005, that proposes a control structure that is similar to the control structure in Publication 3.

- Publication 4 has been published as the conference paper "Controller tuning based on transient selection and optimization for a diesel engine with EGR and VGT" by Johan Wahlström, Lars Eriksson, and Lars Nielsen, SAE Technical paper 2008-01-0985, Detroit, USA, 2008. Parts of this material were presented in the Licentiate thesis "Control of EGR and VGT for emission control and pumping work minimization in diesel engines" by Johan Wahlström".

- Publication 5 is also available as the technical report "Non-linear compensator for handling non-linear Effects in EGR VGT Diesel Engines" by Johan Wahlström and Lars Eriksson. Related to this publication is the conference paper "Performance gains with EGR-flow inversion for handling non-linear dynamic effects in EGR VGT CI engines" by Johan Wahlström and Lars Eriksson, Fifth IFAC Symposium on Advances in Automotive Control, 2007.

- An earlier version of Publication 6 has been published as the conference paper "Robust Nonlinear EGR and VGT Control with Integral Action for Diesel Engines" by Johan Wahlström and Lars Eriksson, 17th IFAC World Congress, 2008.

1.2   Overview and Contributions of the Publications

An overview of the six publications in this thesis is presented below and for each publication its contributions.

1.2.1   Publication 1 - Modeling

When developing and validating a controller for a diesel engine with VGT and EGR, it is desirable to have a model that describes the system dynamics and the nonlinear effects. Therefore, the objective of Publication 1 is to construct a mean value diesel engine model with VGT and EGR. For these systems, several models with different selections of states and complexity have been published [1, 6, 7, 9, 16, 18].

Here the model should be able to describe stationary operations and dynamics that are important for gas flow control. The intended applications of the model are system analysis, simulation, and development of model-based control systems. The goal is to construct a model that describes the dynamics in the manifold pressures, turbocharger, EGR, and actuators with few states in order to have short simulation times. Therefore the model has only eight states: intake and exhaust manifold pressures, oxygen mass fraction in the intake and exhaust manifold, turbocharger speed, and three states describing the actuator dynamics. The structure of the model can be seen in Fig. 1.2. The model is more complex than e.g. the third
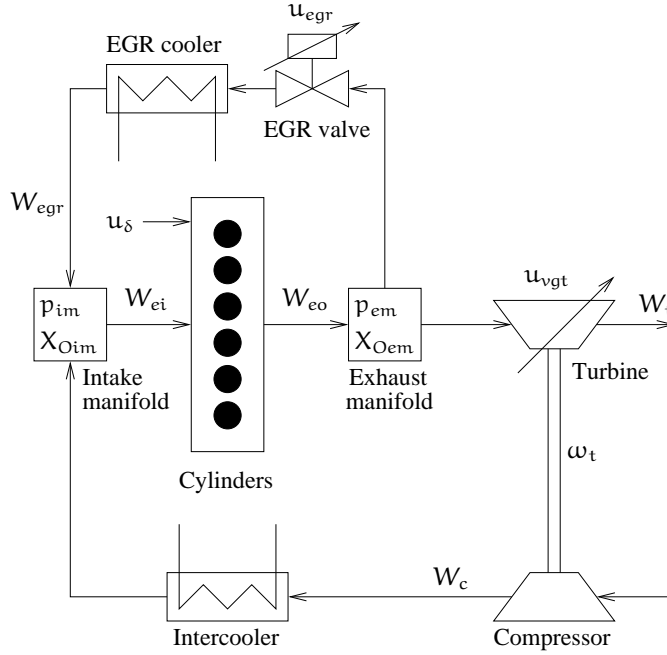
Figure 1.2 *A model structure of the diesel engine. It has three control inputs and five main states related to the engine (p_{im}, p_{em}, X_{Oim}, X_{Oem}, and ω_t). In addition, there are three states for actuator dynamics ($\tilde{u}_{egr1}$, $\tilde{u}_{egr2}$, and $\tilde{u}_{vgt}$).*

order model in [6] that only describes the pressure and turbocharger dynamics, but it is considerably less complex than a GT-POWER model that is based on one-dimensional gas dynamics [17].

Many models in the literature, that have approximately the same complexity as the model proposed here, use three states for each control volume in order to describe the temperature dynamics [6, 9, 16]. However, the model proposed here uses only two states for each manifold. Model extensions are investigated showing that inclusion of temperature states and pressure drop over the intercooler only have minor effects on the dynamic behavior in pressure, oxygen mass fraction, and turbocharger speed and does not improve the model quality. Therefore, these extensions are not included in the proposed model.

Model equations and tuning methods are described for each subsystem in the model. In order to have a low number of model parameters, flows and efficiencies are modeled using physical relationships and parametric models instead of look-up tables. To tune and validate the model, stationary and dynamic measurements have been performed in an engine laboratory at Scania CV AB. Static and dynamic validations of the entire model using dynamic experimental data show that the
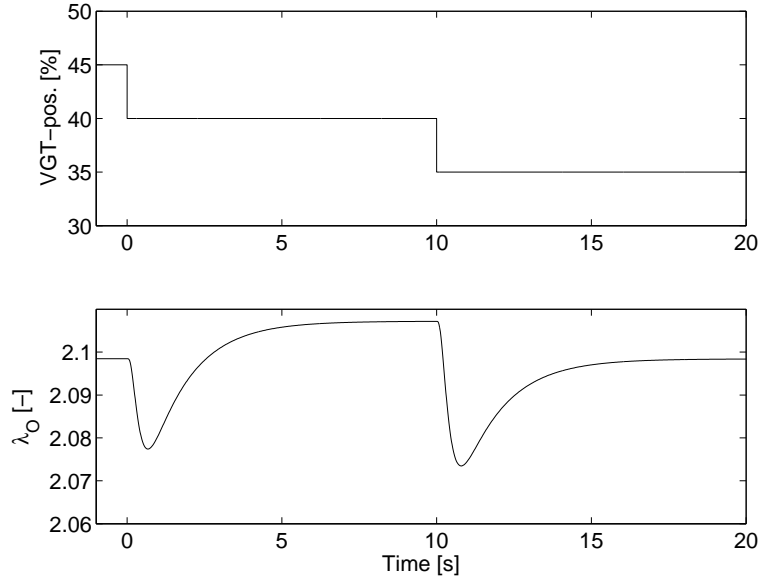
Figure 1.3 *Non-minimumphase behavior and sign reversal in the channel VGT-position to λ_O. The DC-gain in the first step is negative and the DC-gain in the second step is positive.*

mean relative errors are 12.7 % or lower for all measured variables. The validations also show that the proposed model captures the essential system properties, i.e. a non-minimum phase behavior in the channel u_{egr} to p_{im} and a non-minimum phase behavior, an overshoot, and a sign reversal in the channel u_{vgt} to W_c.

1.2.2   Publication 2 - System analysis

An analysis of the characteristics and the behavior of a system aims at obtaining insight into the control problem. This is known to be important for a successful design of an EGR and VGT controller due to non-trivial intrinsic properties, see for example [9]. Therefore, the goal is to make a system analysis of the diesel engine model proposed in Publication 1.

Step responses over the entire operating region show that the channels $u_{vgt} \rightarrow \lambda_O$, $u_{egr} \rightarrow \lambda_O$, and $u_{vgt} \rightarrow x_{egr}$ have non-minimum phase behaviors and sign reversals. See for example Fig. 1.3 that shows these system properties for $u_{vgt} \rightarrow \lambda_O$. The fundamental physical explanation of these system properties is that the system consists of two dynamic effects that interact: a fast pressure dynamics in the manifolds and a slower turbocharger dynamics. It is shown that the engine frequently operates in operating points where the non-minimum phase behaviors and sign reversals occur for the channels $u_{vgt} \rightarrow \lambda_O$ and $u_{vgt} \rightarrow x_{egr}$, and consequently, it is
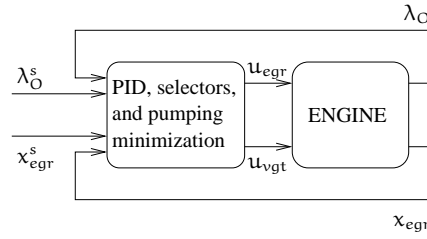
Figure 1.4 *A control structure with PID controllers, min/max selectors, and pumping minimization. It handles the sign reversal in Fig. 1.3 by avoiding the loop VGT-position to λ_O.*

important to consider these properties in a control design. Further, an analysis of zeros for linearized multiple input multiple output models of the engine shows that they are non-minimum phase over the complete operating region. A mapping of the performance variables λ_O and x_{egr} and the relative gain array show that the system from u_{egr} and u_{vgt} to λ_O and x_{egr} is strongly coupled in a large operating region. It is also illustrated that the pumping losses $p_{em} - p_{im}$ decrease with increasing EGR-valve and VGT opening for almost the complete operating region.

1.2.3 Publication 3 - EGR-VGT Control for Pumping Work Minimization

A control structure with PID controllers and selectors (see Fig. 1.4) is proposed and investigated for coordinated control of oxygen/fuel ratio λ_O and intake manifold EGR-fraction x_{egr}. These were chosen both as performance and feedback variables since they give information about when it is possible to minimize the pumping work. This pumping work minimization is a novel and simple strategy and compared to another control structure which closes the EGR-valve and the VGT more, the pumping work is substantially reduced. Further, the chosen variables are strongly coupled to the emissions which makes it easy to adjust set-points, e.g. depending on measured emissions during an emission calibration process. This is more straightforward than control of manifold pressure and air mass flow which is a common choice of feedback variables in the literature [8, 11, 12, 15, 16]. Other choices of feedback variables in the literature are intake manifold pressure and EGR-fraction [12], exhaust manifold pressure and compressor air mass flow [6], intake manifold pressure and EGR flow [14], intake manifold pressure and cylinder air mass-flow [1], or compressor air mass flow and EGR flow [3].

Based on the system analysis in Publication 2, λ_O is controlled by the EGR-valve and x_{egr} by the VGT-position, mainly to handle the sign reversal from VGT to λ_O in Fig. 1.3.

Besides controlling the two main performance variables, λ_O and x_{egr}, the control structure also successfully handles torque control, including torque limitation

due to smoke control, and supervisory control of turbo charger speed for avoiding over-speeding. Further, the control objectives are mapped to the controller structure via a systematic analysis of the control problem, and this conceptual coupling to objectives gives the foundation for systematic tuning. This is utilized to develop an automatic controller tuning method. The objectives to minimize pumping work and ensure the minimum limit of λ_O are handled by the structure, while the other control objectives are captured in a cost function, and the tuning is formulated as a non-linear least squares problem. The details of the tuning method are described in Publication 4.

Different performance trade-offs are necessary and they are illustrated on the European Transient Cycle. The proposed controller is validated in an engine test cell, where it is experimentally demonstrated that the controller achieves all control objectives and that the current production controller has at least 26% higher pumping losses compared to the proposed controller.

1.2.4   Publication 4 - Controller Tuning

Efficient calibration is important and as mentioned above a control tuning method has been developed. The proposed tuning method is based on control objectives that are captured in a cost function, and the tuning is formulated as a non-linear least squares problem. The method is illustrated by applying it on the control structure in Publication 3 and it is also used for the control structures in Publication 5 and 6. To aid the tuning, a systematic method is developed for selecting significant transients that exhibit different challenges for the controller, and an important step in obtaining the solution is precautions in a separate phase to avoid ending up in an unsatisfactory local minimum.

The performance is evaluated on the European Transient Cycle. It is demonstrated how the weights in the cost function influence behavior, and that the tuning method is important in order to improve the control performance compared to if only the initialization method is used. Furthermore, it is shown that the control structure in Publication 3 with parameters based on the proposed tuning method achieves all the control objectives, and it is successfully applied in an engine test cell.

The most important sections in Publication 4 is the automatic tuning method in Sec. 5 and the simulation results in Sec. 6. The control approach in Sec. 2, the control structure in Sec. 4, and the experimental validations in Sec. 7 are more completely described in Publication 3. The simulations in Publication 3 and 4 are performed with an earlier version of the model in Publication 1 that only has two states for the actuator dynamics. However, simulations with the model in Publication 1 that has three states for the actuator dynamics have been performed showing the same results as the results in Publication 3 and 4.
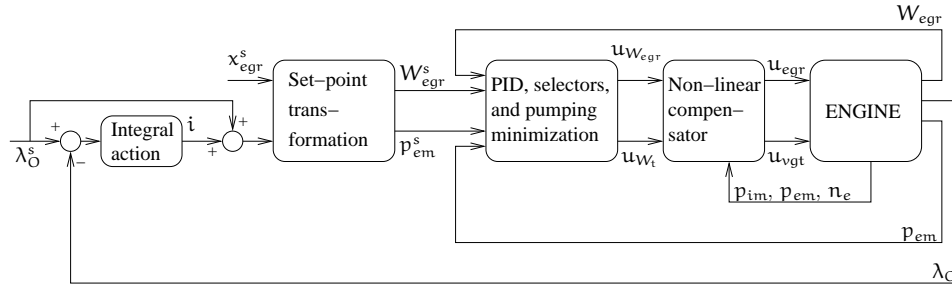
Figure 1.5 *The control structure in Fig. 1.4 is extended with a non-linear compensator.*

1.2.5 Publication 5 - Non-linear compensator

Inspired by an approach in [6], the control structure in Fig. 1.4 is extended with a non-linear compensator according to Fig. 1.5. The goal is to investigate if this non-linear compensator improves the control performance compared to the controller in Fig. 1.4. The non-linear compensator is a non-linear state dependent input transformation that is developed by inverting the models, for EGR-flow and turbine flow, that have actuator position as input and flow as output. This leads to two new control inputs, $u_{W_{egr}}$ and u_{W_t}, which are equal to the EGR-flow W_{egr} and the turbine flow W_t if there are no model errors in the non-linear compensator.

A system analysis of the open-loop system with a non-linear compensator shows that it handles sign reversals and non-linear effects. Further, the analysis shows that this open-loop system is unstable in a large operating region. This instability is stabilized by a control structure that consists of PID controllers, min/max-selectors, and a pumping minimization mechanism similar to the structure in Fig. 1.4. The EGR flow W_{egr} and the exhaust manifold pressure p_{em} are chosen as feedback variables in this structure. Further, the set-points for EGR-fraction and oxygen/fuel ratio are transformed to set-points for the feedback variables. In order to handle model errors in this set-point transformation, an integral action on λ_O is used in an outer loop. Experimental validations of the control structure in Fig. 1.5 show that it handles nonlinear effects (see Fig. 1.6), and that it reduces EGR-errors but increases the pumping losses compared to the control structure in Fig. 1.4.

1.2.6 Publication 6 - Non-linear control

A non-linear controller based on a design in [6] that utilizes a control Lyapunov function and inverse optimal control is investigated. The feedback variables are compressor flow W_c and exhaust manifold pressure p_{em}, see Fig. 1.7. The PID controllers in Fig. 1.5 are thus replaced by a non-linear multivariable controller according to Fig. 1.7, and the goal is to investigate if this non-linear controller improves the control performance compared to the controller in Fig. 1.5. Simulations
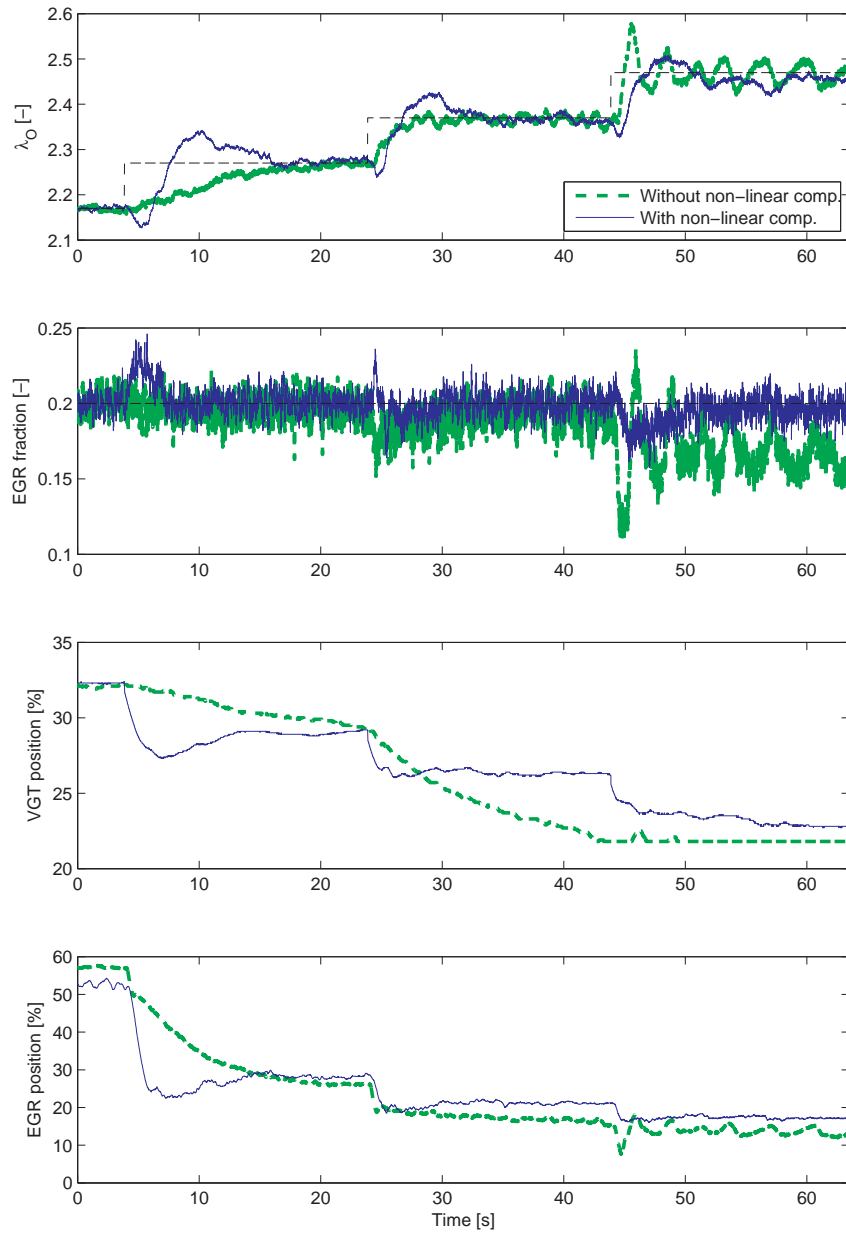
Figure 1.6 *The control structure without non-linear compensator (Fig. 1.4) gives slow control and oscillations at different steps, i.e. it does not handle non-linear effects. The control structure with non-linear compensator (Fig. 1.5) gives less oscillations and fast control, i.e. it handles nonlinear effects.*
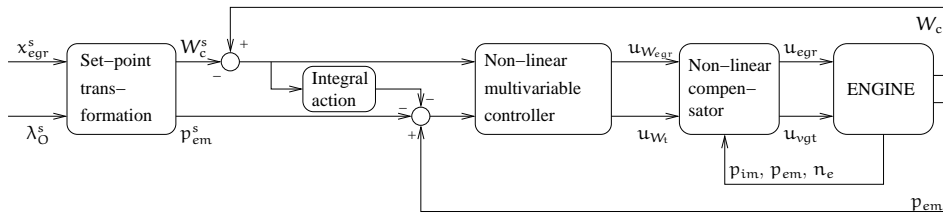
Figure 1.7 *The PID controllers in Fig. 1.5 are replaced by a non-linear multivariable controller that is based on a Lyapunov function and inverse optimal control. Simulations show that this design is not robust to model errors in the non-linear compensator while the control structure in Fig. 1.5 is. If there are no model errors in the non-linear compensator Fig. 1.5 and 1.7 have approximately the same control performance.*

show that integral action is necessary to handle model errors, so the design in [6] is extended with integral action on the compressor flow W_c as depicted in Fig. 1.7 so that the controller can track the performance variables specified in the outer loop.

Comparisons by simulation show that the proposed control design handles non-linear effects in the diesel engine, and that the non-linear compensator is important to achieve this. If there are no model errors in the non-linear compensator, the controllers in Fig. 1.5 and 1.7 have approximately the same control performance. However, it is shown that the proposed control design in Fig. 1.7 is not robust to model errors in the non-linear compensator while the control structure in Fig. 1.5 is, and due to these results, the control structure in Publication 6 is not experimentally validated. Instead, the control structure in Publication 5 is recommended.

Bibliography

[1] M. Ammann, N.P. Fekete, L. Guzzella, and A.H. Glattfelder. Model-based Control of the VGT and EGR in a Turbocharged Common-Rail Diesel Engine: Theory and Passenger Car Implementation. *SAE Technical paper 2003-01-0357*, January 2003.

[2] A. Amstutz and L. Del Re. EGO sensor based robust output control of EGR in diesel engines. *IEEE Transactions on Control System Technology*, pages 37–48, 1995.

[3] Jonathan Chauvin, Gilles Corde, Nicolas Petit, and Pierre Rouchon. Motion planning for experimental airpath control of a diesel homogeneous charge-compression ignition engine. *Control Engineering Practice*, 2008.

[4] L. Guzzella and A. Amstutz. Control of diesel engines. *IEEE Control Systems Magazine*, 18:53–71, 1998.

[5] J.B. Heywood. *Internal Combustion Engine Fundamentals*. McGraw-Hill Book Co, 1988.

[6] M. Jankovic, M. Jankovic, and I.V. Kolmanovsky. Constructive lyapunov control design for turbocharged diesel engines. *IEEE Transactions on Control Systems Technology*, 2000.

[7] M. Jung. *Mean-Value Modelling and Robust Control of the Airpath of a Turbocharged Diesel Engine*. PhD thesis, University of Cambridge, 2003.

[8] Merten Jung, Keith Glover, and Urs Christen. Comparison of uncertainty parameterisations for H-infinity robust control of turbocharged diesel engines. *Control Engineering Practice*, 2005.

[9] I.V. Kolmanovsky, A.G. Stefanopoulou, P.E. Moraal, and M. van Nieuwstadt. Issues in modeling and control of intake flow in variable geometry turbocharged engines. In *Proceedings of 18th IFIP Conference on System Modeling and Optimization*, Detroit, July 1997.

[10] Shigeki Nakayama, Takao Fukuma, Akio Matsunaga, Teruhiko Miyake, and Toru Wakimoto. A new dynamic combustion control method based on charge oxygen concentration for diesel engines. In *SAE Technical Paper 2003-01-3181*, 2003. SAE World Congress 2003.

[11] M. Nieuwstadt, P.E. Moraal, I.V. Kolmanovsky, A. Stefanopoulou, P. Wood, and M. Widdle. Decentralized and multivariable designs for EGR–VGT control of a diesel engine. In *IFAC Workshop, Advances in Automotive Control*, 1998.

[12] M.J. Nieuwstadt, I.V. Kolmanovsky, P.E. Moraal, A.G. Stefanopoulou, and M. Jankovic. EGR–VGT control schemes: Experimental comparison for a high-speed diesel engine. *IEEE Control Systems Magazine*, 2000.

[13] R. Rajamani. Control of a variable-geometry turbocharged and wastegated diesel engine. *Proceedings of the I MECH E Part D Journal of Automobile Engineering*, November 2005.

[14] J. Rückert, F. Richert, A. Schloßer, D. Abel, O. Herrmann, S. Pischinger, and A. Pfeifer. A model based predictive attempt to control boost pressure and EGR–rate in a heavy duty diesel engine. In *IFAC Symposium on Advances in Automotive Control*, 2004.

[15] J. Rückert, A. Schloßer, H. Rake, B. Kinoo, M. Krüger, and S. Pischinger. Model based boost pressure and exhaust gas recirculation rate control for a diesel engine with variable turbine geometry. In *IFAC Workshop: Advances in Automotive Control*, 2001.

[16] A.G. Stefanopoulou, I.V. Kolmanovsky, and J.S. Freudenberg. Control of variable geometry turbocharged diesel engines for reduced emissions. *IEEE Transactions on Control Systems Technology*, 8(4), July 2000.

[17] Gamma Technologies. *GT-POWER User's Manual 6.1.* Gamma Technologies Inc, 2004.

[18] C. Vigild. *The Internal Combustion Engine Modelling, Estimation and Control Issues.* PhD thesis, Technical University of Denmark, Lyngby, 2001.

[19] Kemin Zhou, John C. Doyle, and Keith Glover. *Robust and optimal control.* Prentice-Hall, Inc., Upper Saddle River, NJ, USA, 1996.

Part II

Publications

$$\text{P{\small UBLICATION} 1}$$

Modeling of a Diesel Engine with VGT and EGR capturing Sign Reversal and Non-minimum Phase Behaviors[1]

Johan Wahlström and Lars Eriksson

Vehicular Systems, Department of Electrical Engineering,
Linköping University, S-581 83 Linköping,
Sweden.

---

[1]This report is also available from Department of Electrical Engineering, Linköping University, S-581 83 Linköping. Technical Report Number: LiTH-R-2882

Abstract

A mean value model of a diesel engine with VGT and EGR is developed and validated. The intended model applications are system analysis, simulation, and development of model-based control systems. The goal is to construct a model that describes the dynamics in the manifold pressures, turbocharger, EGR, and actuators with few states in order to have short simulation times. Therefore the model has only eight states: intake and exhaust manifold pressures, oxygen mass fraction in the intake and exhaust manifold, turbocharger speed, and three states describing the actuator dynamics. The model is more complex than e.g. the third order model in [12] that only describes the pressure and turbocharger dynamics, but it is considerably less complex than a GT-POWER model or a Ricardo WAVE model. Many models in the literature, that approximately have the same complexity as the model proposed here, use three states for each control volume in order to describe the temperature dynamics. However, the model proposed here uses only two states for each manifold. Model extensions are investigated showing that inclusion of temperature states and pressure drop over the intercooler only have minor effects on the dynamic behavior and does not improve the model quality. Therefore, these extensions are not included in the proposed model. Model equations and tuning methods are described for each subsystem in the model. In order to have a low number of tuning parameters, flows and efficiencies are modeled using physical relationships and parametric models instead of look-up tables. To tune and validate the model, stationary and dynamic measurements have been performed in an engine laboratory at Scania CV AB. Static and dynamic validations of the entire model using dynamic experimental data show that the mean relative errors are 12.7 % or lower for all measured variables. The validations also show that the proposed model captures the essential system properties, i.e. a non-minimum phase behavior in the channel u_{egr} to p_{im} and a non-minimum phase behavior, an overshoot, and a sign reversal in the channel u_{vgt} to W_c.

1 Introduction

Legislated emission limits for heavy duty trucks are constantly reduced. To fulfill the requirements, technologies like Exhaust Gas Recirculation (EGR) systems and Variable Geometry Turbochargers (VGT) have been introduced. The primary emission reduction mechanisms utilized to control the emissions are that NO_x can be reduced by increasing the intake manifold EGR-fraction x_{egr} and smoke can be reduced by increasing the oxygen/fuel ratio λ_O [11]. However x_{egr} and λ_O depend in complicated ways on the actuation of the EGR and VGT. It is therefore necessary to have coordinated control of the EGR and VGT to reach the legislated emission limits in NO_x and smoke. When developing and validating a controller for this system, it is desirable to have a model that describes the system dynamics and the nonlinear effects that are important for gas flow control. For example in [14], [13], and [19] it is shown that this system has non-minimum phase behaviors, overshoots, and sign reversals. Therefore, the objective of this report is to construct a mean value diesel engine model, from actuator input to system output, that captures these properties. The intended usage of the model are system analysis, simulation and development of model-based control systems. The model shall describe the dynamics in the manifold pressures, turbocharger, EGR, and actuators with few states in order to have short simulation times.

Several models with different selections of states and complexity have been published for diesel engines with EGR and VGT. A third order model that describes the intake and exhaust manifold pressure and turbocharger dynamics is developed in [12]. The model in [13] has 6 states describing intake and exhaust manifold pressure and temperature dynamics, and turbocharger and compressor mass flow dynamics. A 7:th order model that describes intake and exhaust manifold pressure, temperature, and air-mass fraction dynamics, and turbocharger dynamics is proposed in [1]. These dynamics are also described by the 7:th order models in [12, 14, 19] where burned gas fraction is used instead of air-mass fraction in the manifolds. Another model that describes these dynamics is the 9:th order model in [18] that also has two states for the actuator dynamics. The models described above are lumped parameter models. Other model families, that have considerably more states are those based on one-dimensional gas dynamics, for example GT-POWER and Ricardo WAVE models.

The model proposed here has eight states: intake and exhaust manifold pressures, oxygen mass fraction in the intake and exhaust manifold, turbocharger speed, and three states describing the actuator dynamics. In order to have a low number of tuning parameters, flows and efficiencies are modeled based upon physical relationships and parametric models instead of look-up tables. The model is implemented in MATLAB/SIMULINK using a component library.

1.1 Outline and model extensions

The structure of the model as well as the tuning and the validation data are described in Sec. 1.2 to 1.6. Model equations and model tuning are described for each

sub-model in Sec. 2 to 6. A summary of the model assumptions and the model equations is given in Sec. 7 while Sec. 8 summarizes the tuning and a model validation. The goal is also to investigate if the proposed model can be improved with model extensions in Sec. 9. These model extensions are inclusions of temperature states and a pressure drop over the intercooler and they are investigated due to that they are used in many models in the literature [2, 8, 12, 14, 18].

1.2   Selection of number of states

The model has eight states: intake and exhaust manifold pressures (p_{im} and p_{em}), oxygen mass fraction in the intake and exhaust manifold (X_{Oim} and X_{Oem}), turbocharger speed (ω_t), and three states describing the actuator dynamics for the two control signals ($\tilde{u}_{egr1}$, $\tilde{u}_{egr2}$, and $\tilde{u}_{vgt}$). These states are collected in a state vector x

$$x = (p_{im} \quad p_{em} \quad X_{Oim} \quad X_{Oem} \quad \omega_t \quad \tilde{u}_{egr1} \quad \tilde{u}_{egr2} \quad \tilde{u}_{vgt})^{\mathsf{T}} \qquad (1)$$

Descriptions of the nomenclature, the variables and the indices can be found in Appendix A and the structure of the model can be seen in Fig. 1.

The states p_{im}, p_{em}, and ω_t describe the main dynamics and the most important system properties, such as non-minimum phase behaviors, overshoots, and sign reversals. In order to model the dynamics in the oxygen/fuel ratio λ_O, the states X_{Oim} and X_{Oem} are used. Finally, the states $\tilde{u}_{egr1}$, $\tilde{u}_{egr2}$, and $\tilde{u}_{vgt}$ describe the actuator dynamics where the EGR-valve actuator model has two states ($\tilde{u}_{egr1}$ and $\tilde{u}_{egr2}$) in order to describe an overshoot in the actuator.

Many models in the literature, that approximately have the same complexity as the model proposed here, use three states for each control volume in order to describe the temperature dynamics [12, 14, 18]. However, the model proposed here uses only two states for each manifold: pressure and oxygen mass fraction. Model extensions are investigated in Sec. 9.1 showing that inclusion of temperature states has only minor effects on the dynamic behavior. Furthermore, the pressure drop over the intercooler is not modeled since this pressure drop has only small effects on the dynamic behavior. However, this pressure drop has large effects on the stationary values, but these effects do not improve the complete engine model, see Sec. 9.2.

1.3   Model structure

It is important that the model can be utilized both for different vehicles and for engine testing and calibration. In these situations the engine operation is defined by the rotational speed n_e, for example given as an input from a drivecycle, and therefore it is natural to parameterize the model using engine speed. The resulting model is thus expressed in state space form as

$$\dot{x} = f(x, u, n_e) \qquad (2)$$

Figure 1 *A model structure of the diesel engine. It has three control inputs and five main states related to the engine (p_{im}, p_{em}, X_{Oim}, X_{Oem}, and ω_t). In addition, there are three states for actuator dynamics ($\tilde{u}_{egr1}$, $\tilde{u}_{egr2}$, and $\tilde{u}_{vgt}$).*

where the engine speed n_e is considered to be an input to the model, and u is the control input vector

$$u = (u_\delta \quad u_{egr} \quad u_{vgt})^\mathsf{T} \tag{3}$$

which contains mass of injected fuel u_δ, EGR-valve position u_{egr}, and VGT actuator position u_{vgt}. The EGR-valve is closed when $u_{egr} = 0\,\%$ and open when $u_{egr} = 100\,\%$. The VGT is closed when $u_{vgt} = 0\,\%$ and open when $u_{vgt} = 100\,\%$.

1.4 Measurements

To tune and validate the model, stationary and dynamic measurements have been performed in an engine laboratory at Scania CV AB, and these are described below.

Table 1 *Measured variables during stationary measurements.*

Variable	Description	Unit
M_e	Engine torque	Nm
n_e	Rotational engine speed	rpm
n_t	Rotational turbine speed	rpm
p_{amb}	Ambient pressure	Pa
p_c	Pressure after compressor	Pa
p_{em}	Exhaust manifold pressure	Pa
p_{im}	Intake manifold pressure	Pa
T_{amb}	Ambient temperature	K
T_c	Temperature after compressor	K
T_{em}	Exhaust manifold temperature	K
T_{im}	Intake manifold temperature	K
T_t	Temperature after turbine	K
u_{egr}	EGR control signal. 0 - closed, 100 - open	%
u_{vgt}	VGT control signal. 0 - closed, 100 - open	%
u_δ	Injected amount of fuel	mg/cycle
W_c	Compressor mass flow	kg/s
x_{egr}	EGR fraction	—

Stationary measurements

The stationary data consists of measurements at stationary conditions in 82 operating points, that are scattered over a large operating region covering different loads, speeds, VGT- and EGR-positions. These 82 operating points also include the European Stationary Cycle (ESC) at 13 operating points. The variables that were measured during stationary measurements can be seen in Tab. 1. The EGR fraction is calculated by measuring the carbon dioxide concentration in the intake and exhaust manifolds.

All the stationary measurements are used for tuning of parameters in static models. The static models are then validated using dynamic measurements.

Dynamic measurements

The dynamic data consists of measurements at dynamic conditions with steps in VGT control signal, EGR control signal, and fuel injection in several different operating points according to Tab. 2. The steps in VGT-position and EGR-valve are performed in 9 different operating points (data sets A-H, J) and the steps in fuel injection are performed in one operating point (data set I). The data set J is used for tuning of dynamic actuator models and the data sets E and I are used for tuning of dynamic models in the manifolds, in the turbocharger, and in the engine torque. Further, the data sets A-D and F-I are used for validation of essential system properties and time constants and the data sets A-I are used for validation of static models. The dynamic measurements are limited in sample rate with a

Table 2 *Dynamic tuning and validation data that consist of steps in VGT-position, EGR-valve, and fuel injection. The data sets E, I, and J are used for tuning of dynamic models, the data sets A-D and F-I are used for validation of essential system properties and time constants, and the data sets A-I are used for validation of static models.*

	VGT-EGR steps								u_δ steps	VGT-EGR steps
Data set	A	B	C	D	E	F	G	H	I	J
Speed [rpm]		1200			1500		1900		1500	-
Load [%]	25	40	50	75	50	25	75	100	-	-
Number of steps	77	35	2	77	77	77	55	1	7	48
Sample frequency [Hz]	1	100	100	1	1	1	1	100	10	100

sample frequency of 1 Hz for the data sets A, D-G, 10 Hz for the data set I, and 100 Hz for the data sets B, C, H, and J. This leads to that the data sets A, D-G, and I do not capture the fastest dynamics in the system, while the data sets B, C, H, and J do. Further, the data sets B, C, H, and J were measured 3.5 years after the data sets A, D, E, F, G, I and the stationary data. The variables that were measured during dynamic measurements can be seen in Tab. 3.

Sensor time constants and system dynamics

To justify that the model captures the system dynamics and not the sensor dynamics, the dynamics of the sensors are analyzed and compared with the dynamics seen in the measurements. The time constants of the sensors for the measured outputs during dynamic measurements are shown in Tab. 3. These time constants are based on sensor data sheets, except for the time constant for the engine torque sensor that is calculated from dynamic measurements according to Sec. 8.1. The time constants of the sensors for n_t, p_{em}, p_{im}, and W_c are significantly faster than the dynamics seen in the measurements in Fig. 20–22 and these sensor dynamics are therefore neglected. The time constants for the EGR and VGT position sensors are significantly faster than the actuator dynamics and these sensor dynamics are therefore neglected. The time constant for the engine torque sensor is large and it is therefore considered in the validation. However, this time constant is not considered in the proposed model due to that the model will be used for gas flow control and not for engine torque feedback control. Finally, the sensor dynamics for the engine speed does not effect the dynamic validation results since the engine speed is an input to the model and it is also constant in all measurements used here.

Table 3 *Measured variables during dynamic measurements and sensor time constants.*

Variable	Description	Unit	Maximum time constant for the sensor dynamics [ms]
n_t	Rotational turbine speed	rpm	6
p_{em}	Exhaust manifold pressure	Pa	20
p_{im}	Intake manifold pressure	Pa	15
W_c	Compressor mass flow	kg/s	20
$\tilde{u}_{egr}$	EGR position 0 - closed, 100 - open	%	$\ll 50$
$\tilde{u}_{vgt}$	VGT position 0 - closed, 100 - open	%	$\ll 25$
M_e	Engine torque	Nm	1000
n_e	Rotational engine speed	rpm	26
u_{egr}	EGR control signal 0 - closed, 100 - open	%	-
u_{vgt}	VGT control signal 0 - closed, 100 - open	%	-
u_δ	Injected amount of fuel	mg/cycle	-

1.5   Parameter estimation and validation

Parameters in static models are estimated automatically using least squares optimization and data from stationary measurements. The parameters in the dynamic models are estimated in two steps. Firstly, the actuator parameters are estimated by adjusting these parameters manually until simulations of the actuator models follow the dynamic responses in data set J. Secondly, the manifold volumes, the turbocharger inertia, and the time constant for the engine torque are estimated by adjusting these parameters manually until simulations of the complete model follow the dynamic responses in the data sets E and I.

Systematic tuning methods for each parameter are described in detail in Sec. 2 to 5. Since these methods are systematic and general, it is straightforward to re-create the values of the model parameters and to apply the tuning methods on different diesel engines with EGR and VGT.

Due to that the stationary measurements are few, both the static and the dynamic models are validated by simulating the complete model and comparing it with dynamic measurements. The model is validated in stationary points using the data sets A-I and dynamic properties are validated using the data sets A-D and F-I.

1.6 Relative error

Relative errors are calculated and used to evaluate the tuning and the validation of the model. Relative errors for stationary measurements between a measured variable $y_{meas,stat}$ and a modeled variable $y_{mod,stat}$ are calculated as

$$\text{stationary relative error}(i) = \frac{y_{meas,stat}(i) - y_{mod,stat}(i)}{\frac{1}{N} \sum_{i=1}^{N} y_{meas,stat}(i)} \tag{4}$$

where i is an operating point. Relative errors for dynamic measurements between a measured variable $y_{meas,dyn}$ and a modeled variable $y_{mod,dyn}$ are calculated as

$$\text{dynamic relative error}(j) = \frac{y_{meas,dyn}(j) - y_{mod,dyn}(j)}{\frac{1}{N} \sum_{i=1}^{N} y_{meas,stat}(i)} \tag{5}$$

where j is a time sample. In order to make a fair comparison between these relative errors, both the stationary and the dynamic relative error have the same stationary measurement in the denominator and the mean value of this stationary measurement is calculated in order to avoid large relative errors when $y_{meas,stat}$ is small.

2 Manifolds

The intake and exhaust manifolds are modeled as dynamic systems with two states each, and these are pressure and oxygen mass fraction. The standard isothermal model [11], that is based upon mass conservation, the ideal gas law, and that the manifold temperature is constant or varies slowly, gives the differential equations for the manifold pressures

$$\begin{aligned}
\frac{d}{dt} p_{im} &= \frac{R_a \, T_{im}}{V_{im}} \left(W_c + W_{egr} - W_{ei} \right) \\
\frac{d}{dt} p_{em} &= \frac{R_e \, T_{em}}{V_{em}} \left(W_{eo} - W_t - W_{egr} \right)
\end{aligned} \tag{6}$$

There are two sets of thermodynamic properties: air has the ideal gas constant R_a and the specific heat capacity ratio γ_a, and exhaust gas has the ideal gas constant R_e and the specific heat capacity ratio γ_e. The intake manifold temperature T_{im} is assumed to be constant and equal to the cooling temperature in the intercooler, the exhaust manifold temperature T_{em} will be described in Sec. 3.2, and V_{im} and V_{em} are the manifold volumes. The mass flows W_c, W_{egr}, W_{ei}, W_{eo}, and W_t will be described in Sec. 3 to 5.

The EGR fraction in the intake manifold is calculated as

$$x_{egr} = \frac{W_{egr}}{W_c + W_{egr}} \tag{7}$$

Note that the EGR gas also contains oxygen that affects the oxygen fuel ratio in the cylinder. This effect is considered by modeling the oxygen concentrations X_{Oim}

and X_{Oem} in the control volumes. These concentrations are defined in the same way as in [19]

$$X_{Oim} = \frac{m_{Oim}}{m_{totim}}, \quad X_{Oem} = \frac{m_{Oem}}{m_{totem}} \tag{8}$$

where m_{Oim} and m_{Oem} are the oxygen masses, and m_{totim} and m_{totem} are the total masses in the intake and exhaust manifolds. Differentiating X_{Oim} and X_{Oem} and using mass conservation [19] give the following differential equations

$$
\begin{aligned}
\frac{d}{dt} X_{Oim} &= \frac{R_a\, T_{im}}{p_{im}\, V_{im}} \left(\left(X_{Oem} - X_{Oim} \right) W_{egr} + \left(X_{Oc} - X_{Oim} \right) W_c \right) \\
\frac{d}{dt} X_{Oem} &= \frac{R_e\, T_{em}}{p_{em}\, V_{em}} \left(X_{Oe} - X_{Oem} \right) W_{eo}
\end{aligned}
\tag{9}
$$

where X_{Oc} is the constant oxygen concentration passing the compressor, i.e. air with $X_{Oc} = 23.14\%$, and X_{Oe} is the oxygen concentration in the exhaust gases coming from the engine cylinders, X_{Oe} will be described in Sec. 3.1.

Another way to consider the oxygen in the EGR gas, is to model the burned gas ratios in the control volumes which are a frequent choice for states in many papers [12, 14, 18]. The oxygen concentration and the burned gas ratio have exactly the same effect on the oxygen fuel ratio and therefore these states are equivalent.

Tuning parameters

- V_{im} and V_{em}: manifold volumes.

Tuning method

The tuning parameters V_{im} and V_{em} are determined by adjusting these parameters manually until simulations of the complete model follow the dynamic responses in the dynamic data set E in Tab. 2.

3   Cylinder

Three sub-models describe the behavior of the cylinder, these are:

- A mass flow model that describes the gas and fuel flows that enter and leave the cylinder, the oxygen to fuel ratio, and the oxygen concentration out from the cylinder.

- A model of the exhaust manifold temperature

- An engine torque model.

3.1 Cylinder flow

The total mass flow W_{ei} from the intake manifold into the cylinders is modeled using the volumetric efficiency η_{vol} [11]

$$W_{ei} = \frac{\eta_{vol}\, p_{im}\, n_e\, V_d}{120\, R_a\, T_{im}} \tag{10}$$

where p_{im} and T_{im} are the pressure and temperature in the intake manifold, n_e is the engine speed and V_d is the displaced volume. The volumetric efficiency is in its turn modeled as

$$\eta_{vol} = c_{vol1}\sqrt{p_{im}} + c_{vol2}\sqrt{n_e} + c_{vol3} \tag{11}$$

The fuel mass flow W_f into the cylinders is controlled by u_δ, which gives the injected mass of fuel in mg per cycle and cylinder

$$W_f = \frac{10^{-6}}{120}\, u_\delta\, n_e\, n_{cyl} \tag{12}$$

where n_{cyl} is the number of cylinders. The mass flow W_{eo} out from the cylinder is given by the mass balance as

$$W_{eo} = W_f + W_{ei} \tag{13}$$

The oxygen to fuel ratio λ_O in the cylinder is defined as

$$\lambda_O = \frac{W_{ei}\, X_{Oim}}{W_f\, (O/F)_s} \tag{14}$$

where $(O/F)_s$ is the stoichiometric relation between the oxygen and fuel masses. The oxygen to fuel ratio is equivalent to the air fuel ratio which is a common choice of performance variable in the literature [12, 15, 16, 18].

During the combustion, the oxygen is burned in the presence of fuel. In diesel engines $\lambda_O > 1$ to avoid smoke. Therefore, it is assumed that $\lambda_O > 1$ and the oxygen concentration out from the cylinder can then be calculated as the unburned oxygen fraction

$$X_{Oe} = \frac{W_{ei}\, X_{Oim} - W_f\, (O/F)_s}{W_{eo}} \tag{15}$$

Tuning parameters

- c_{vol1}, c_{vol2}, c_{vol3}: volumetric efficiency constants

Tuning method

The tuning parameters c_{vol1}, c_{vol2}, and c_{vol3} are determined by solving a linear least-squares problem that minimizes $(W_{ei} - W_{ei,meas})^2$ with c_{vol1}, c_{vol2}, and c_{vol3} as the optimization variables. The variable W_{ei} is the model in (10) and
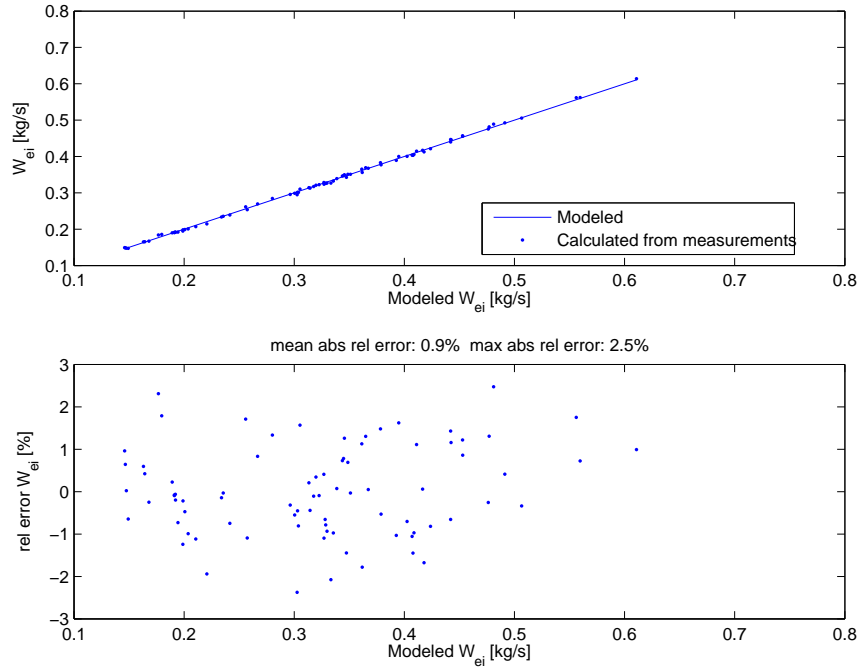
Figure 2 Top: *Comparison of modeled mass flow W_{ei} into the cylinders and calculated W_{ei} from measurements.* **Bottom:** *Relative errors for modeled W_{ei} as function of modeled W_{ei} at steady state.*

(11) and $W_{ei,meas}$ is calculated from stationary measurements as $W_{ei,meas} = W_c/(1 - x_{egr})$. Stationary measurements are used as inputs to the model during the tuning. The result of the tuning is shown in Fig. 2 that shows that the cylinder mass flow model has small absolute relative errors with a mean and a maximum absolute relative error of 0.9 % and 2.5 % respectively.

3.2   Exhaust manifold temperature

The exhaust manifold temperature model consists of a model for the cylinder out temperature and a model for the heat losses in the exhaust pipes.

Cylinder out temperature

The cylinder out temperature T_e is modeled in the same way as in [17]. This approach is based upon ideal gas Seliger cycle (or limited pressure cycle [11]) cal-

culations that give the cylinder out temperature

$$T_e = \eta_{sc}\,\Pi_e^{1-1/\gamma_a}\,r_c^{1-\gamma_a}\,x_p^{1/\gamma_a-1}\left(q_{in}\left(\frac{1-x_{cv}}{c_{pa}}+\frac{x_{cv}}{c_{va}}\right)+T_1\,r_c^{\gamma_a-1}\right) \qquad (16)$$

where η_{sc} is a compensation factor for non ideal cycles and x_{cv} the ratio of fuel consumed during constant volume combustion. The rest of the fuel $(1-x_{cv})$ is used during constant pressure combustion. The model (16) also includes the following 6 components: the pressure quotient over the cylinder

$$\Pi_e = \frac{p_{em}}{p_{im}} \qquad (17)$$

the pressure quotient between point 3 (after combustion) and point 2 (before combustion) in the Seliger cycle

$$x_p = \frac{p_3}{p_2} = 1 + \frac{q_{in}\,x_{cv}}{c_{va}\,T_1\,r_c^{\gamma_a-1}} \qquad (18)$$

the specific energy contents of the charge

$$q_{in} = \frac{W_f\,q_{HV}}{W_{ei}+W_f}\,(1-x_r) \qquad (19)$$

the temperature at inlet valve closing after intake stroke and mixing

$$T_1 = x_r\,T_e + (1-x_r)\,T_{im} \qquad (20)$$

the residual gas fraction

$$x_r = \frac{\Pi_e^{1/\gamma_a}\,x_p^{-1/\gamma_a}}{r_c\,x_v} \qquad (21)$$

and the volume quotient between point 3 (after combustion) and point 2 (before combustion) in the Seliger cycle

$$x_v = \frac{v_3}{v_2} = 1 + \frac{q_{in}\,(1-x_{cv})}{c_{pa}\left(\frac{q_{in}\,x_{cv}}{c_{va}}+T_1\,r_c^{\gamma_a-1}\right)} \qquad (22)$$

Solution to the cylinder out temperature

Since the equations above are non-linear and depend on each other, the cylinder out temperature is calculated numerically using a fixed point iteration which starts with the initial values $x_{r,0}$ and $T_{1,0}$. Then the following equations are applied in

each iteration k

$$
q_{in,k+1} = \frac{W_f \, q_{HV}}{W_{ei} + W_f} \, (1 - x_{r,k})
$$

$$
x_{p,k+1} = 1 + \frac{q_{in,k+1} \, x_{cv}}{c_{va} \, T_{1,k} \, r_c^{\gamma_a - 1}}
$$

$$
x_{v,k+1} = 1 + \frac{q_{in,k+1} \, (1 - x_{cv})}{c_{pa} \left(\frac{q_{in,k+1} \, x_{cv}}{c_{va}} + T_{1,k} \, r_c^{\gamma_a - 1} \right)}
$$

$$
x_{r,k+1} = \frac{\Pi_e^{1/\gamma_a} \, x_{p,k+1}^{-1/\gamma_a}}{r_c \, x_{v,k+1}}
$$

$$
T_{e,k+1} = \eta_{sc} \, \Pi_e^{1 - 1/\gamma_a} \, r_c^{1 - \gamma_a} \, x_{p,k+1}^{1/\gamma_a - 1} \left(q_{in,k+1} \left(\frac{1 - x_{cv}}{c_{pa}} + \frac{x_{cv}}{c_{va}} \right) + T_{1,k} \, r_c^{\gamma_a - 1} \right)
$$

$$
T_{1,k+1} = x_{r,k+1} \, T_{e,k+1} + (1 - x_{r,k+1}) \, T_{im}
$$

(23)

In each sample during the simulation, the initial values $x_{r,0}$ and $T_{1,0}$ are set to the solutions of x_r and T_1 from the previous sample.

Heat losses in the exhaust pipes

The cylinder out temperature model above does not describe the exhaust manifold temperature completely due to heat losses. This is illustrated in Fig. 3a which shows a comparison between measured and modeled exhaust manifold temperature and in this figure it is assumed that the exhaust manifold temperature is equal to the cylinder out temperature, i.e. $T_{em} = T_e$. The relative error between model and measurement seems to increase from a negative error to a positive error for increasing mass flow W_{eo} out from the cylinder. This is due to that the exhaust manifold temperature is measured in the exhaust manifold and that there are heat losses to the surroundings in the exhaust pipes between the cylinder and the exhaust manifold. Therefore the nest step is to include a sub-model for these heat losses.

This temperature drop is modeled in the same way as Model 1, presented in [6], where the temperature drop is described as a function of mass flow out from the cylinder

$$
T_{em} = T_{amb} + (T_e - T_{amb}) \, e^{-\frac{h_{tot} \, \pi \, d_{pipe} \, l_{pipe} \, n_{pipe}}{W_{eo} \, c_{pe}}}
$$

(24)

where T_{amb} is the ambient temperature, h_{tot} the total heat transfer coefficient, d_{pipe} the pipe diameter, l_{pipe} the pipe length and n_{pipe} the number of pipes. Using this model, the mean and maximum absolute relative error is reduced, see Fig. 3b.

Approximating the solution to the cylinder out temperature

As explained above, the cylinder out temperature is calculated numerically using the fixed point iteration (23). A simulation of the complete engine model during

a. Without a model for heat losses in the exhaust pipes, i.e. $T_{em} = T_e$.

b. With model (24) for heat losses in the exhaust pipes.
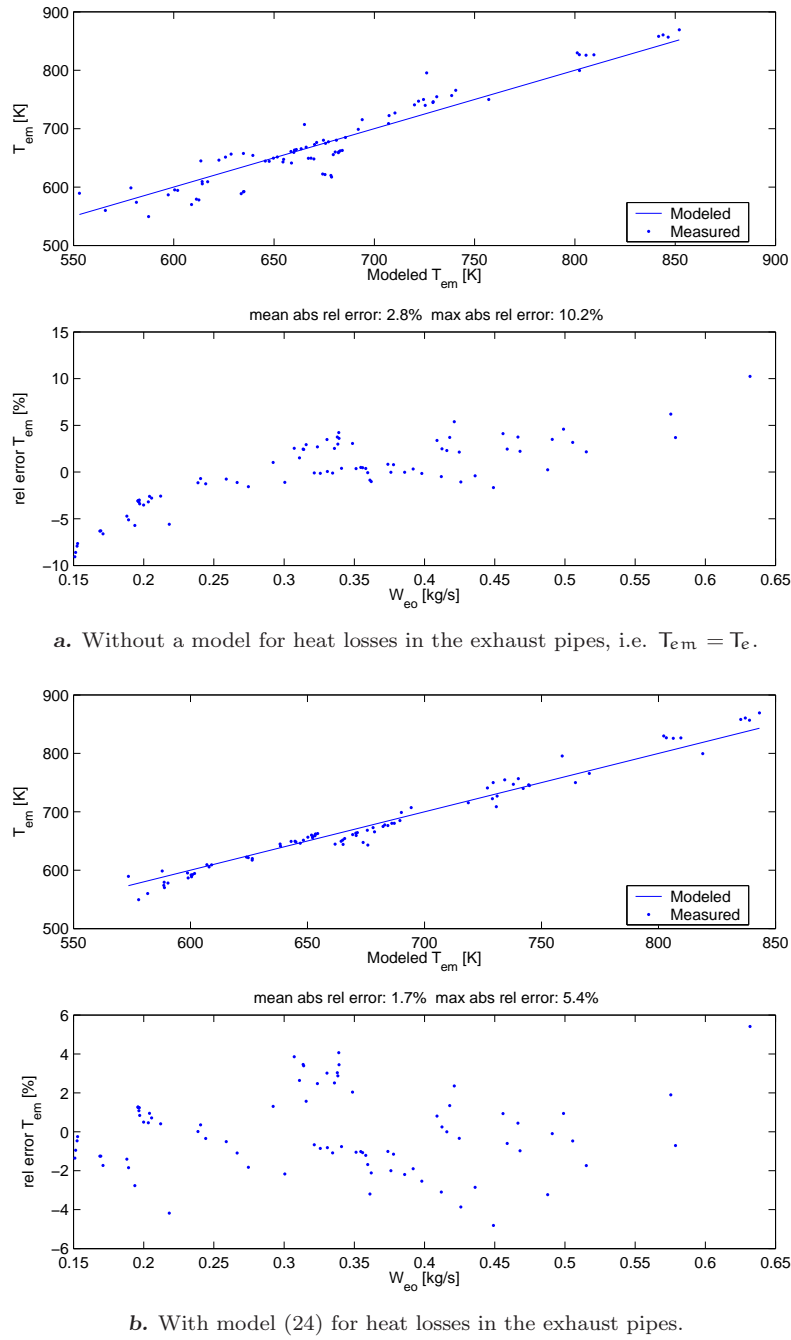
Figure 3 *Modeled and measured exhaust manifold temperature T_{em} and relative errors for modeled T_{em} at steady state.*
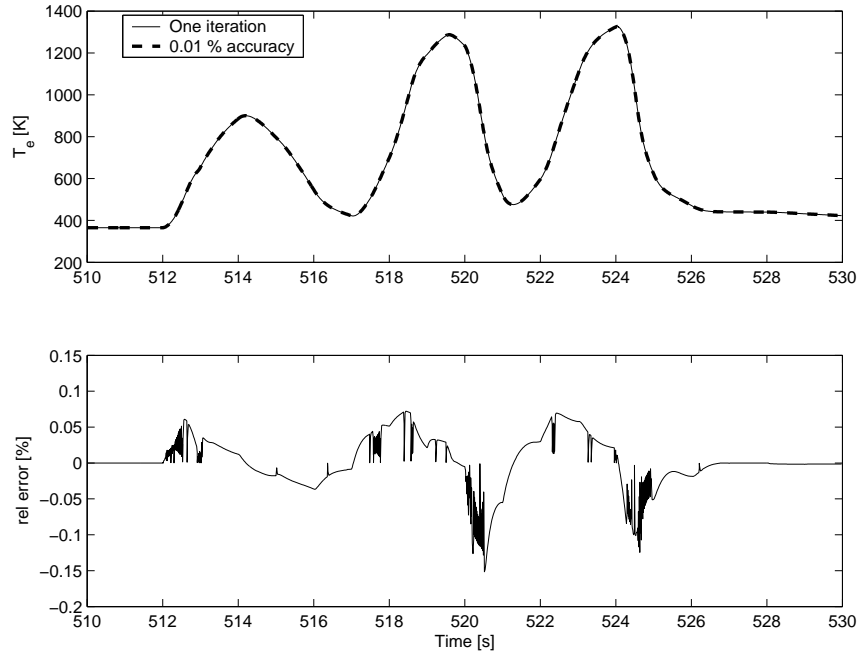
Figure 4 *The cylinder out temperature* T_e *is calculated by simulating the total engine model during the complete European Transient Cycle. This figure shows the part of the European Transient Cycle that consists of the maximum relative error.* **Top:** *The fixed point iteration (23) is used in two ways: by using one iteration and to get 0.01 % accuracy.* **Bottom:** *Relative errors between the solutions from one iteration and 0.01 % accuracy.*

the European Transient Cycle in Fig. 4 shows that it is sufficient to use one iteration in this iterative process. This is shown by comparing the solution from one iteration with one that has sufficiently many iterations to give a solution with 0.01 % accuracy. The maximum absolute relative error of the solution from one iteration (compared to the solution with 0.01 % accuracy) is 0.15 %. This error is small because the fixed point iteration (23) has initial values that are close to the solution. Consequently, when using this method in simulation it is sufficient to use one iteration in this model since the mean absolute relative error of the exhaust manifold temperature model (compared to the measurements in Fig. 3b) is 1.7 %.

Tuning parameters

- η_{sc}: compensation factor for non ideal cycles

- x_{cv}: the ratio of fuel consumed during constant volume combustion

- h_{tot}: the total heat transfer coefficient

Tuning method

The tuning parameters η_{sc}, x_{cv}, and h_{tot} are determined by solving a non-linear least-squares problem that minimizes $(T_{em} - T_{em,meas})^2$ with η_{sc}, x_{cv}, and h_{tot} as the optimization variables. The variable T_{em} is the model in (23) and (24) with stationary measurements as inputs to the model, and $T_{em,meas}$ is a stationary measurement. The result of the tuning is shown in Fig. 3b which shows that the model describes the exhaust manifold temperature well, with a mean and a maximum absolute relative error of 1.7 % and 5.4 % respectively.

3.3 Engine torque

The torque produced by the engine M_e is modeled using three different engine components; the gross indicated torque M_{ig}, the pumping torque M_p, and the friction torque M_{fric} [11].

$$M_e = M_{ig} - M_p - M_{fric} \tag{25}$$

The pumping torque is modeled using the intake and exhaust manifold pressures.

$$M_p = \frac{V_d}{4\pi}\left(p_{em} - p_{im}\right) \tag{26}$$

The gross indicated torque is coupled to the energy that comes from the fuel

$$M_{ig} = \frac{u_\delta\,10^{-6}\,n_{cyl}\,q_{HV}\,\eta_{ig}}{4\pi} \tag{27}$$

Assuming that the engine is always running at optimal injection timing, the gross indicated efficiency η_{ig} is modeled as

$$\eta_{ig} = \eta_{igch}\left(1 - \frac{1}{r_c^{\gamma_{cyl}-1}}\right) \tag{28}$$

where the parameter η_{igch} is estimated from measurements, r_c is the compression ratio, and γ_{cyl} is the specific heat capacity ratio for the gas in the cylinder. The friction torque is assumed to be a quadratic polynomial in engine speed [11].

$$M_{fric} = \frac{V_d}{4\pi}10^5\left(c_{fric1}\,n_{eratio}^2 + c_{fric2}\,n_{eratio} + c_{fric3}\right) \tag{29}$$

where

$$n_{eratio} = \frac{n_e}{1000} \tag{30}$$

Tuning parameters

- η_{igch}: combustion chamber efficiency

- c_{fric1}, c_{fric2}, c_{fric3}: coefficients in the polynomial function for the friction torque
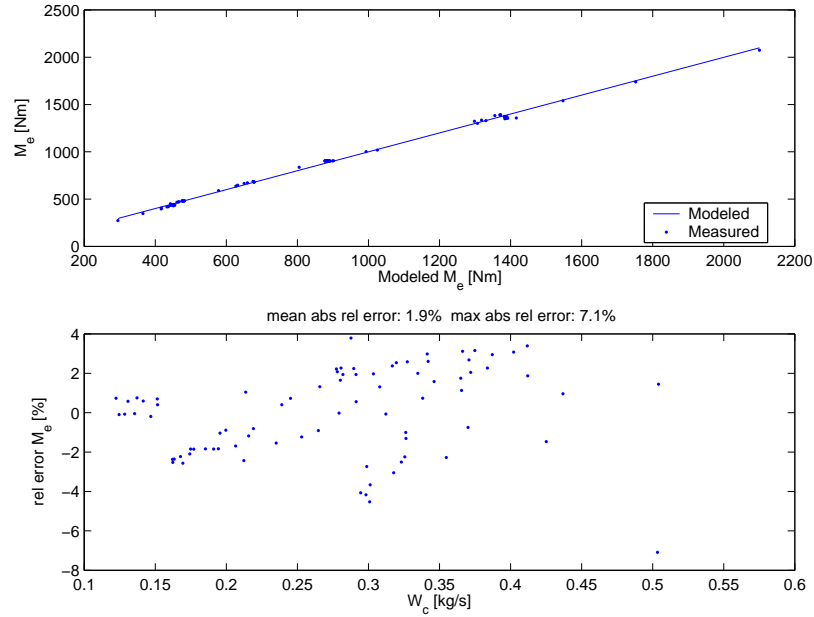
Figure 5 *Comparison of measurements and model for the engine torque M_e at steady state.* **Top:** *Modeled and measured engine torque M_e.* **Bottom:** *Relative errors for modeled M_e.*

Tuning method

The tuning parameters η_{igch}, c_{fric1}, c_{fric2}, and c_{fric3} are determined by solving a linear least-squares problem that minimizes $(M_e + M_p - M_{e,meas} - M_{p,meas})^2$ with the tuning parameters as the optimization variables. The model of $M_e + M_p$ is obtained by solving (25) for $M_e + M_p$ and $M_{e,meas} + M_{p,meas}$ is calculated from stationary measurements as $M_{e,meas} + M_{p,meas} = M_e + V_d(p_{em} - p_{im})/(4\pi)$. Stationary measurements are used as inputs to the model. The result of the tuning is shown in Fig. 5 which shows that the engine torque model has small absolute relative errors with a mean and a maximum absolute relative error of 1.9 % and 7.1 % respectively.

4   EGR-valve

The EGR-valve model consists of sub-models for the EGR-valve mass flow and the EGR-valve actuator.

4.1   EGR-valve mass flow

The mass flow through the EGR-valve is modeled as a simplification of a compressible flow restriction with variable area [11] and with the assumption that there is no reverse flow when $p_{em} < p_{im}$. The motive for this assumption is to construct a simple model. The model can be extended with reverse flow, but this increases the complexity of the model since a reverse flow model requires mixing of different temperatures and oxygen fractions in the exhaust manifold and a change of the temperature and the gas constant in the EGR mass flow model. However, p_{em} is larger than p_{im} in normal operating points, consequently the assumption above will not effect the model behavior in these operating points. Furthermore, reverse flow is not measured and can therefore not be validated.

The mass flow through the restriction is

$$W_{egr} = \frac{A_{egr}\, p_{em}\, \Psi_{egr}}{\sqrt{T_{em}\, R_e}} \tag{31}$$

where

$$\Psi_{egr} = \sqrt{\frac{2\,\gamma_e}{\gamma_e - 1}\left(\Pi_{egr}^{2/\gamma_e} - \Pi_{egr}^{1+1/\gamma_e}\right)} \tag{32}$$

Measurement data shows that (32) does not give a sufficiently accurate description of the EGR flow. Pressure pulsations in the exhaust manifold or the influence of the EGR-cooler could be two different explanations for this phenomenon. In order to maintain the density influence ($p_{em}/(\sqrt{T_{em}\, R_e})$) in (31) and the simplicity in the model, the function Ψ_{egr} is instead modeled as a parabolic function (see Fig. 6 where Ψ_{egr} is plotted as function of Π_{egr}).

$$\Psi_{egr} = 1 - \left(\frac{1 - \Pi_{egr}}{1 - \Pi_{egropt}} - 1\right)^2 \tag{33}$$

The pressure quotient Π_{egr} over the valve is limited when the flow is choked, i.e. when sonic conditions are reached in the throat, and when $1 < p_{im}/p_{em}$, i.e. no backflow can occur.

$$\Pi_{egr} = \begin{cases} \Pi_{egropt} & \text{if } \frac{p_{im}}{p_{em}} < \Pi_{egropt} \\[2mm] \frac{p_{im}}{p_{em}} & \text{if } \Pi_{egropt} \leq \frac{p_{im}}{p_{em}} \leq 1 \\[2mm] 1 & \text{if } 1 < \frac{p_{im}}{p_{em}} \end{cases} \tag{34}$$

For a compressible flow restriction, the standard model for Π_{egropt} is

$$\Pi_{egropt} = \left(\frac{2}{\gamma_e + 1}\right)^{\frac{\gamma_e}{\gamma_e - 1}} \tag{35}$$

but the accuracy of the EGR flow model is improved by replacing the physical value of Π_{egropt} in (35) with a tuning parameter [2].
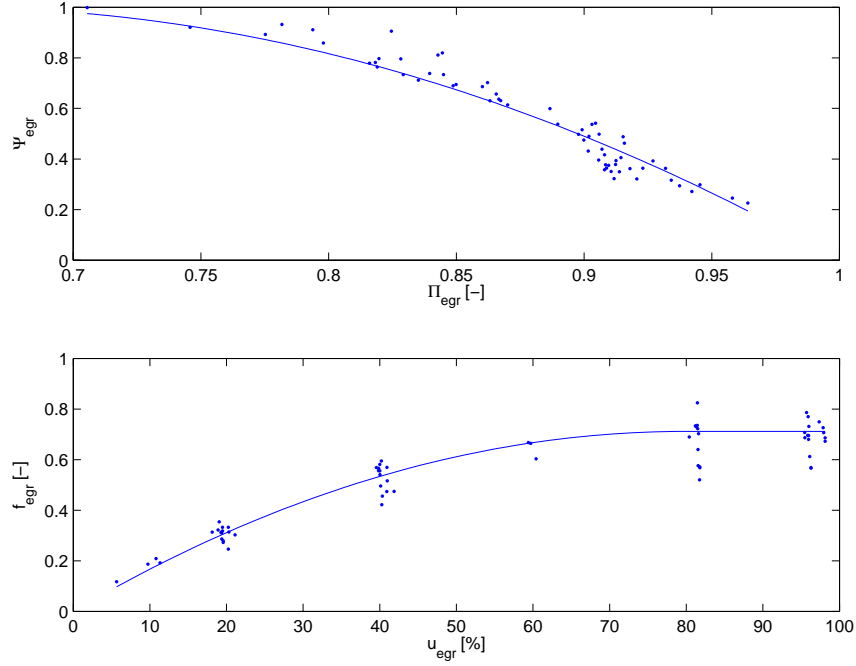
Figure 6 *Comparison of calculated points from measurements and two sub-models for the EGR flow W_{egr} at steady state showing how different variables in the sub-models depend on each other. Note that this is not a validation of the sub-models since the calculated points for the sub-models depend on the model tuning.* **Top:** *The line shows Ψ_{egr} (33) as function of pressure quotient Π_{egr}. The data points are calculated by solving (31) for Ψ_{egr}.* **Bottom:** *The line shows the effective area ratio f_{egr} (37) as function of control signal u_{egr}. The data points are calculated by solving (31) for f_{egr}.*

The effective area

$$A_{egr} = A_{egrmax} \, f_{egr}(\tilde{u}_{egr}) \tag{36}$$

is modeled as a polynomial function of the EGR valve position $\tilde{u}_{egr}$ (see Fig. 6 where f_{egr} is plotted as function of u_{egr})

$$f_{egr}(\tilde{u}_{egr}) = \begin{cases} c_{egr1} \, \tilde{u}_{egr}^2 + c_{egr2} \, \tilde{u}_{egr} + c_{egr3} & \text{if } \tilde{u}_{egr} \leq -\frac{c_{egr2}}{2\,c_{egr1}} \\ c_{egr3} - \frac{c_{egr2}^2}{4\,c_{egr1}} & \text{if } \tilde{u}_{egr} > -\frac{c_{egr2}}{2\,c_{egr1}} \end{cases} \tag{37}$$

where $\tilde{u}_{egr}$ describes the EGR actuator dynamics, see Sec. 4.2. The EGR-valve is open when $\tilde{u}_{egr} = 100\%$ and closed when $\tilde{u}_{egr} = 0\%$.

Tuning parameters

- Π_{egropt}: optimal value of Π_{egr} for maximum value of the function Ψ_{egr} in (33)

- c_{egr1}, c_{egr2}, c_{egr3}: coefficients in the polynomial function for the effective area

Tuning method

The tuning parameters above are determined by solving a separable non-linear least-squares problem, see [3] for details about the solution method. The non-linear part of this problem minimizes $(W_{egr} - W_{egr,meas})^2$ with Π_{egropt} as the optimization variable. In each iteration in the non-linear least-squares solver, the values for c_{egr1}, c_{egr2}, and c_{egr3} are set to be the solution of a linear least-squares problem that minimizes $(W_{egr} - W_{egr,meas})^2$ for the current value of Π_{egropt}. The variable W_{egr} is described by the model (31) and $W_{egr,meas}$ is calculated from measurements as $W_{egr,meas} = W_c\, x_{egr}/(1 - x_{egr})$. Stationary measurements are used as inputs to the model. The result of the tuning is shown in Fig. 7 which shows that the absolute relative errors are larger than 15 % in some points. However, the model describes the EGR mass flow well in the other points, and the mean and maximum absolute relative error are equal to 6.1 % and 22.2 % respectively.

4.2   EGR-valve actuator

The EGR-valve actuator dynamics is modeled as a second order system with an overshoot and a time delay, see Fig. 8. This model consist of a subtraction between two first order systems with different gains and time constants according to

$$\tilde{u}_{egr} = K_{egr}\, \tilde{u}_{egr1} - (K_{egr} - 1)\tilde{u}_{egr2} \tag{38}$$

$$\frac{d}{dt}\, \tilde{u}_{egr1} = \frac{1}{\tau_{egr1}}(u_{egr}(t - \tau_{degr}) - \tilde{u}_{egr1}) \tag{39}$$

$$\frac{d}{dt}\, \tilde{u}_{egr2} = \frac{1}{\tau_{egr2}}(u_{egr}(t - \tau_{degr}) - \tilde{u}_{egr2}) \tag{40}$$

Tuning parameters

- τ_{egr1}, τ_{egr2}: time constants for the two different first order systems

- τ_{degr}: time delay

- K_{egr}: a parameter that affects the size of the overshoot
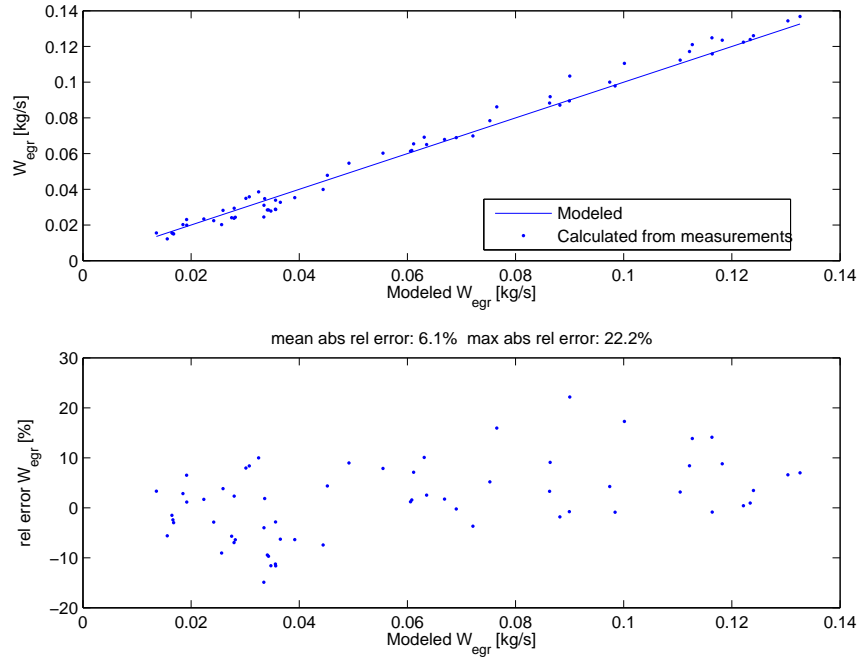
Figure 7 Top: *Comparison between modeled EGR flow* W_{egr} *and calculated* W_{egr} *from measurements at steady state.* **Bottom:** *Relative errors for* W_{egr} *at steady state.*

Tuning method

The tuning parameters above are determined by adjusting these parameters manually until simulations of the EGR-valve actuator model follow the dynamic responses in the dynamic data set J in Tab. 2. This data consist of 18 steps in EGR-valve position with a step size of 10% going from 0% up to 90% and then back again to 0% with a step size of 10%. The measurements also consist of 1 step with a step size of 30%, 1 step with a step size of 75%, 3 steps with a step size of 80%, and 1 step with a step size of 90%. These 24 steps are normalized and shifted in time in order to achieve the same starting point of the input step. These measurements are then compared with the unit step response for the linear system (38)-(40) in Fig. 8, which shows that the measurements have both large overshoots and no overshoots in some steps. However, the model describes the actuator well in average.
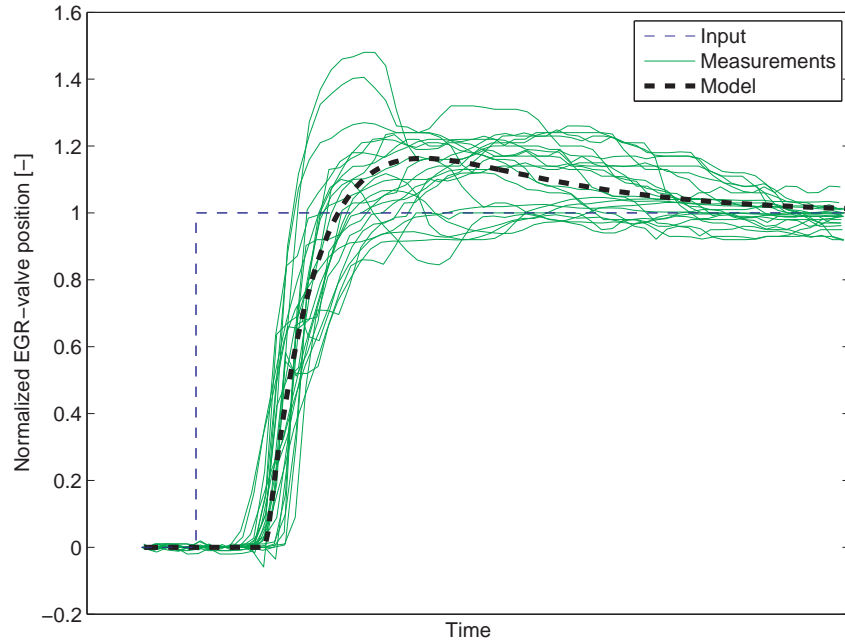
Figure 8 *Comparison between EGR-actuator dynamic simulation and dynamic tuning data during steps in EGR-valve position.*

5   Turbocharger

The turbocharger consists of a turbo inertia model, a turbine model, a VGT actuator model, and a compressor model.

5.1   Turbo inertia

For the turbo speed ω_t, Newton's second law gives

$$\frac{\mathrm{d}}{\mathrm{d}t}\omega_t = \frac{P_t\,\eta_m - P_c}{J_{tc}\,\omega_t} \tag{41}$$

where J_t is the inertia, P_t is the power delivered by the turbine, P_c is the power required to drive the compressor, and η_m is the mechanical efficiency in the turbocharger.

Tuning parameter

- J_t: turbo inertia

Tuning method

The tuning parameter J_t is determined by adjusting this parameter manually until simulations of the complete model follow the dynamic responses in the dynamic data set E in Tab. 2.

5.2 Turbine

The turbine model consists of sub-models for the total turbine efficiency and the turbine mass flow, which also includes the VGT actuator as a sub-model.

Turbine efficiency

One way to model the power P_t is to use the turbine efficiency η_t, which is defined as [11]

$$\eta_t = \frac{P_t}{P_{t,s}} = \frac{T_{em} - T_t}{T_{em}(1 - \Pi_t^{1-1/\gamma_e})} \tag{42}$$

where T_t is the temperature after the turbine, Π_t is the pressure ratio

$$\Pi_t = \frac{p_{amb}}{p_{em}} \tag{43}$$

and $P_{t,s}$ is the power from the isentropic process

$$P_{t,s} = W_t\, c_{pe}\, T_{em} \left(1 - \Pi_t^{1-1/\gamma_e}\right) \tag{44}$$

where W_t is the turbine mass flow.

In (42) it is assumed that there are no heat losses in the turbine, i.e. it is assumed that there are no temperature drops between the temperatures T_{em} and T_t that is due to heat losses. This assumption leads to errors in η_t if (42) is used to calculate η_t from measurements. One way to improve this model is to model these temperature drops, but it is difficult to tune these models since there exists no measurements of these temperature drops. Another way to improve the model, that is frequently used in the literature [7], is to use another efficiency that are approximatively equal to η_t. This approximation utilizes that

$$P_t\, \eta_m = P_c \tag{45}$$

at steady state according to (41). Consequently, $P_t \approx P_c$ at steady state. Using this approximation in (42), another efficiency η_{tm} is obtained

$$\eta_{tm} = \frac{P_c}{P_{t,s}} = \frac{W_c\, c_{pa}(T_c - T_{amb})}{W_t\, c_{pe}\, T_{em} \left(1 - \Pi_t^{1-1/\gamma_e}\right)} \tag{46}$$

where T_c is the temperature after the compressor and W_c is the compressor mass flow. The temperature T_{em} in (46) introduces less errors compared to the temperature difference $T_{em} - T_t$ in (42) due to that the absolute value of T_{em} is larger than

the absolute value of $T_{em} - T_t$. Consequently, (46) introduces less errors compared to (42) since (46) does not consist of $T_{em} - T_t$. The temperatures T_c and T_{amb} are low and they introduce less errors compared to T_{em} and T_t since the heat losses in the compressor are comparatively small. Another advantage of using (46) is that the individual variables P_t and η_m in (41) do not have to be modeled. Instead, the product $P_t \eta_m$ is modeled using (45) and (46)

$$P_t \eta_m = \eta_{tm} P_{t,s} = \eta_{tm} W_t c_{pe} T_{em} \left(1 - \Pi_t^{1-1/\gamma_e}\right) \tag{47}$$

Measurements show that η_{tm} depends on the blade speed ratio (BSR) as a parabolic function [20], see Fig. 9 where η_{tm} is plotted as function of BSR.

$$\eta_{tm} = \eta_{tm,max} - c_m(BSR - BSR_{opt})^2 \tag{48}$$

The blade speed ratio is the quotient of the turbine blade tip speed and the speed which a gas reaches when expanded isentropically at the given pressure ratio Π_t

$$BSR = \frac{R_t \omega_t}{\sqrt{2 c_{pe} T_{em} \left(1 - \Pi_t^{1-1/\gamma_e}\right)}} \tag{49}$$

where R_t is the turbine blade radius. The parameter c_m in the parabolic function varies due to mechanical losses and c_m is therefore modeled as a function of the turbo speed

$$c_m = c_{m1}(\max(0, \omega_t - c_{m2}))^{c_{m3}} \tag{50}$$

see Fig. 9 where c_m is plotted as function of ω_t.

Tuning parameters

- $\eta_{tm,max}$: maximum turbine efficiency

- BSR_{opt}: optimum BSR value for maximum turbine efficiency

- c_{m1}, c_{m2}, c_{m3}: parameters in the model for c_m

Tuning method

The tuning parameters above are determined by solving a separable non-linear least-squares problem, see [3] for details about the solution method. The non-linear part of this problem minimizes $(\eta_{tm} - \eta_{tm,meas})^2$ with BSR_{opt}, c_{m2}, and c_{m3} as the optimization variables. In each iteration in the non-linear least-squares solver, the values for $\eta_{tm,max}$ and c_{m1} are set to be the solution of a linear least-squares problem that minimizes $(\eta_{tm} - \eta_{tm,meas})^2$ for the current values of BSR_{opt}, c_{m2}, and c_{m3}. The efficiency η_{tm} is described by the model (48) and $\eta_{tm,meas}$ is calculated from measurements using (46). Stationary measurements are used as inputs to the model. The result of the tuning is shown in Fig. 9 and 10 which show that the model describes the total turbine efficiency well with a mean and a maximum absolute relative error of 4.2 % and 13.2 % respectively.
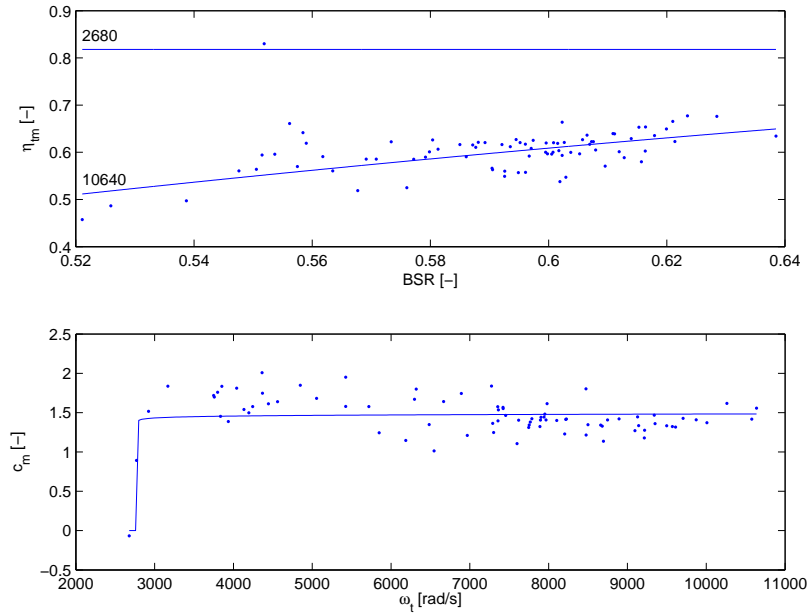
Figure 9 *Comparison of calculated points from measurements and the model for the turbine efficiency η_{tm} at steady state.* **Top:** *The lines show η_{tm} (48) at two different turbo speeds as function of blade speed ratio* BSR. *The data points are calculated by using (46) and (49).* **Bottom:** *The line shows the parameter c_m (50) as function of turbo speed ω_t. The data points are calculated by solving (48) for c_m. Note that this plot is not a validation of c_m since the calculated points for c_m depend on the model tuning.*
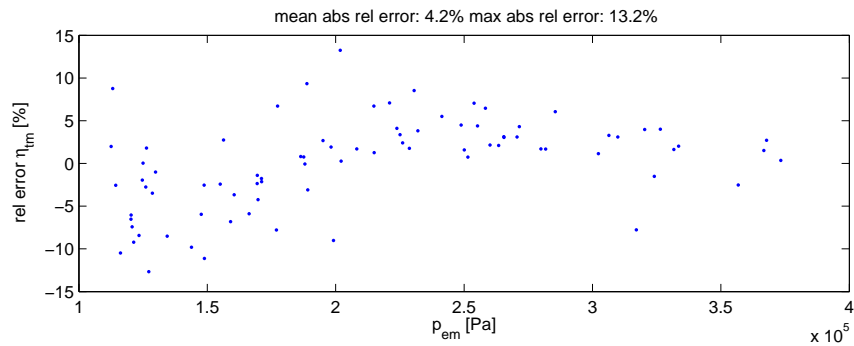
Figure 10 *Relative errors for the total turbine efficiency η_{tm} as function of exhaust manifold pressure p_{em} at steady state.*

Turbine mass flow

The turbine mass flow W_t is modeled using the corrected mass flow in order to consider density variations in the mass flow [11, 20]

$$\frac{W_t \sqrt{T_{em} R_e}}{p_{em}} = A_{vgtmax} f_{\Pi t}(\Pi_t) f_{vgt}(\tilde{u}_{vgt}) \tag{51}$$

where A_{vgtmax} is the maximum area in the turbine that the gas flows through. Measurements show that the corrected mass flow depends on the pressure ratio Π_t and the VGT actuator signal $\tilde{u}_{vgt}$. As the pressure ratio decreases, the corrected mass flow increases until the gas reaches the sonic condition and the flow is choked. This behavior can be described by a choking function

$$f_{\Pi t}(\Pi_t) = \sqrt{1 - \Pi_t^{K_t}} \tag{52}$$

which is not based on the physics of the turbine, but it gives good agreement with measurements using few parameters [8], see Fig. 11 where $f_{\Pi t}$ is plotted as function of Π_t.

When the VGT control signal u_{vgt} increases, the effective area increases and hence also the flow increases. Due to the geometry in the turbine, the change in effective area is large when the VGT control signal is large. This behavior can be described by a part of an ellipse (see Fig. 11 where f_{vgt} is plotted as function of u_{vgt})

$$\left(\frac{f_{vgt}(\tilde{u}_{vgt}) - c_{f2}}{c_{f1}}\right)^2 + \left(\frac{\tilde{u}_{vgt} - c_{vgt2}}{c_{vgt1}}\right)^2 = 1 \tag{53}$$

where f_{vgt} is the effective area ratio function and $\tilde{u}_{vgt}$ describes the VGT actuator dynamics.

The flow can now be modeled by solving (51) for W_t giving

$$W_t = \frac{A_{vgtmax} p_{em} f_{\Pi t}(\Pi_t) f_{vgt}(\tilde{u}_{vgt})}{\sqrt{T_{em} R_e}} \tag{54}$$

and solving (53) for f_{vgt} giving

$$f_{vgt}(\tilde{u}_{vgt}) = c_{f2} + c_{f1} \sqrt{\max(0, 1 - \left(\frac{\tilde{u}_{vgt} - c_{vgt2}}{c_{vgt1}}\right)^2)} \tag{55}$$

Tuning parameters

- K_t: exponent in the choking function for the turbine flow

- c_{f1}, c_{f2}, c_{vgt1}, c_{vgt2}: parameters in the ellipse for the effective area ratio function
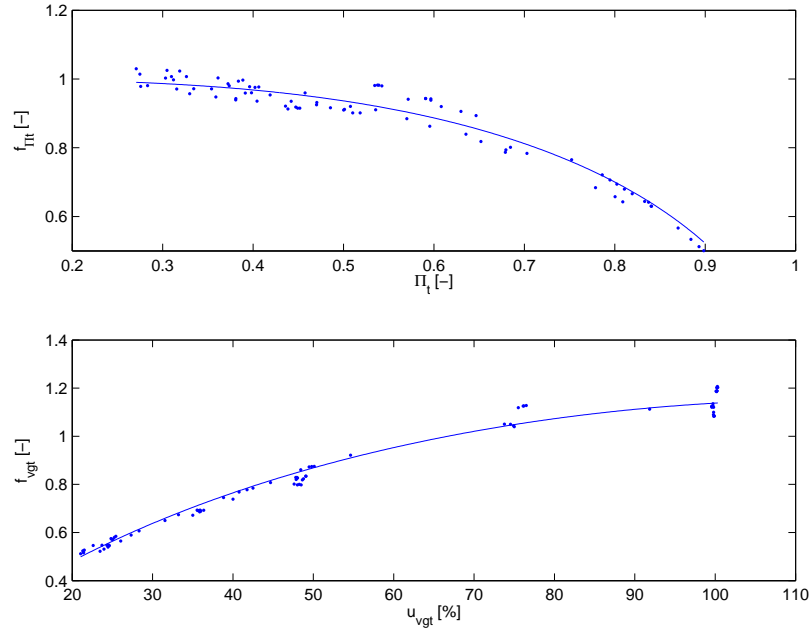
Figure 11 *Comparison of calculated points from measurements and two sub-models for the turbine mass flow at steady state showing how different variables in the sub-models depend on each other. Note that this is not a validation of the sub-models since the calculated points for the sub-models depend on the model tuning.* **Top:** *The line shows the choking function* $f_{\Pi t}$ *(52) as function of the pressure ratio* Π_t. *The data points are calculated by solving (51) for* $f_{\Pi t}$. **Bottom:** *The line shows the effective area ratio function* f_{vgt} *(55) as function of the control signal* u_{vgt}. *The data points are calculated by solving (51) for* f_{vgt}.

Tuning method

The tuning parameters above are determined by solving a non-linear least-squares problem that minimizes $(W_t - W_{t,meas})^2$ with the tuning parameters as the optimization variables. The flow W_t is described by the model (54), (55), and (52), and $W_{t,meas}$ is calculated from measurements as $W_{t,meas} = W_c + W_f$, where W_f is calculated using (12). Stationary measurements are used as inputs to the model. The result of the tuning is shown in Fig. 12 which shows small absolute relative errors with a mean and a maximum absolute relative error of 2.8 % and 7.6 % respectively.
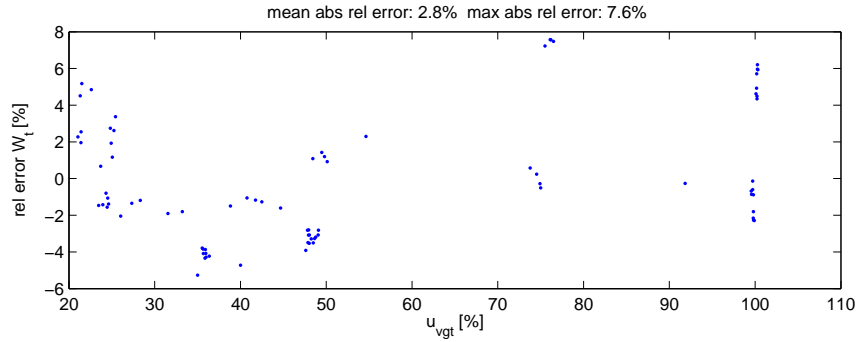
Figure 12 *Relative errors for turbine flow* W_t *as function of control signal* u_{vgt} *at steady state.*

VGT actuator

The VGT actuator dynamics is modeled as a first order system with a time delay according to

$$\frac{d}{dt}\tilde{u}_{vgt} = \frac{1}{\tau_{vgt}}(u_{vgt}(t - \tau_{dvgt}) - \tilde{u}_{vgt}) \tag{56}$$

Tuning parameters

- τ_{vgt}: time constant

- τ_{dvgt}: time delay

Tuning method

The tuning parameters above are determined by adjusting these parameters manually until simulations of the VGT actuator model follow the dynamic responses in the dynamic data set J in Tab. 2. This data consist of 18 steps in VGT position with a step size of 10% going from 100% down to 10% and then back again to 100% with a step size of 10%. The measurements also consist of 5 steps with a step size of 5% and 1 step with a step size of 20%. These 24 steps are then normalized and shifted in time in order to achieve the same starting point of the input step. These measurements are then compared with the unit step response for the linear system (56) in Fig. 13 which shows that the model describes the actuator well.

5.3 Compressor

The compressor model consists of sub-models for the compressor efficiency and the compressor mass flow.
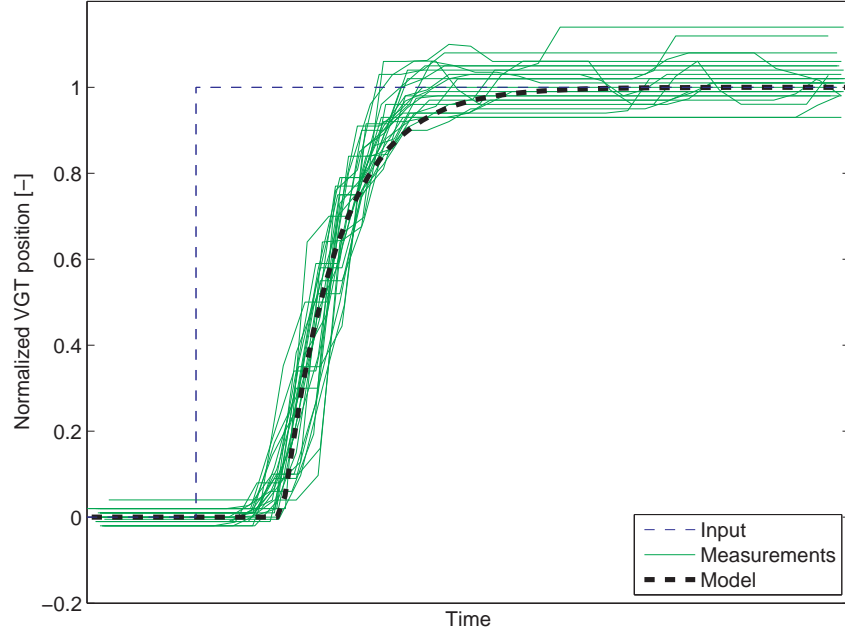
Figure 13 *Comparison between VGT-actuator dynamic simulation and dynamic tuning data during steps in VGT position.*

Compressor efficiency

The compressor power P_c is modeled using the compressor efficiency η_c, which is defined as [11]

$$\eta_c = \frac{P_{c,s}}{P_c} = \frac{T_{amb}\left(\Pi_c^{1-1/\gamma_a} - 1\right)}{T_c - T_{amb}} \tag{57}$$

where T_c is the temperature after the compressor, Π_c is the pressure ratio

$$\Pi_c = \frac{p_{im}}{p_{amb}} \tag{58}$$

and $P_{c,s}$ is the power from the isentropic process

$$P_{c,s} = W_c \, c_{pa} \, T_{amb} \left(\Pi_c^{1-1/\gamma_a} - 1\right) \tag{59}$$

where W_c is the compressor mass flow. The power P_c is modeled by solving (57) for P_c and using (59)

$$P_c = \frac{P_{c,s}}{\eta_c} = \frac{W_c \, c_{pa} \, T_{amb}}{\eta_c} \left(\Pi_c^{1-1/\gamma_a} - 1\right) \tag{60}$$

The efficiency is modeled using ellipses similar to [9], but with a non-linear transformation on the axis for the pressure ratio similar to [2]. The inputs to the efficiency model are Π_c and W_c (see Fig. 18). The flow W_c is not scaled by the inlet temperature and the inlet pressure, in the current implementation, since these two variables are constant. However, this model can easily be extended with corrected mass flow in order to consider variations in the environmental conditions.

The ellipses can be described as

$$\eta_c = \eta_{cmax} - \chi^\mathsf{T} Q_c \chi \tag{61}$$

χ is a vector which contains the inputs

$$\chi = \left[\begin{array}{c} W_c - W_{copt} \\ \pi_c - \pi_{copt} \end{array} \right] \tag{62}$$

where the non-linear transformation for Π_c is

$$\pi_c = (\Pi_c - 1)^{c_\pi} \tag{63}$$

and the symmetric and positive definite matrix Q_c consists of three parameters

$$Q_c = \left[\begin{array}{cc} a_1 & a_3 \\ a_3 & a_2 \end{array} \right] \tag{64}$$

Tuning model parameters

- η_{cmax}: maximum compressor efficiency

- W_{copt} and π_{copt}: optimum values of W_c and π_c for maximum compressor efficiency

- c_π: exponent in the scale function, (63)

- a_1, a_2 and a_3: parameters in the matrix Q_c

Tuning method

The tuning parameters above are determined by solving a separable non-linear least-squares problem, see [3] for details about the solution method. The non-linear part of this problem minimizes $(\eta_c - \eta_{c,meas})^2$ with W_{copt}, π_{copt}, and c_π as the optimization variables. In each iteration in the non-linear least-squares solver, the values for η_{cmax}, a_1, a_2 and a_3 are set to be the solution of a linear least-squares problem that minimizes $(\eta_c - \eta_{c,meas})^2$ for the current values of W_{copt}, π_{copt}, and c_π. The efficiency η_c is described by the model (61) to (64) and $\eta_{c,meas}$ is calculated from measurements using (57). Stationary measurements are used as inputs to the model. This method does not guarantee that the matrix Q_c becomes positive definite, therefore it is important to check that Q_c is positive
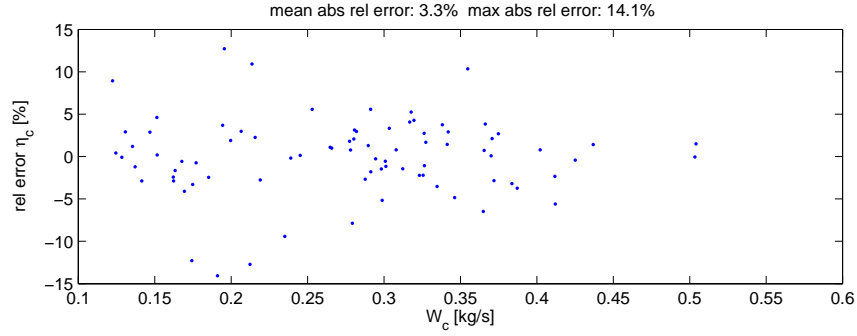
Figure 14 *Relative errors for η_c as function of W_c at steady state.*

definite after the tuning. For the stationary tuning data in Sec. 1.4 Q_c is positive definite. The result of the tuning is shown in Fig. 14 which shows small absolute relative errors with a mean and a maximum absolute relative error of 3.3 % and 14.1 % respectively.

Compressor mass flow

The mass flow W_c through the compressor is modeled using two dimensionless variables. The first variable is the energy transfer coefficient [5]

$$\Psi_c = \frac{2 c_{pa} T_{amb} \left(\Pi_c^{1-1/\gamma_a} - 1 \right)}{R_c^2 \omega_t^2} \tag{65}$$

which is the quotient of the isentropic kinetic energy of the gas at the given pressure ratio Π_c and the kinetic energy of the compressor blade tip where R_c is compressor blade radius. The second variable is the volumetric flow coefficient [5]

$$\Phi_c = \frac{W_c/\rho_{amb}}{\pi R_c^3 \omega_t} = \frac{R_a T_{amb}}{p_{amb} \pi R_c^3 \omega_t} W_c \tag{66}$$

which is the quotient of volume flow rate of air into the compressor and the rate at which volume is displaced by the compressor blade where ρ_{amb} is the density of the ambient air. The relation between Ψ_c and Φ_c can be described by a part of an ellipse [2, 7], see Fig. 15 where Φ_c is plotted as function of Ψ_c

$$c_{\Psi 1}(\omega_t) \left(\Psi_c - c_{\Psi 2} \right)^2 + c_{\Phi 1}(\omega_t) \left(\Phi_c - c_{\Phi 2} \right)^2 = 1 \tag{67}$$

where $c_{\Psi 1}$ and $c_{\Phi 1}$ varies with turbo speed ω_t and are modeled as polynomial functions.

$$c_{\Psi 1}(\omega_t) = c_{\omega\Psi 1} \omega_t^2 + c_{\omega\Psi 2} \omega_t + c_{\omega\Psi 3} \tag{68}$$

$$c_{\Phi 1}(\omega_t) = c_{\omega\Phi 1} \omega_t^2 + c_{\omega\Phi 2} \omega_t + c_{\omega\Phi 3} \tag{69}$$
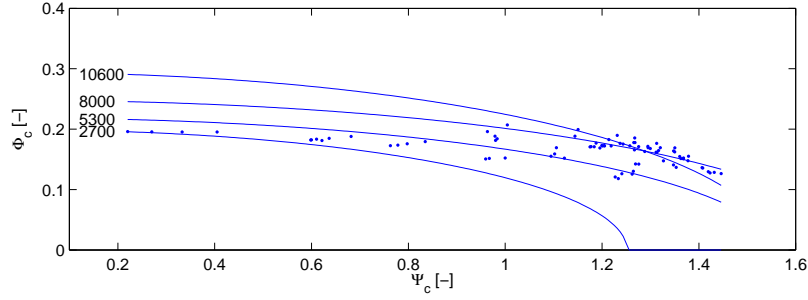
Figure 15 *Comparison of calculated points from measurements and model for the compressor mass flow W_c at steady state. The lines show the volumetric flow coefficient Φ_c (70) at four different turbo speeds as function of energy transfer coefficient Ψ_c. The data points are calculated using (65) and (66).*

In Fig. 16 the variables $c_{\Psi1}$ and $c_{\Phi1}$ are plotted as function of the turbo speed ω_t. The mass flow is modeled by solving (67) for Φ_c and solving (66) for W_c.

$$\Phi_c = \sqrt{\max\left(0, \frac{1 - c_{\Psi1}\,(\Psi_c - c_{\Psi2})^2}{c_{\Phi1}}\right)} + c_{\Phi2} \qquad (70)$$

$$W_c = \frac{p_{amb}\,\pi\,R_c^3\,\omega_t}{R_a\,T_{amb}}\,\Phi_c \qquad (71)$$

Tuning model parameters

- $c_{\Psi2}$, $c_{\Phi2}$: parameters in the ellipse model for the compressor mass flow

- $c_{\omega\Psi1}$, $c_{\omega\Psi2}$, $c_{\omega\Psi3}$: coefficients in the polynomial function (68)

- $c_{\omega\Phi1}$, $c_{\omega\Phi2}$, $c_{\omega\Phi3}$: coefficients in the polynomial function (69)

Tuning method

The tuning parameters above are determined by solving a separable non-linear least-squares problem, see [3] for details about the solution method. The non-linear part of this problem minimizes $(c_{\Psi1}(\omega_t)\,(\Psi_c - c_{\Psi2})^2 + c_{\Phi1}(\omega_t)\,(\Phi_c - c_{\Phi2})^2 - 1)^2$ with $c_{\Psi2}$ and $c_{\Phi2}$ as the optimization variables. In each iteration in the non-linear least-squares solver, the values for $c_{\omega\Psi1}$, $c_{\omega\Psi2}$, $c_{\omega\Psi3}$, $c_{\omega\Phi1}$, $c_{\omega\Phi2}$, and $c_{\omega\Phi3}$ are set to be the solution of a linear least-squares problem that minimizes $(c_{\Psi1}(\omega_t)\,(\Psi_c - c_{\Psi2})^2 + c_{\Phi1}(\omega_t)\,(\Phi_c - c_{\Phi2})^2 - 1)^2$ for the current values of $c_{\Psi2}$ and $c_{\Phi2}$. Stationary measurements are used as inputs to the model. The result of
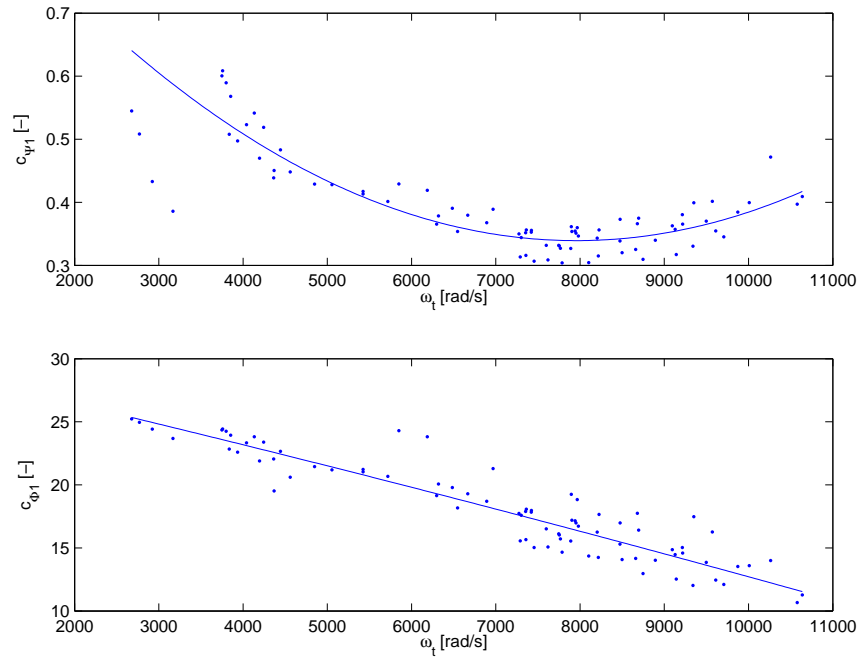
Figure 16 *Comparison of calculated points from measurements and two sub-models for the compressor mass flow at steady state showing how different variables in the sub-models depend on each other. Note that this is not a validation of the sub-models since the calculated points for the sub-models depend on the model tuning. The lines show the sub-models $c_{\Psi 1}$ (68) and $c_{\Phi 1}$ (69) as function of turbo speed ω_t. The data points are calculated by solving (67) for $c_{\Psi 1}$ and $c_{\Phi 1}$.*

the tuning is shown in Fig. 17 which shows that the model describes the compressor mass flow well with a mean and a maximum absolute relative error of 3.4 % and 13.7 % respectively.

Compressor map

Compressor performance is usually presented in terms of a map with Π_c and W_c on the axes showing lines of constant efficiency and constant turbo speed. This is shown in Fig. 18 which has approximatively the same characteristics as Fig. 2.10 in [20]. Consequently, the proposed model of the compressor efficiency (61) and the compressor flow (71) has the expected behavior.
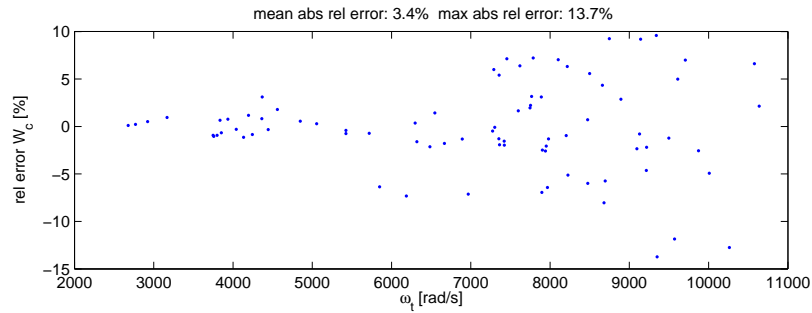
Figure 17 *Relative errors for compressor flow W_c as function of tur-bocharger speed ω_t at steady state.*
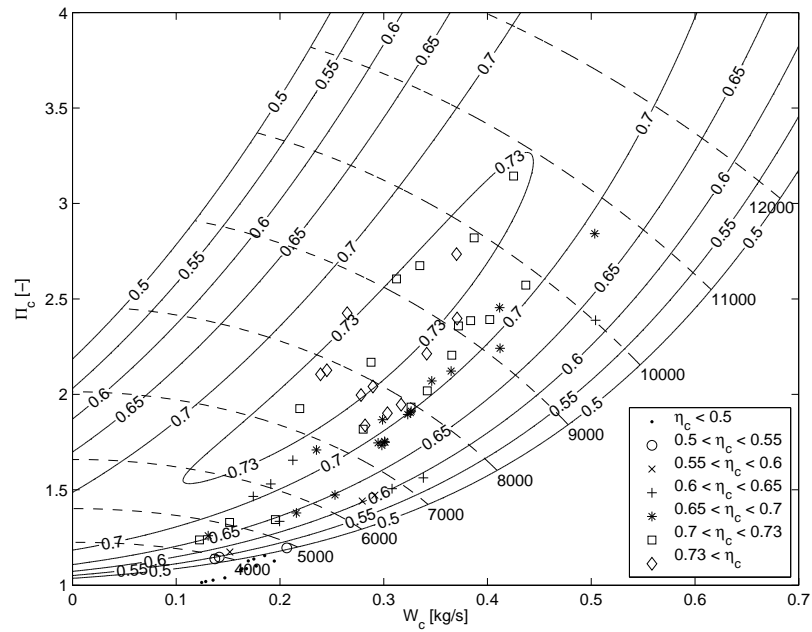
Figure 18 *Compressor map with modeled efficiency lines (solid line), mod-eled turbo speed lines (dashed line with turbo speed in rad/s), and calculated efficiency from measurements using (57). The calculated points are divided into different groups. The turbo speed lines are described by the compressor flow model.*

6 Intercooler and EGR-cooler

To construct a simple model, that captures the important system properties, the intercooler and the EGR-cooler are assumed to be ideal, i.e. there is no pressure loss, no mass accumulation, and perfect efficiency, which give the following equations

$$
\begin{aligned}
p_{out} &= p_{in} \\
W_{out} &= W_{in} \\
T_{out} &= T_{cool}
\end{aligned}
\tag{72}
$$

where T_{cool} is the cooling temperature. The model can be extended with non-ideal coolers, but these increase the complexity of the model since non-ideal coolers require that there are states for the pressures both before and after the coolers.

7 Summary of assumptions and model equations

A summary of the model assumptions is given in Sec. 7.1 and the proposed model equations are given in Sec. 7.2 to 7.5.

7.1 Assumptions

To develop a simple model, that captures the dominating effects in the mass flows, the following assumptions were made:

1. The manifolds are modeled as standard isothermal models.

2. All gases are considered to be ideal and there are two sets of thermodynamic properties:

   (a) Air has the gas constant R_a and the specific heat capacity ratio γ_a.
   (b) Exhaust gas has the gas constant R_e and the specific heat capacity ratio γ_e.

3. The EGR gas in the intake manifold affects neither the gas constant nor the specific heat capacity in the intake manifold.

4. No heat transfer to or from the gas inside of the intake manifold.

5. No backflow can occur in the EGR-valve, compressor, turbine, or the cylinder.

6. The oxygen fuel ratio λ_O is always larger than one.

7. The intercooler and the EGR-cooler are ideal, i.e. the equations for the coolers are

$$
\begin{aligned}
p_{out} &= p_{in} \\
W_{out} &= W_{in} \\
T_{out} &= T_{cool}
\end{aligned}
\tag{73}
$$

where T_{cool} is the cooling temperature.

Note that assumptions 1 and 7 above lead to that the intake manifold temperature is constant.

7.2   Manifolds

$$
\begin{aligned}
\frac{\mathrm{d}}{\mathrm{dt}} p_{im} &= \frac{R_a\, T_{im}}{V_{im}} \left(W_c + W_{egr} - W_{ei} \right) \\
\frac{\mathrm{d}}{\mathrm{dt}} p_{em} &= \frac{R_e\, T_{em}}{V_{em}} \left(W_{eo} - W_t - W_{egr} \right)
\end{aligned}
\tag{74}
$$

$$
x_{egr} = \frac{W_{egr}}{W_c + W_{egr}}
\tag{75}
$$

$$
\begin{aligned}
\frac{\mathrm{d}}{\mathrm{dt}} X_{Oim} &= \frac{R_a\, T_{im}}{p_{im}\, V_{im}} \left((X_{Oem} - X_{Oim})\, W_{egr} + (X_{Oc} - X_{Oim})\, W_c \right) \\
\frac{\mathrm{d}}{\mathrm{dt}} X_{Oem} &= \frac{R_e\, T_{em}}{p_{em}\, V_{em}} \left(X_{Oe} - X_{Oem} \right) W_{eo}
\end{aligned}
\tag{76}
$$

7.3   Cylinder

Cylinder flow

$$
W_{ei} = \frac{\eta_{vol}\, p_{im}\, n_e\, V_d}{120\, R_a\, T_{im}}
\tag{77}
$$

$$
\eta_{vol} = c_{vol1} \sqrt{p_{im}} + c_{vol2} \sqrt{n_e} + c_{vol3}
\tag{78}
$$

$$
W_f = \frac{10^{-6}}{120}\, u_\delta\, n_e\, n_{cyl}
\tag{79}
$$

$$
W_{eo} = W_f + W_{ei}
\tag{80}
$$

$$
\lambda_O = \frac{W_{ei}\, X_{Oim}}{W_f\, (O/F)_s}
\tag{81}
$$

$$
X_{Oe} = \frac{W_{ei}\, X_{Oim} - W_f\, (O/F)_s}{W_{eo}}
\tag{82}
$$

Cylinder out temperature

$$q_{in,k+1} = \frac{W_f\,q_{HV}}{W_{ei} + W_f}\,(1 - x_{r,k})$$

$$x_{p,k+1} = 1 + \frac{q_{in,k+1}\,x_{cv}}{c_{va}\,T_{1,k}\,r_c^{\gamma_a - 1}}$$

$$x_{v,k+1} = 1 + \frac{q_{in,k+1}\,(1 - x_{cv})}{c_{pa}\left(\frac{q_{in,k+1}\,x_{cv}}{c_{va}} + T_{1,k}\,r_c^{\gamma_a - 1}\right)}$$

$$x_{r,k+1} = \frac{\Pi_e^{1/\gamma_a}\,x_{p,k+1}^{-1/\gamma_a}}{r_c\,x_{v,k+1}}$$

$$T_{e,k+1} = \eta_{sc}\,\Pi_e^{1 - 1/\gamma_a}\,r_c^{1-\gamma_a}\,x_{p,k+1}^{1/\gamma_a - 1}\left(q_{in,k+1}\left(\frac{1 - x_{cv}}{c_{pa}} + \frac{x_{cv}}{c_{va}}\right) + T_{1,k}\,r_c^{\gamma_a - 1}\right)$$

$$T_{1,k+1} = x_{r,k+1}\,T_{e,k+1} + (1 - x_{r,k+1})\,T_{im}$$

$$\tag{83}$$

$$T_{em} = T_{amb} + (T_e - T_{amb})\,e^{-\frac{h_{tot}\,\pi\,d_{pipe}\,l_{pipe}\,n_{pipe}}{W_{eo}\,c_{pe}}} \tag{84}$$

Cylinder torque

$$M_e = M_{ig} - M_p - M_{fric} \tag{85}$$

$$M_p = \frac{V_d}{4\,\pi}\,(p_{em} - p_{im}) \tag{86}$$

$$M_{ig} = \frac{u_\delta\,10^{-6}\,n_{cyl}\,q_{HV}\,\eta_{ig}}{4\,\pi} \tag{87}$$

$$\eta_{ig} = \eta_{igch}\left(1 - \frac{1}{r_c^{\gamma_{cyl} - 1}}\right) \tag{88}$$

$$M_{fric} = \frac{V_d}{4\,\pi}10^5\left(c_{fric1}\,n_{eratio}^2 + c_{fric2}\,n_{eratio} + c_{fric3}\right) \tag{89}$$

$$n_{eratio} = \frac{n_e}{1000} \tag{90}$$

7.4 EGR-valve

$$W_{egr} = \frac{A_{egr}\,p_{em}\,\Psi_{egr}}{\sqrt{T_{em}\,R_e}} \tag{91}$$

$$\Psi_{egr} = 1 - \left(\frac{1 - \Pi_{egr}}{1 - \Pi_{egropt}} - 1\right)^2 \tag{92}$$

$$\Pi_{egr} = \begin{cases} \Pi_{egropt} & \text{if } \frac{p_{im}}{p_{em}} < \Pi_{egropt} \\[2mm] \frac{p_{im}}{p_{em}} & \text{if } \Pi_{egropt} \leq \frac{p_{im}}{p_{em}} \leq 1 \\[2mm] 1 & \text{if } 1 < \frac{p_{im}}{p_{em}} \end{cases} \tag{93}$$

$$A_{egr} = A_{egrmax}\, f_{egr}(\tilde{u}_{egr}) \tag{94}$$

$$f_{egr}(\tilde{u}_{egr}) = \begin{cases} c_{egr1}\, \tilde{u}_{egr}^2 + c_{egr2}\, \tilde{u}_{egr} + c_{egr3} & \text{if } \tilde{u}_{egr} \leq -\frac{c_{egr2}}{2\, c_{egr1}} \\[3mm] c_{egr3} - \frac{c_{egr2}^2}{4\, c_{egr1}} & \text{if } \tilde{u}_{egr} > -\frac{c_{egr2}}{2\, c_{egr1}} \end{cases} \tag{95}$$

$$\tilde{u}_{egr} = K_{egr}\, \tilde{u}_{egr1} - (K_{egr} - 1)\tilde{u}_{egr2} \tag{96}$$

$$\frac{d}{dt}\, \tilde{u}_{egr1} = \frac{1}{\tau_{egr1}}(u_{egr}(t - \tau_{degr}) - \tilde{u}_{egr1}) \tag{97}$$

$$\frac{d}{dt}\, \tilde{u}_{egr2} = \frac{1}{\tau_{egr2}}(u_{egr}(t - \tau_{degr}) - \tilde{u}_{egr2}) \tag{98}$$

7.5 Turbo

Turbo inertia

$$\frac{d}{dt}\omega_t = \frac{P_t\, \eta_m - P_c}{J_{tc}\, \omega_t} \tag{99}$$

Turbine efficiency

$$P_t\, \eta_m = \eta_{tm}\, W_t\, c_{pe}\, T_{em} \left(1 - \Pi_t^{1-1/\gamma_e}\right) \tag{100}$$

$$\Pi_t = \frac{p_{amb}}{p_{em}} \tag{101}$$

$$\eta_{tm} = \eta_{tm,max} - c_m(BSR - BSR_{opt})^2 \tag{102}$$

$$BSR = \frac{R_t\, \omega_t}{\sqrt{2\, c_{pe}\, T_{em} \left(1 - \Pi_t^{1-1/\gamma_e}\right)}} \tag{103}$$

$$c_m = c_{m1}(\max(0, \omega_t - c_{m2}))^{c_{m3}} \tag{104}$$

Turbine mass flow

$$W_t = \frac{A_{vgtmax}\, p_{em}\, f_{\Pi t}(\Pi_t)\, f_{vgt}(\tilde{u}_{vgt})}{\sqrt{T_{em}\, R_e}} \tag{105}$$

$$f_{\Pi t}(\Pi_t) = \sqrt{1 - \Pi_t^{K_t}} \tag{106}$$

$$f_{vgt}(\tilde{u}_{vgt}) = c_{f2} + c_{f1}\sqrt{\max\left(0, 1 - \left(\frac{\tilde{u}_{vgt} - c_{vgt2}}{c_{vgt1}}\right)^2\right)} \tag{107}$$

$$\frac{d}{dt}\tilde{u}_{vgt} = \frac{1}{\tau_{vgt}}(u_{vgt}(t - \tau_{dvgt}) - \tilde{u}_{vgt}) \tag{108}$$

Compressor efficiency

$$P_c = \frac{W_c\, c_{pa}\, T_{amb}}{\eta_c}\left(\Pi_c^{1-1/\gamma_a} - 1\right) \tag{109}$$

$$\Pi_c = \frac{p_{im}}{p_{amb}} \tag{110}$$

$$\eta_c = \eta_{cmax} - \chi^{\mathsf{T}}\, Q_c\, \chi \tag{111}$$

$$\chi = \begin{bmatrix} W_c - W_{copt} \\ \pi_c - \pi_{copt} \end{bmatrix} \tag{112}$$

$$\pi_c = (\Pi_c - 1)^{c_\pi} \tag{113}$$

$$Q_c = \begin{bmatrix} a_1 & a_3 \\ a_3 & a_2 \end{bmatrix} \tag{114}$$

Compressor mass flow

$$W_c = \frac{p_{amb}\, \pi\, R_c^3\, \omega_t}{R_a\, T_{amb}}\Phi_c \tag{115}$$

$$\Phi_c = \sqrt{\max\left(0, \frac{1 - c_{\Psi 1}\,(\Psi_c - c_{\Psi 2})^2}{c_{\Phi 1}}\right)} + c_{\Phi 2} \tag{116}$$

$$\Psi_c = \frac{2\, c_{pa}\, T_{amb}\left(\Pi_c^{1-1/\gamma_a} - 1\right)}{R_c^2\, \omega_t^2} \tag{117}$$

$$c_{\Psi 1} = c_{\omega\Psi 1}\, \omega_t^2 + c_{\omega\Psi 2}\, \omega_t + c_{\omega\Psi 3} \tag{118}$$

$$c_{\Phi 1} = c_{\omega\Phi 1}\, \omega_t^2 + c_{\omega\Phi 2}\, \omega_t + c_{\omega\Phi 3} \tag{119}$$

8 Model tuning and validation

One step in the development of a model that describes the system dynamics and the nonlinear effects is the tuning and validation. In Sec. 8.1 a summary of the model tuning is given and in Sec. 8.2 a validation of the complete model is performed using dynamic data. In the validation, it is important to investigate if the model captures the essential dynamic behaviors and nonlinear effects. The data that is used in the tuning and validation are described in Sec. 1.4.

8.1 Summary of tuning

A summary of the tuning of static and dynamic models and its results are given in the following sections. In order to validate the engine torque model during dynamic responses, a time constant for the engine torque is modeled and tuned below.

Static models

As described in Sec. 1.5, parameters in static models are estimated automatically using least squares optimization and tuning data from stationary measurements. The tuning methods for each parameter and the tuning results are described in Sec. 3 to 5. The tuning results are summarized in Tab. 4 showing the absolute relative model errors between static sub-models and stationary tuning data. The mean absolute relative errors are 6.1 % or lower. The EGR mass flow model has the largest mean absolute relative error and the cylinder mass flow model has the smallest mean absolute relative error.

Table 4 *The mean and maximum absolute relative errors between static models and the stationary tuning data for each subsystem in the diesel engine model, i.e. a summary of the mean and maximum absolute relative errors in Sec. 3 to 5.*

Subsystem	Mean absolute relative error [%]	Maximum absolute relative error [%]
Cylinder mass flow	0.9	2.5
Exhaust gas temperature	1.7	5.4
Engine torque	1.9	7.1
EGR mass flow	6.1	22.2
Turbine efficiency	4.2	13.2
Turbine mass flow	2.8	7.6
Compressor efficiency	3.3	14.1
Compressor mass flow	3.4	13.7

Dynamic models

As described in Sec. 1.5, parameters in dynamic models are estimated in two steps. Firstly, the actuator parameters are estimated using the method in Sec. 4.2 and 5.2. These sections also show the tuning results for the actuators. Secondly, the manifold volumes and the turbocharger inertia are estimated using the method in Sec. 2 and 5.1. The tuning result of the second step is shown in Tab. 5 for the data set E that shows that the mean absolute relative errors are 8 % or lower.

A dynamometer is fitted to the engine via an axle-shaft in order to brake or supply torque to the engine. This dynamometer and axle-shaft lead to that the measured engine torque has a time constant that is not modeled due to that the torque will not be used as a feedback in the controller. However, in order to validate the engine torque model during dynamic responses, this dynamics is modeled in the validation as a first order system

$$\frac{\mathrm{d}}{\mathrm{dt}}\, M_{e,meas} = \frac{1}{\tau_{Me}}(M_e - M_{e,meas}) \tag{120}$$

where $M_{e,meas}$ is the measured torque and M_e is the output torque from the engine. The time constant τ_{Me} is tuned by adjusting it manually until simulations of the complete model follow the measured torque during steps in fuel injection at 1500 rpm, i.e. the data set I in Tab. 5 which gives a mean absolute relative error of 7.3 % for the engine torque. The result of the tuning is shown in Fig. 19 showing that the model captures the dynamic in the engine torque.

Table 5 *The mean absolute relative errors between diesel engine model simulation and dynamic tuning or validation data that consist of steps in VGT-position, EGR-valve, and fuel injection. The data sets E and I are used for tuning of dynamic models, the data sets A-D and F-I are used for validation of essential system properties and time constants, and all the data sets are used for validation of static models.*

Data set	VGT-EGR steps								u_δ steps
	A	B	C	D	E	F	G	H	I
Speed [rpm]		1200			1500		1900		1500
Load [%]	25	40	50	75	50	25	75	100	-
Number of steps	77	35	2	77	77	77	55	1	7
p_{im}	2.0	1.6	7.2	10.6	6.3	5.0	4.5	4.9	2.9
p_{em}	2.4	4.7	4.9	6.8	5.5	4.5	4.6	4.8	4.7
W_c	3.2	4.7	5.6	10.7	8.0	6.7	6.7	7.4	3.8
n_t	4.4	8.9	4.6	11.9	7.0	6.0	4.1	12.7	3.0
M_e	-	-	-	-	-	-	-	-	7.3

Figure 19 *Comparison between diesel engine model simulation and dynamic tuning data during steps in fuel injection showing that the model captures the dynamic in $M_{e,meas}$. Data set I. Operating point: n_e=1500 rpm, u_{vgt}=26 %, and u_{egr}=19 %.*

8.2   Validation

Due to that the stationary measurements are few, both the static and the dynamic models are validated by simulating the total model and comparing it with the dynamic validation data sets A-I in Tab. 2. The result of this validation can be seen in Tab. 5 that shows that the mean absolute relative errors are 12.7 % or lower. Note that the engine torque is not measured during VGT and EGR steps. The relative errors are due to mostly steady state errors, but since the engine model will be used in a controller the steady state accuracy is less important since a controller will take care of steady state errors. However, in order to design a successful controller, it is important that the model captures the essential dynamic behaviors and nonlinear effects. Therefore, essential system properties and time constants are validated in the following section.
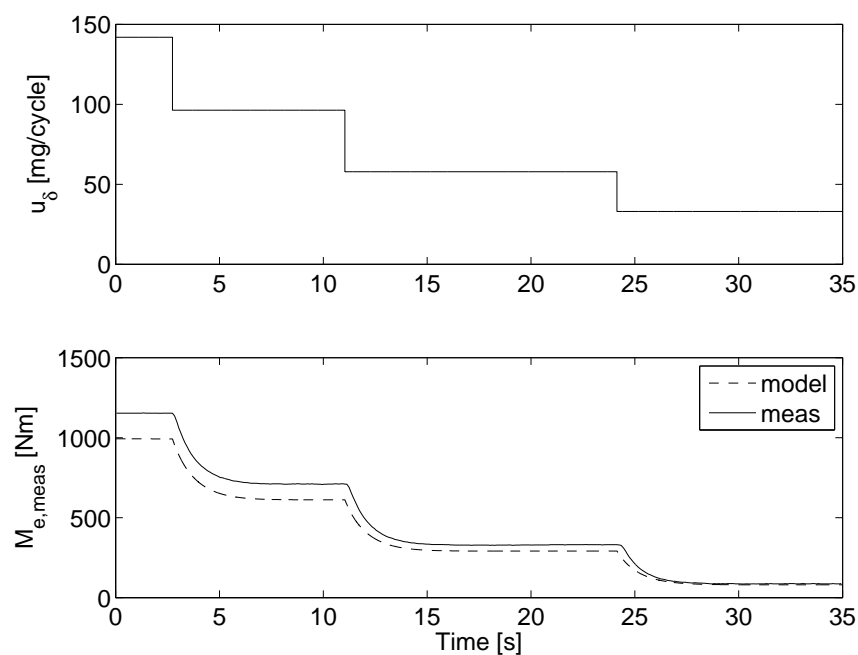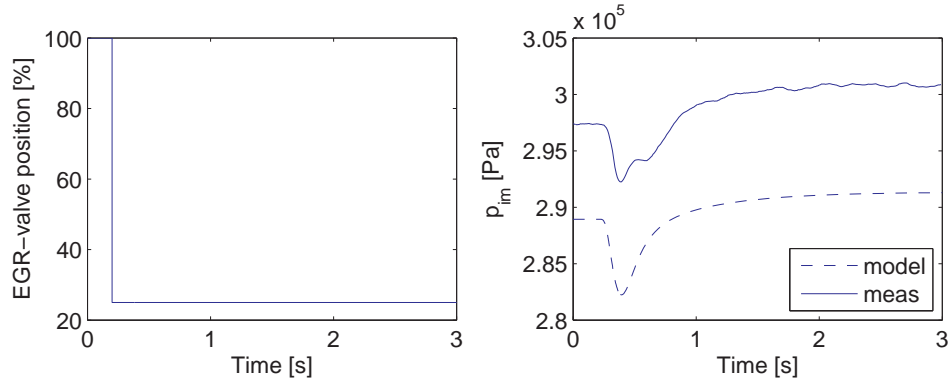
Figure 20 *Comparison between diesel engine model simulation and dynamic validation data during a step in EGR-valve position showing that the model captures the non-minimum phase behavior in p_{im}. Data set H. Operating point: 100 % load, n_e=1900 rpm and u_{vgt}=60 %.*

Validation of essential system properties and time constants

The references [14] and [13] show the essential system properties for the pressures and the flows in a diesel engine with VGT and EGR. Some of these properties are a non-minimum phase behavior in the intake manifold pressure and a non-minimum phase behavior, an overshoot, and a sign reversal in the compressor mass flow. These system properties and time constants are validated using the dynamic validation data sets A-D and F-I in Tab. 5. Three validations are performed in Fig. 20-22. Fig. 20 shows that the model captures the non-minimum phase behavior in the channel u_{egr} to p_{im}. Fig. 21 shows that the model captures the non-minimum phase behavior in the channel u_{vgt} to W_c. Fig. 22 shows that the model captures the overshoot in the channel u_{vgt} to W_c and a small non-minimum phase behavior in the channel u_{vgt} to n_t. Fig. 20 to 22 also show that the model captures the fast dynamics in the beginning of the responses and the slow dynamics in the end of the responses. Further, by comparing Fig. 21 and 22, it can be seen that the model captures the sign reversal in u_{vgt} to W_c. In Fig. 21 the DC-gain is negative and in Fig. 22 the DC-gain is positive.

Figure 21 *Comparison between diesel engine model simulation and dynamic validation data during steps in VGT position showing that the model captures the non-minimum phase behavior in W_c. Data set B. Operating point: 40 % load, n_e=1200 rpm and u_{egr}=100 %.*

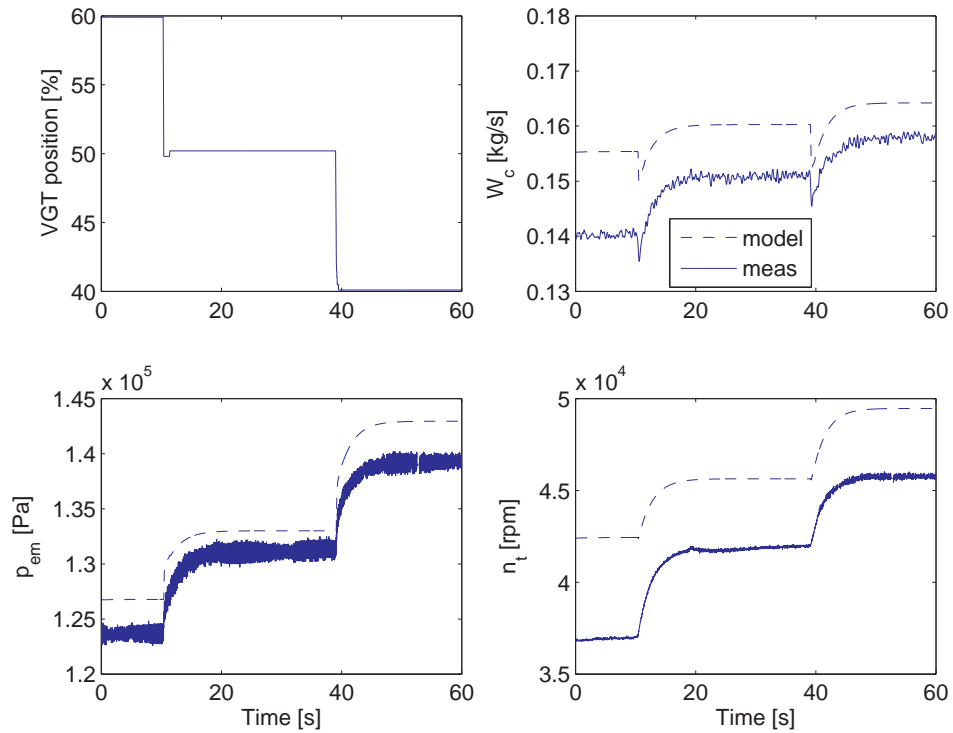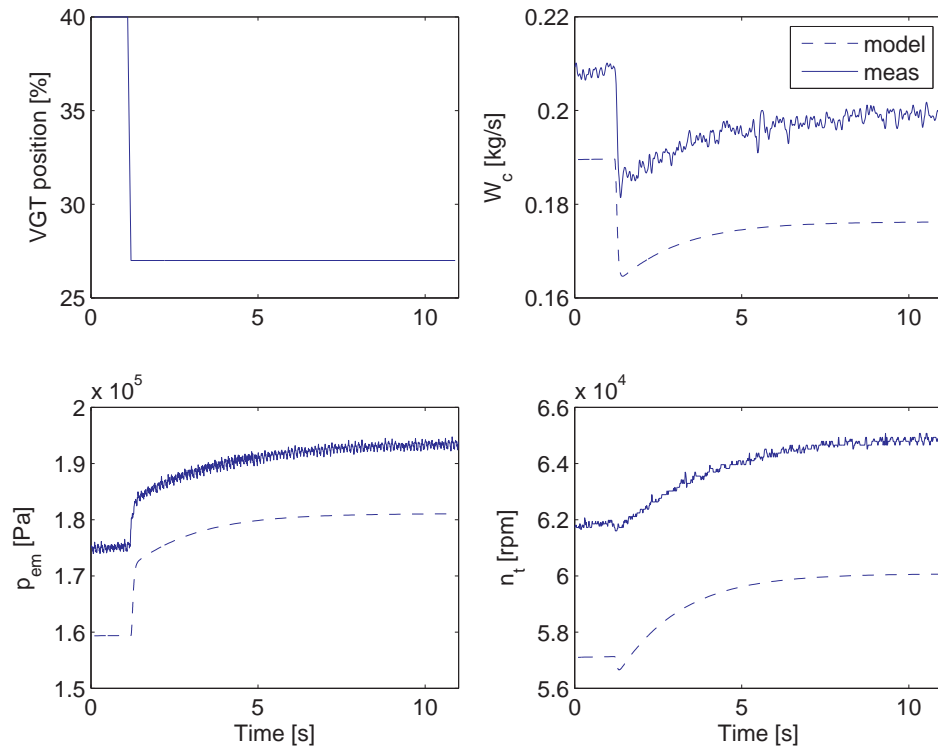**Figure 22** *Comparison between diesel engine model simulation and dynamic validation data during a step in VGT position showing that the model captures the overshoot in W_c and a small non-minimum phase behavior in n_t. A comparison between Fig. 21 and 22 also shows that the model captures the sign reversal in W_c. Data set C. Operating point: 50 % load, n_e=1200 rpm and u_{egr}=100 %.*

9   Model extensions

The proposed model in Sec. 2 to 8 is a small model with 8 states that describes the important dynamics and non-linear system properties according to Sec. 8. In the following sections the goal is to investigate if this model can be improved substantially with model extensions. In Sec. 9.1 the proposed model is extended with temperature states and in Sec. 9.2 the proposed model is extended with temperature states, a pressure drop over the intercooler, and an extra control volume.

9.1   Extensions: temperature states

To investigate if temperature states in the manifolds improve the model substantially, the 8:th order model in Sec. 2 to 6 is extended with two temperature states (T_{im} and T_{em}) which leads to a 10:th order model with the states

$$x = (p_{im} \quad p_{em} \quad T_{im} \quad T_{em} \quad X_{Oim} \quad X_{Oem} \quad \omega_t \quad \tilde{u}_{egr1} \quad \tilde{u}_{egr2} \quad \tilde{u}_{vgt})^\mathsf{T} \quad (121)$$

Extended model equations

The intake and exhaust manifold models in Sec. 2 are extended with temperatures states T_{im} and T_{em} according to the adiabatic model [4, 10]

$$\frac{d}{dt} T_{im} = \frac{R_a\, T_{im}}{p_{im}\, V_{im}\, c_{va}}\cdot$$
$$(c_{va}(W_{ic} + W_{egr})(T_{im,in} - T_{im}) + R_a(T_{im,in}(W_{ic} + W_{egr}) - T_{im}\, W_{ei})) \quad (122)$$
$$\frac{d}{dt} p_{im} = \frac{R_a\, T_{im}}{V_{im}} (W_{ic} + W_{egr} - W_{ei}) + \frac{p_{im}}{T_{im}} \frac{d}{dt} T_{im}$$

$$\frac{d}{dt} T_{em} = \frac{R_e\, T_{em}}{p_{em}\, V_{em}\, c_{ve}}\cdot$$
$$(c_{ve}\, W_{eo}(T_{em,in} - T_{em}) + R_e(T_{em,in}\, W_{eo} - T_{em}(W_t + W_{egr}))) \quad (123)$$
$$\frac{d}{dt} p_{em} = \frac{R_e\, T_{em}}{V_{em}} (W_{eo} - W_t - W_{egr}) + \frac{p_{em}}{T_{em}} \frac{d}{dt} T_{em}$$

where the temperature $T_{im,in}$ for the flows into the intake manifold is assumed to be constant and the temperature $T_{em,in}$ for the flow into the exhaust manifold is equal to T_{em} in (24). The intercooler is assumed to be ideal, i.e.

$$W_{ic} = W_c \quad (124)$$

The differential equations for the oxygen mass fractions are the same as in Sec. 2 if (124) is applied to

$$\frac{d}{dt} X_{Oim} = \frac{R_a\, T_{im}}{p_{im}\, V_{im}} ((X_{Oem} - X_{Oim})\, W_{egr} + (X_{Oc} - X_{Oim})\, W_{ic})$$
$$\frac{d}{dt} X_{Oem} = \frac{R_e\, T_{em}}{p_{em}\, V_{em}} (X_{Oe} - X_{Oem})\, W_{eo} \quad (125)$$

The values of all the tuning parameters are the same as for the 8:th order model.

Figure 23 *Comparison between 8:th and 10:th order model during a step in EGR-valve position showing that these two models have approximately the same dynamic response with a non-minimum phase behavior in p_{im}. Operating point: $u_\delta = 110$ mg/cycle, $n_e = 1500$ rpm, and $u_{vgt} = 30$ %.*

Comparison between 8:th and 10:th order model

To investigate how the states T_{im} and T_{em} affect the system properties, step responses are compared for the 8:th and 10:th order model. Fig. 23 to Fig. 25 show that the two models have approximately the same dynamic response with approximately the same non-minimum phase behavior in p_{im} and approximately the same non-minimum phase behavior, overshoot, and sign reversal in W_c. Consequently, the temperature states only have minor effects on the system properties and therefore there are no major improvements of the model if it is extended with temperature states.

9.2   Extensions: temperature states and pressure drop over intercooler

To investigate if additional temperature states and a pressure drop over the intercooler improve the model substantially, the 10:th order model in Sec. 9.1 is extended with a control volume between the compressor and the intercooler. This control volume consists of a temperature state T_{ic} and a pressure state p_c. This leads to a 12:th order model with the states

$$x = (p_{im} \quad p_{em} \quad p_c \quad T_{im} \quad T_{em} \quad T_{ic} \quad X_{Oim} \quad X_{Oem} \quad \omega_t \quad \tilde{u}_{egr1} \quad \tilde{u}_{egr2} \quad \tilde{u}_{vgt})^\mathsf{T}$$
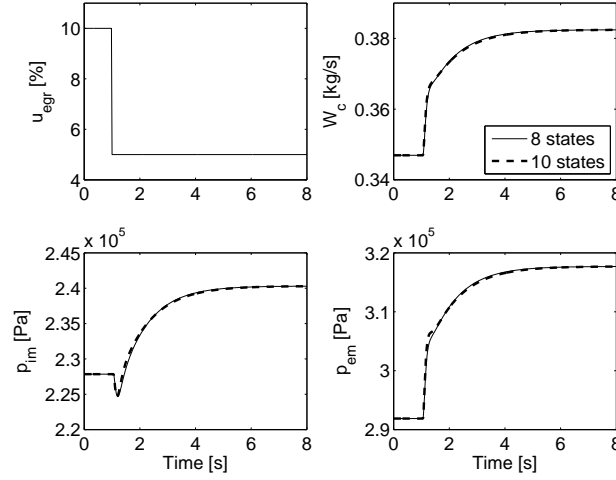$$(126)$$

Figure 24 *Comparison between 8:th and 10:th order model during a step in VGT position showing that these two models have approximately the same dynamic response with a non-minimum phase behavior in W_c. Operating point:* $u_\delta = 110$ *mg/cycle,* $n_e = 1500$ *rpm, and* $u_{egr} = 80$ %.
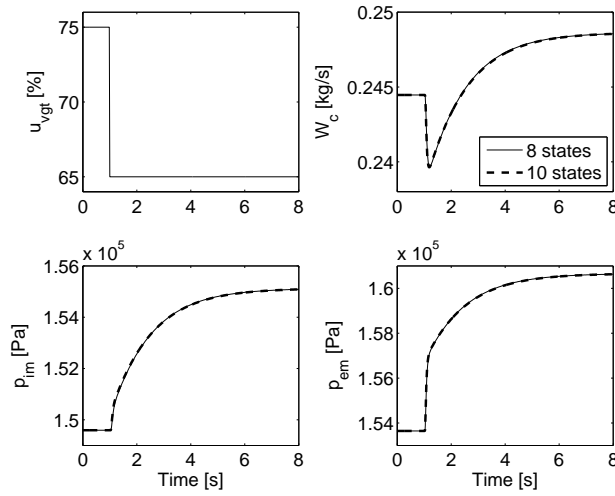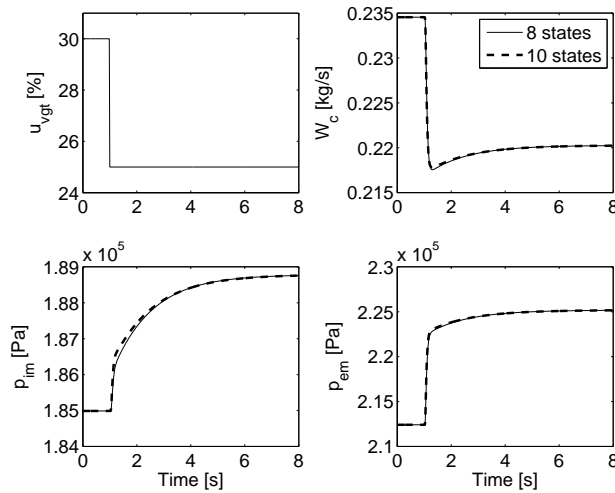

Figure 25 *Comparison between 8:th and 10:th order model during a step in VGT position showing that these two models have approximately the same dynamic response with an overshoot and a sign reversal in W_c. Operating point:* $u_\delta = 110$ *mg/cycle,* $n_e = 1500$ *rpm, and* $u_{egr} = 80$ %.

Extended model equations

The control volume before the intercooler is modeled as an adiabatic model with a temperature state T_{ic} and a pressure state p_c

$$
\begin{aligned}
\frac{d}{dt}\, T_{ic} &= \frac{R_a\, T_{ic}}{p_c\, V_{ic}\, c_{va}} \left(c_{va}\, W_c (T_c - T_{ic}) + R_a (T_c\, W_c - T_{ic}\, W_{ic}) \right) \\
\frac{d}{dt}\, p_c &= \frac{R_a\, T_{ic}}{V_{ic}} \left(W_c - W_{ic} \right) + \frac{p_c}{T_{ic}} \frac{d}{dt}\, T_{ic}
\end{aligned}
\tag{127}
$$

where V_{ic} is the volume of the control volume and it is set to a reasonable value. The flow W_{ic} through the intercooler is modeled as an incompressible flow [20, 8]

$$
W_{ic} = \sqrt{\frac{p_c (p_c - p_{im})}{T_{ic}\, k_{ic}}}
\tag{128}
$$

Equation (128) is used instead of (124) and the pressure quotient over the compressor

$$
\Pi_c = \frac{p_c}{p_{amb}}
\tag{129}
$$

is used instead of (58).

Tuning parameters

- k_{ic}: parameter for the model in (128)

- V_{im}: intake manifold volume

- η_{cmax}, W_{copt}, π_{copt}, c_π, a_1, a_2, and a_3: parameters for the compressor efficiency

- $c_{\Psi 2}$, $c_{\Phi 2}$, $c_{\omega\Psi 1}$, $c_{\omega\Psi 2}$, $c_{\omega\Psi 3}$, $c_{\omega\Phi 1}$, $c_{\omega\Phi 2}$, and $c_{\omega\Phi 3}$: parameters for the compressor flow

Tuning

The tuning parameter k_{ic} is determined by solving a linear least-squares problem that minimizes $(p_c - p_{im} - (p_{c,meas} - p_{im,meas}))^2$ with k_{ic} as the optimization variable. The model of $p_c - p_{im}$ is obtained by solving (128) for $p_c - p_{im}$. The variables $p_{c,meas}$ and $p_{im,meas}$ are stationary measurements.

The intake manifold volume V_{im} is re-tuned according to the method in Sec. 8.1 due to that the extended dynamics in the intercooler affects the dynamics in the intake manifold.

The tuning parameters for the compressor efficiency and the compressor flow are re-tuned using the method in Sec. 5.3 with the new definition of the pressure quotient (129).

The values of all the other tuning parameters are the same as for the 8:th order model.

Figure 26 *Comparison between 8:th and 12:th order model during a step in EGR-valve position showing that there are stationary differences. However, the dynamic behavior are approximately the same with a non-minimum phase behavior in p_{im}. Operating point: $u_\delta = 110$ mg/cycle, $n_e = 1500$ rpm, and $u_{vgt} = 30$ %.*

Comparison between 8:th and 12:th order model

To investigate how the additional temperature states, control volume before the intercooler, and pressure drop over the intercooler affect the system properties, step responses are compared for the 8:th and 12:th order model. Fig. 26 and Fig. 27 show that there are stationary differences between the two models. However, the dynamic behavior are qualitatively the same considering the amplitudes, the time constants, and the non-minimum phase behaviors in p_{im} and W_c. In Fig. 28 there are differences in both stationary conditions and in dynamic behavior, e.g. the 12:th order model gives a non-minimum phase behavior and a positive DC-gain in p_{im} while the 8:th order model gives a response without a non-minimum phase behavior and with a negative DC-gain in p_{im}. However, by simulating the same step in an adjacent operating point, see Fig. 29, the dynamic behavior are approximately the same for the two models with a non-minimum phase behavior in p_{im} and an overshoot in p_{em}. Consequently, the two models have approximately the same dynamic behavior except that the two models change their dynamic behavior at different but adjacent operating points. Therefore, the conclusion is that temperature states, a pressure drop over the intercooler, and a control volume before the intercooler have only small effects on the dynamic behavior but the addition of the pressure drop has an effect on the stationary values.
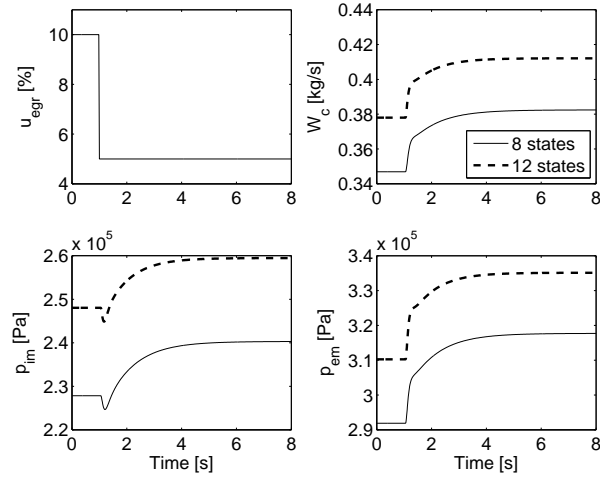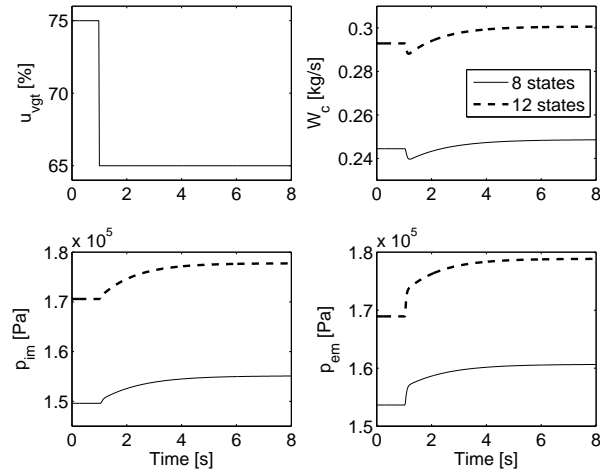
Figure 27 *Comparison between 8:th and 12:th order model during a step in VGT position showing that there are stationary differences. However, the dynamic behavior are approximately the same with a non-minimum phase behavior in W_c. Operating point: $u_\delta = 110$ mg/cycle, $n_e = 1500$ rpm, and $u_{egr} = 80$ %.*
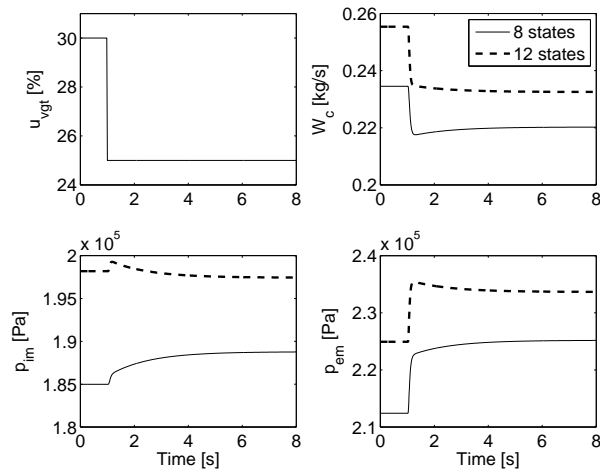
Figure 28 *Comparison between 8:th and 12:th order model during a step in VGT position showing that there are differences in both stationary conditions and in dynamic behavior. Operating point: $u_\delta = 110$ mg/cycle, $n_e = 1500$ rpm, and $u_{egr} = 80$ %.*
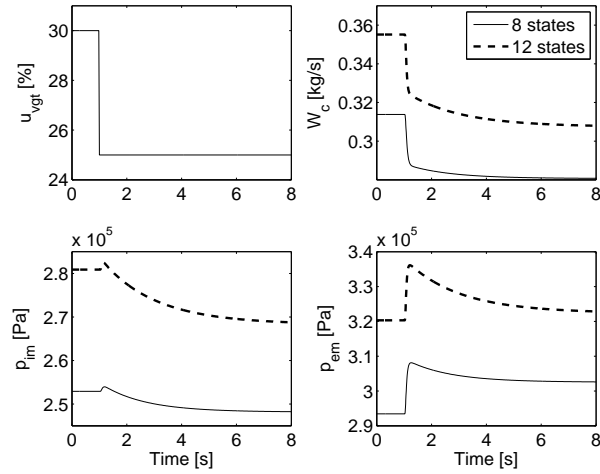
Figure 29 *Comparison between 8:th and 12:th order model during a step in VGT position at an adjoining operating point compared to Fig. 28 showing that the two models have approximately the same dynamic response with a non-minimum phase behavior in p_{im} and an overshoot in p_{em}. Operating point: $u_\delta = 180$ mg/cycle, $n_e = 1500$ rpm, and $u_{egr} = 80$ %.*

Comparison between experimental data and 12:th order model

The previous section shows that there are stationary differences between the 8:th and 12:th order model. In this section, the goal is to investigate if these stationary differences improve the validation results in Sec. 8.2.

The 12:th order model is validated by calculating the mean absolute relative errors between 12:th order model and dynamic tuning or validation data, see Tab. 6. These mean absolute relative errors are calculated in the same way as for the 8:th order model in Tab. 5. Comparing these two tables, the 12:th order model gives larger mean absolute relative errors in almost all operating points and for almost all signals. There are only 6 of 37 errors that are lower. Consequently, the inclusion of temperature states, a pressure drop over the intercooler, and a control volume before the intercooler did not improve the model quality on the validation data.

Table 6 *The mean absolute relative errors between diesel engine model of the 12:th order and dynamic tuning or validation data that consist of steps in VGT-position, EGR-valve, and fuel injection. These mean absolute relative errors are calculated in the same way as the mean absolute relative errors for the 8:th order model in Tab. 5. Comparing Tab. 5 and 6, the 12:th order model gives larger mean absolute relative errors for 31 of 37 errors.*

	VGT-EGR steps								u_δ steps
Data set	A	B	C	D	E	F	G	H	I
Speed [rpm]		1200			1500		1900		1500
Load [%]	25	40	50	75	50	25	75	100	-
Number of steps	77	35	2	77	77	77	55	1	7
p_{im}	5.0	6.6	5.1	12.2	9.7	10.3	11.6	4.5	9.6
p_{em}	3.7	9.6	2.0	7.6	7.1	6.7	9.6	5.2	9.1
W_c	4.3	13.0	7.3	12.0	14.2	17.8	18.5	7.8	11.7
n_t	6.4	14.8	4.3	12.3	8.1	8.6	6.1	9.0	6.3
M_e	-	-	-	-	-	-	-	-	7.2

10   Conclusions

A mean value model of a diesel engine with VGT and EGR was developed and validated. The intended applications of the model are system analysis, simulation, and development of model-based control systems. The goal is to construct a model that describes the dynamics in the manifold pressures, turbocharger, EGR, and actuators with few states in order to have short simulation times. Therefore the model has only eight states: intake and exhaust manifold pressures, oxygen mass fraction in the intake and exhaust manifold, turbocharger speed, and three states describing the actuator dynamics. Many models in the literature, that approximately have the same complexity as the model proposed here, use three states for each control volume in order to describe the temperature dynamics. However, the model proposed here uses only two states for each manifold. Model extensions are investigated showing that inclusion of temperature states and pressure drop over the intercooler only has minor effects on the dynamic behavior and does not improve the model quality. Therefore, these extensions are not included in the proposed model.

Model equations and tuning methods for the parameters were described for each subsystem in the model. In order to have a low number of tuning parameters, flows and efficiencies are modeled using physical relationships and parametric models instead of look-up tables. The parameters in the static models are tuned automatically using least squares optimization and stationary measurements in 82 different operating points. The parameters in the dynamic models are tuned by adjusting these parameters manually until simulations of the complete model follow the dynamic responses in the dynamic measurements.

Static and dynamic validations of the entire model were performed using dynamic measurements, consisting of steps in fuel injection, EGR control signal, and VGT control signal. The validations show that the mean relative errors are 12.7 % or lower for all measured variables. They also show that the proposed model captures the essential system properties, i.e. a non-minimum phase behavior in the channel u_{egr} to p_{im} and a non-minimum phase behavior, an overshoot, and a sign reversal in the channel u_{vgt} to W_c.

References

[1] M. Ammann, N.P. Fekete, L. Guzzella, and A.H. Glattfelder. Model-based Control of the VGT and EGR in a Turbocharged Common-Rail Diesel Engine: Theory and Passenger Car Implementation. *SAE Technical paper 2003-01-0357*, January 2003.

[2] Per Andersson. *Air Charge Estimation in Turbocharged Spark Ignition Engines*. PhD thesis, Linköpings Universitet, December 2005.

[3] Å. Björk. *Numerical Methods for Least Squares Problems*. SIAM, 1996.

[4] Alain Chevalier, Martin Müeller, and Elbert Hendricks. On the validity of mean value engine models during transient operation. *SAE Technical paper 2000-01-1261*, 2000.

[5] S.L. Dixon. *Fluid Mechanics and Thermodynamics of Turbomachinery*. Butterworth Heinemann, Woburn, 4:th edition, 1998.

[6] Lars Eriksson. Mean value models for exhaust system temperatures. *SAE 2002 Transactions, Journal of Engines, 2002-01-0374*, 111(3), September 2002.

[7] Lars Eriksson. Modeling and control of turbocharged SI and DI engines. *Oil & Gas Science and Technology - Rev. IFP*, 62(4):523–538, 2007.

[8] Lars Eriksson, Lars Nielsen, Jan Brugård, Johan Bergström, Fredrik Pettersson, and Per Andersson. Modeling and simulation of a turbo charged SI engine. *Annual Reviews in Control*, 26(1):129–137, October 2002.

[9] L. Guzzella and A. Amstutz. Control of diesel engines. *IEEE Control Systems Magazine*, 18:53–71, 1998.

[10] Elbert Hendricks. Isothermal vs. adiabatic mean value SI engine models. In *IFAC Workshop: Advances in Automotive Control*, 2001.

[11] J.B. Heywood. *Internal Combustion Engine Fundamentals*. McGraw-Hill Book Co, 1988.

[12] M. Jankovic, M. Jankovic, and I.V. Kolmanovsky. Constructive lyapunov control design for turbocharged diesel engines. *IEEE Transactions on Control Systems Technology*, 2000.

[13] M. Jung. *Mean-Value Modelling and Robust Control of the Airpath of a Turbocharged Diesel Engine*. PhD thesis, University of Cambridge, 2003.

[14] I.V. Kolmanovsky, A.G. Stefanopoulou, P.E. Moraal, and M. van Nieuwstadt. Issues in modeling and control of intake flow in variable geometry turbocharged engines. In *Proceedings of 18th IFIP Conference on System Modeling and Optimization*, Detroit, July 1997.

[15] M.J. Nieuwstadt, I.V. Kolmanovsky, P.E. Moraal, A.G. Stefanopoulou, and M. Jankovic. EGR–VGT control schemes: Experimental comparison for a high-speed diesel engine. *IEEE Control Systems Magazine*, 2000.

[16] R. Rajamani. Control of a variable-geometry turbocharged and wastegated diesel engine. *Proceedings of the I MECH E Part D Journal of Automobile Engineering*, November 2005.

[17] P. Skogtjärn. Modelling of the exhaust gas temperature for diesel engines. Master's thesis LiTH-ISY-EX-3379, Department of Electrical Engineering, Linköping University, Linköping, Sweden, December 2002.

[18] A.G. Stefanopoulou, I.V. Kolmanovsky, and J.S. Freudenberg. Control of variable geometry turbocharged diesel engines for reduced emissions. *IEEE Transactions on Control Systems Technology*, 8(4), July 2000.

[19] C. Vigild. *The Internal Combustion Engine Modelling, Estimation and Control Issues*. PhD thesis, Technical University of Denmark, Lyngby, 2001.

[20] N. Watson and M.S. Janota. *Turbocharging the Internal Combustion Engine*. The Mechanical Press Ltd, Hong Kong, 1982.

A Notation

Table 7 Symbols used in the report

Symbol	Description	Unit
A	Area	m^2
BSR	Blade speed ratio	—
c_p	Spec. heat capacity, constant pressure	$J/(kg \cdot K)$
c_v	Spec. heat capacity, constant volume	$J/(kg \cdot K)$
J	Inertia	$kg \cdot m^2$
M	Torque	Nm
M_e	Engine torque	Nm
M_p	Pumping torque	Nm
n_{cyl}	Number of cylinders	—
n_e	Rotational engine speed	rpm
n_t	Rotational turbine speed	rpm
$(O/F)_s$	Stoichiometric oxygen-fuel ratio	—
p	Pressure	Pa
P	Power	W
q_{HV}	Heating value of fuel	J/kg
r_c	Compression ratio	—
R	Gas constant	$J/(kg \cdot K)$
R	Radius	m
T	Temperature	K
u_{egr}	EGR control signal. 100 - open, 0 - closed	$\%$
u_{vgt}	VGT control signal. 100 - open, 0 - closed	$\%$
u_δ	Injected amount of fuel	$mg/cycle$
V	Volume	m^3
W	Mass flow	kg/s
x_{egr}	EGR fraction	—
X_O	Oxygen mass fraction	—
γ	Specific heat capacity ratio	—
η	Efficiency	—
λ_O	Oxygen-fuel ratio	—
Π	Pressure quotient	—
ρ	Density	kg/m^3
τ	Time constant	s
Φ_c	Volumetric flow coefficient	—
Ψ_c	Energy transfer coefficient	—
ω	Rotational speed	rad/s

Table 8 *Indices used in the report*

Index	Description
a	air
amb	ambient
c	compressor
d	displaced
e	exhaust
egr	EGR
ei	engine cylinder in
em	exhaust manifold
eo	engine cylinder out
f	fuel
fric	friction
ig	indicated gross
im	intake manifold
m	mechanical
t	turbine
tc	turbocharger
vgt	VGT
vol	volumetric
δ	fuel injection

Table 9 *Abbreviations used in the report*

Abbreviation	Description
EGR	Exhaust gas recirculation
VGT	Variable geometry turbocharger

System analysis of a Diesel Engine with VGT and EGR[1]

Johan Wahlström, Lars Eriksson, and Lars Nielsen

Vehicular Systems, Department of Electrical Engineering,
Linköping University, S-581 83 Linköping,
Sweden.

Abstract

A system analysis of a diesel engine with VGT and EGR is performed in order to obtain insight into a VGT and EGR control problem where the goal is to control the performance variables oxygen fuel ratio λ_O and EGR-fraction x_{egr} using the VGT actuator u_{vgt} and the EGR actuator u_{egr}. Step responses over the entire operating region show that the channels $u_{vgt} \to \lambda_O$, $u_{egr} \to \lambda_O$, and $u_{vgt} \to x_{egr}$ have non-minimum phase behaviors and sign reversals. The fundamental physical explanation of these system properties is that the system consists of two dynamic effects that interact: a fast pressure dynamics in the manifolds and a slow turbocharger dynamics. It is shown that the engine frequently operates in operating points where the non-minimum phase behaviors and sign reversals occur for the channels $u_{vgt} \to \lambda_O$ and $u_{vgt} \to x_{egr}$, and consequently, it is important to consider these properties in a control design. Further, an analysis of zeros for linearized multiple input multiple output models of the engine shows that they are non-minimum phase over the complete operating region. A mapping of the performance variables λ_O and x_{egr} and the relative gain array show that the system from u_{egr} and u_{vgt} to λ_O and x_{egr} is strongly coupled in a large operating region. It is also illustrated that the pumping losses $p_{em} - p_{im}$ decrease with increasing EGR-valve and VGT opening for almost the complete operating region.

---

[1]This report is also available from Department of Electrical Engineering, Linköping University, S-581 83 Linköping. Technical Report Number: LiTH-R-2881

1   Introduction

Legislated emission limits for heavy duty trucks are constantly reduced. To fulfill the requirements, technologies like Exhaust Gas Recirculation (EGR) systems and Variable Geometry Turbochargers (VGT) have been introduced. The primary emission reduction mechanisms utilized to control the emissions are that NO_x can be reduced by increasing the intake manifold EGR-fraction x_{egr} and smoke can be reduced by increasing the oxygen/fuel ratio λ_O [1]. Therefore, it is natural to choose x_{egr} and λ_O as the main performance variables. However x_{egr} and λ_O depend in complicated ways on the EGR and VGT actuation, and it is therefore necessary to have coordinated control of the EGR and VGT to reach the legislated emission limits in NO_x and smoke. When developing a controller for this system, it is desirable to perform an analysis of the characteristics and the behavior of the system in order to obtain insight into the control problem. This is known to be important for a successful design of an EGR and VGT controller due to non-trivial intrinsic properties, see for example [3]. Therefore, the goal is to make a system analysis of the diesel engine model in Sec. 2. The essential system properties for this model are physically explained in Sec. 3 by looking at step responses. In Sec. 4 a mapping of these system properties is performed by simulating step responses over the entire operating region and by analyzing zeros for linearized models. This is done for the main performance variables oxygen/fuel ratio, λ_O, and EGR-fraction, x_{egr}. Further, λ_O and x_{egr} are mapped in Sec. 5 in order to investigate the interactions in the system. Also, the pumping work is mapped in Sec. 5 to give insight into how the pumping losses can be minimized.

2   Diesel engine model

A model for a heavy duty diesel engine is used in the system analysis in this report. This diesel engine model is focused on the gas flows, see Fig. 1, and it is a mean value model with eight states: intake and exhaust manifold pressures (p_{im} and p_{em}), oxygen mass fraction in the intake and exhaust manifold (X_{Oim} and X_{Oem}), turbocharger speed (ω_t), and three states describing the actuator dynamics for the two control signals ($\tilde{u}_{egr1}$, $\tilde{u}_{egr2}$, and $\tilde{u}_{vgt}$). These states are collected in a state vector x

$$x = [p_{im} \quad p_{em} \quad X_{Oim} \quad X_{Oem} \quad \omega_t \quad \tilde{u}_{egr1} \quad \tilde{u}_{egr2} \quad \tilde{u}_{vgt}]^\mathsf{T}$$

There are no state equations for the manifold temperatures, since the pressures and the turbocharger speed govern the most important system properties, such as non-minimum phase behaviors, overshoots, and sign reversals, while the temperature states have only minor effects on these system properties [7].

The resulting model is expressed in state space form as
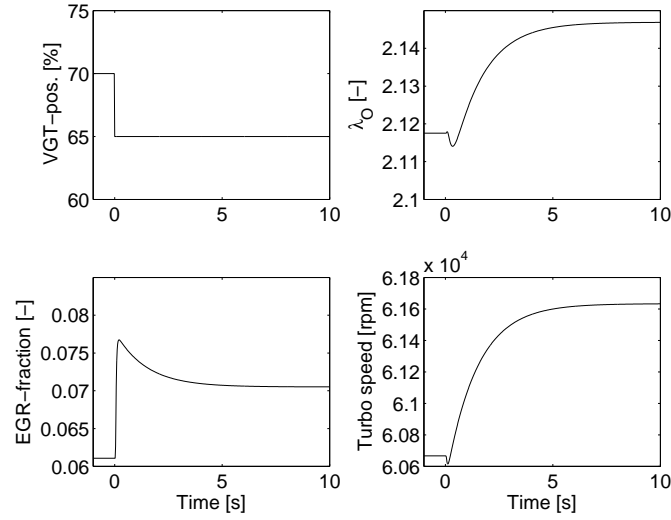
$$\dot{x} = f(x, u, n_e)$$

Figure 1 *Sketch of the diesel engine model used for the system analysis. It has five states related to the engine (p_{im}, p_{em}, X_{Oim}, X_{Oem}, and ω_t) and three for actuator dynamics ($\tilde{u}_{egr1}$, $\tilde{u}_{egr2}$, and $\tilde{u}_{vgt}$).*

where the engine speed n_e is considered as an input to the model, and u is the control input vector

$$u = [u_\delta \quad u_{egr} \quad u_{vgt}]^\mathsf{T}$$

which contains mass of injected fuel u_δ, EGR-valve position u_{egr}, and VGT actuator position u_{vgt}.

A detailed description and derivation of the model together with a model tuning and a validation against test cell measurements is given in [7]. The validation shows that the model captures the essential system properties that exist in the diesel engine, i.e. non-minimum phase behaviors, overshoots, and sign reversals. The references [3], [2], and [4] also show that the diesel engine has these system properties.

3 Physical intuition for system properties

As mentioned in Sec. 2, the diesel engine has non-minimum phase behaviors, overshoots, and sign reversals. The fundamental physical explanation of these system properties is that the system consists of two dynamic effects that interact: a fast pressure dynamics in the manifolds and a slow turbocharger dynamics. These two

Figure 2 *Responses to a step in VGT position showing non-minimum phase behaviors in λ_O and in the turbo speed. Operating point: u_δ=110 mg/cycle, n_e=1500 rpm and u_{egr}=80 %. Initial u_{vgt}=70 %.*

dynamic effects often work against each other which results in the system properties above. For example, if the fast dynamic effect is small and the slow dynamic effect is large, the result will be a non-minimum phase behavior, see λ_O in Fig. 2. Note that the DC-gain is negative. However, if the fast dynamic effect is large and the slow dynamic effect is small, the result will be an overshoot and a sign reversal, see λ_O in Fig. 3. The precise conditions for this sign reversal are due to complex interactions between flows, temperatures, and pressures in the entire engine. More physical explanations of the system properties for VGT position and EGR-valve responses are found in the following sections.

3.1   Physical intuition for VGT position response

Model responses to steps in VGT position are shown in Fig. 2 and 3. In Fig. 2 a closing of the VGT leads to an increase in exhaust manifold pressure and therefore an increase in EGR-fraction which leads to a decrease in intake manifold oxygen mass fraction and a decrease in λ_O in the beginning of the step. However, an increase in exhaust manifold pressure thereafter leads to an increase in turbocharger speed and thus compressor mass flow. The result is an increase in λ_O and in this case the increase is larger than the initial decrease. The increase in λ_O is slower due to the slower dynamics of the turbocharger speed, which means that VGT position to λ_O has a non-minimum phase behavior. There is also a non-minimum phase behavior in the turbocharger speed response. The non-minimum phase behavior
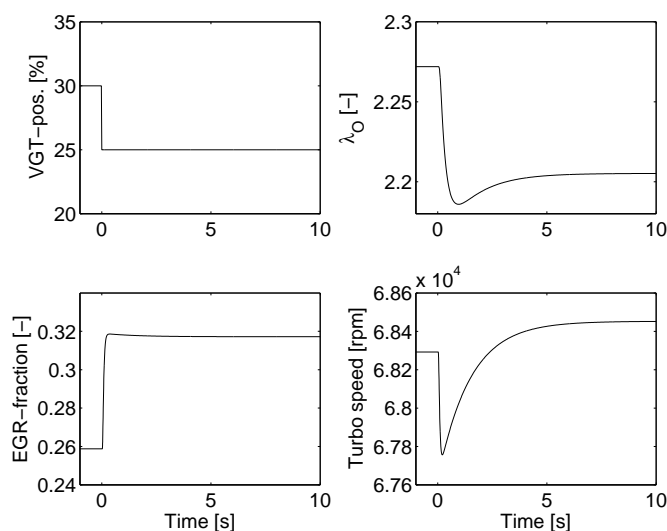
Figure 3 *Responses to a step in VGT position showing a sign reversal in* λ_O *compared to Fig. 2. Operating point:* u_δ=*110 mg/cycle,* n_e=*1500 rpm and* u_{egr}=*80 %. Initial* u_{vgt}=*30 %.*

in λ_O increases with increasing EGR-valve opening and decreasing VGT opening until the sign of the DC-gain is reversed and the non-minimum phase behavior becomes an overshoot instead. The sign reversal can be seen in Fig. 3, where the size of the step is the same but the initial VGT position is more closed compared to Fig. 2. Contrary to Fig. 2, Fig. 3 shows that a closing of the VGT position leads to a total decrease in λ_O. Further, the non-minimum phase behavior in the turbocharger speed response in Fig. 3 is larger than in Fig. 2.

3.2   Physical intuition for EGR-valve response

Model responses to steps in the EGR-valve are shown in Fig. 4 and 5. In Fig. 4, λ_O has a non-minimum phase behavior which has the following physical explanation. The closing of the EGR-valve leads to an immediate decrease in EGR-fraction, yielding an immediate decrease in p_{im} and increase in p_{em}. However, closing the EGR-valve also means that less exhaust gases are recirculated and there are thus more exhaust gases to drive the turbine. This causes the turbocharger to speed up and produce more compressor flow which results in a subsequent increase in p_{im} that is larger than the initial decrease. This effect is slower though due to the slower dynamics of the turbocharger speed, which gives that EGR-valve to p_{im} has a non-minimum phase behavior. Since p_{im} affects the total flow into the engine and thereby λ_O, there is also a non-minimum phase behavior in λ_O. Note that the DC-gain from EGR-valve to λ_O is negative in Fig. 4. The non-minimum phase
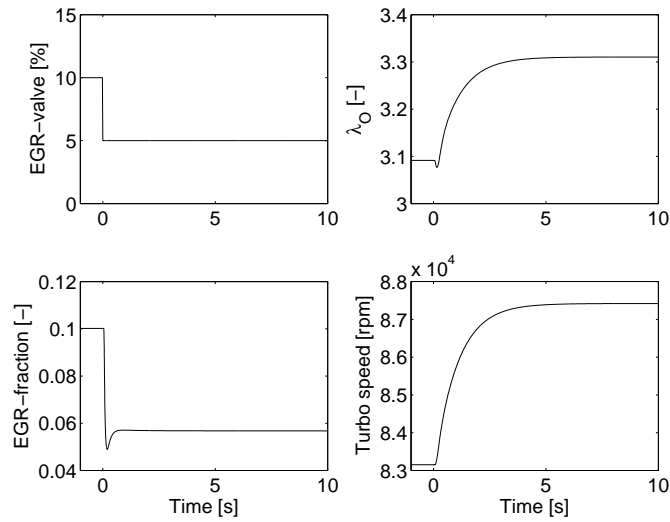
Figure 4 *Responses to a step in EGR-valve showing a non-minimum phase behavior in λ_O. Operating point: u_δ=110 mg/cycle, n_e=1500 rpm and u_{vgt}=30 %.*
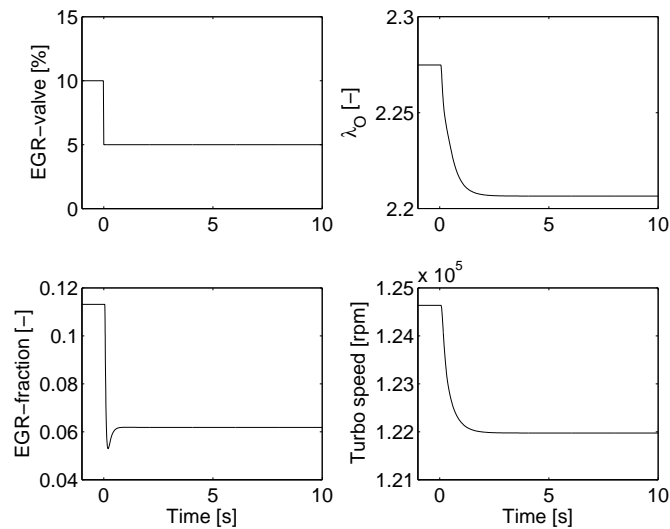

Figure 5 *Responses to a step in EGR-valve showing sign reversals in λ_O and in the turbo speed compared to Fig. 4. Operating point: u_δ=230 mg/cycle, n_e=2000 rpm and u_{vgt}=30 %.*

behavior increases with decreasing EGR-valve opening and increasing engine speed until the sign of the DC-gain is reversed. The sign reversal can be seen in Fig. 5, where the step in EGR-valve is performed in an operating point with higher torque and higher engine speed compared to Fig. 4. In contrast to Fig. 4, Fig. 5 shows that a closing of the EGR-valve leads to a total decrease in λ_O and in n_t.

4 Mapping of system properties

The step responses in Sec. 3 show that there are non-minimum phase behaviors and sign reversals in the main performance variables λ_O and x_{egr}. Knowledge about these system properties and response times in the entire operating region is important when developing a control structure. Therefore, the DC-gain K, the non-minimum phase behavior with an relative undershoot x_N, and the response time τ are mapped by simulating step responses in the entire operating region. The DC-gain K is defined as

$$K = \frac{y_2 - y_0}{\Delta u} \qquad (1)$$

where y_0 is the initial value and y_2 is the final value of a step response according to Fig. 6 where the input has a step size Δu. The relative undershoot x_N is defined as

$$x_N = \frac{y_0 - y_1}{y_2 - y_1} \qquad (2)$$

where y_1 is the minimum value of the step response in Fig. 6. The response time τ is defined in Fig. 6, i.e

$$\tau = \{t : y(t) = 0.63(y_2 - y_0) + y_0\} \qquad (3)$$

For a first order system with time delay, the response time according to this definition would be the sum of the time constant and the time delay.

The mapping of the system properties is based on step responses simulated at 20 different u_{vgt} points, 20 different u_{egr} points, 3 different n_e points, and 3 different u_δ points. The sizes of the steps in u_{vgt} and u_{egr} are 5% of the difference between two adjoining operating points. Sec. 4.1 presents the results regarding the DC-gains (1). Non-minimum phase zeros for linearized multiple input multiple output (MIMO) models of the engine are analyzed in Sec. 4.2 in order to determine the non-minimum-phase characteristics of these models. A root locus for one operating point is presented in Sec. 4.2 in order to illustrate the poles for the closed loop system. Non-minimum phase behaviors with the relative undershoots (2) are mapped in Sec. 4.3. In addition to a mapping of the system properties over the operating region for the engine, a mapping of the operating points where the engine frequently operates is performed in Sec. 4.4. This is performed by simulating the European Transient Cycle and calculating the relative frequency for different sub-regions. Finally, the response times (3) are mapped in Sec. 4.5.
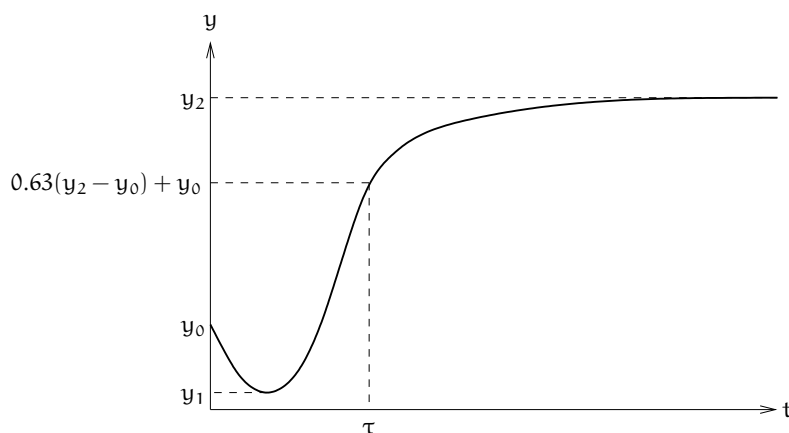
Figure 6 *A step response with an initial value y_0, a final value y_2, a non-minimum phase behavior with an undershoot y_1, and a response time τ.*

4.1   DC-gains

A sign reversal in a channel causes problems when controlling the corresponding feedback loop. These sign reversals are investigated by mapping the DC-gain, K, for the channels $u_{vgt} \rightarrow \lambda_O$, $u_{egr} \rightarrow \lambda_O$, $u_{vgt} \rightarrow x_{egr}$, and $u_{egr} \rightarrow x_{egr}$ in Fig. 7 to 10. The channels $u_{vgt} \rightarrow \lambda_O$, $u_{egr} \rightarrow \lambda_O$, and $u_{vgt} \rightarrow x_{egr}$ have negative DC-gain in large operating regions and reversed sign (positive sign) in small operating regions, while $u_{egr} \rightarrow x_{egr}$ has positive DC-gain in the entire operating region.

The DC-gain for the channel $u_{vgt} \rightarrow \lambda_O$ (see Fig. 7) has reversed sign (positive sign) in operating points with closed to half open VGT, half to fully open EGR-valve, low to medium n_e, and medium to large u_δ or in operating points with half to fully open VGT, low n_e, and small u_δ. The left bottom plot shows that for almost all EGR-valve positions the sign is reversed twice when the VGT goes from closed to fully open. Further, the DC-gain for the channel $u_{egr} \rightarrow \lambda_O$ (see Fig. 8) has reversed sign (positive sign) in a smaller operating region, compared to $u_{vgt} \rightarrow \lambda_O$, which is in operating points with closed to half open EGR-valve, high n_e, and medium to large u_δ. Finally, the DC-gain for the channel $u_{vgt} \rightarrow x_{egr}$ (see Fig. 9) also has reversed sign (positive sign) in a smaller operating region, compared to $u_{vgt} \rightarrow \lambda_O$, which is in operating points with half to fully open VGT, half to fully open EGR-valve, low to medium n_e, and small u_δ.

The DC-gains for all four channels (Fig. 7 to 10) are equal to zero also in some other operating points than where sign reversal occurs. The DC-gains for the channels $u_{egr} \rightarrow \lambda_O$, $u_{vgt} \rightarrow x_{egr}$, and $u_{egr} \rightarrow x_{egr}$ are equal to zero in operating points with half to fully open VGT, low to medium n_e and medium to large u_δ. In these operating points $p_{em} < p_{im}$ (see Fig. 18) which leads to that $x_{egr} = 0$ since no backflow is modeled in the EGR-flow model. As a consequence,

the control signal u_{egr} cannot influence the system and the control signal u_{vgt} cannot influence the EGR-fraction. The DC-gain for the channels $u_{egr} \rightarrow \lambda_O$ and $u_{egr} \rightarrow x_{egr}$ are also equal to zero when $u_{egr} = 80$ % and the DC-gain for the channel $u_{vgt} \rightarrow x_{egr}$ is also equal to zero when $u_{egr} = 0$ %.

The mapping of the DC-gains shows that the DC-gains vary much between different operating points in all four channels. A common trend is that the DC-gains for the channels $u_{vgt} \rightarrow \lambda_O$ and $u_{vgt} \rightarrow x_{egr}$ are large when the VGT is closed and small when the VGT is open. Similarly, the DC-gains for the channels $u_{egr} \rightarrow \lambda_O$ and $u_{egr} \rightarrow x_{egr}$ are large when the EGR-valve is closed and small when the EGR-valve is open.
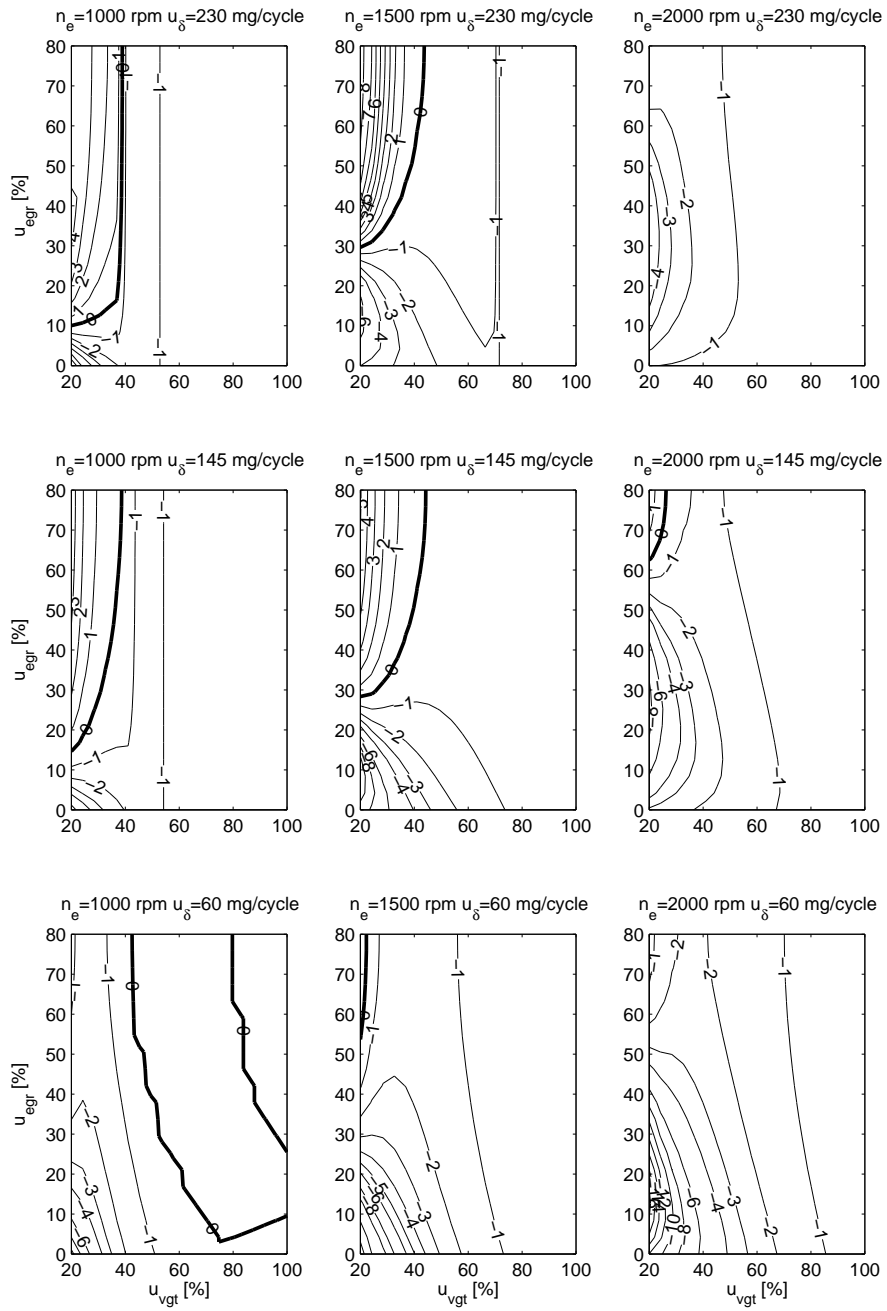
Figure 7 *Contour plots of the DC-gain, $100 \cdot K$, for the channel $u_{vgt} \to \lambda_O$ at 3 different n_e and 3 different u_δ. The DC-gain has a sign reversal that occurs at the thick line.*
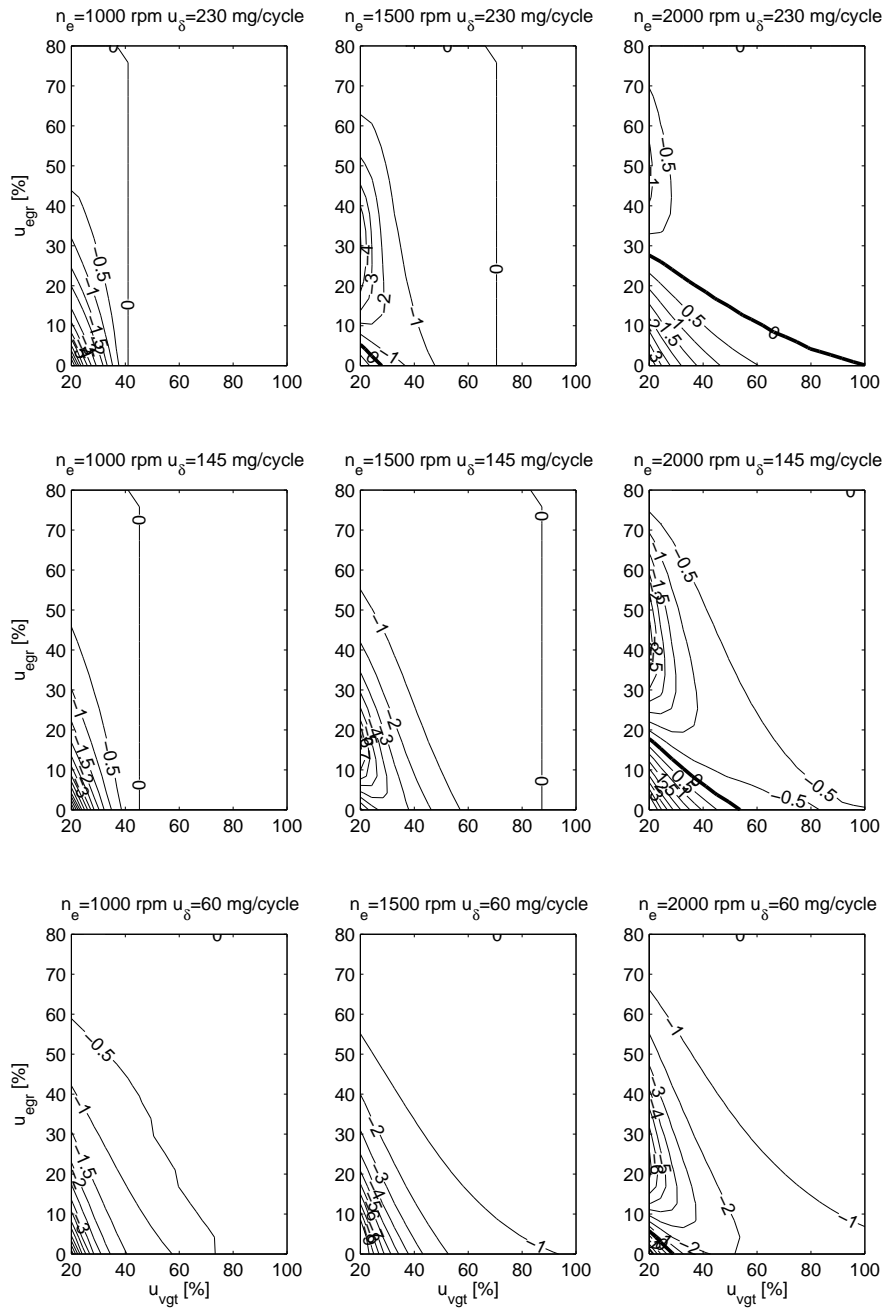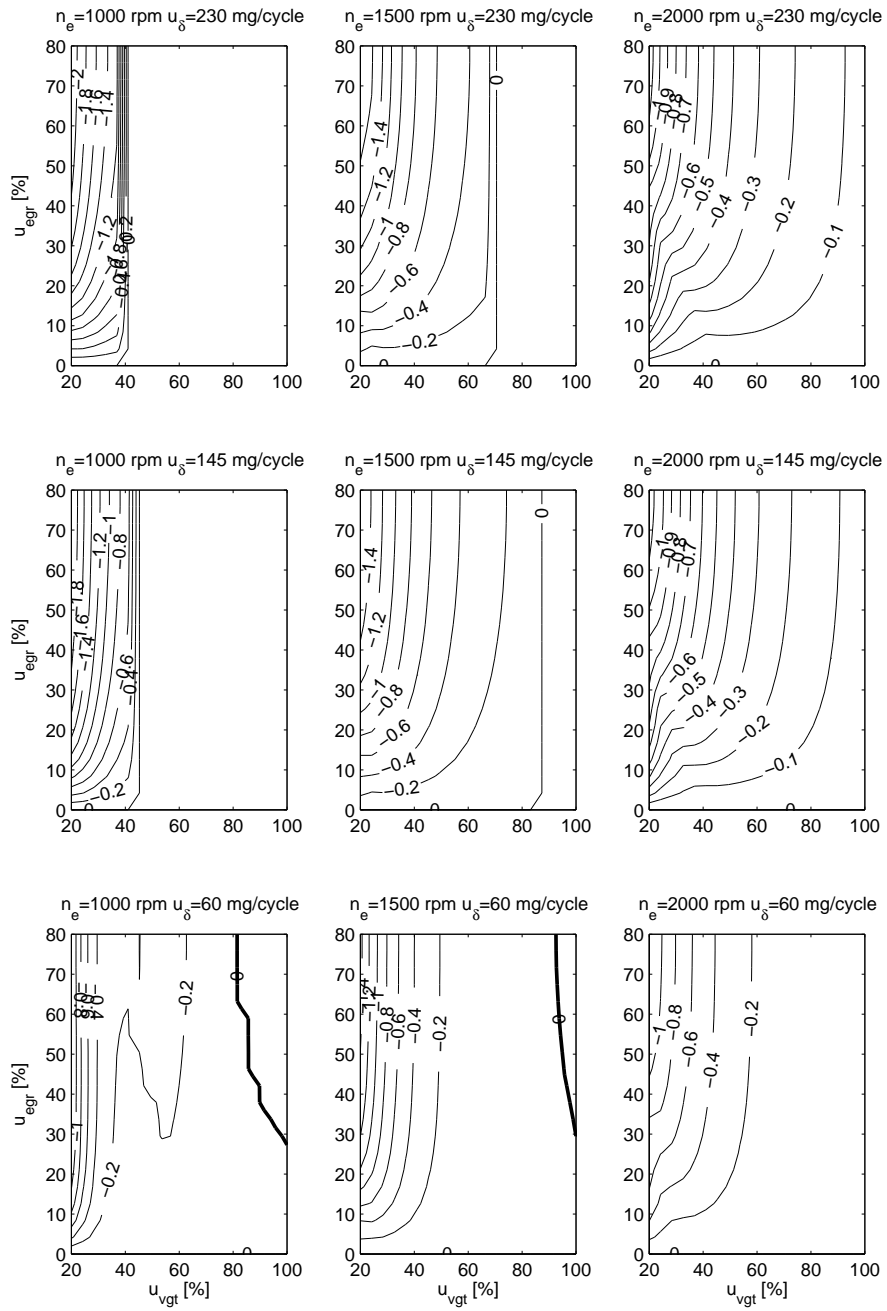
Figure 8 *Contour plots of the DC-gain, $100 \cdot K$, for the channel $u_{egr} \to \lambda_O$ at 3 different n_e and 3 different u_δ. The DC-gain has a sign reversal that occurs at the thick line.*

Figure 9 *Contour plots of the DC-gain, $100 \cdot K$, for the channel $u_{vgt} \to x_{egr}$ at 3 different n_e and 3 different u_δ. The DC-gain has a sign reversal that occurs at the thick line.*
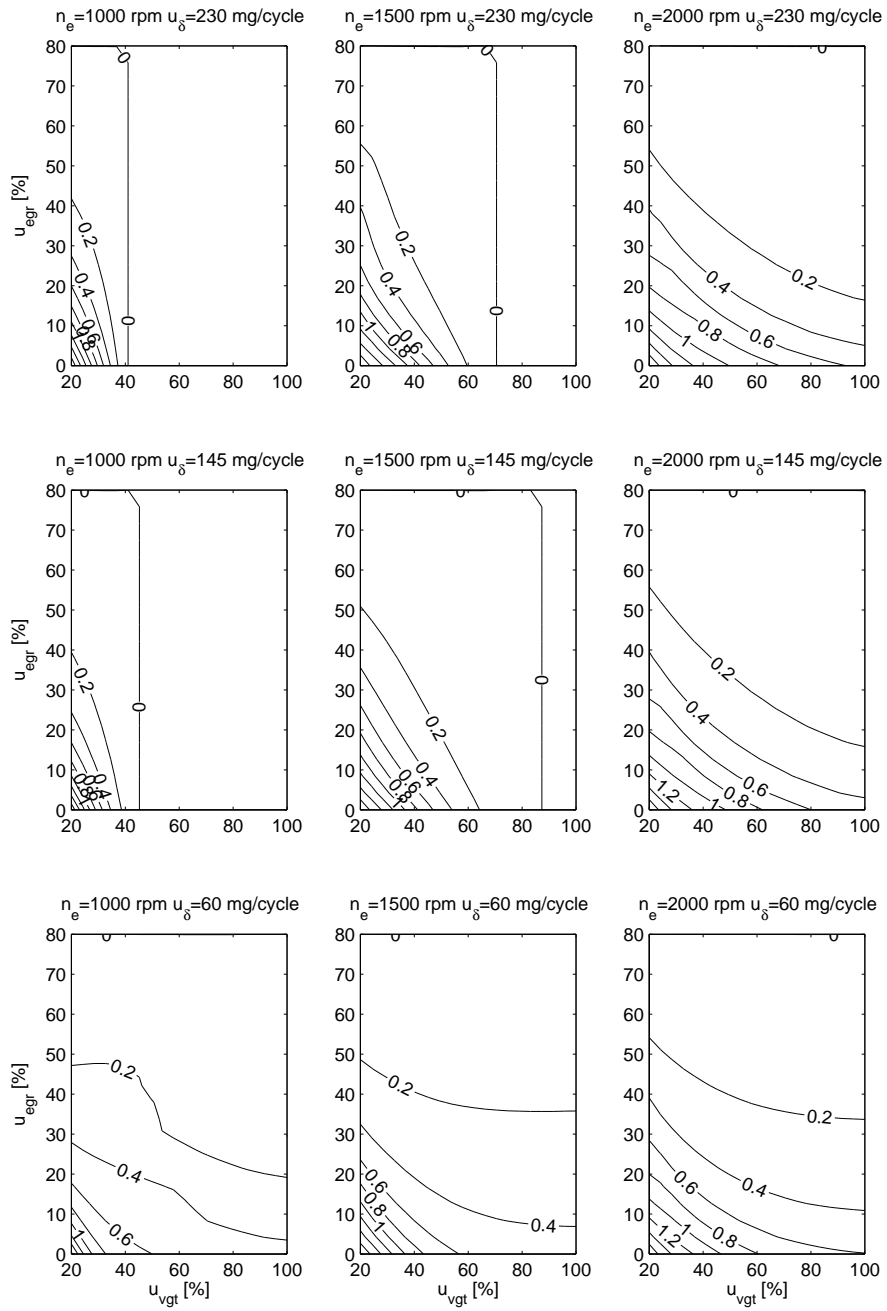
Figure 10 *Contour plots of the DC-gain, $100 \cdot K$, for the channel $u_{egr} \rightarrow x_{egr}$ at 3 different n_e and 3 different u_δ. The DC-gain is positive and also equal to zero in some operating points.*

4.2   Zeros and a root locus

A mapping of zeros for linearized MIMO models of the engine over the entire operating region is performed in order to determine the non-minimum-phase characteristics of these models. The linear models are constructed by linearizing the non-linear model in Sec. 2 in the same operating points as the operating points in Fig. 7 to 10, i.e. 20 different u_{vgt} points, 20 different u_{egr} points, 3 different n_e points, and 3 different u_δ points. The linear models have the form

$$\dot{x} = A_i\, x + B_i\, u$$
$$y = C_i\, x \qquad\qquad (4)$$

where i is the operating point number and

$$u = [u_{egr} \quad u_{vgt}]^{\mathsf{T}}$$
$$x = [p_{im} \quad p_{em} \quad X_{Oim} \quad X_{Oem} \quad \omega_t \quad \tilde{u}_{egr1} \quad \tilde{u}_{egr2} \quad \tilde{u}_{vgt}]^{\mathsf{T}}$$
$$y = [\lambda_O \quad x_{egr}]^{\mathsf{T}}$$

An analysis of the poles and zeros for the models (4) shows that there are 8 poles in the left complex half plane for the complete operating region, one zero in the right complex half plane for the complete operating region, 3 zeros in the left complex half plane when $p_{em} > p_{im}$, and 2 zeros in the left complex half plane when $p_{em} < p_{im}$. In this latter case the EGR-valve is closed. The value of the zero in the right complex half plane is mapped in Fig. 11 showing that this zero is positive for the complete operating region. Consequently, the linear diesel engine models (4) are non-minimum phase in the complete operating region.

A root locus for the model (4) in one operating point where $p_{em} > p_{im}$ is presented in Fig. 12. This root locus is based on the feedback

$$u = k \left(\begin{array}{cc} \frac{1}{K_{u_{egr} \to \lambda_O}} & 0 \\ 0 & \frac{1}{K_{u_{vgt} \to x_{egr}}} \end{array} \right) (r - y) \qquad\qquad (5)$$

where the signal r is the set-point for the output y and the choice of feedback loops is motivated in [5]. The constants $K_{u_{egr} \to \lambda_O}$ and $K_{u_{vgt} \to x_{egr}}$ are the DC-gains for the channels $u_{egr} \to \lambda_O$ and $u_{vgt} \to x_{egr}$ in the operating point $n_e = 1500$ rpm, $u_\delta = 145$ mg/cycle, $u_{egr} = 16.8$ %, and $u_{vgt} = 36.8$ %, and k is a scalar parameter. The root locus in Fig. 12 shows the closed-loop pole trajectories as function of the parameter k. These trajectories have 4 asymptotes due to that the difference between the number of poles and the number of zeros for the open-loop system is 4. Two closed-loop poles become unstable for large k and two poles in the left complex half plane have large imaginary parts for large k, i.e. these poles gives oscillations with low damping. Root loci for other operating points (where $p_{em} > p_{im}$) have approximately the same behavior. Root loci for operating points where $p_{em} < p_{im}$ are not investigated since $x_{egr} = 0$ in these operating points and u_{egr} can not influence the system which leads to that other control modes have to be used in these operating points.
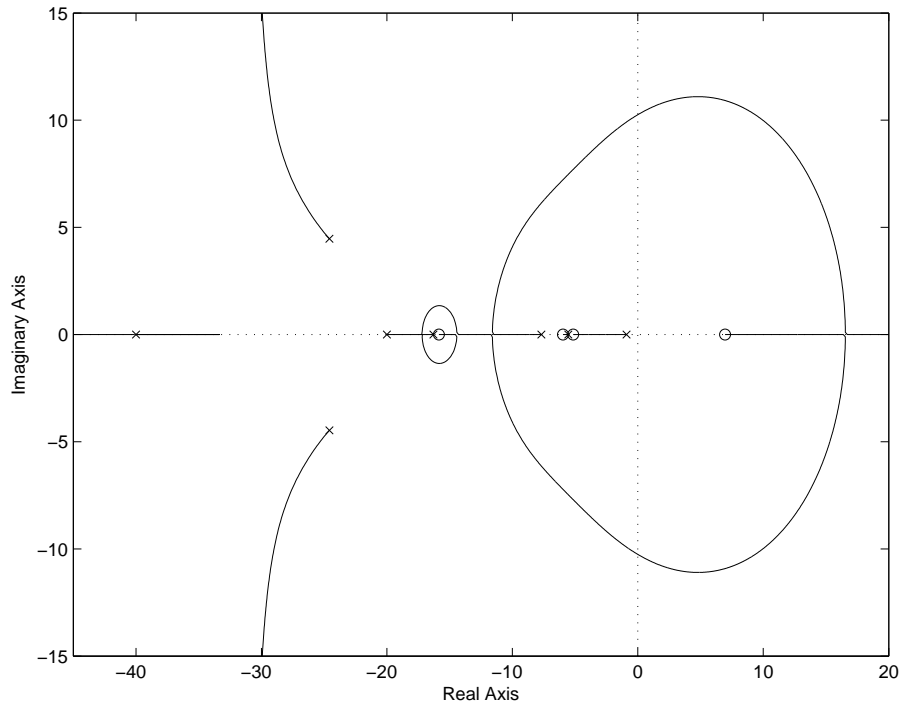
Figure 11 *Contour plots of the zero that exists in the right complex half plane showing that this zero is positive for the complete operating region.*

Figure 12 *A pole-zero map and a root locus for the model* (4) *in the operating point* $n_e = 1500$ *rpm,* $u_\delta = 145$ *mg/cycle,* $u_{egr} = 16.8$ *%, and* $u_{vgt} = 36.8$ *%. The crosses are the poles and the circles are the zeros for the model* (4). *The root locus shows the closed-loop pole trajectories as function of the scalar parameter* k *in the feedback* (5). *The trajectories start at the crosses (poles) with* $k = 0$ *and ends at the circles (zeros) or along 4 asymptotes with* $k = +\infty$.

4.3   Non-minimum phase behaviors

In the previous section, it is shown that the linearized MIMO diesel engine models (4) have a zero in the right half plane and are therefore non-minimum phase. In this section, the size of the undershoot in a non-minimum phase behavior is investigated by mapping the relative undershoot x_N, defined by (2), over the entire operating region. This is performed for the channels $u_{vgt} \to \lambda_O$, $u_{egr} \to \lambda_O$, and $u_{vgt} \to x_{egr}$ in Fig. 13 to 15, but not for the channel $u_{egr} \to x_{egr}$ as it has no non-minimum phase behavior.

By comparing Fig. 7 with Fig. 13 and comparing Fig. 8 with Fig. 14 it can be seen that the non-minimum phase behaviors in the channels $u_{vgt} \to \lambda_O$ and $u_{egr} \to \lambda_O$ only occur in operating points with negative DC-gain. Further, the relative undershoots are 40 to 100 % only in operating points near the sign reversal for these two channels. Consequently, the relative undershoot for the channel $u_{egr} \to \lambda_O$ is larger than 40 % in a smaller operating region compared to $u_{vgt} \to \lambda_O$ since the sign reversal for $u_{egr} \to \lambda_O$ occurs in a smaller operating region. In the operating points with reversed sign (positive sign) the non-minimum phase behavior becomes an overshoot instead (see also Fig. 2 and Fig. 3 where the non-minimum phase behavior in λ_O becomes an overshoot).

By comparing Fig. 9 with Fig. 15 it can be seen that the non-minimum phase behavior in $u_{vgt} \to x_{egr}$ occurs only in a small operating region with reversed sign (positive sign) for the DC-gain where the relative undershoots are 40 to 100 %. In the operating points with negative DC-gain the non-minimum phase behavior becomes an overshoot instead.
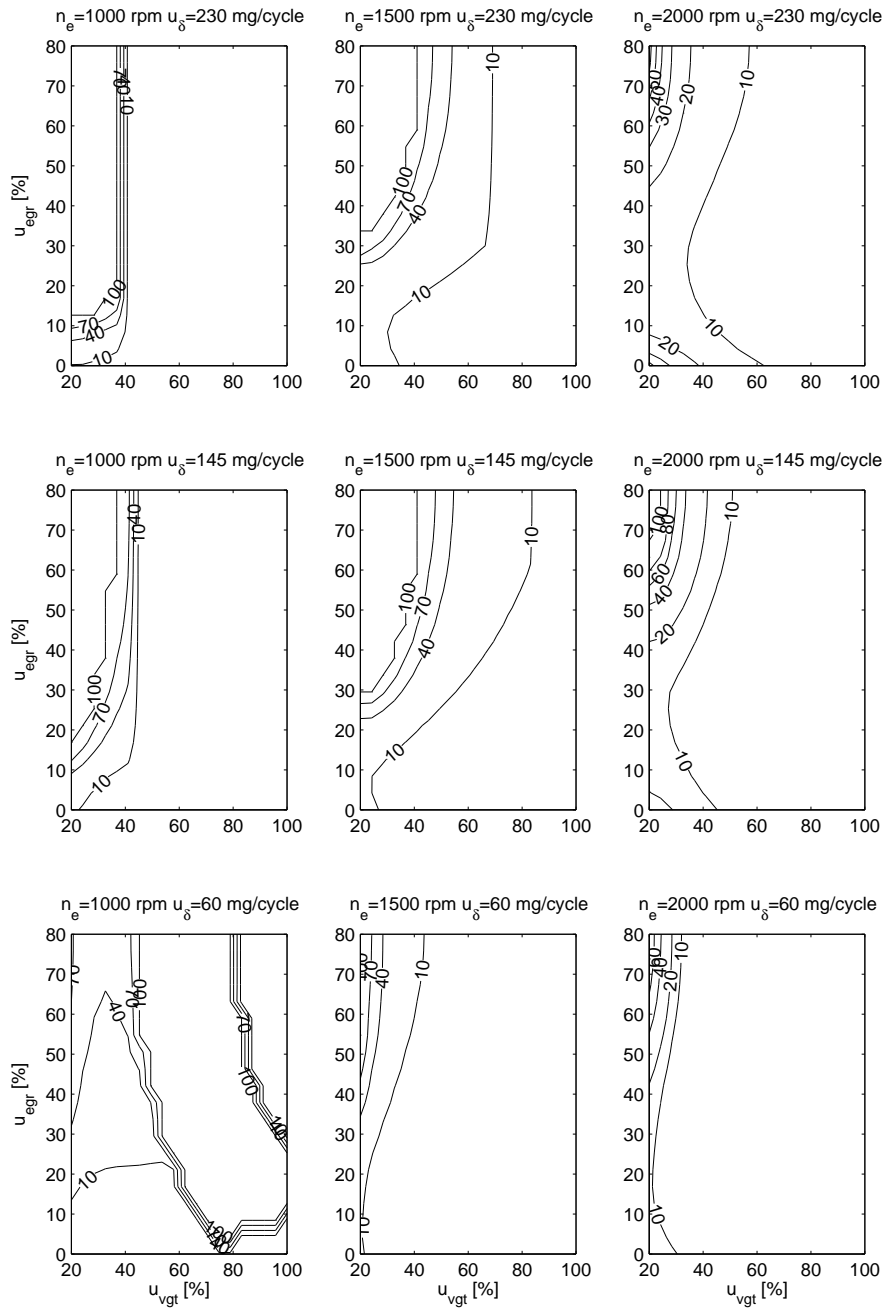
Figure 13 *Contour plots of the relative undershoot, x_N [%], (see Eq. (2)) in a non-minimum phase behavior for the channel $u_{vgt} \rightarrow \lambda_O$ at 3 different n_e and 3 different u_δ.*

Figure 14 *Contour plots of the relative undershoot, x_N [%], (see Eq. (2)) in a non-minimum phase behavior for the channel $u_{egr} \to \lambda_O$ at 3 different n_e and 3 different u_δ.*
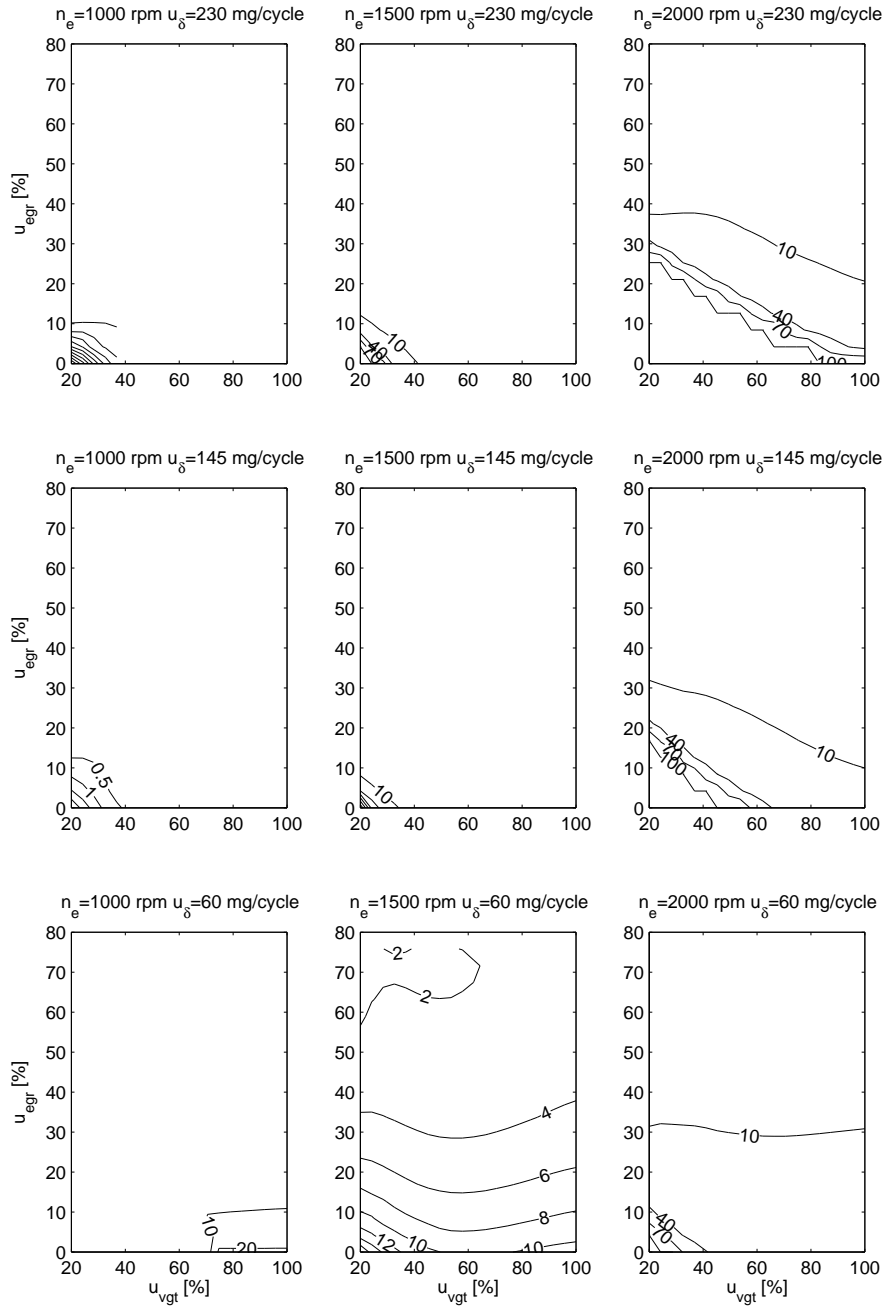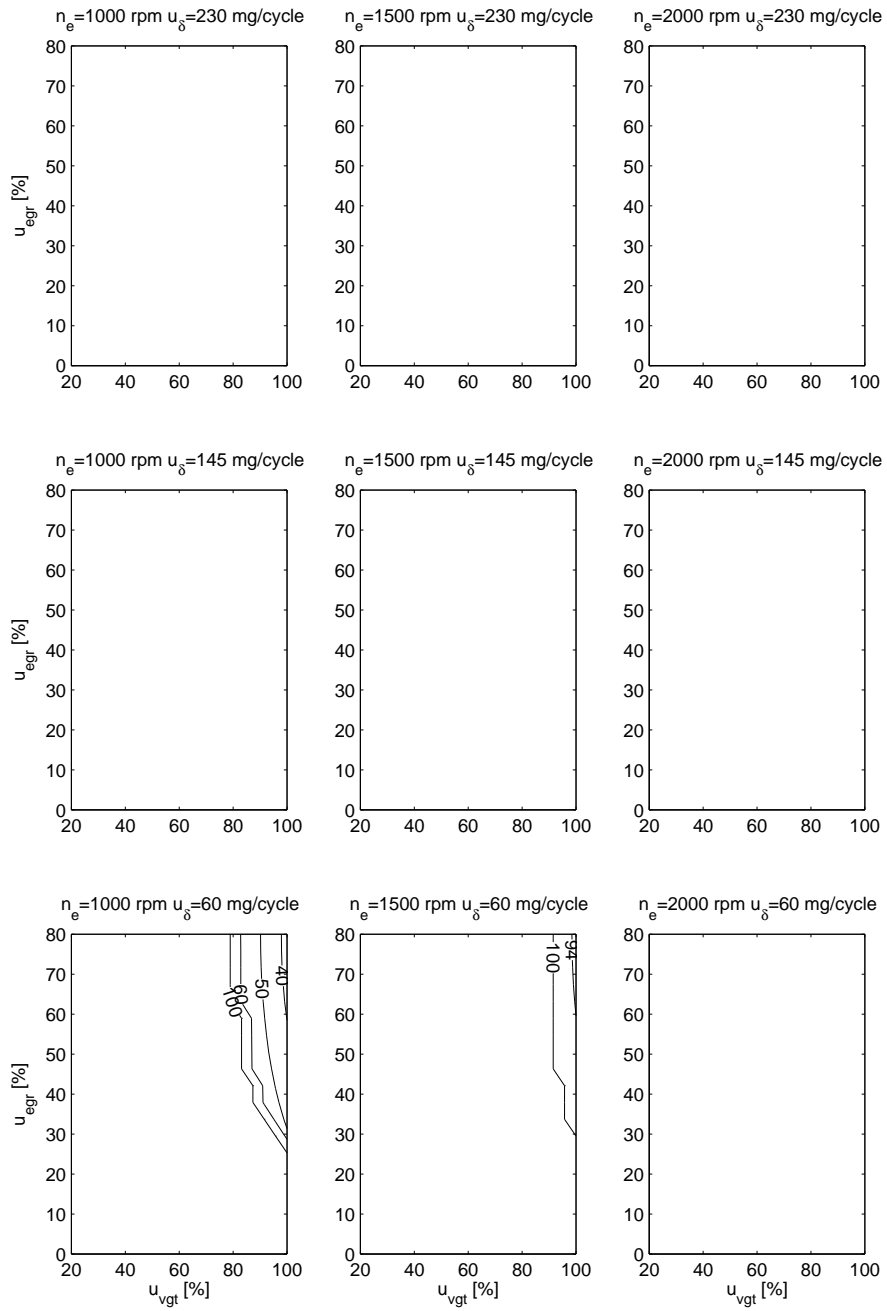
Figure 15 *Contour plots of the relative undershoot, x_N [%], (see Eq. (2)) in a non-minimum phase behavior for the channel $u_{vgt} \rightarrow x_{egr}$ at 3 different n_e and 3 different u_δ.*

4.4   Operation pattern for the European Transient Cycle

A mapping of the operating points where the engine frequently operates is important in order to understand what system properties in the sections above that should be considered in the control design. This mapping is performed by simulating the complete control system in [5] during the European Transient Cycle. The control parameters are tuned using the method in [6] and the weighting factors $\gamma_{Me} = 1$ and $\gamma_{egr} = 1$. In Fig. 16, this simulation is plotted by first sampling the signals n_e, u_δ, u_{vgt}, and u_{egr} with a frequency of 10 Hz, and then dividing these simulated points into 9 different operating regions by selecting the nearest operating region to each simulated point. These operating regions correspond to the 9 different plots in Fig. 16 where each plot has u_{egr} on the y-axis and u_{vgt} on the x-axis, i.e. exactly as the contour plots in the previous sections. The percentage of simulated points in each operating region is also shown in the plots. Further, the lines where the sign reversals occur for the channels $u_{vgt} \to \lambda_O$, $u_{egr} \to \lambda_O$, and $u_{vgt} \to x_{egr}$ are shown in the plots.

   Comparing Fig. 16 with Fig. 13 to 15, the conclusion is that the engine frequently operates in operating points where the sign reversal and the non-minimum phase occur for the channels $u_{vgt} \to \lambda_O$ and $u_{vgt} \to x_{egr}$, and that the engine does not frequently operate in operating points where the sign reversal and the non-minimum phase occur for $u_{egr} \to \lambda_O$. Consequently, it is important to consider the sign reversal and the non-minimum phase for $u_{vgt} \to \lambda_O$ and $u_{vgt} \to x_{egr}$ in a control design. The engine does not operate at $n_e > 1750$ rpm since the European Transient Cycle only consists of n_e that are lower than 1750 rpm.

4.5   Response time

The response time τ for the channels $u_{vgt} \to \lambda_O$, $u_{egr} \to \lambda_O$, $u_{vgt} \to x_{egr}$, and $u_{egr} \to x_{egr}$, respectively, are mapped over the entire operating region using the definition in Fig. 6. The result is presented in Appendix A, while the minimum, mean, and maximum value for each τ are shown in Tab. 1.

   The variations of τ for the channels $u_{vgt} \to \lambda_O$, $u_{egr} \to \lambda_O$, and $u_{vgt} \to x_{egr}$ are larger compared to τ for the channel $u_{egr} \to x_{egr}$. This is because the channels $u_{vgt} \to \lambda_O$, $u_{egr} \to \lambda_O$, and $u_{vgt} \to x_{egr}$ have sign reversals. These three channels have small τ when the overshoot is large, which is in operating points with positive

Table 1 *The minimum, mean, and maximum value of the response time τ in the entire operating region for the channels $u_{vgt} \to \lambda_O$, $u_{egr} \to \lambda_O$, $u_{vgt} \to x_{egr}$, and $u_{egr} \to x_{egr}$.*

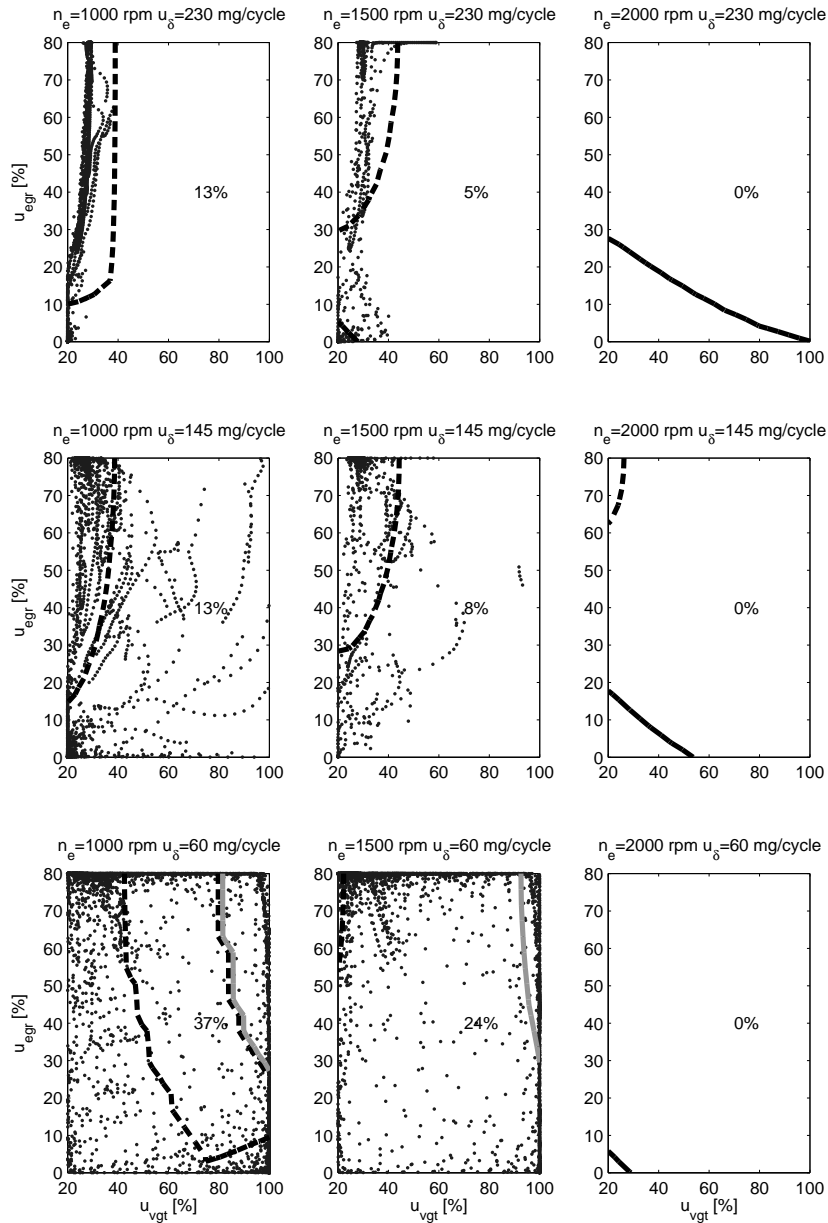| Channel	$u_{vgt} \to \lambda_O$	$u_{egr} \to \lambda_O$	$u_{vgt} \to x_{egr}$	$u_{egr} \to x_{egr}$
Minimum τ	0.10	0.12	0.07	0.16
Mean τ	1.10	0.97	0.20	0.17
Maximum τ	5.91	3.83	10.04	0.76

Figure 16 *Operating points during European Transient Cycle simulations of a control system showing that the engine frequently operates in operating points where the sign reversal occurs for the channels $u_{vgt} \to \lambda_O$ (dashed black line) and $u_{vgt} \to x_{egr}$ (solid gray line), and that the engine does not frequently operate in operating points where the sign reversal occurs for the channel $u_{egr} \to \lambda_O$ (solid black line).*

DC-gains near the sign reversals for $u_{vgt} \rightarrow \lambda_O$ and $u_{egr} \rightarrow \lambda_O$ and with negative DC-gains for $u_{vgt} \rightarrow x_{egr}$. The channels $u_{vgt} \rightarrow \lambda_O$, $u_{egr} \rightarrow \lambda_O$, and $u_{egr} \rightarrow x_{egr}$ have large τ in operating points with fully open EGR-valve, almost closed VGT, low n_e, and small u_δ. The channel $u_{vgt} \rightarrow x_{egr}$ has a large τ in operating points with half to fully open EGR-valve, fully open VGT, medium n_e, and small u_δ.

5 Mapping of performance variables

Besides looking at dynamic responses of different loops, it is valuable to study the interaction. This is done in Sec. 5.1 for λ_O and x_{egr}. Further, in Sec. 5.2 the pumping losses are mapped to give insight into how to minimize the pumping losses.

5.1 System coupling in steady state

A mapping of the main performance variables λ_O and x_{egr} as function of u_{egr} and u_{vgt} in steady state is given in Fig. 17. The system is decoupled, in steady state, in one point if one of the contour lines is horizontal at the same time as the other line is vertical. This is almost the case in the gray areas in Fig. 17, see also the cross in the middle plot showing that the tangents to the contour lines are almost perpendicular in one point. The gray areas are near the sign reversals for $u_{vgt} \rightarrow \lambda_O$, $u_{egr} \rightarrow \lambda_O$, and $u_{vgt} \rightarrow x_{egr}$ since one of the contour lines is either horizontal or vertical at the sign reversals. In the operating regions that are not gray, the system is strongly coupled.

In the gray areas near the sign reversal for the channel $u_{vgt} \rightarrow \lambda_O$ (thick dashed line), u_{vgt} almost only affects x_{egr} and u_{egr} almost only affects λ_O. However, in the gray areas near the sign reversals for the channels $u_{egr} \rightarrow \lambda_O$ (thick solid line) and $u_{vgt} \rightarrow x_{egr}$ (dotted line) u_{egr} almost only affects x_{egr} and u_{vgt} almost only affects λ_O.

System coupling is also investigated in Appendix B by analyzing the relative gain array (RGA) showing that the system is strongly coupled. Input-output pairing for SISO controllers are also investigated showing that the best input-output pairing is

$$u_{egr} \rightarrow \lambda_O$$
$$u_{vgt} \rightarrow x_{egr}$$

5.2 Pumping losses in steady state

A mapping of the pumping losses in steady state over the entire operating region gives insight into how to minimize the pumping work. Fig. 18 shows that the pumping losses $p_{em} - p_{im}$ decrease with increasing EGR-valve and VGT openings except at operating points with low torque, low engine speed, half to fully open EGR-valve, and half to fully open VGT, where there is a sign reversal in the gain from VGT to pumping losses. Further, the pumping losses are negative in operating
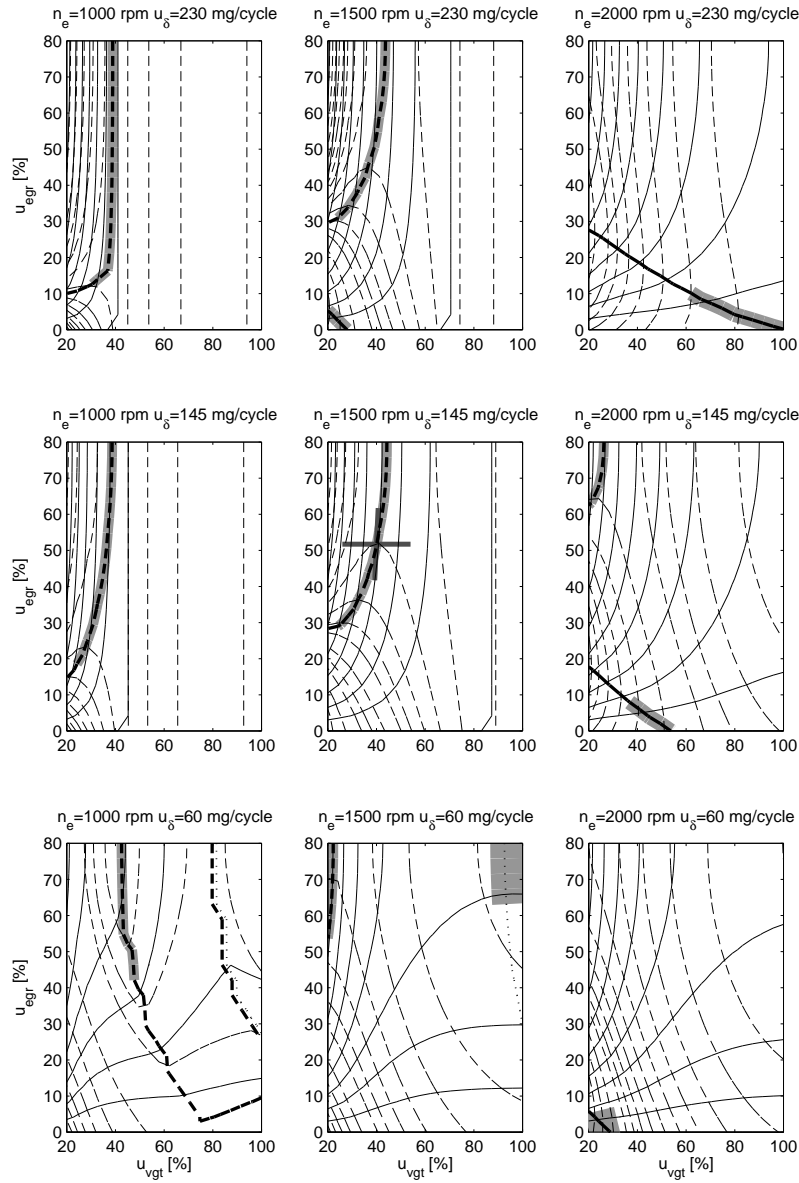
Figure 17 *Contour plots of λ_O (thin dashed line) and x_{egr} (thin solid line) in steady-state at 3 different n_e and 3 different u_δ. The system from u_{egr} and u_{vgt} to λ_O and x_{egr} is strongly coupled in steady state in almost the entire operating region except for operating points in the gray areas. These areas are near the sign reversals for the channels $u_{vgt} \rightarrow \lambda_O$ (thick dashed line), $u_{egr} \rightarrow \lambda_O$ (thick solid line), and $u_{vgt} \rightarrow x_{egr}$ (dotted line). The cross in the middle plot shows an example of a point where the system is almost decoupled.*

Figure 18 *Contour plots of* $p_{em} - p_{im}$ *[bar] in steady-state at 3 different* n_e *and 3 different* u_δ*, showing that* $p_{em} - p_{im}$ *decreases with increasing EGR-valve and VGT opening, except in the left bottom plot where there is a sign reversal in the gain from* u_{vgt} *to* $p_{em} - p_{im}$*.*
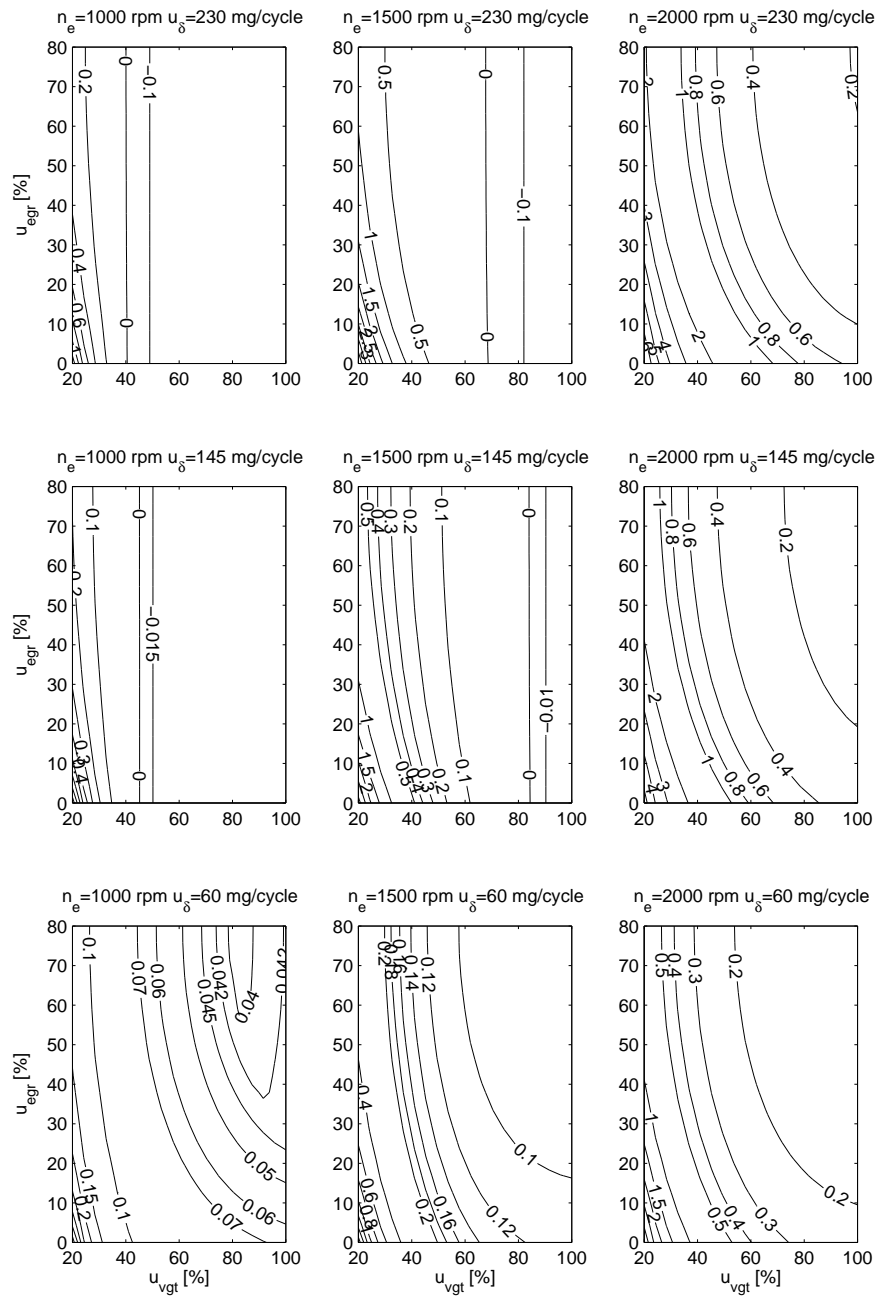
points with half to fully open VGT, low to medium n_e, and medium to large u_δ, and the pumping losses are high in operating points with closed VGT and high n_e.

These observations are valuable since they give the basis for the development of a controller that besides control of the performance variables λ_O and x_{egr} also minimizes the pumping work. Further, the specific structure revealed in Fig. 18 makes it possible to employ a non-complicated control principle in an industrially adapted control structure, see [5].

6   Conclusions

A system analysis of a diesel engine has been performed showing that the channels $u_{vgt} \to \lambda_O$, $u_{egr} \to \lambda_O$, and $u_{vgt} \to x_{egr}$ have non-minimum phase behaviors and sign reversals. The fundamental physical explanation of these system properties is that the system consists of two dynamic effects that interact: a fast pressure dynamics in the manifolds and a slow turbocharger dynamics. These two dynamic effects often work against each other which results in the system properties above. The analysis also shows that the engine frequently operates in operating points where these properties occur for the channels $u_{vgt} \to \lambda_O$ and $u_{vgt} \to x_{egr}$, and consequently, it is important to consider the sign reversal and the non-minimum phase behavior for these channels in a control design. Further, it was demonstrated that the four channels $(u_{vgt}, u_{egr}) \to (\lambda_O, x_{egr})$ have varying DC-gains and time constants. Furthermore, an analysis of linearized MIMO models of the engine shows that there is one zero in the right half plane over the complete operating region. Consequently, these MIMO models are non-minimum phase over the complete operating region. A mapping of the performance variables λ_O and x_{egr} and the relative gain array show that the system from u_{egr} and u_{vgt} to λ_O and x_{egr} is strongly coupled in a large operating region. It was also illustrated that the pumping losses $p_{em} - p_{im}$ decrease with increasing EGR-valve and VGT opening except for a small operating region (with low torque, low engine speed, half to fully open EGR-valve, and half to fully open VGT, where there is a sign reversal in the gain from VGT to pumping losses).

References

[1] J.B. Heywood. *Internal Combustion Engine Fundamentals.* McGraw-Hill Book Co, 1988.

[2] M. Jung. *Mean-Value Modelling and Robust Control of the Airpath of a Turbocharged Diesel Engine.* PhD thesis, University of Cambridge, 2003.

[3] I.V. Kolmanovsky, A.G. Stefanopoulou, P.E. Moraal, and M. van Nieuwstadt. Issues in modeling and control of intake flow in variable geometry turbocharged engines. In *Proceedings of* 18th *IFIP Conference on System Modeling and Optimization*, Detroit, July 1997.

[4] C. Vigild. *The Internal Combustion Engine Modelling, Estimation and Control Issues.* PhD thesis, Technical University of Denmark, Lyngby, 2001.

[5] Johan Wahlström. Control of EGR and VGT for emission control and pumping work minimization in diesel engines. Licentiate Thesis, Linköping University, 2006.

[6] Johan Wahlström, Lars Eriksson, and Lars Nielsen. Controller tuning based on transient selection and optimization for a diesel engine with EGR and VGT. In *Electronic Engine Controls*, number 2008-01-0985 in SAE Technical paper series SP-2159, SAE World Congress, Detroit, USA, 2008.

[7] Johan Wahlström and Lars Eriksson. Modeling of a diesel engine with VGT and EGR capturing sign reversal and non-minimum phase behaviors. Technical report, Linköping University, 2009.

A   Response time

The response time τ (see Fig. 6) for the channels $u_{vgt} \to \lambda_O$, $u_{egr} \to \lambda_O$, $u_{vgt} \to x_{egr}$, and $u_{egr} \to x_{egr}$ are shown in Fig. 19 to 22 over a large operating region.
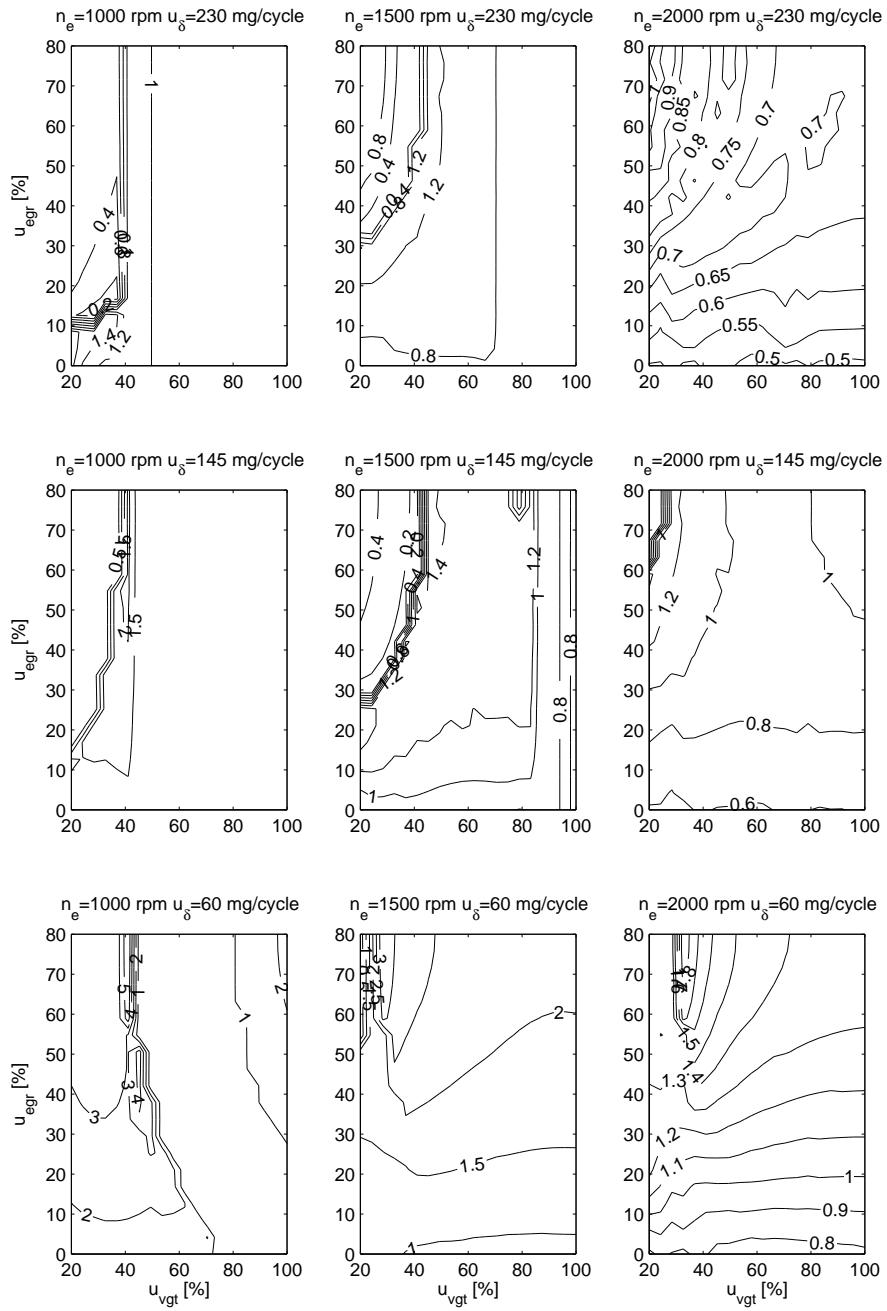
Figure 19 Contour plots of the response time, τ [s], for the channel $u_{vgt} \rightarrow$ λ_O at 3 different n_e and 3 different u_δ, i.e. 3*3=9 different n_e and u_δ points.

Figure 20 *Contour plots of the response time, τ [s], for the channel $u_{egr} \rightarrow \lambda_O$ at 3 different n_e and 3 different u_δ, i.e. $3*3=9$ different n_e and u_δ points.*

Figure 21 *Contour plots of the response time, τ [s], for the channel $u_{vgt} \rightarrow$ x_{egr} at 3 different n_e and 3 different u_δ, i.e. 3*3=9 different n_e and u_δ points.*
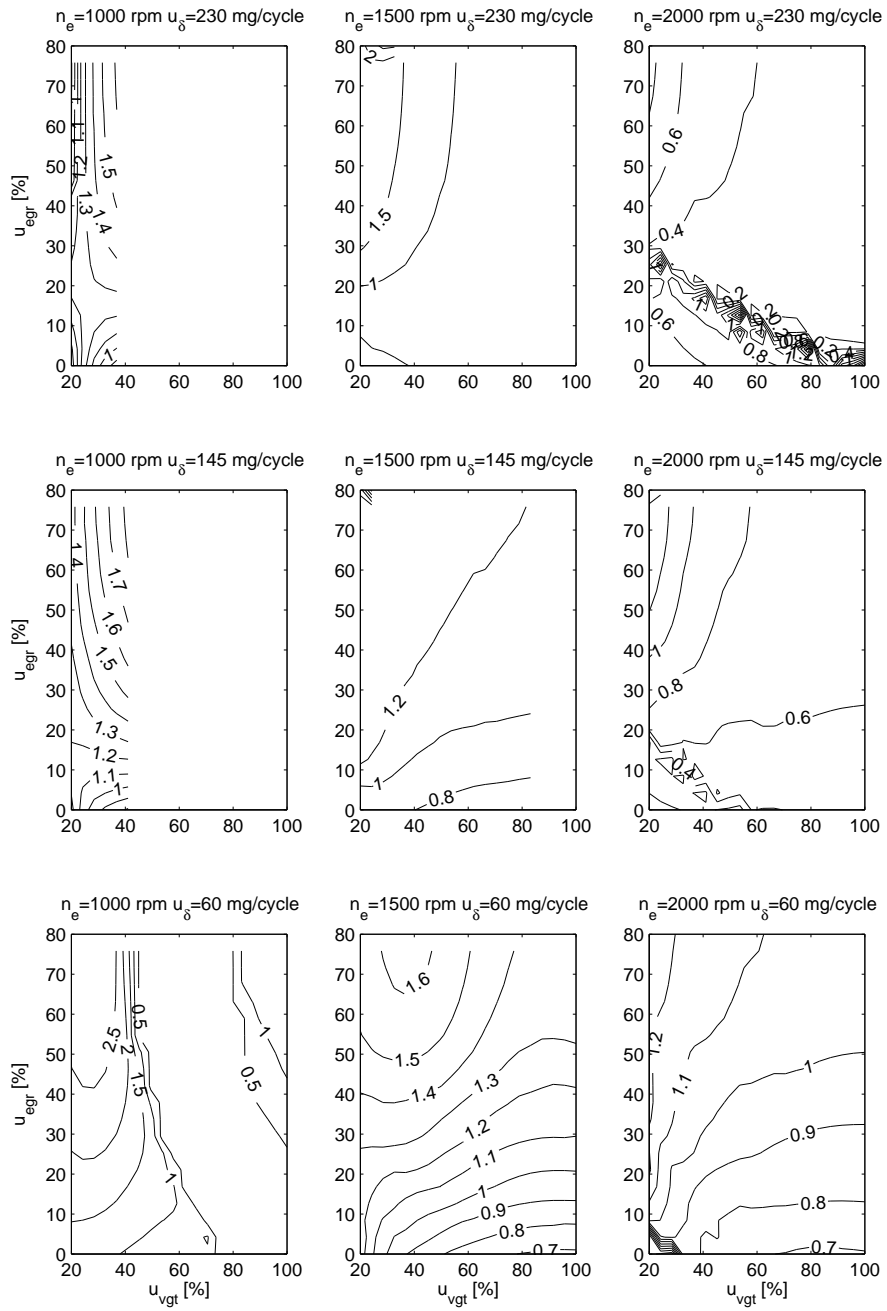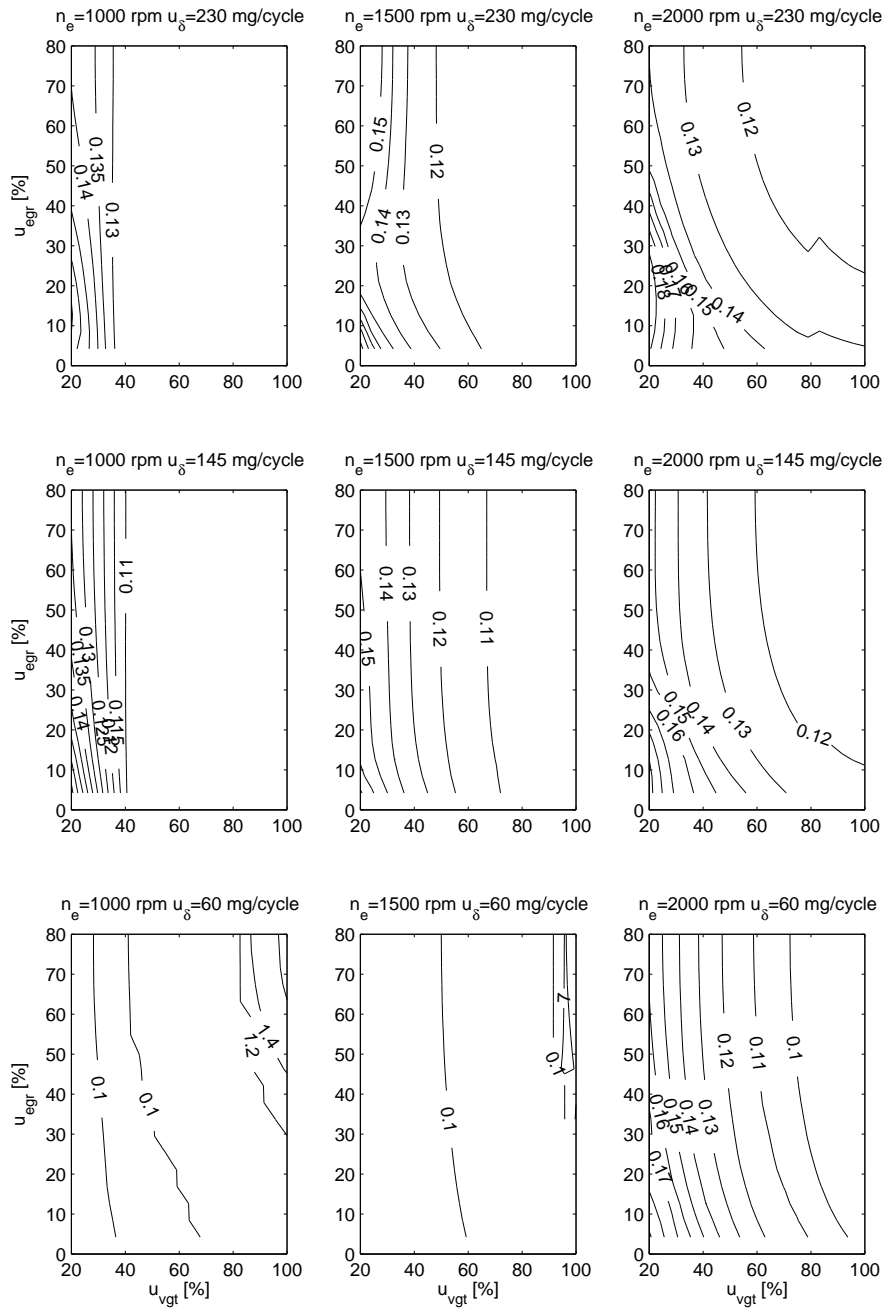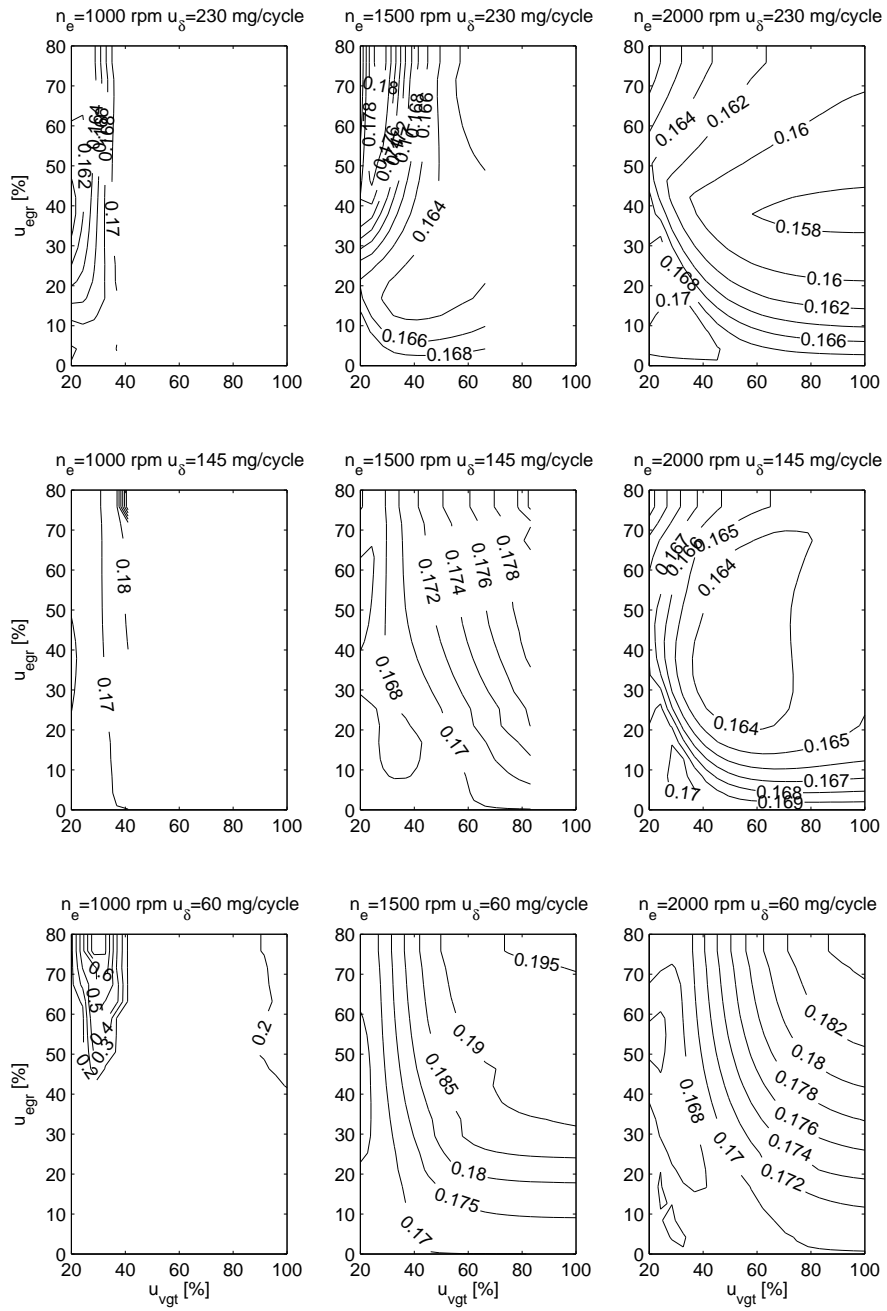
Figure 22 *Contour plots of the response time, τ [s], for the channel $u_{egr} \rightarrow x_{egr}$ at 3 different n_e and 3 different u_δ, i.e. 3*3=9 different n_e and u_δ points.*

B   Relative gain array

Mappings of the relative gain array (RGA) for linearized MIMO models of the engine over the entire operating region are performed in order investigate system coupling and input-output pairing for SISO controllers. For a matrix G, RGA is defined as

$$\mathrm{RGA}(\mathsf{G}) = \mathsf{G} .* (\mathsf{G}^{\dagger})^{\mathsf{T}} \tag{6}$$

where ".*" is the element-by-element multiplication and the pseudo inverse is defined as

$$\mathsf{G}^{\dagger} = (\mathsf{G}^* \mathsf{G})^{-1} \mathsf{G}^* \tag{7}$$

where G^* is the conjugate transpose of the matrix G.

RGA is analyzed for the linearized models (4) in Sec. 4.2, giving the following transfer functions

$$\mathsf{G}_i(s) = \mathsf{C}_i(s\,\mathsf{I} - \mathsf{A}_i)^{-1}\mathsf{B}_i \tag{8}$$

for each operating point i and the following relation between inputs and outputs

$$\begin{pmatrix} \lambda_O \\ x_{egr} \end{pmatrix} = \mathsf{G}_i(s) \cdot \begin{pmatrix} u_{egr} \\ u_{vgt} \end{pmatrix} \tag{9}$$

When investigating the best input-output pairing for SISO controllers, there are two main rules to follow:

1. Choose input-output pairings where the corresponding elements in the matrix $\mathrm{RGA}(\mathsf{G}_i(j\omega_c))$ are close to 1 in the complex plane. Here, ω_c is the desired bandwidth of the closed-loop system.
2. Avoid input-output pairings where the corresponding elements in the matrix $\mathrm{RGA}(\mathsf{G}_i(0))$ are negative.

In order to follow rule 1 above, RGA is mapped in the following way. For

$$\mathrm{RGA}(\mathsf{G}_i(j\omega_c)) = \begin{pmatrix} g_{11} & g_{12} \\ g_{21} & g_{22} \end{pmatrix} \tag{10}$$

with $\omega_c = 1/4$ rad/s

$$s_1 = |g_{11} - 1| + |g_{22} - 1| \tag{11}$$
$$s_2 = |g_{21} - 1| + |g_{12} - 1| \tag{12}$$

are calculated. If s_1 or s_2 are small, the corresponding elements in (10) are close to 1. The variables s_1 and s_2 are mapped in Fig. 23 and 24 respectively showing that each of these variables are smaller than 1 in the gray areas. The points where the engine operates during the European Transient Cycle are also mapped in the figures in the same way as in Fig. 16. Consequently, the goal is to choose an input-output pairing so that the engine frequently operates in the gray areas. It can be seen that the engine operates outside the gray areas in both Fig. 23 and 24 for some operating points. Consequently, the system is strongly coupled in these

points. For $u_\delta \geq 145$ mg/cycle the engine operates more frequently in the gray areas in Fig. 23 than in Fig. 24. However, for $u_\delta = 60$ mg/cycle it is the reversed relation, i.e. the engine operates more frequently in the gray areas in Fig. 24 than in Fig. 23. On the other hand, one of the control inputs are often saturated when $u_\delta = 60$ mg/cycle and when this occur, there is no pairing problem. Consequently, according to rule 1 the best input-output pairing is

$$u_{egr} \rightarrow \lambda_O$$
$$u_{vgt} \rightarrow x_{egr}$$

In order to follow rule 2 above, RGA is mapped in the following way. For

$$\text{RGA}(G_i(0)) = \begin{pmatrix} h_{11} & h_{12} \\ h_{21} & h_{22} \end{pmatrix} \tag{13}$$

the variables h_{11} and h_{21} are mapped in Fig. 25 and 26 respectively showing that each of these variables are greater or equal to zero in the gray areas. The variable h_{12} is greater or equal to zero in the same area as h_{21} and h_{22} is greater or equal to zero in the same area as h_{11}. In the same way as in Fig. 23 and 24 the goal is to choose an input-output pairing so that the engine frequently operates in the gray areas. The result is that the engine operates more frequently in the gray areas in Fig. 25 than in Fig. 26. It is only a small white area in the left bottom plot in Fig. 25 where $h_{11} < 0$ and where the engine operates for some few operating points. Consequently, even for rule 2 the best input-output pairing is

$$u_{egr} \rightarrow \lambda_O$$
$$u_{vgt} \rightarrow x_{egr}$$

Figure 23 *A mapping of s_1, defined by (11), showing that $s_1 < 1$ in the gray areas. The points where the engine operates during the European Transient Cycle are also mapped showing that for $u_\delta \geq 145$ mg/cycle the engine operates more frequently in the gray areas than in Fig. 24.*

Figure 24 *A mapping of* s_2, *defined by* (12), *showing that* $s_2 < 1$ *in the gray areas. The points where the engine operates during the European Transient Cycle are also mapped.*

Figure 25 *A mapping of* h_{11}, *defined by* (13), *showing that* $h_{11} \geq 0$ *in the gray areas. The points where the engine operates during the European Transient Cycle are also mapped showing that the engine operates more frequently in the gray areas than in Fig. 26.*
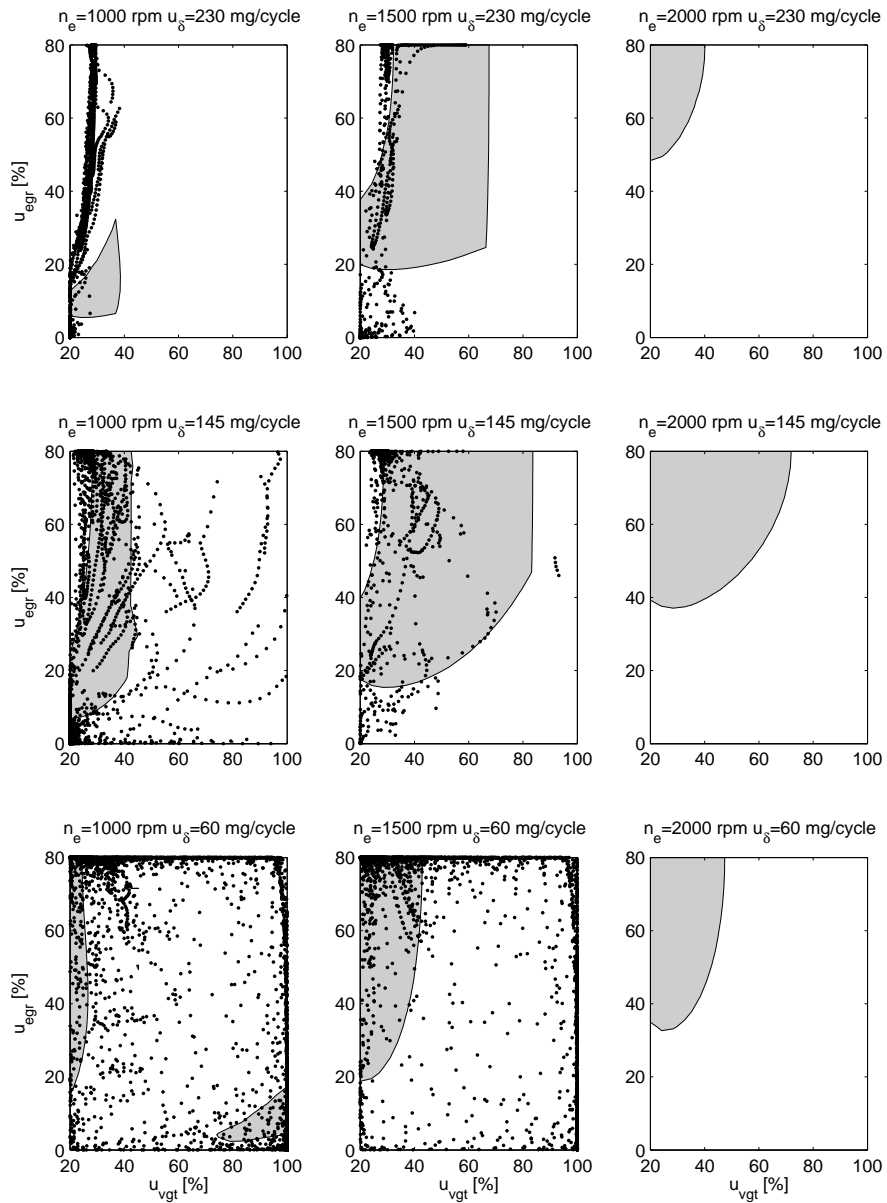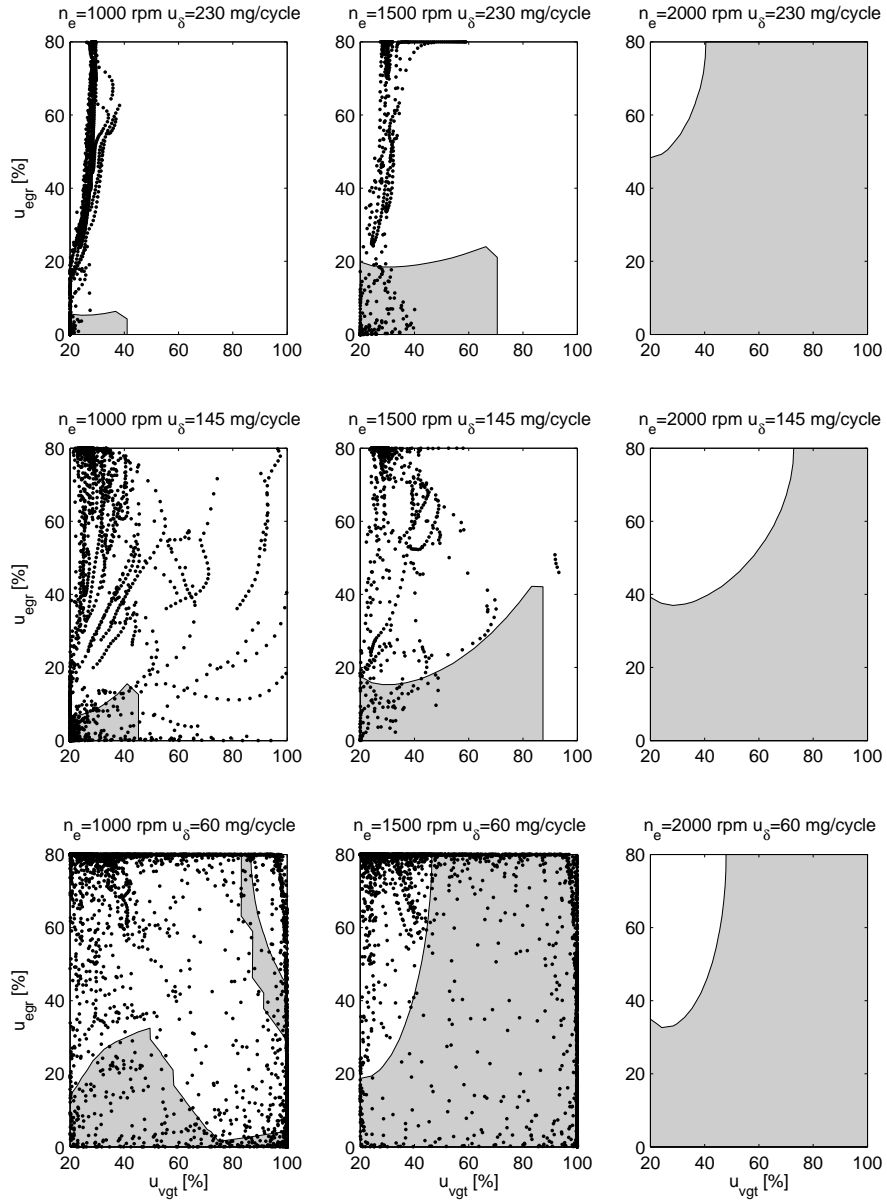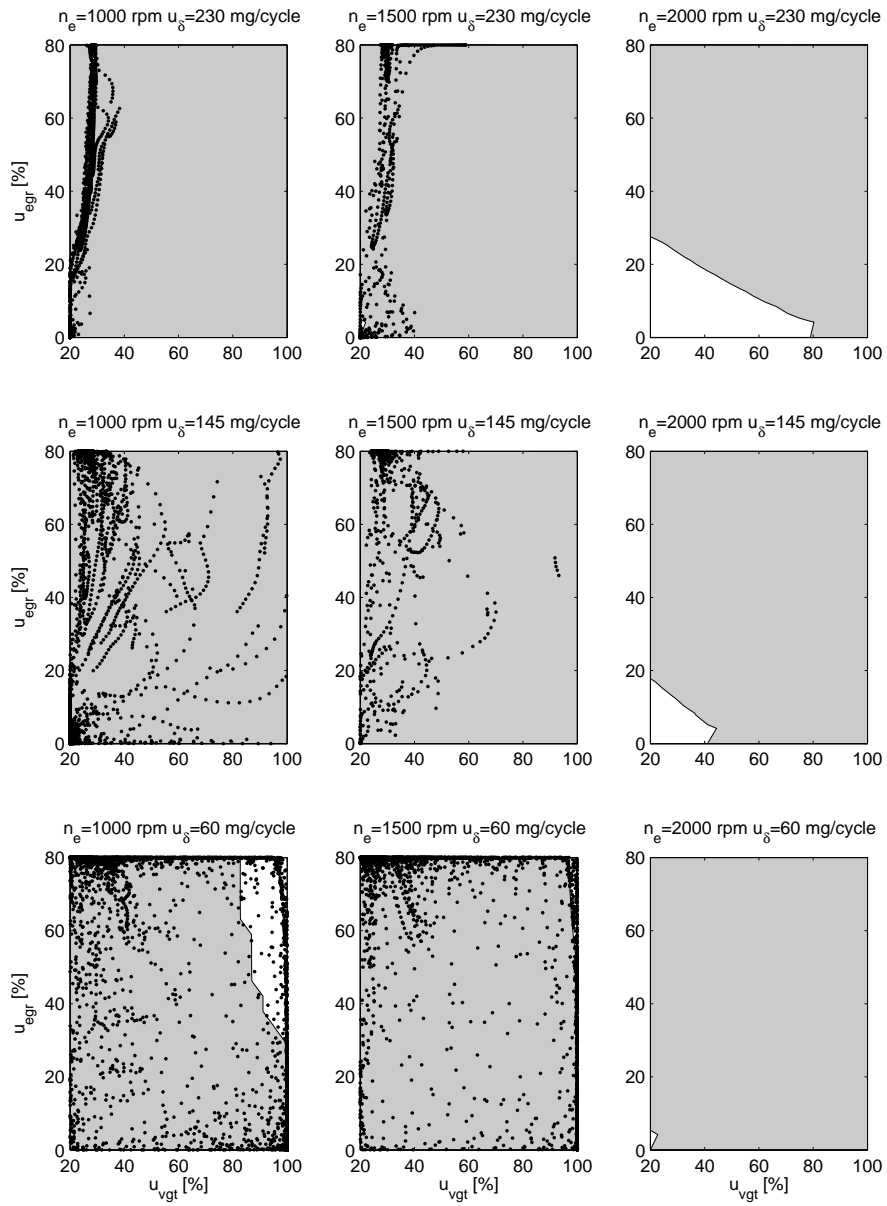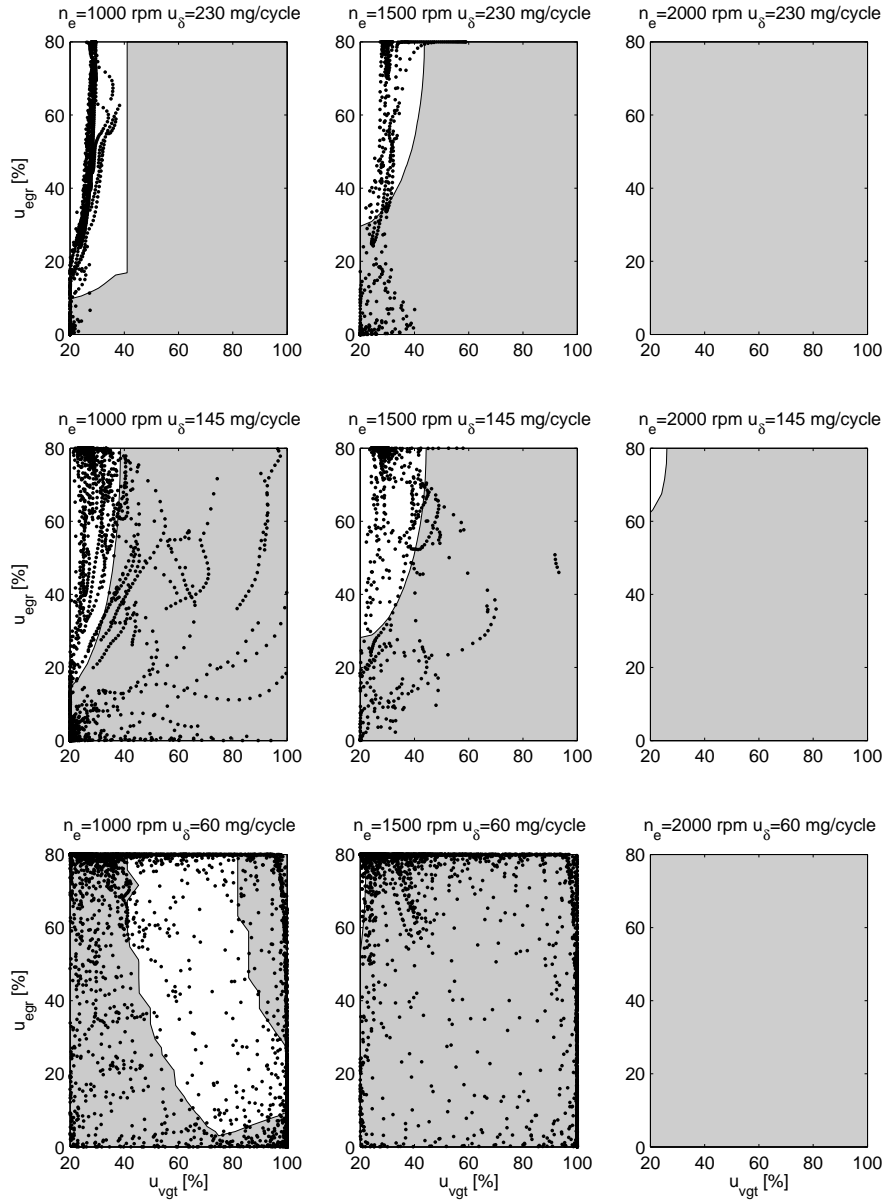
Figure 26 A mapping of h_{21}, defined by (13), showing that $h_{21} \geq 0$ in the gray areas. The points where the engine operates during the European Transient Cycle are also mapped.

EGR-VGT Control and Tuning for Pumping Work Minimization and Emission Control[1]

Johan Wahlström, Lars Eriksson, and Lars Nielsen

Vehicular Systems, Department of Electrical Engineering,
Linköping University, S-581 83 Linköping,
Sweden.

3

Abstract

A control structure is proposed and investigated for coordinated control of EGR valve and VGT position in heavy duty diesel engines. Main control goals are to fulfill the legislated emission levels, to reduce the fuel consumption, and to fulfill safe operation of the turbocharger. These goals are achieved through regulation of normalized oxygen/fuel ratio, λ_O, and intake manifold EGR-fraction. These are chosen both as main performance variables and feedback variables since they contain information about when it is possible to decrease the fuel consumption by minimizing the pumping work. Based on this a novel and simple pumping work minimization strategy is developed. The proposed performance variables are also strongly coupled to the emissions which makes it easier to adjust set-points, e.g. depending on measured emissions during an emission calibration process, since it is more straightforward than control of manifold pressure and air mass flow. Further, internally the controller is structured to handle the different control objectives. Controller tuning is important for performance but can be time consuming and to meet this end a method is developed where the controller objectives are captured in a cost function, which makes automatic tuning possible even though objectives are conflicting. Performance trade-offs are necessary and are illustrated on the European Transient Cycle. The proposed controller is validated in an engine test cell, where it is experimentally demonstrated that the controller achieves all the control objectives and that the current production controller has at least 26% higher pumping losses compared to the proposed controller.

---

[1]This paper has been submitted for publication.

1   Introduction

Legislated emission limits for heavy duty trucks are constantly reduced while at the same time there is a significant drive for good fuel economy. To fulfill the requirements, technologies like Exhaust Gas Recirculation (EGR) systems and Variable Geometry Turbochargers (VGT) have been introduced. The primary emission reduction mechanisms utilized are that NO_x can be reduced by increasing the intake manifold EGR-fraction and smoke can be reduced by increasing the air/fuel ratio [5]. However the EGR fraction and air/fuel ratio depend in complicated ways on the EGR and VGT actuation and it is therefore necessary to have coordinated control of the EGR and VGT to reach the legislated emission limits. Various approaches have been published, and an overview of different control aspects is given in [4]. A multi-variable controller is presented in [6], some approaches that differ in the selection of performance variables are compared in [12], and in [15] decoupling control is investigated. Other control approaches are described in [1, 2, 3, 7, 11, 13, 16].

This paper presents the scientifically interesting results from an academic and industrial collaboration where a structure for coordinated EGR and VGT control was developed and investigated. The structure provides a convenient way for handling emission requirements and introduces a novel and straightforward approach for optimizing the engine efficiency by minimizing pumping work. Added to that, the paper covers requirements regarding additional control objectives, interfaces between inner and outer loops, and calibration that have been important for a successful industrial validation and application. The key ideas behind the structure are described in Sec. 2, and Sec. 2.2 summarizes the control objectives related to EGR and VGT control. A mean value diesel engine model, focused on gas flows, is described in Sec. 3. It is first used for system analysis in Sec. 4 and later used both for controller tuning and in simulation evaluations of the closed-loop system. An important part is Sec. 5 that systematically develops the control structure based on the analysis of control objectives and the key properties that were observed in the preceding system analysis. Sec. 5.4 discusses the pumping minimizing mechanism and compares it to another structure with respect to pumping work. In Sec. 6 a tuning methodology is developed that is achieved by formulating a cost function that reflects the control objectives. Performance trade-offs are inevitable in this system and simulations on a European Transient Cycle (ETC) are used in Sec. 7 to illustrate how these can be handled. Finally Sec. 8 discusses the results from the experimental validation performed in an engine test cell at Scania CV AB.

2   Proposed control approach

To deliver low fuel consumption and fast response to the driver's command while fulfilling the emission requirements are the goals for engine control. The control of EGR and VGT for emission abatement is considered first, and then the other goals are considered as they are also important for a successful application. The selection of performance and feedback variables is an important first step [22], and

for emission control it should be noted that exhaust gases, present in the intake from EGR, also contain oxygen. This makes it more suitable to define and use the oxygen/fuel ratio instead of the traditional air/fuel ratio. The main motive is that it is the oxygen content that is crucial for smoke generation, and the idea is to use the oxygen content of the cylinder instead of air mass flow, see e.g. [10]. The exact definition of the normalized oxygen/fuel ratio λ_O is given by (16) in Sec. 3. Thus, EGR-fraction x_{egr} and oxygen/fuel ratio λ_O are a natural selection for performance variables as they are directly related to the emissions. These performance variables are equivalent to cylinder air/fuel ratio and burned gas ratio which are a frequent choice for performance variables in many papers [6, 12, 16, 13].

The choice of feedback variables defines the overall controller structure, and the most common choice in the literature are compressor air mass flow and intake manifold pressure [7, 11, 12, 15, 16]. Other choices are intake manifold pressure and EGR-fraction [12], exhaust manifold pressure and compressor air mass flow [6], intake manifold pressure and EGR flow [14], intake manifold pressure and cylinder air mass-flow [1], or compressor air mass flow and EGR flow [3]. Based on the close relation to the emissions, x_{egr} and λ_O are here used also as feedback variables. Simulations are presented in [13], but to our knowledge our work is the first that have utilized and verified this choice of feedback variables experimentally.

2.1   Advantages of this choice

There are three main advantages with the choice of EGR-fraction x_{egr} and oxygen/fuel ratio λ_O as both performance and feedback variables.

The first advantage is that these variables provide direct information about when it is possible/allowed to minimize the pumping work, compared to e.g. manifold pressure and air mass flow. To facilitate improved fuel economy the proposed control structure also has a novel and simple mechanism for optimizing the fuel consumption by minimizing the pumping work. In diesel engines a large λ_O is allowed and there is thus an extra degree of freedom, when λ_O is greater than its set-point, that can be used to minimize the pumping work. Pumping minimization is an important feature, however the performance variables x_{egr} and λ_O are always controlled as they are the major variables in the controller.

The second advantage is as mentioned above that these variables are strongly connected to the emissions and gives a natural separation within the engine management system. The performance variables are handled in a fast inner loop, whereas trade-offs between e.g. emissions and response time for different operating conditions are made in an outer loop. The idea with two loops is depicted in Fig. 1.

The third follows from the second in that it fits well into industry's engineering process where the inner control loops are first tuned for performance. Then the total system is calibrated to get stable combustion and to meet the emission limits by adjusting set-points for different operating conditions, different hardware configurations, and different legislative requirements depending on the measured emissions during the emission calibration process.
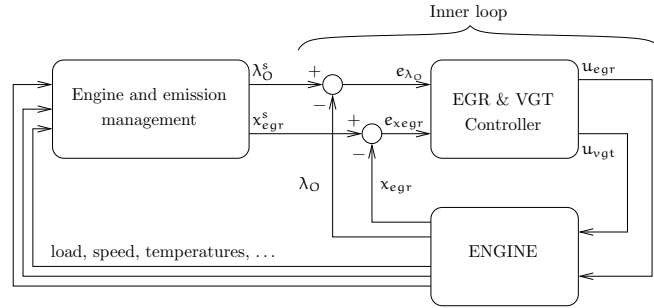
Figure 1 *A cascade control structure, with an inner loop where EGR and VGT actuators are controlled using the main performance variables EGR fraction x_{egr} and oxygen/fuel ratio λ_O. This sketch is a simplified illustration of the main idea that will be completed in Sec. 5 to also include fuel control and turbo protection.*

Normally, neither x_{egr} nor λ_O are measured and have to be estimated using observers. The observer design is important, but it is not the focus in this paper. Here it is assumed that an observer exist similar to that in [13]. This means that the known issues about oxygen estimation are handled and in the experiments such an observer of industrial production type is available and used. Engines could in the future be equipped with a sensor for λ_O, and if so, then nothing has to be changed in the proposed controller structure, which is an additional advantage.

2.2   Control objectives

In addition to control of x_{egr} and λ_O it is also necessary to have load control, since the driver's demand must be actuated. This is achieved through basic fuel control using feedforward. Furthermore it is also important to monitor and control turbocharger speed since aggressive transients can cause damage through overspeeding.

The primary variables to be controlled are engine torque M_e, normalized oxygen/fuel ratio λ_O, intake manifold EGR-fraction x_{egr}, and turbocharger speed n_t. The goal is to follow a driving cycle while maintaining low emissions, low fuel consumption, and suitable turbocharger speeds, which together with the discussion above gives the following control objectives for the performance variables.

1. λ_O should be greater than a soft limit, a set-point λ_O^s, which enables a trade-off between emission, fuel consumption, and response time.

2. λ_O is not allowed to go below a hard minimum limit λ_O^{min}, otherwise there will be too much smoke. λ_O^{min} is always smaller than λ_O^s.

3. x_{egr} should follow its set-point x_{egr}^s. There will be more NO_x if the EGR-fraction is too low and there will be more smoke if the EGR-fraction is too high.
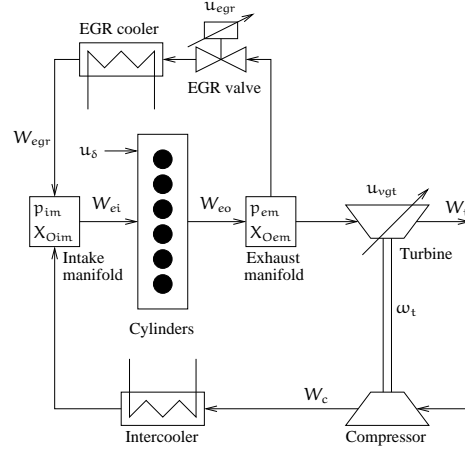
Figure 2 *Sketch of the diesel engine model used for simulation, control design, and tuning. It has five main states related to the engine (p_{im}, p_{em}, X_{Oim}, X_{Oem}, and ω_t) and two states for actuator dynamics ($\tilde{u}_{egr}$ and $\tilde{u}_{vgt}$).*

4. The engine torque, M_e, should follow the set-point M_e^s from the drivers demand.
5. The turbocharger speed, n_t, is not allowed to exceed a maximum limit n_t^{max}, preventing turbocharger damage.
6. The pumping losses, M_p, should be minimized in order to decrease the fuel consumption.

The aim is now to develop a control structure that achieves all these control objectives when the set-points for EGR-fraction and engine torque are reachable.

3   Diesel engine model

A diesel engine model is used to capture and give insight into the important system properties and also used in simulations for tuning and validation of the developed controller structure. The model is focused on the gas flows, see Fig. 2, and has seven states: intake and exhaust manifold pressures (p_{im} and p_{em}), oxygen mass fraction in the intake and exhaust manifold (X_{Oim} and X_{Oem}), turbocharger speed (ω_t), and two states describing the actuator dynamics for the two control signals ($\tilde{u}_{egr}$ and $\tilde{u}_{vgt}$). These states are collected in a state vector x

$$x = (p_{im} \quad p_{em} \quad X_{Oim} \quad X_{Oem} \quad \omega_t \quad \tilde{u}_{egr} \quad \tilde{u}_{vgt})^\mathsf{T} \tag{1}$$

There are no state equations for the manifold temperatures. The reason is that the pressures and the turbocharger speed govern the system properties in Sec. 4,

while the temperature states have only minor effects on these system properties.

It is important that the model can be utilized both for different vehicles having the same engine but different driveline parameters and for engine testing, calibration, and certification in an engine test cell. In many of these situations the engine operation is defined by the rotational speed n_e, for example given as a drivecycle, and therefore it is natural to parameterize the model using engine speed. The resulting model is thus expressed in state space form as

$$\dot{x} = f(x, u, n_e) \tag{2}$$

where the engine speed n_e is considered as an input to the model, and u is the control input vector

$$u = (u_\delta \quad u_{egr} \quad u_{vgt})^\mathsf{T} \tag{3}$$

which contains mass of injected fuel u_δ, EGR-valve position u_{egr}, and VGT actuator position u_{vgt}. The EGR-valve is closed when $u_{egr} = 0\,\%$ and open when $u_{egr} = 100\,\%$. The VGT is closed when $u_{vgt} = 0\,\%$ and open when $u_{vgt} = 100\,\%$.

The model is a mean value engine model [8], and the equations are given below. A detailed description and derivation of the model is given in [20] together with a tuning methodology and a validation against test cell measurements. Descriptions of the nomenclature, the variables and the indices can be found in the Appendix. The derivatives of the state variables are given by (4)–(7) where the right hand sides are given by (8)–(15). The performance variables are defined by (16)–(17).

Manifolds

$$\begin{aligned}
\frac{d}{dt}\,p_{im} &= \frac{R_a\,T_{im}}{V_{im}}\,(W_c + W_{egr} - W_{ei}) \\
\frac{d}{dt}\,p_{em} &= \frac{R_e\,T_{em}}{V_{em}}\,(W_{eo} - W_t - W_{egr})
\end{aligned} \tag{4}$$

$$\begin{aligned}
\frac{d}{dt}\,X_{Oim} &= \frac{R_a\,T_{im}}{p_{im}\,V_{im}}((X_{Oem} - X_{Oim})\,W_{egr} + \\
&\quad (X_{Oc} - X_{Oim})\,W_c)
\end{aligned} \tag{5}$$

$$\frac{d}{dt}\,X_{Oem} = \frac{R_e\,T_{em}}{p_{em}\,V_{em}}\,(X_{Oe} - X_{Oem})\,W_{eo} \tag{6}$$

Actuator dynamics and turbo speed

$$\begin{aligned}
\frac{d}{dt}\,\tilde{u}_{egr} &= \frac{1}{\tau_{egr}}(u_{egr}(t - \tau_{degr}) - \tilde{u}_{egr}) \\
\frac{d}{dt}\,\tilde{u}_{vgt} &= \frac{1}{\tau_{vgt}}(u_{vgt} - \tilde{u}_{vgt}), \quad \frac{d}{dt}\,\omega_t = \frac{P_t\,\eta_m - P_c}{J_t\,\omega_t}
\end{aligned} \tag{7}$$

Cylinder

$$W_{ei} = \frac{p_{im}\, n_e\, V_d}{120\, R_a\, T_{im}} \eta_{vol}(p_{im}, n_e), \quad W_f = \frac{10^{-6}}{120}\, u_\delta\, n_e\, n_{cyl} \tag{8}$$

$$W_{eo} = W_f + W_{ei}, \quad X_{Oe} = \frac{W_{ei}\, X_{Oim} - W_f\, (O/F)_s}{W_{eo}} \tag{9}$$

$$T_{em} = T_{em}\left(\frac{p_{em}}{p_{im}}, W_f, W_{eo}\right) \tag{10}$$

EGR-valve

$$W_{egr} = \frac{A_{egr}(\tilde{u}_{egr})\, p_{em}\, \Psi_{egr}\left(\frac{p_{im}}{p_{em}}\right)}{\sqrt{T_{em}\, R_e}} \tag{11}$$

Turbine

$$\frac{W_t\, \sqrt{T_{em}}}{p_{em}} = A_{vgtmax}\, f_{\Pi t}(\Pi_t)\, f_{vgt}(\tilde{u}_{vgt}), \quad \Pi_t = \frac{p_{amb}}{p_{em}} \tag{12}$$

$$P_t\, \eta_m = \eta_{tm}(\omega_t, T_{em}, \Pi_t)\, W_t\, c_{pe}\, T_{em}\left(1 - \Pi_t^{1-1/\gamma_e}\right) \tag{13}$$

Compressor

$$W_c = \frac{p_{amb}\, \pi\, R_c^3\, \omega_t}{R_a\, T_{amb}}\, \Phi_c(\omega_t, \Pi_c), \quad \Pi_c = \frac{p_{im}}{p_{amb}} \tag{14}$$

$$P_c = \frac{W_c\, c_{pa}\, T_{amb}}{\eta_c(W_c, \Pi_c)}\left(\Pi_c^{1-1/\gamma_a} - 1\right) \tag{15}$$

Performance variables

$$x_{egr} = \frac{W_{egr}}{W_c + W_{egr}}, \quad \lambda_O = \frac{W_{ei}\, X_{Oim}}{W_f\, (O/F)_s}, \quad n_t = \omega_t\, \frac{30}{\pi} \tag{16}$$

$$M_p = \frac{V_d}{4\,\pi}\left(p_{em} - p_{im}\right), \quad M_e = M_{ig} - M_p - M_{fric} \tag{17}$$

$$M_{ig} = \frac{1}{4\,\pi}\, u_\delta\, 10^{-6}\, n_{cyl}\, q_{HV}\, \eta_{igch}\left(1 - \frac{1}{r_c^{\gamma_{cyl}-1}}\right) \tag{18}$$

$$M_{fric} = \frac{V_d}{4\,\pi} 10^5\left(c_{fric1}\, n_e^2 + c_{fric2}\, n_e + c_{fric3}\right) \tag{19}$$

4   System properties

An analysis of the behavior and characteristics of the system gives valuable insight into the control problem and is important for a successful design of the control structure (see for example [9]). An extensive system analysis has been performed and is given in [21]. Sec. 4.1 summarizes the main results and uses step changes in VGT position and EGR-valve to illustrate the properties, while Sec. 4.2 compiles the results from an analysis of linearized diesel engine models. In Sec. 4.3 the pumping losses are analyzed to give insight into how to handle objective 6 in Sec. 2.2.

4.1   Steps in VGT position and EGR-valve

Model responses to steps in VGT position and EGR-valve in Fig. 3 show that λ_O has non-minimum phase behaviors, overshoots, and sign reversals (this is well known and shown in [9]). The fundamental physical explanation of these system properties is that the system consists of two dynamic effects that interact: a fast pressure dynamics in the manifolds and a slow turbocharger dynamics. These two dynamic effects often work against each other and change in size which results in the system properties above. For example, when the fast dynamic effect is small and the slow dynamic effect is large, the result is a non-minimum phase behavior, see λ_O at 0 s for the VGT and the EGR step. However, when the fast dynamic effect is large and the slow dynamic effect is small, the result is an overshoot and a sign reversal for the VGT step at 10 s and a sign reversal for the EGR step at 10 s. The precise condition for the sign reversal is due to a complex interaction between flows, temperatures, and pressures in the entire engine.

Both the non-minimum phase behavior and the sign reversal in the channel $u_{vgt} \to \lambda_O$ occur in operating points where the engine frequently operates. Therefore, these two properties must be considered in the control design (this will be discussed in Sec. 5.2). For the other channel $u_{egr} \to \lambda_O$ both the non-minimum phase behavior and the sign reversal only occur in operating points where λ_O, pumping loss M_p, and turbocharger speed n_t are high. Consequently, there are significant drawbacks when operating in these operating points. Therefore, the control structure should be designed so that these operating points are avoided (this will be discussed in Sec. 5.2).

The channel $u_{egr} \to x_{egr}$ has a positive DC-gain. The channel $u_{vgt} \to x_{egr}$ has a negative DC-gain, except for a sign reversal that occur in a small operating region with low torque, low to medium engine speed, half to fully open EGR-valve, and half to fully open VGT.

4.2   Results from an analysis of linearized diesel engine models

Linearized diesel engine models are analyzed over the entire operating region in [21] showing that these models have a zero in the right half plane and are therefore non-
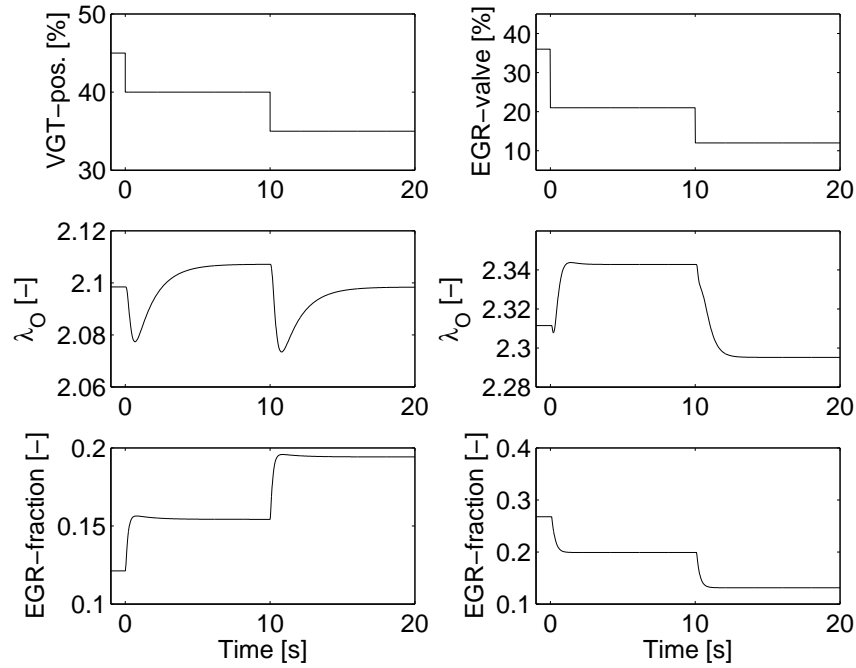
Figure 3 *Responses to steps in VGT position (left column) and EGR valve (right column) showing non-minimum phase behaviors and sign reversals in λ_O. Operating point for the VGT steps: u_δ=145 mg/cycle, n_e=1500 rpm and u_{egr}=50 %. Operating point for the EGR steps: u_δ=230 mg/cycle, n_e=2000 rpm and u_{vgt}=30 %.*

minimum phase. Further, the relative gain array is analyzed for these models in [21] showing that the best input-output pairing for SISO controllers is $u_{egr} \rightarrow \lambda_O$ and $u_{vgt} \rightarrow x_{egr}$ in the regions where the engine frequently operates.

4.3 Pumping losses in steady state

A mapping of the pumping losses in steady state, is shown in Fig. 4, covering the entire operating region (at 20 different u_{vgt} points, 20 different u_{egr} points, 3 different n_e points, and 3 different u_δ points). It gives insight into how to achieve the pumping work minimization in the control structure. Fig. 4 shows that the pumping losses $p_{em} - p_{im}$ decrease with increasing EGR-valve and VGT openings except in a small operating region with low torque, low engine speed, half to fully open EGR-valve, and half to fully open VGT, where there is a sign reversal in the gain from VGT to pumping losses. In Sec. 5.5 the resulting control behavior in this corner is discussed.
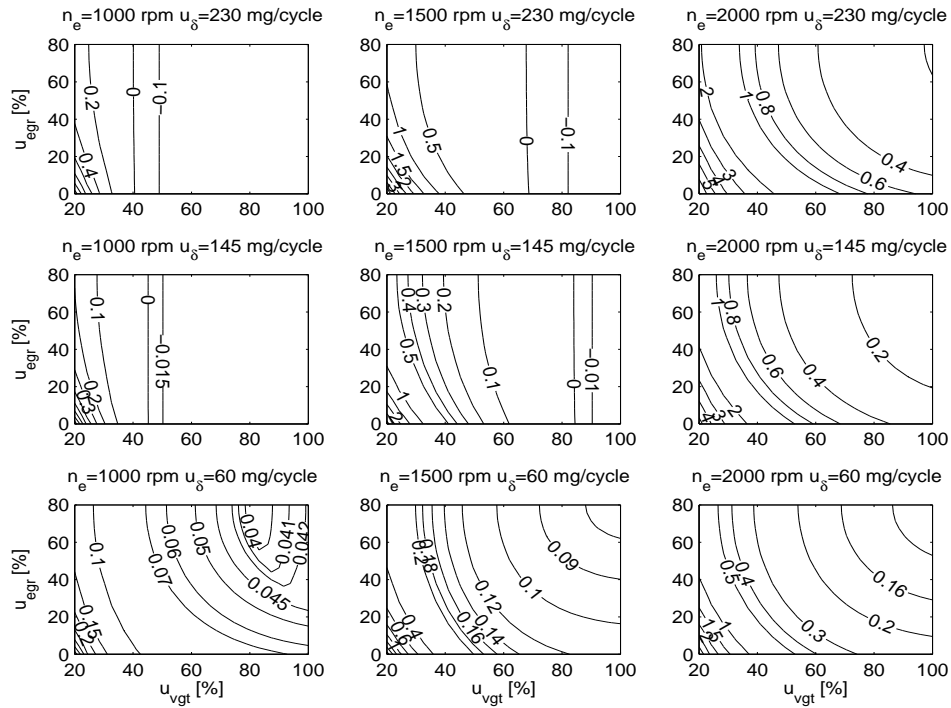
Figure 4 Contour plots of $p_{em} - p_{im}$ [bar] in steady-state at 3 different n_e and 3 different u_δ, showing that $p_{em} - p_{im}$ decreases with increasing EGR-valve and VGT opening, except in the left bottom plot where there is a sign reversal in the gain from u_{vgt} to $p_{em} - p_{im}$.

5   Control structure

The control design objective is to coordinate u_δ, u_{egr}, and u_{vgt} in order to achieve the control objectives stated in Sec. 2.2. The diesel engine is a non-linear and coupled system and one could consider using a multivariable non-linear controller. However, based on the system analysis in the previous section, it is possible to build a controller structure using min/max-selectors and SISO controllers for EGR and VGT control, and to use feedforward for fuel control. As will be shown, this can be done systematically by mapping each loop to the control objectives via the system analysis. The resulting structure of loops is the main result together with the rationale for it, but within the structure different SISO controllers could be used. However, throughout the presentation PID controllers will be used. The foremost reasons are that all control objectives will be shown to be met and that PID controllers are widely accepted by industry.

The solution is presented step by step in the following sections, but a MAT-
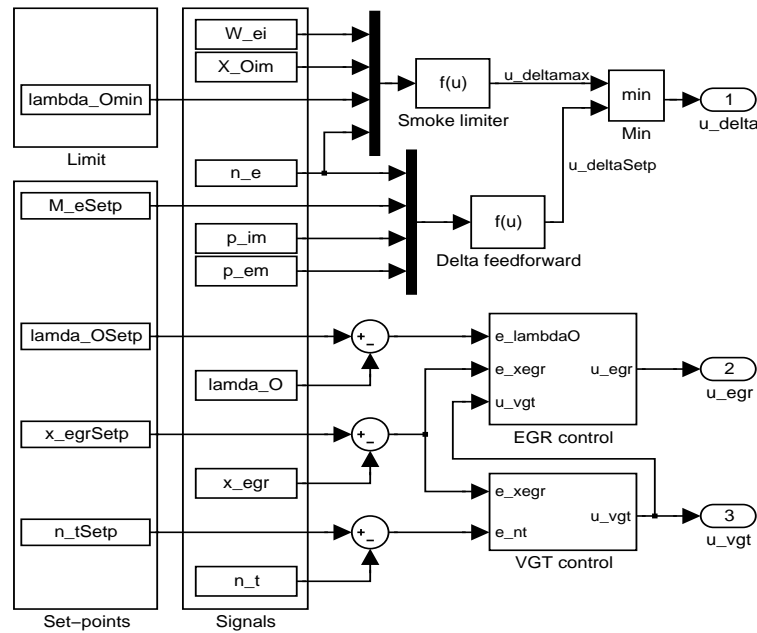
Figure 5 *The proposed control structure, as* MATLAB/SIMULINK *block diagram, showing; a limit, set-points, measured and observed signals, fuel control with smoke limiter, together with the controllers for EGR and VGT.*

LAB/SIMULINK schematic of the full control structure is shown in Fig. 5, where all signals and the fuel controller are included together with the EGR and VGT controller depicted in Fig. 1.

5.1   Signals, set-points, and a limit

The signals needed for the controller are assumed to be either measured or estimated using observers. The measured signals are engine speed (n_e), intake and exhaust manifold pressure (p_{im}, p_{em}) and turbocharger speed (n_t). The observed signals are the mass flow into the engine W_{ei}, oxygen mass fraction X_{Oim}, λ_O and x_{egr}. All these signals can be seen in the block "Signals" in Fig. 5.

The set-points and the limit needed for the controller (see Fig. 5) vary with operation conditions during driving. These signals are provided by an engine and emission management system as depicted in Fig. 1. The limit and the set-points are obtained from measurements and tuned to achieve stable combustion and the legislated emissions requirements. They are then represented as look-up tables being functions of operating conditions.

5.2   Main feedback loops

The starting point for the design is the structure in Fig. 1 in Sec. 2. Based on an analysis of the system properties in Sec. 4 two main feedback loops are chosen. In the presentation to follow the resulting choice (Eqs. (20) and (21)) is presented first and then the analysis that motivates it is given.

The main loops are

$$u_{egr} = -\mathrm{PID}\left(e_{\lambda_O}\right) \tag{20}$$

$$u_{vgt} = -\mathrm{PID}\left(e_{xegr}\right) \tag{21}$$

where $e_{\lambda_O} = \lambda_O^s - \lambda_O$ and $e_{xegr} = x_{egr}^s - x_{egr}$. These two main feedback loops are selected to handle items 1 and 3 of the control objectives stated in Sec. 2.2. In the first loop λ_O is controlled to a set-point λ_O^s with the control signal u_{egr} and in the second loop intake manifold EGR-fraction, x_{egr}, is controlled to its set-point, x_{egr}^s, with the control signal u_{vgt}. The PID controllers have a minus sign since the corresponding channels have negative DC-gains in almost the entire operating region (see Sec. 4).

The rationale behind the choice of the two main feedback loops are as follows. Relating to the system properties in Sec. 4, both actuators could straightforwardly be chosen for control of the EGR-fraction. However, for both actuators the λ_O performance variable requires care, and the proposed choice of main control loops relies on the following facts. Firstly, the channel from u_{vgt} to λ_O has a sign reversal and a non-minimum phase behavior (see Sec. 4.1), that are avoided in the proposed structure (20) because u_{egr} is used to control λ_O. Secondly, also the channel from u_{egr} to λ_O has a sign reversal and a non-minimum phase behavior in some few operating points where the EGR-valve is closed to half open (see Sec. 4.1). However, in all these operating points λ_O is much larger than its set-point λ_O^s which makes the EGR-valve to open up (according to (20)). Consequently, the system will leave these operating points, and the influence of the non-minimum phase behavior and the sign reversal thus only have effects in transients passing these operating points.

Another reason for the choice of the main control loops are that more undershoots in λ_O will appear if the main control loops are switched. In such a case a system analysis shows that the fast decrease in λ_O, coupled to a load increase, will cause a closing of the VGT before a closing of the EGR-valve, leading to an increase in the EGR mass flow and therefore an unnecessary decrease in λ_O in the beginning of the transient (see [17] for more details). Further, an analysis of the relative gain array supports the proposed input-output pairing for the main control loops according to Sec. 4.2.

5.3   Additional feedback loops

In order to achieve the control objectives 3 and 5 stated in Sec. 2.2, two additional feedback loops are added to the main control loops (20)–(21). Also in this section, the equations are stated first, and then the reasons are given. Two loops are added

according to

$$u_{egr} = \min(-\text{PID}_1(e_{\lambda_O}), \text{PID}_2(e_{xegr})) \tag{22}$$

$$u_{vgt} = \max(-\text{PID}_3(e_{xegr}), -\text{PID}_4(e_{nt})) \tag{23}$$

where $e_{nt} = n_t^s - n_t$. Note that there is no minus sign for PID_2 since the corresponding channel has positive DC-gain. All other channels have negative DC-gain in almost the entire operating region (see Sec. 4). All the PID controllers have integral action, and their derivative part will be discussed in Sec. 5.7.

The additional feedback loops in the structure (22)–(23), are motivated as follows. In operating points with low engine torque there is too much EGR, although the VGT is fully open. To achieve control objective 3 also for these operating points, a lower EGR-fraction x_{egr} is obtainable by closing the EGR-valve u_{egr} using $\text{PID}_2(e_{xegr})$ in (22). The appropriate value for u_{egr} is then the smallest value of the outputs from the two different PID controllers i.e. the more closed EGR setting is used. In order to get a simple control structure, x_{egr}^s is set larger than zero in operating points where $e_{\lambda_O} > 0$ and $u_{egr} = 0$ so that $\text{PID}_3(e_{xegr})$ in (23) closes the VGT in order to increase λ_O. To achieve control objective 5 and avoid over-speeding of the turbo, the VGT is also influenced by the turbine speed n_t in (23). In this case n_t is controlled with u_{vgt} to a set-point n_t^s which has a value slightly lower than the maximum limit n_t^{max} in order to avoid that overshoots shall exceed n_t^{max}. The appropriate value for u_{vgt} is then the largest value of the outputs from the two different controllers, which means that the VGT is opened up, thereby decreasing the input torque to the turbocharger, and thereby keeping its speed within limits.

5.4   Minimizing pumping work

The control structure (22)–(23) is not guaranteed to minimize the pumping work. This can be understood from the model equations as follows. It is clear from (11) that a given flow W_{egr} can be achieved for different combinations of flow area $A_{egr}(\tilde{u}_{egr})$ and $\frac{p_{em} \Psi_{egr}\left(\frac{p_{im}}{p_{em}}\right)}{\sqrt{T_{em}}}$. The key observation is that there are many combinations of the flow area and pressure loss that can give the same flow, and consequently there are many u_{egr} and u_{vgt} that can give the same x_{egr} in cases when $\lambda_O > \lambda_O^s$. Thus in some cases when $\lambda_O > \lambda_O^s$ both u_{egr} and u_{vgt} are governed by e_{xegr}. In stationary conditions, when $\text{PID}_2(e_{xegr})$ and $\text{PID}_3(e_{xegr})$ in (22)–(23) have converged, the controller fulfills the control objectives but the EGR-valve and VGT are not guaranteed to minimize the pumping work.

To achieve control objective 6, i.e. to minimize the pumping work, two additional control modes are added to the control structure (22)–(23) according to

$$u_{egr}(t_i) = \begin{cases} \min\left(-\text{PID}_1(e_{\lambda_O}), \\ \text{PID}_2(e_{xegr})\right) & , \text{if } u_{vgt}(t_{i-1}) = 100 \\ \\ -\text{PID}_1(e_{\lambda_O}) & , \text{else} \end{cases} \tag{24}$$

$$u_{vgt}(t_i) = \begin{cases} 100 & , \text{if } (u_{vgt}(t_{i-1}) = 100) \\ & \& \, (e_{xegr} < 0.01) \\ \\ \max\left(-\text{PID}_3(e_{xegr}), \right. \\ \left. -\text{PID}_4(e_{nt})\right) & , \text{else} \end{cases} \tag{25}$$

In this structure u_{egr} is calculated using a minimum selector only when $u_{vgt} = 100$, compared to (22) that always has a minimum selector. This subtle difference results in minimized pumping work in stationary points by striving to open the actuators as much as possible. Looking at the pumping work minimization in more detail the important controller action is coupled to λ_O, and in particular the operating conditions where there is a degree of freedom i.e. when $\lambda_O > \lambda_O^s$. For these conditions there are now two cases. In the first case the proposed controller strives to reduce λ_O by opening the EGR-valve, through the second row in (24). To maintain x_{egr}^s, this action also forces the VGT to be opened as much as possible. Either λ_O^s is reached or $\text{PID}_1(e_{\lambda_O})$ saturates at fully open, due to the integral action. In the other case, coupled to the first rows in (24)–(25), the VGT is fully open and it is necessary to reduce x_{egr} by closing the EGR-valve to reach x_{egr}^s. In both cases the actuators are thus opened as much as possible while achieving control objectives 1 and 3.

From the physics we know that opening a valve reduces the pressure differences over the corresponding restriction, in particular (11) results in a lower pressure loss and minimized pumping work (17). Therefore control objective 6 is achieved through the mechanism that was explained above and that opens the EGR-valve and VGT. These properties are also confirmed in Fig. 4, which shows that the lowest pumping work is achieved when the EGR-valve and VGT are opened as much as possible while keeping the control objectives. The only exceptions are in operating points with low torque, low engine speed, half to fully open EGR-valve, and half to fully open VGT. In these operating points there is a sign reversal in the gain from VGT to pumping work. However, the proposed control structure is not extended to handle this sign reversal, since the maximum profit according to simulations would only be 2.5 mBar, which is an insignificant value.

In case 1 in (25) the VGT is locked to fully open (the value 100) until $e_{xegr} > 0.01$ in order to avoid oscillations between case 1 and 2 in (24).

Simulations have been performed, under the same conditions as in [19], and they show that the proposed control structure (24)–(25) reduces the pumping work with 66% compared to the control structure (22)–(23). However, when considering the modeling and measurements errors the reduction is calculated to be at least 56%, and this leads to a reduction in fuel consumption with 4%.

5.5   Effect of sign reversal in VGT to EGR-fraction

The system properties in Sec. 4.1 show that the DC-gain from u_{vgt} to x_{egr} has a sign reversal in a small operating region, and an important question is what effect this sign reversal has on the control performance. This sign reversal occurs in operating points with half to fully open EGR-valve and half to fully open VGT

and in these operating points λ_O is much larger than its set-point λ_O^s which makes the EGR-valve to be fully open if $u_{vgt} < 100$ (according to case 2 in (24)). If $u_{vgt} < 100$ and $x_{egr} < x_{egr}^s$ in the beginning of a transient the VGT position decreases until $x_{egr} = x_{egr}^s$ (according to PID$_3(e_{xegr})$ in (25)), consequently the system will leave the operating region with reversed sign. If $u_{vgt} < 100$ and $x_{egr} > x_{egr}^s$ in the beginning of a transient the VGT position increases until it is fully open and then PID$_2(e_{xegr})$ in (24) becomes active and closes the EGR-valve until $x_{egr} = x_{egr}^s$. Consequently, the system can not get caught in the operating region with reversed sign while PID$_3(e_{xegr})$ in (25) is active, i.e. the system can not get caught in an unstable mode. However, the effect of this sign reversal is that there exist two sets of solutions for the EGR-valve and the VGT-position for the same value of x_{egr}^s depending on if $x_{egr} < x_{egr}^s$ or if $x_{egr} > x_{egr}^s$ in the beginning of a transient. However, the proposed control structure is not extended to handle this sign reversal, since the maximum profit in pumping work would only be 2.5 mBar, which is the same value as the maximum profit in the previous section due to that the sign reversal in VGT to EGR-fraction occurs partly in the same operating points as the sign reversal in VGT to pumping work.

5.6   Feedforward fuel control

Engine torque control, control objective 4, is achieved by feedforward from the set-point M_e^s by utilizing the torque model and calculating the set-point value for u_δ according to

$$u_\delta^s = c_1 M_e^s + c_2(p_{em} - p_{im}) + c_3 n_e^2 + c_4 n_e + c_5$$

which is obtained by solving u_δ from (17)–(19). This feedforward control is implemented in the block "Delta feedforward" in Fig. 5.

Aggressive transients can cause λ_O to go below its hard limit λ_O^{min} resulting in exhaust smoke. The PID controller in the main loop (20) is not designed to handle this problem. To handle control objective 2, a smoke limiter is used which calculates the maximum value of u_δ. The calculation is based on engine speed n_e, mass flow into the engine W_{ei}, oxygen mass fraction X_{Oim} and lower limit of oxygen/fuel ratio λ_O^{min}

$$u_\delta^{max} = \frac{W_{ei}\, X_{Oim}\, 120}{\lambda_O^{min}\, (O/F)_s\, 10^{-6}\, n_{cyl}\, n_e}$$

which is implemented in the block "Smoke limiter" in the top of Fig. 5.

Combining these two the final fuel control command is given by

$$u_\delta = \min(u_\delta^{max}, u_\delta^s) \tag{26}$$

which concludes the description and the motivation of the control structure in Fig. 5.

5.7   Derivative parts

It has been found that the loop from VGT-position to turbocharger speed ($\text{PID}_4(e_{nt})$ in (25)) benefits from a derivative part in order to predict high turbocharger speeds. This is due to the large time constant in the corresponding open-loop channel. The channel $u_{egr} \to \lambda_O$ also has a large time constant, but there is a lower demand on the band width for $\text{PID}_1(e_{\lambda_O})$ compared to $\text{PID}_4(e_{nt})$, and consequently $\text{PID}_1(e_{\lambda_O})$ does not need a derivative part. None of the other PID controllers need a derivative part due to smaller time constants in the corresponding channels.

5.8   PID parameterization and tuning

Each PID controller has the following parameterization

$$\text{PID}_j(e) = K_j \left(e + \frac{1}{T_{ij}} \int e \, dt + T_{dj} \frac{de}{dt} \right) \tag{27}$$

where the index j is the number of the different PID controllers in (24)–(25). The PID controllers are implemented in incremental form which leads to anti-windup and bump-less transfer between the different control modes [23].

Regarding tuning, the systematic analysis of the control problem in Sec. 4 has in this section been used to map the control objectives to the controller structure. This coupling to objectives gives the foundation for systematic tuning, be it manual or automatic. In the next section this will be utilized for automatic tuning, and it is also an advantage to have this conceptual coupling when doing manual fine tuning.

6   Automatic Controller Tuning

In the proposed structure there are four PID controllers that need tuning. There are conflicting goals as it is not possible to get both good transient response and good EGR tracking at the same time and trade-offs have to be made. This can be a cumbersome work and therefore an efficient and systematic method, for tuning the parameters K_j, T_{ij}, and T_{dj} in (27), has been developed. As a result the following non-linear least squares problem is formulated

$$\begin{aligned} \min \ &V(\theta) \\ \text{s.t.} \ &\theta > 0 \end{aligned} \tag{28}$$

where θ is the parameter vector

$$\theta = [K_1, \, T_{i1}, \, K_2, \, T_{i2}, \, K_3, \, T_{i3}, \, K_4, \, T_{i4}, \, T_{d4}]^T \tag{29}$$

The control objectives in Sec. 2.2 and the system properties in Sec. 4 are mapped to a quadratic performance measure, where each term reflects either control objectives or actuator stress. The motivation for each term is given below, and the cost function is calculated as

$$V(\theta) = \sum_{i=1}^{N} \gamma_{Me} \left(\frac{e_{Me}(t_i, \theta)}{M_{eNorm}} \right)^2 + \gamma_{egr} \left(\frac{e_{xegr}(t_i, \theta)}{x_{egrNorm}} \right)^2$$

$$+ \left(\frac{u_{egr}(t_i, \theta) - u_{egr}(t_{i-1}, \theta)}{u_{egrNorm}} \right)^2$$

$$+ \left(\frac{u_{vgt}(t_i, \theta) - u_{vgt}(t_{i-1}, \theta)}{u_{vgtNorm}} \right)^2$$

$$+ \gamma_{nt} \left(\frac{\max(n_t(t_i, \theta) - n_t^{max}, 0)}{n_{tNorm}} \right)^2$$

(30)

where t_i is the time at sample number i. All terms in (30) are normalized to get the same order of magnitude for the five terms, and this means that the weighting factors have an order of magnitude as $\gamma_{Me} \approx 1$ and $\gamma_{egr} \approx 1$.

These terms have been derived by analyzing the control objectives and system properties, and the connections and motives for them are given in the following paragraphs. Objectives 2 and 6 are fulfilled directly as they are built into the structure in terms of the smoke limiter and the pumping work minimization presented in Sec. 5.

Term 1

This term is the most intricate one and it is coupled to objectives 1 and 4 and they are in their turn related to each other through the system properties. They are related since a good transient response, especially during tip-in maneuvers, is connected to availability of oxygen and thus a fast λ_O-controller will give good transient response.

A further motivation for choosing to minimize engine torque deficiency, $e_{Me} = M_e^s - M_e$ comes from the fact that negative values of $e_{\lambda_O} = \lambda_O^s - \lambda_O$ are allowed, and it is positive e_{λ_O} values that have to be decreased. Now noting that torque deficiency occurs when the smoke limiter in Sec. 5.6 restricts the amount of fuel injected, i.e. when $\lambda_O = \lambda_O^{min}$ (see Fig. 7 between 309 s and 313 s). Since $\lambda_O^{min} < \lambda_O^s$ a positive e_{λ_O} exists when torque deficiency occurs.

One could also consider using e_{λ_O} directly but such a choice is not sufficiently sensitive during transients where there is a need for air. Due to the smoke limiter, e_{λ_O} will be limited to the difference $\lambda_O^s - \lambda_O^{min}$ when the smoke limiter is active and this does not reflect the actual demand for air and λ_O during transients. Thus the torque deficiency is selected as performance measure.

Term 2

This term is directly coupled to objective 3 and strives to minimize the EGR error $(e_{xegr} = x_{egr}^s - x_{egr})$.

Terms 3 and 4

These terms are coupled to the general issue of avoiding actuator stress, e.g. oscillatory behavior in the EGR valve or in the VGT control signals. The terms have equal weight since the control signals are of the same magnitude.

Term 5

This term is a direct consequence of objective 5 and avoids that the turbocharger speed exceeds its maximum limit. A high penalty is used, $\gamma_{nt} \approx 10^3$, to capture that this is a safety critical control loop.

In summary all control objectives are considered and handled in the tuning. Furthermore, the difficulty of tuning of the individual controllers, related to the trade-off between transient response (λ_O) and EGR errors, is efficiently handled by the two weighting factors γ_{Me} and γ_{egr}. This will be further illustrated in Sec. 7.2.

6.1   Solving (28)

A methodology for solving the optimization problem has been developed and the details are described in [18]. The important constituents are; a transient selection method and a solver for the optimization problem. Transient selection is made to reduce the computational time and the method identifies representative and aggressive transients where different control modes are excited. As a result computational time is reduced from 30 to 3 hours when using only the selected transients instead of a full ETC cycle.

The numerical solver for (28), described in [18], has three steps. Firstly, the tuning parameters are initialized using the Åström-Hägglund step-response method for pole-placement [23]. Secondly, a heuristic globalization-method is used to scan a large region around the initial values. Thirdly, a standard non-linear local least squares solver is used. It is worth to point out that the heuristics in the second step is important for avoiding that the local solver ends up in an unsatisfactory local minimum, see [18] for details.

7   European Transient Cycle simulations

The control tuning method is illustrated and applied, and a simulation study is performed on the European Transient Cycle (ETC). The cycle consists of three parts representing different driving conditions: urban (0-600 s), rural (600-1200 s), and high-way (1200-1800 s) driving.

The closed loop system, consisting of the model in Sec. 3 and the proposed control structure in Sec. 5 (depicted in Fig. 5), is simulated in Matlab/Simulink. The set points for λ_O and x_{egr} are authentic recordings that have been provided by industry. A remark is that an observer is not used in the simulations. Instead a low pass filter, with the time constant 0.02 s, is used to model the observer dynamics for all variables assumed to come from an observer. This is done in the block
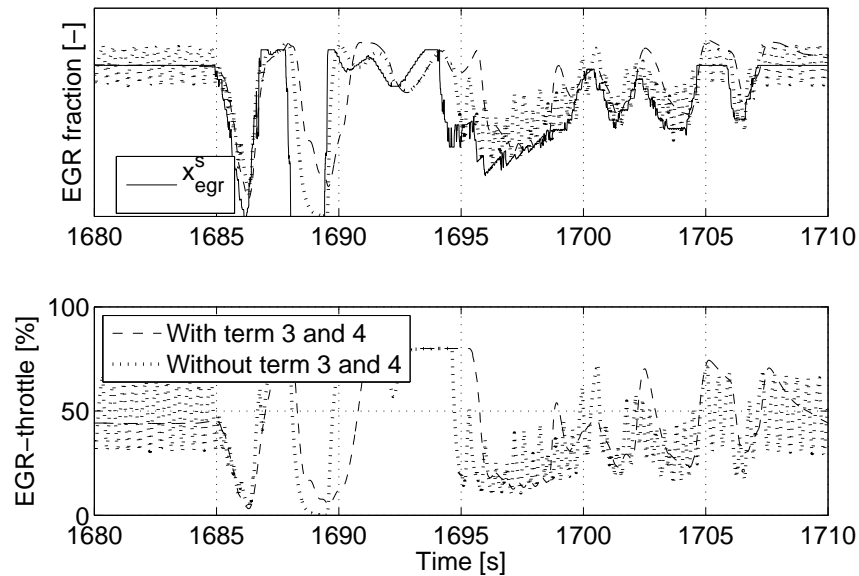
Figure 6 *Comparison in simulation between two sets of PID parameters. The first set of PID parameters is optimized using the cost function (30) and the second is optimized without term 3 and 4. The second set of PID parameters gives oscillations in the control signals. Consequently term 3 and 4 in the cost function are important in order to avoid oscillations.*

"Signals" in Fig. 5. The different signals in the cost function (30) are calculated by simulating the complete system and sampling the signals with a frequency of 100 Hz.

7.1   Actuator oscillations

The importance of terms 3 and 4 (actuator oscillations) in the cost function is illustrated in Fig. 6, where the control system is simulated with two sets of PID parameters. The first set of PID parameters is optimized using the cost function (30) and the second is optimized without terms 3 and 4. The second set of PID parameters gives oscillations in the control signals. Consequently terms 3 and 4 in the cost function are important in order to decrease actuator oscillations. Further, a tuning rule for avoiding oscillations in the control signals u_{egr} and u_{vgt} is to decrease the sum $\gamma_{Me} + \gamma_{egr}$ until the oscillations in the control signals disappear.

7.2   Balancing control objectives

The weighting factors γ_{Me}, γ_{egr}, and γ_{nt} in the cost function (30) are tuning parameters. When tuning these, trade-offs are made between torque deficiency, EGR error, pumping losses, and turbo over-speed.

   A tuning strategy for the relation between γ_{Me} and γ_{egr} is to increase γ_{Me} when a controller tuner wants to decrease the torque deficiency and increase γ_{egr} when a controller tuner wants to decrease the EGR error and the pumping losses. It is important that the sum $\gamma_{Me} + \gamma_{egr}$ is constant in order to avoid influence of the third and fourth term in the cost function when tuning the first and the second term. In the following section $\gamma_{Me} + \gamma_{egr} = 2$. A tuning strategy for avoiding turbo over-speeding is to increase γ_{nt} until the fifth term becomes equal to zero.

Illustration of performance trade-offs

The trade-offs between torque deficiency, EGR error, and pumping losses are illustrated in Fig. 7–8, where the control system is simulated on an aggressive transient from the ETC cycle with two sets of weighting factors. The first set is $\gamma_{Me} = 1$ and $\gamma_{egr} = 1$ and the second set is $\gamma_{Me} = 3/2$ and $\gamma_{egr} = 1/2$. The latter set of weighting factors punishes the torque deficiency more than the first one. Fig. 8 also shows the control modes for the EGR valve

$$\mathtt{mode}_{egr} = \begin{cases} 1 & \text{, if } \mathrm{PID}_1(e_{\lambda_O}) \text{ active} \\ 2 & \text{, if } \mathrm{PID}_2(e_{xegr}) \text{ active} \end{cases} \tag{31}$$

and the VGT position

$$\mathtt{mode}_{vgt} = \begin{cases} 1 & \text{, if } u_{vgt} = 100 \\ 2 & \text{, if } \mathrm{PID}_3(e_{xegr}) \text{ active} \\ 3 & \text{, if } \mathrm{PID}_4(e_{nt}) \text{ active} \end{cases} \tag{32}$$

   The setting $\gamma_{Me} = 3/2$ and $\gamma_{egr} = 1/2$ gives less torque deficiency but more EGR error and more pumping losses compared to $\gamma_{Me} = 1$ and $\gamma_{egr} = 1$, which is seen in Fig. 7–8 in the following way. Between 305 and 308 s the engine torque is low which leads to a high λ_O, an open EGR-valve, and that the VGT position controls the EGR-fraction so that the EGR error is low. Thereafter, an increase in engine torque at 308 s leads to a decrease in λ_O and therefore a closing of the EGR-valve. This closing is faster if γ_{Me}/γ_{egr} is increased from 1 to 3 which leads to a lower EGR-fraction (i.e. more EGR error), a more closed VGT position, a faster increase in turbocharger speed, and consequently a lower torque deficiency. Note that the torque deficiency and the EGR error can not be low at the same time during the aggressive transient. Note also that there are more pumping losses at $\gamma_{Me} = 3/2$ and $\gamma_{egr} = 1/2$ due to that the EGR-valve and the VGT position are more closed. Consequently, in dynamic conditions trade-offs are made between torque deficiency
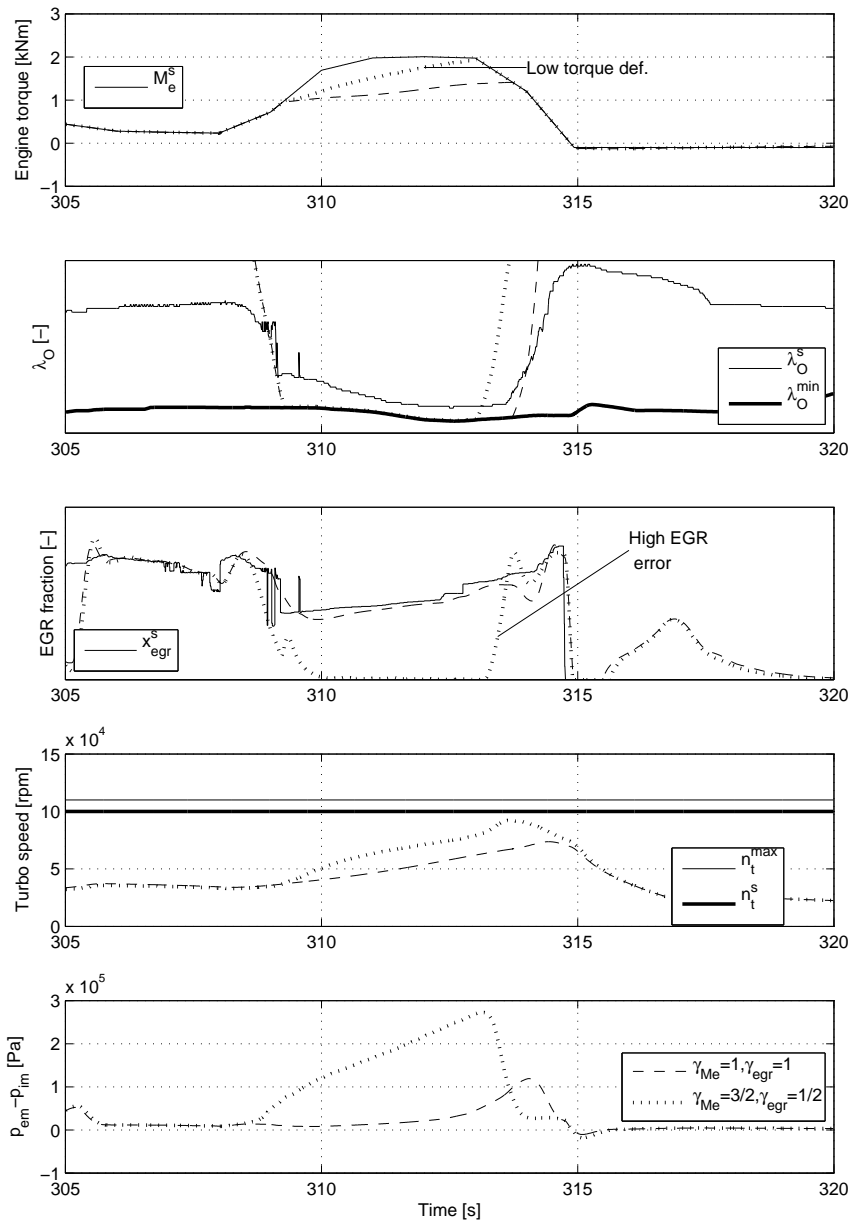
Figure 7 *Comparison between two simulations of the control system using two sets of weighting factors. The first set is $\gamma_{Me} = 1$ and $\gamma_{egr} = 1$ and the second set is $\gamma_{Me} = 3/2$ and $\gamma_{egr} = 1/2$. The latter set of weighting factors gives less torque deficiency but more EGR error and more pumping losses compared to the first set of weighting factors.*
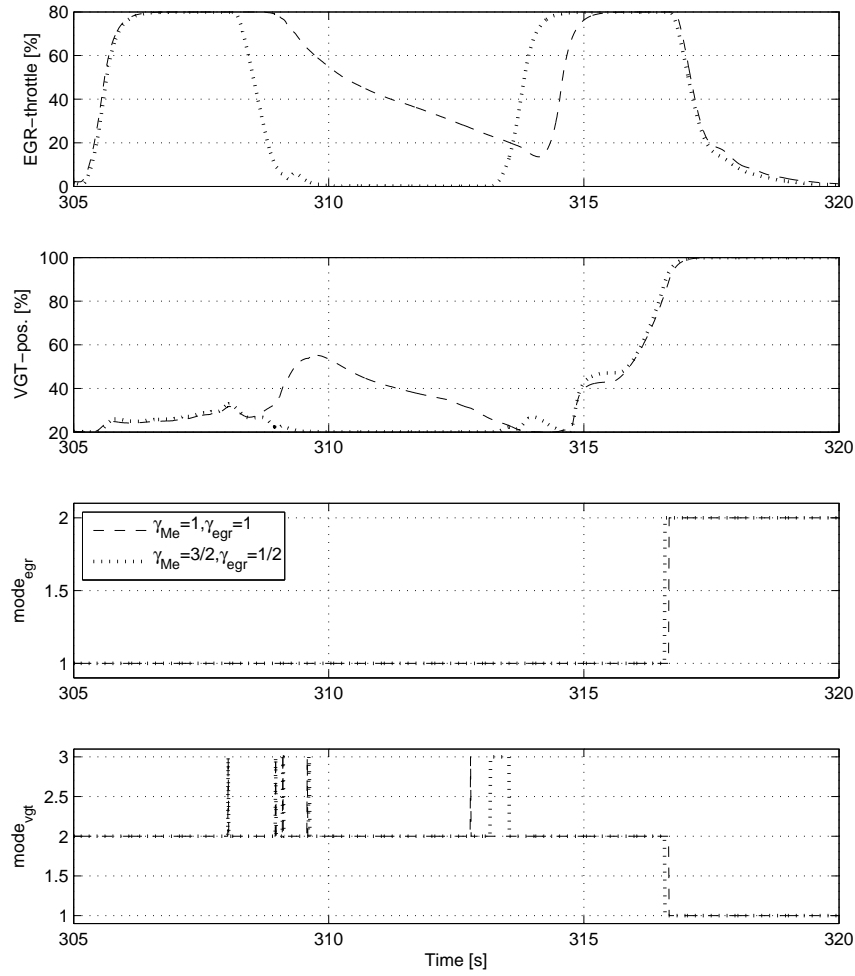
Figure 8 *Control inputs and control modes for the simulations in Fig. 7.*

and pumping loss. However, it is important to note that the pumping loss is still minimized in stationary points by the proposed control structure in both cases in Fig. 7–8 compared to the other control structure in Sec. 5.3 that gives higher pumping losses.

All the trade-offs between different performance variables described in this section are also valid for the complete cycle. This is illustrated by simulating the complete ETC cycle [17].

8   Engine test cell experiments

The control structure proposed in Sec. 5 (depicted in Fig. 5) is applied and validated in an engine test cell on the complete ETC cycle. The goal is to experimentally verify that the control structure achieves the control objectives stated in Sec. 2.2 and to compare it to the current production control system.

An available production observer, similar to the one in [13], is used to estimate the oxygen mass fraction X_{Oim}. Once X_{Oim} is estimated, the mass flow into the engine W_{ei}, λ_O and x_{egr} are calculated using (8) and (16). The engine speed (n_e), intake and exhaust manifold pressure (p_{im}, p_{em}) and turbocharger speed (n_t) are measured with production sensors. The set points for λ_O and x_{egr} are given as functions of the operating point and have been provided by industry and are the same for all controllers. The injection timing control has been provided by industry. The PID parameters are initially tuned using the method in Sec. 6 with $\gamma_{Me} = 3/2$ and $\gamma_{egr} = 1/2$, and are then manually fine tuned in the engine test cell experiments. The motive for choosing these weighting factors is that they represent a worst case scenario concerning the EGR-error and the pumping work. This worst case scenario is used in the experiments in order to show that the proposed control system reduces the pumping work compared to the current production control system for all reasonable sets of weighting factors. This can be understood as follows. According to Fig. 7–8, the selected weighting factors $\gamma_{Me} = 3/2$ and $\gamma_{egr} = 1/2$ give low torque deficiency, high pumping work, and high EGR-errors and consequently NO_x emissions that perhaps do not fulfill the legislated emission limits. The pumping work becomes higher when increasing γ_{Me}/γ_{egr}, however this leads to even higher EGR-errors and increases the NO_x emissions which is undesirable. Therefore, $\gamma_{Me} = 3/2$ and $\gamma_{egr} = 1/2$ are considered to be a worst case scenario concerning the EGR-error and the pumping work.

8.1   Investigation of the control objectives

The validation of the control structure on the complete ETC cycle shows that it achieves the control objectives in Sec. 2.2. This is illustrated by showing an aggressive transient from the ETC cycle in Fig. 9–10. Note that this transient was not used in the automatic tuning process in Sec. 6. The fulfillment is assessed in the following way.

Control objective 1 is achieved since λ_O is larger than the set-point λ_O^s except when the torque increases rapidly at 253 s and when λ_O has a small undershoot at 263 s. To handle this, the controller closes both the EGR-throttle and the VGT-position at 253 s and the controller closes the EGR-throttle at 263 s in order to increase λ_O as fast as possible. Control objective 2 is achieved since λ_O is always larger than or equal to the minimum limit λ_O^{min}. Note that the smoke limiter is active when $\lambda_O = \lambda_O^{min}$. Control objective 3 is achieved since x_{egr} follows its set-point x_{egr}^s except when $\lambda_O = \lambda_O^{min}$ at 253.5 s and when λ_O decreases rapidly at 259 s. At these points it is important to increase λ_O, so therefore the EGR-throttle is closed which results in an EGR-error. Control objective 4 is achieved
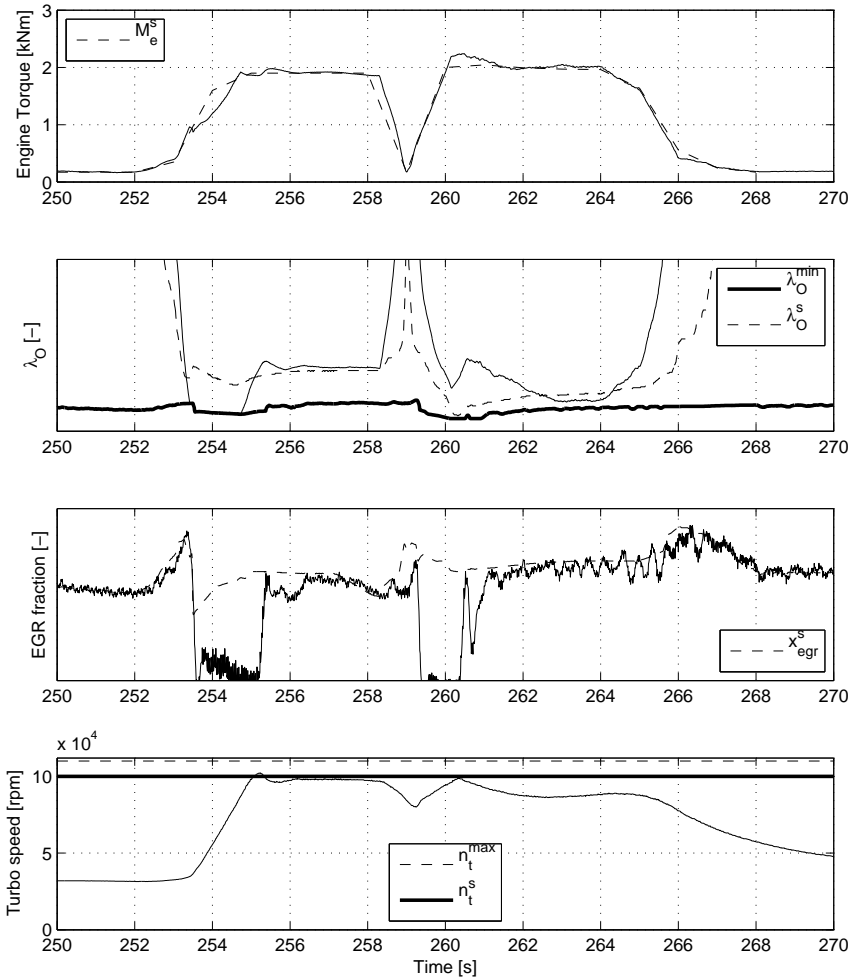
Figure 9 *Validation of the proposed control structure in an engine test cell on an aggressive transient from the ETC cycle. Note that this transient was not used in the automatic tuning process in Sec. 6. The proposed control structure achieves all the control objectives stated in Sec. 2.2.*
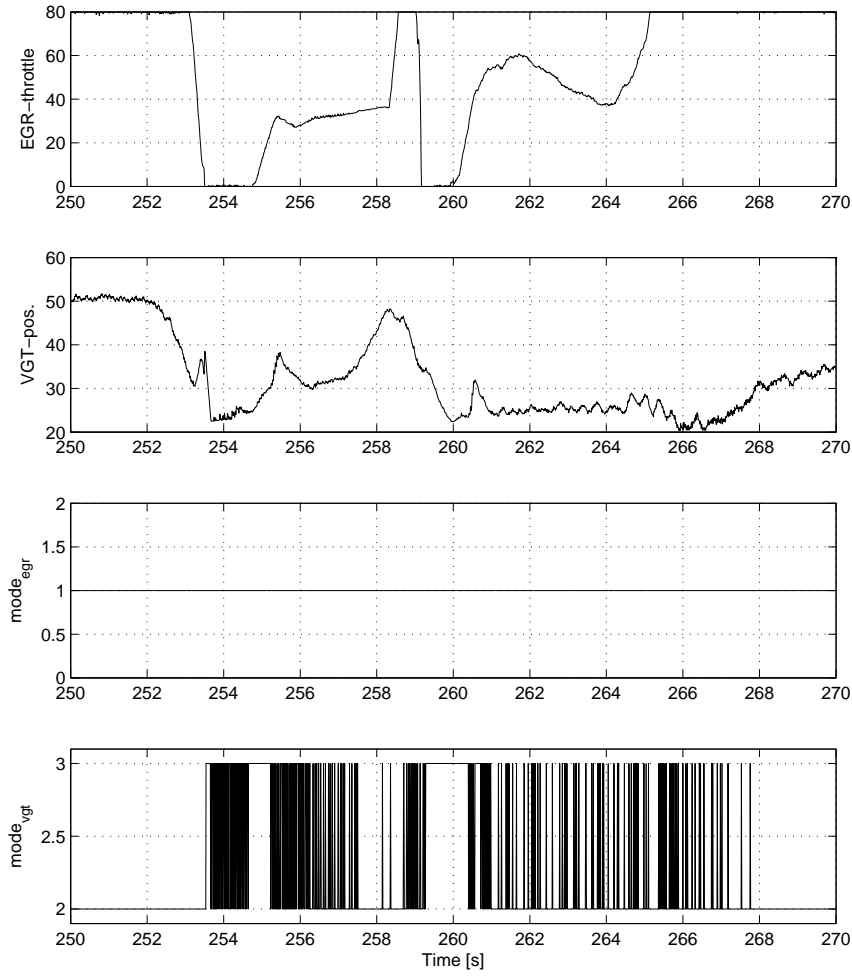
Figure 10 *Control inputs and control modes for the experiment in Fig. 9.*

since M_e follows its set-point M_e^s except when the smoke limiter is active at 253.5 s. Control objective 5 is achieved since the turbocharger speed is always smaller than its maximum value n_t^{max}. Finally, control objective 6 is achieved since the EGR-throttle is opened as much as possible when $\lambda_O > \lambda_O^s$, yielding minimized pumping loss. This can been seen at 250 s, 258.5 s, and 265 s where the EGR-throttle is fully open while the VGT controls the EGR-fraction. Quantitatively, following the calculation in Sec. 5.4, the pumping losses are calculated to be reduced at least 50%. The oscillations in $mode_{vgt}$ are due to measurement noise and that the outputs from $\text{PID}_3(e_{xegr})$ and $\text{PID}_4(e_{nt})$ have approximately the same values at these points. These oscillations are not harmful, since the PID controllers are

implemented in incremental form yielding bump-less transfer.

Consequently, the proposed control structure achieves all the control objectives in Sec. 2.2. Further, the experiment shows that the control structure has good control performance with fast control of the performance variables and systematic handling of trade-offs.

8.2   Comparison to the current production control system

The proposed control structure is compared to the current production system on the complete ETC cycle by comparing λ_O-error, x_{egr}-error, and pumping losses

$$E_{\lambda_O} = \sum_{i=1}^{N} \max(e_{\lambda_O}(t_i), 0)$$

$$E_{x_{egr}} = \sum_{i=1}^{N} |e_{xegr}(t_i)| \tag{33}$$

$$PMEP = \sum_{i=1}^{N} (p_{em}(t_i) - p_{im}(t_i))$$

where t_i is the time at sample number i. The comparison in Tab. 1 shows that the two controllers have approximately the same control performance in the main performance variables λ_O and x_{egr} and that the production controller has 26% higher pumping losses yielding 1.4% higher fuel consumption, that is significant for a truck engine. The differences in E_{λ_O} and $E_{x_{egr}}$ between the controllers are only due to that the tuning of the controllers have different trade-offs between λ_O-error and x_{egr}-error. The tuning of the proposed controller is selected to be a worst case scenario concerning the EGR-error and the pumping work according to Sec. 8. Since the production controller gives more pumping losses for this worst case scenario, it will have at least 26% higher pumping losses for all reasonable sets of weighting factors in the tuning of the proposed controller.

Table 1 *The measures (33) for two different controllers over the ETC cycle, showing that the production controller has 26% higher pumping losses. The measures are normalized with respect to the proposed controller.*

Controller	E_{λ_O}	$E_{x_{egr}}$	PMEP
Proposed controller	1.00	1.00	1.00
Production controller	1.50	0.60	1.26

9   Conclusions

A control structure with PID controllers and selectors has been proposed and investigated for coordinated control of oxygen/fuel ratio λ_O and intake manifold

EGR-fraction x_{egr}. These were chosen both as performance and feedback variables since they give information about when it is allowed to minimize the pumping work. This pumping work minimization is a novel and simple strategy and compared to another control structure which closes the EGR-valve and the VGT more, the pumping work is substantially reduced. Further, the chosen variables are strongly coupled to the emissions and therefore they give advantages in an industrial perspective where the inner loop is combined with an outer loop in an engine management system in a way suited for efficient calibration.

Based on a system analysis, λ_O is controlled by the EGR-valve and x_{egr} by the VGT-position, mainly to handle the sign reversal from VGT to λ_O. Besides controlling the two main performance variables, λ_O and x_{egr}, the control structure also successfully handles torque control, including torque limitation due to smoke control, and supervisory control of turbo charger speed for avoiding over-speeding. Further, the systematic analysis of the control problem in Section 4 was used to map the control objectives to the controller structure, and this conceptual coupling to objectives gives the foundation for systematic tuning, be it manual or automatic. This was utilized to develop an automatic controller tuning method. The objectives to minimize pumping work and ensure the minimum limit of λ_O are handled by the structure, while the other control objectives are captured in a cost function, and the tuning is formulated as a non-linear least squares problem.

Different performance trade-offs are necessary and they were illustrated on the European Transient Cycle. The proposed controller is validated in an engine test cell, where it is experimentally demonstrated that the controller achieves all control objectives and that the current production controller has at least 26% higher pumping losses compared to the proposed controller.

Acknowledgments

Notation

Table 2 *Symbols used in the paper.*

Symbol	Description	Unit
A	Area	m^2
c_p	Spec. heat capacity, constant pressure	$J/(kg \cdot K)$
e	Control error	—
J	Inertia	$kg \cdot m^2$
K_j	Gain in a PID	—
M	Torque	Nm
M_e	Engine torque	Nm
n_{cyl}	Number of cylinders	—

Symbol	Description	Unit
n_e	Rotational engine speed	rpm
n_t	Rotational turbine speed	rpm
$(O/F)_s$	Stoichiometric oxygen-fuel ratio	—
p	Pressure	Pa
P	Power	W
q_{HV}	Heating value of fuel	J/kg
r_c	Compression ratio	—
R	Gas constant	$J/(kg \cdot K)$
R	Radius	m
t	Time	s
T	Temperature	K
T_{dj}	Derivative time in a PID	s
T_{ij}	Integral time in a PID	s
T_s	Sample time	s
u_{egr}	EGR control signal. 100:open 0:closed	%
u_{vgt}	VGT control signal. 100:open 0:closed	%
u_δ	Injected amount of fuel	mg/cycle
V	Volume	m^3
V	Cost function	—
W	Mass flow	kg/s
x_{egr}	EGR fraction	—
X_O	Oxygen mass fraction	—
γ	Specific heat capacity ratio	—
γ	Weighting factor	—
η	Efficiency	—
θ	PID parameters	—
λ_O	Oxygen-fuel ratio	—
Π	Pressure quotient	—
τ	Time constant	s
Φ_c	Volumetric flow coefficient	—
ω	Rotational speed	rad/s

Table 3 *Indices used in the paper.*

Index	Description	Index	Description
a	air	fric	friction
amb	ambient	ig	indicated gross
c	compressor	im	intake manifold
d	displaced	m	mechanical
e	exhaust	Norm	normalized
egr	EGR	Setp	set-point
ei	engine cylinder in	t	turbine
em	exhaust manifold	vgt	VGT
eo	engine cylinder out	vol	volumetric
f	fuel	δ	fuel injection

References

[1] M. Ammann, N.P. Fekete, L. Guzzella, and A.H. Glattfelder. Model-based Control of the VGT and EGR in a Turbocharged Common-Rail Diesel Engine:

Theory and Passenger Car Implementation. *SAE Technical paper 2003-01-0357*, January 2003.

[2] A. Amstutz and L. Del Re. EGO sensor based robust output control of EGR in diesel engines. *IEEE Transactions on Control System Technology*, pages 37–48, 1995.

[3] Jonathan Chauvin, Gilles Corde, Nicolas Petit, and Pierre Rouchon. Motion planning for experimental airpath control of a diesel homogeneous charge-compression ignition engine. *Control Engineering Practice*, 2008.

[4] L. Guzzella and A. Amstutz. Control of diesel engines. *IEEE Control Systems Magazine*, 18:53–71, 1998.

[5] J.B. Heywood. *Internal Combustion Engine Fundamentals*. McGraw-Hill Book Co, 1988.

[6] M. Jankovic, M. Jankovic, and I.V. Kolmanovsky. Constructive lyapunov control design for turbocharged diesel engines. *IEEE Transactions on Control Systems Technology*, 2000.

[7] Merten Jung, Keith Glover, and Urs Christen. Comparison of uncertainty parameterisations for H-infinity robust control of turbocharged diesel engines. *Control Engineering Practice*, 2005.

[8] Uwe Kiencke and Lars Nielsen. *Automotive Control Systems For Engine, Driveline, and Vehicle*. Springer-Verlag, second edition, 2005.

[9] I.V. Kolmanovsky, A.G. Stefanopoulou, P.E. Moraal, and M. van Nieuwstadt. Issues in modeling and control of intake flow in variable geometry turbocharged engines. In *Proceedings of 18$^{\text{th}}$ IFIP Conference on System Modeling and Optimization*, Detroit, July 1997.

[10] Shigeki Nakayama, Takao Fukuma, Akio Matsunaga, Teruhiko Miyake, and Toru Wakimoto. A new dynamic combustion control method based on charge oxygen concentration for diesel engines. In *SAE Technical Paper 2003-01-3181*, 2003. SAE World Congress 2003.

[11] M. Nieuwstadt, P.E. Moraal, I.V. Kolmanovsky, A. Stefanopoulou, P. Wood, and M. Widdle. Decentralized and multivariable designs for EGR–VGT control of a diesel engine. In *IFAC Workshop, Advances in Automotive Control*, 1998.

[12] M.J. Nieuwstadt, I.V. Kolmanovsky, P.E. Moraal, A.G. Stefanopoulou, and M. Jankovic. EGR–VGT control schemes: Experimental comparison for a high-speed diesel engine. *IEEE Control Systems Magazine*, 2000.

[13] R. Rajamani. Control of a variable-geometry turbocharged and wastegated diesel engine. *Proceedings of the I MECH E Part D Journal of Automobile Engineering*, November 2005.

[14] J. Rückert, F. Richert, A. Schloßer, D. Abel, O. Herrmann, S. Pischinger, and A. Pfeifer. A model based predictive attempt to control boost pressure and EGR–rate in a heavy duty diesel engine. In *IFAC Symposium on Advances in Automotive Control*, 2004.

[15] J. Rückert, A. Schloßer, H. Rake, B. Kinoo, M. Krüger, and S. Pischinger. Model based boost pressure and exhaust gas recirculation rate control for a

diesel engine with variable turbine geometry. In *IFAC Workshop: Advances in Automotive Control*, 2001.

[16] A.G. Stefanopoulou, I.V. Kolmanovsky, and J.S. Freudenberg. Control of variable geometry turbocharged diesel engines for reduced emissions. *IEEE Transactions on Control Systems Technology*, 8(4), July 2000.

[17] Johan Wahlström. Control of EGR and VGT for emission control and pumping work minimization in diesel engines. Licentiate Thesis, Linköping University, 2006.

[18] Johan Wahlström, Lars Eriksson, and Lars Nielsen. Controller tuning based on transient selection and optimization for a diesel engine with EGR and VGT. In *Electronic Engine Controls*, number 2008-01-0985 in SAE Technical paper series SP-2159, SAE World Congress, Detroit, USA, 2008.

[19] Johan Wahlström, Lars Eriksson, Lars Nielsen, and Magnus Pettersson. PID controllers and their tuning for EGR and VGT control in diesel engines. In *Preprints of the 16th IFAC World Congress*, Prague, Czech Republic, 2005.

[20] Johan Wahlström and Lars Eriksson. Modeling of a diesel engine with VGT and EGR including oxygen mass fraction. Technical report, Linköping University, 2006.

[21] Johan Wahlström, Lars Eriksson, and Lars Nielsen. System analysis of a diesel engine with VGT and EGR. Technical report, Linköping University, 2009.

[22] Kemin Zhou, John C. Doyle, and Keith Glover. *Robust and optimal control*. Prentice-Hall, Inc., Upper Saddle River, NJ, USA, 1996.

[23] K. J. Åström and T. Hägglund. *PID Controllers: Theory, Design and Tuning*. Research Triangle Park, Instrument Society of America, 2nd edition, 1995.

Controller Tuning based on Transient Selection and Optimization for a Diesel Engine with EGR and VGT[1]

Johan Wahlström, Lars Eriksson, and Lars Nielsen

Vehicular Systems, Department of Electrical Engineering,
Linköping University, S-581 83 Linköping,
Sweden.

4

Abstract

In modern Diesel engines Exhaust Gas Recirculation (EGR) and Variable Geometry Turbochargers (VGT) have been introduced to meet the new emission requirements. A control structure that coordinates and handles emission limits and low fuel consumption has been developed. This controller has a set of PID controllers with parameters that need to be tuned. To be able to achieve good performance, an optimization based tuning method is developed and tested. In the optimization the control objectives are captured by a cost function. To aid the tuning a systematic method has been developed for selecting representative and significant transients that excite different modes in the controller. The performance is evaluated on the European Transient Cycle. It is demonstrated how weighting factors in the cost function influence control behavior, and that the proposed tuning method gives a significant improvement in control performance compared to standardized tuning methods for PID controllers. Further, the proposed tuning method and the control structure are applied and validated on an engine in a test cell, where it is demonstrated that the control structure achieves all stated control objectives.

---

[1]This paper has been published as the conference paper "Controller tuning based on transient selection and optimization for a diesel engine with EGR and VGT" by Johan Wahlström, Lars Eriksson, and Lars Nielsen, SAE Technical paper 2008-01-0985, Detroit, USA, 2008. The most important sections in this publication is the automatic tuning method in Sec. 5 and the simulation results in Sec. 6. The control approach in Sec. 2, the control structure in Sec. 4, and the experimental validations in Sec. 7 are more completely described in Publication 3.

1   Introduction

Legislated emission limits for heavy duty trucks are constantly reduced. To fulfill the requirements, technologies like Exhaust Gas Recirculation (EGR) systems and Variable Geometry Turbochargers (VGT) have been introduced. The primary emission reduction mechanisms utilized to control the emissions are that NO_x can be reduced by increasing the intake manifold EGR-fraction and smoke can be reduced by increasing the air/fuel ratio [5]. Note that recirculated exhaust gases, present in the intake, also contain oxygen which makes it more suitable to define and use the oxygen/fuel ratio λ_O instead of the traditional air/fuel ratio [17]. The main motive for this is that it is the oxygen contents that is crucial for smoke generation and the idea is to use the oxygen content of the cylinder instead of air mass flow, see e.g. [10]. Besides λ_O it is natural to use EGR-fraction x_{egr} as the other main performance variable, but one could also use the burned gas fraction instead of the EGR-fraction. Note that the emissions NO_x and smoke are not used as performance variables, since this would require either sensors or observers for these.

The oxygen/fuel ratio λ_O and EGR fraction x_{egr} depend in complicated ways on the EGR and VGT actuation. It is therefore necessary to have coordinated control of the EGR and VGT to reach the legislated emission limits in NO_x and smoke and various approaches have been published. Reference [4] presents a good overview of different control aspects of diesel engines with EGR and VGT. In [12] there is a comparison of some control approaches with different selections of performance variables, and in [14] decoupling control is investigated. Other control approaches are described in [2, 6, 11, 15, 1, 13, 18].

In a joint industrial collaboration, a coordinated EGR and VGT control structure has been proposed in [17] that provides a convenient way to handle emission requirements and at the same time optimizes the engine efficiency by minimizing the pumping work. This structure formulates the emission control strategy in terms of performance variables, that have a direct relation to the NO_x and smoke emissions, which gives a structure with natural separation between control design and emission fine tuning. The control engineer can focus on the control loop performance while the calibration engineer can fine tune the controller setpoints to fulfill the emission limits. For a successful application of this control structure, it is advantageous that it besides good behavior and good interfaces is straightforward to calibrate and re-calibrate in order to save time when adapting to hardware changes. Therefore, this paper proposes an automatic tuning method for all controller parameters in the controller structure.

1.1   Outline

The proposed tuning method is based on optimization of a cost function, that reflects the control objectives, and the tuning is formulated as a non-linear least squares problem in Sec. 5. To aid the tuning a systematic method is developed for selecting significant transients that exhibit different challenges for the controller.

The fine tuning through optimization is then performed on the selected transients. In Sec. 6 simulations on a European Transient Cycle (ETC) are used to illustrate the transient selection method, and controller tuning and performance. Different performance trade-offs are illustrated and discussed. The proposed tuning method and the control structure are validated in collaboration with Scania CV AB in an engine test cell where the goal is to investigate if the control structure achieves the control objectives and the results are discussed in Sec. 7. Before reaching the main content of the paper (Sec. 5–7) background is provided. Sec. 2 describes the key ideas behind the control structure and the control objectives related to EGR and VGT control. Sec. 3 describes a mean value diesel engine model, focused on gas flows, that is used for tuning and simulation evaluations of the closed-loop system. The recently proposed control structure is reviewed in Sec. 4.

2 Control approach

This paper proposes an automatic tuning method of a recently proposed control structure for coordinated control of EGR-fraction and oxygen/fuel ratio λ_O, which is a novel choice of performance variables. Previous related work as cited above cover other control approaches with different performance variables in the loop. The most common choice of performance variables in the papers above are compressor air mass flow and intake manifold pressure.

The choice of EGR-fraction and oxygen/fuel ratio λ_O as performance variables are described and investigated in [17] and the two main advantages are as follows. The first advantage is as mentioned above that these variables are strongly connected to the emissions, compared to e.g. manifold pressure and air mass flow. The second advantage follows from the first one in that it gives a natural separation within the engine control system. The performance variables are handled in a fast inner loop, whereas trade-offs between e.g. emissions and response time for different operating conditions are made in an outer loop. The idea with two loops is depicted in Fig. 1. The focus in this paper is on the control design of the inner loop. Note that focusing entirely on the emissions during the assessment of the inner loop could be misleading since the emissions depend strongly on the set points that have been generated for the inner loop. Therefore, the goal is to judge the performance in terms of the set point following instead of emissions.

Neither EGR-fraction nor λ_O are normally measured and have to be estimated using observers. The observer design is important, but it is not the focus in this paper. Examples of observer designs for thermodynamic states and gas compositions can be found in [12, 13, 9, 3, 16, 7].

In addition to control EGR-fraction and λ_O it is also necessary to have fuel control, since the driver's demand must be actuated. This is achieved through basic fuel control using feedforward. Furthermore it is also important to monitor and control turbocharger speed since aggressive transients can cause damage through over-speeding.
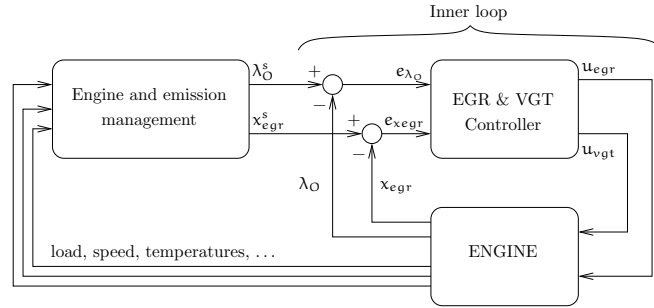
Figure 1 *A cascade control structure, with an inner loop where EGR and VGT actuators are controlled using the main performance variables EGR fraction x_{egr} and oxygen/fuel ratio λ_O. This sketch is a simplified illustration of the main idea that will be completed in Sec. 4 to also include fuel control and turbo protection.*

2.1   Control objectives

The primary performance variables to be controlled are engine torque M_e, normalized oxygen/fuel ratio λ_O, intake manifold EGR-fraction x_{egr} and turbocharger speed n_t. The goal is to follow a driving cycle while maintaining low emissions, low fuel consumption, and suitable turbocharger speeds, which together with the discussion above gives the following control objectives for the performance variables.

1. λ_O should be greater than a soft limit, a set-point λ_O^s, which enables a trade off between emission, fuel consumption, and response time.

2. λ_O is not allowed to go below a hard minimum limit λ_O^{min}, otherwise there will be too much smoke. Note that λ_O^{min} is always smaller than λ_O^s.

3. The EGR-fraction x_{egr} should follow its set-point. There will be more NO_x if the EGR-fraction is too low and there will be more smoke if the EGR-fraction is too high.

4. The engine torque should follow the set-point from the drivers demand.

5. The turbocharger speed is not allowed to exceed a maximum limit, otherwise the turbocharger can be damaged.

6. The pumping losses M_p should be minimized in stationary operating points in order to decrease the fuel consumption.
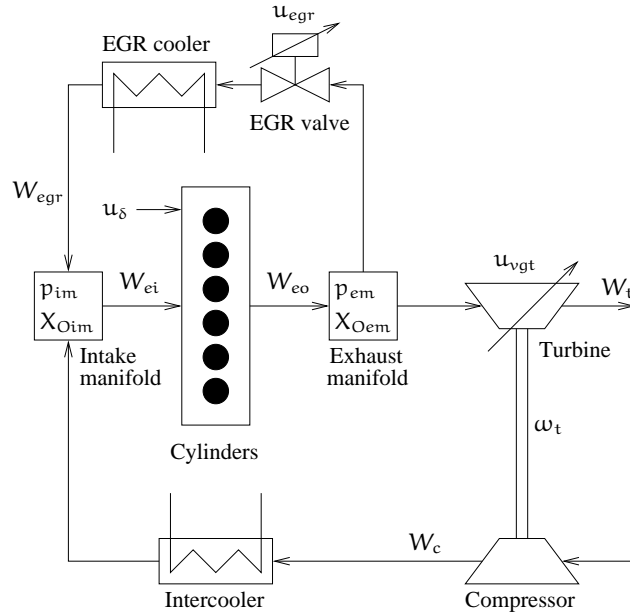
Figure 2 *Sketch of the diesel engine model used for simulation, control design, and tuning. It has five main states related to the engine (p_{im}, p_{em}, X_{Oim}, X_{Oem}, and ω_t) and two states for actuator dynamics ($\tilde{u}_{egr}$ and $\tilde{u}_{vgt}$).*

3   Diesel engine model

A diesel engine model is used for tuning and validation of the developed controller structure, see [19]. This diesel engine model is focused on the gas flows, see Fig. 2, and it is a mean value model with seven states: intake and exhaust manifold pressures (p_{im} and p_{em}), oxygen mass fraction in the intake and exhaust manifold (X_{Oim} and X_{Oem}), turbocharger speed (ω_t), and two states describing the actuator dynamics for the two control signals ($\tilde{u}_{egr}$ and $\tilde{u}_{vgt}$). These states are collected in a state vector x

$$x = (p_{im} \quad p_{em} \quad X_{Oim} \quad X_{Oem} \quad \omega_t \quad \tilde{u}_{egr} \quad \tilde{u}_{vgt})^\mathsf{T} \tag{1}$$

There are no state equations for the manifold temperatures, since the pressures and the turbocharger speed govern the most important system properties, such as non-minimum phase behaviors, overshoots, and sign reversals, while the temperature dynamics have only minor effects on these system properties.

It is important that the model focusing on the gas flows can be utilized both for different vehicles having the same engine but different driveline parameters and for engine testing, calibration, and certification in an engine test cell. In many of these

situations the engine operation is defined by the rotational speed n_e, for example given as a drivecycle, and therefore it is natural to parameterize the model using engine speed. The resulting model is thus expressed in state space form as

$$\dot{x} = f(x, u, n_e) \tag{2}$$

where the engine speed n_e is considered as an input to the model, and u is the control input vector

$$u = (u_\delta \quad u_{egr} \quad u_{vgt})^\mathsf{T} \tag{3}$$

which contains mass of injected fuel u_δ, EGR-valve position u_{egr}, and VGT actuator position u_{vgt}. The EGR-valve is closed when $u_{egr} = 0\,\%$ and open when $u_{egr} = 100\,\%$. The VGT is closed when $u_{vgt} = 0\,\%$ and open when $u_{vgt} = 100\,\%$.

A detailed description and derivation of the model together with a model tuning and a validation against test cell measurements is given in [19].

4 Control structure

The control design objective is to actuate u_δ, u_{egr}, and u_{vgt} in order to achieve the control objectives stated in Sec. 2.1. The diesel engine is a non-linear and coupled system and these properties could be considered using multivariable non-linear controllers. However, here the approach is to build a controller structure using min/max-selectors and SISO controllers for EGR and VGT control, and to use feedforward for fuel control. There are two reasons for looking at SISO controllers. Firstly, SISO controllers are accepted by the industry. Secondly, the idea is to develop a simple structure that captures the essential requirements on a controller handling all the control objectives.

Many different SISO controllers are available, but throughout the presentation PID controllers will be used. The solution is proposed and motivated in [17], but it is reviewed in the following sections and a MATLAB/SIMULINK schematic of the full control structure is shown in Fig. 3, where all signals and the fuel controller are included together with the EGR and VGT controller depicted in Fig. 1.

4.1 Signals, set-points and a limit

The signals needed for the controller are assumed to be either measured or estimated using observers. The measured signals are engine speed (n_e), intake and exhaust manifold pressure (p_{im}, p_{em}) and turbocharger speed (n_t). The observed signals are the mass flow into the engine W_{ei}, oxygen mass fraction X_{Oim}, λ_O and x_{egr}. All these signals can be seen in the block "Signals" in Fig. 3.

The set-points and the limit needed for the controller (see Fig. 3) vary with operation conditions during driving. These signals are provided by an engine and emission management system as depicted in Fig. 1. The limit and the set-points are obtained from measurements and tuned to achieve the legislated emissions requirements. They are then represented as look-up tables being functions of operating conditions.
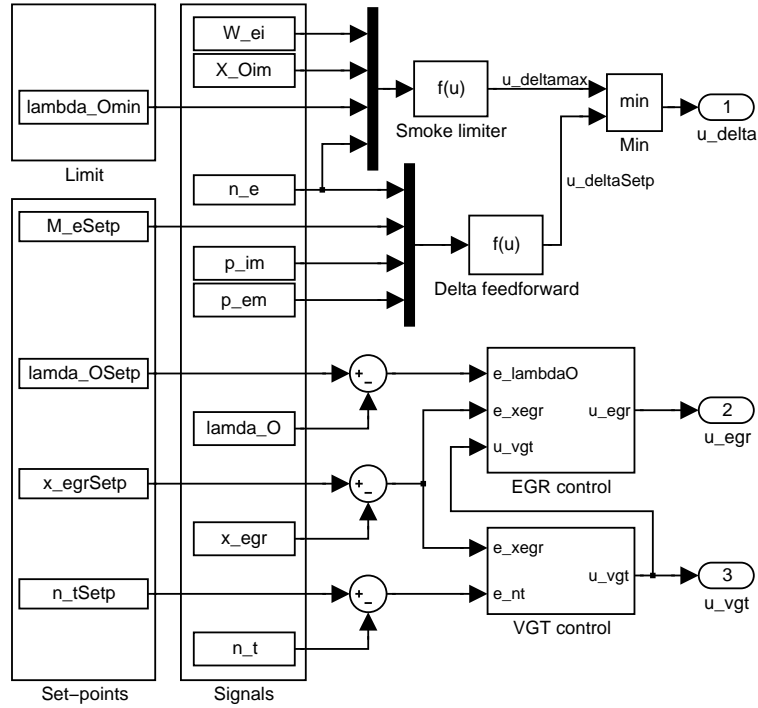
Figure 3 *The control structure, as* MATLAB/SIMULINK *block diagram,
showing; a limit, set-points, measured and observed signals, fuel control
with smoke limiter, together with the main controllers for EGR and VGT.*

4.2   Main feedback loops

The following main feedback loops are used

$$u_{egr} = -\text{PID}\left(e_{\lambda_O}\right) \tag{4}$$

$$u_{vgt} = -\text{PID}\left(e_{xegr}\right) \tag{5}$$

where $e_{\lambda_O} = \lambda_O^s - \lambda_O$ and $e_{xegr} = x_{egr}^s - x_{egr}$. These two main feedback loops
are selected to handle items 1 and 3 of the control objectives stated in Sec. 2.1. It
is known that the DC-gain in $u_{vgt} \to \lambda_O$ changes sign with operating point [8].
However, the main feedback loops in (4)–(5) handle this sign reversal because u_{egr}
is used to control λ_O.

4.3   Additional control modes

In order to achieve the control objectives 3, 5, and 6 stated in Sec. 2.1, additional control modes are added to the main control loops (4)–(5) according to

$$u_{egr}(t_i) = \begin{cases} \begin{aligned} &\min\left(-\text{PID}_1(e_{\lambda_O}),\right. \\ &\left.\text{PID}_2(e_{xegr})\right) \end{aligned} & , \text{if } u_{vgt}(t_{i-1}) = 100 \\[2mm] -\text{PID}_1(e_{\lambda_O}) & , \text{else} \end{cases} \tag{6}$$

$$u_{vgt}(t_i) = \begin{cases} 100 & , \text{if } (u_{vgt}(t_{i-1}) = 100) \\ & \quad \& \,(e_{xegr} < 0.01) \\[2mm] \begin{aligned} &\max\left(-\text{PID}_3(e_{xegr}),\right. \\ &\left.-\text{PID}_4(e_{nt})\right) \end{aligned} & , \text{else} \end{cases} \tag{7}$$

where $e_{nt} = n_t^s - n_t$. Note that there is no minus sign for PID_2 since the corresponding channel has positive DC-gain. All other channels have negative DC-gain in almost the entire operating region [17].

The additional control modes in the structure (6)–(7) are motivated as follows. In operating points with low engine torque there is too much EGR, although the VGT is fully open. To achieve control objective 3 also for these operating points, a lower EGR-fraction x_{egr} is obtainable by closing the EGR-valve u_{egr} when $u_{vgt} = 100$ using $\text{PID}_2(e_{xegr})$ in (6). To achieve control objective 5 and avoid over-speeding of the turbo, the VGT is also influenced by the turbine speed n_t in (7). In this case n_t is controlled with u_{vgt} to a set-point n_t^s which has a value slightly lower than the maximum limit n_t^{max} in order to avoid that overshoots shall exceed n_t^{max}. Further, this structure also minimizes the pumping work in stationary points by striving to open the actuators as much as possible [17]. Consequently, control objective 6 is achieved. Note that there are sign reversals also in $u_{egr} \to \lambda_O$ and $u_{vgt} \to x_{egr}$. However, these sign reversals have only minor effects on the control performance and therefore the control structure is not extended to handle these effects.

In case 1 in (7) the VGT is locked to fully open (the value 100) until $e_{xegr} > 0.01$ in order to avoid oscillations between case 1 and 2 in (6).

4.4   PID parameterization and implementation

Each PID controller has the following parameterization

$$\text{PID}_j(e) = K_j \left(e + \frac{1}{T_{ij}} \int e \, dt + T_{dj} \frac{de}{dt} \right) \tag{8}$$

where the index j is the number of the different PID controllers in (6)–(7). The PID controllers are implemented in incremental form which leads to anti-windup and bump-less transfer between the different control modes [20].

4.5 Derivative parts

It is worth to point out that the loop from VGT-position to turbocharger speed ($\text{PID}_4(e_{nt})$ in (7)) does benefit from a derivative part in order to predict high turbocharger speeds. This is due to the large time constant in the corresponding open-loop channel. The channel $u_{egr} \to \lambda_O$ also has a large time constant, but there is a lower demand on the band width for $\text{PID}_1(e_{\lambda_O})$ compared to $\text{PID}_4(e_{nt})$, and consequently $\text{PID}_1(e_{\lambda_O})$ does not need a derivative part. None of the other PID controllers need a derivative part due to smaller time constants in the corresponding channels.

4.6 Fuel control

Engine torque control, control objective 4, is achieved by feedforward from the set-point M_e^s using the torque model and calculating the set-point value for u_δ according to

$$u_\delta^s = c_1 \, M_e^s + c_2 (p_{em} - p_{im}) + c_3 \, n_e^2 + c_4 \, n_e + c_5$$

This fuel control is implemented in the block "Delta feedforward" in Fig. 3.

Aggressive transients can cause λ_O to go below its hard limit λ_O^{min} resulting in exhaust smoke. The PID controller in the main loop (4) is not designed to handle this problem. Therefore, to handle control objective 2, a smoke limiter is used which calculates the maximum value of u_δ. The calculation is based on engine speed n_e, mass flow into the engine W_{ei}, oxygen mass fraction X_{Oim} and lower limit of oxygen/fuel ratio λ_O^{min}

$$u_\delta^{max} = \frac{W_{ei} \, X_{Oim} \, 120}{\lambda_O^{min} \, (O/F)_s \, 10^{-6} \, n_{cyl} \, n_e}$$

which is implemented in the block "Smoke limiter" in the top of Fig. 3.

Combining these two the final fuel control command is given by

$$u_\delta = \min(u_\delta^{max}, u_\delta^s) \tag{9}$$

which concludes the description and the description of the control structure in Fig. 3.

5 Automatic Controller Tuning

In the control structure (6)–(7) there are four PID controllers that need to be tuned. This can be a cumbersome work and therefore this section proposes an efficient method for automatically finding the tuning parameters K_j, T_{ij}, and T_{dj} in (8) off-line, based upon the control objectives in Sec. 2.1 and the model in Sec. 3.

5.1   Cost function

The automatic tuning method is obtained by formulating the control objectives in Sec. 2.1 as a non-linear least squares problem

$$
\begin{aligned}
& \min V(\theta) \\
& \theta > 0
\end{aligned}
\tag{10}
$$

where θ is the vector of PID parameters

$$
\theta = [K_1,\, T_{i1},\, K_2,\, T_{i2},\, K_3,\, T_{i3},\, K_4,\, T_{i4},\, T_{d4}]^{\mathsf{T}}
\tag{11}
$$

The cost function $V(\theta)$ consists of 5 terms where each term reflects either a control objective or an actuator stress. The first term uses a special signal to penalize λ_O error (see the motive below). The cost function is calculated as

$$
\begin{aligned}
V(\theta) = \sum_{i=1}^{N} \;& \gamma_{Me}\left(\frac{e_{Me}(t_i,\theta)}{M_{eNorm}}\right)^2 + \gamma_{egr}\left(\frac{e_{xegr}(t_i,\theta)}{x_{egrNorm}}\right)^2 \\
& + \left(\frac{u_{egr}(t_i,\theta) - u_{egr}(t_{i-1},\theta)}{u_{egrNorm}}\right)^2 \\
& + \left(\frac{u_{vgt}(t_i,\theta) - u_{vgt}(t_{i-1},\theta)}{u_{vgtNorm}}\right)^2 \\
& + \gamma_{nt}\left(\frac{\max(n_t(t_i,\theta) - n_t^{max}, 0)}{n_{tNorm}}\right)^2
\end{aligned}
\tag{12}
$$

where t_i is the time at sample number i. The motives for the different terms in the cost function are:

Term 1

In order to decrease positive $e_{\lambda_O} = \lambda_O^s - \lambda_O$ (note that negative e_{λ_O} is allowed), term 1 minimizes engine torque deficiency ($e_{Me} = M_e^s - M_e$). Torque deficiency appears when the smoke limiter in Sec. 4.6 restricts the amount of fuel injected, i.e. when $\lambda_O = \lambda_O^{min}$ (see Fig. 6 between 309 s and 313 s). Since $\lambda_O^{min} < \lambda_O^s$, positive e_{λ_O} exists when torque deficiency appears.

Term 2

Minimizes EGR error ($e_{xegr} = x_{egr}^s - x_{egr}$).

Term 3 and 4

Avoid oscillations in the EGR valve and in the VGT control signals. The terms have equal weight.

Term 5

Avoids turbocharger overspeeding. This is a strict limit for machine protection and this limit is enforced using a high penalty, $\gamma_{nt} = 10^3$.

As seen in (12) all the terms are normalized in order to get the same order of magnitude for the five terms, and this means that the weighting factors have an order of magnitude as $\gamma_{Me} \approx 1$ and $\gamma_{egr} \approx 1$.

5.2 Optimization

A solver is proposed for the optimization problem stated in the previous section, and it consists of three phases: an initialization method, a globalization heuristic, and a local solver.

The tuning parameters are initialized using the Åström-Hägglund step-response method for pole-placement [20]. The values of the parameters are calculated in several different operating points since the system is non-linear, and then the mean values of the parameters over the entire operating range are used.

The non-linear least squares problem (10) has several local minima, and therefore precautions must be taken to avoid ending up in a bad local minimum. A global optimization method could be used, but these have the drawback of requiring long computational times. Instead a heuristic method is used to scan a large region around the initial values from Åström-Hägglund. This is done in Phase 2 below, by taking large steps in all directions narrowing in on a good local minimum with relatively short computational times. Then in Phase 3 a tailor made routine for solving least squares problems is used.

Phase 1: Find an initial guess.

1. Initialization: Åström-Hägglund step-response method.

Phase 2: Find a solution near a good local minimum.

1. For all $n = 1$ to 9:

   - Multiply $\theta(n)$ with 3, compute $V(\theta)$ and save its value together with the corresponding θ.

   - Divide $\theta(n)$ with 3, compute $V(\theta)$ and save its value together with the corresponding θ.

2. Choose the set of parameters θ which corresponds to the smallest value of the computed $V(\theta)$ in step 1.

3. Go to step 1 until the calculations don't find any smaller $V(\theta)$.

Phase 3: Finds the solution for the good local minimum.

1. Initial guess: Solution from phase 2.

2. Use a standard Matlab non-linear least squares problem solver.

This algorithm results in a better local minimum compared to if only phases 1 and 3 are used, so the heuristic in phase 2 is valuable.

5.3   Transient selection

If a complete driving cycle is used in the automatic tuning when calculating the cost function (12) it gives a long computational time. This computational time can be decreased if only some few transients are used. For example the European Transient Cycle (ETC) gives a computational time of 30 hours, but if only three transients from the ETC cycle are used the computational time is reduced to 3 hours. When selecting transients it is important that they are representative and significant, and therefore the following selection criteria are formulated.

Selection criterion 1

Below the EGR error measure E_{xegr} and the torque deficiency measure E_{Me} are introduced. The selected transients should be such that both these measures and the turbocharger speed n_t are high. This is achieved by selecting transients that consist of at least one of the ten highest values of each of these three.

The EGR error measure, E_{xegr}, increases linearly as function of time when $|e_{xegr}| > 1.5\%$ according to

$$E_{xegr}(t_i) = \begin{cases} E_{xegr}(t_{i-1}) + T_s & \text{, if } (|e_{xegr}(t_i)| > 1.5\%) \,\&\, (i \geq 1) \\ 0 & \text{, else} \end{cases}$$

where T_s is the sample time and $e_{xegr} = x^s_{egr} - x_{egr}$. The torque deficiency measure, E_{Me}, increases when $e_{Me} > 0$ according to

$$E_{Me}(t_i) = \begin{cases} E_{Me}(t_{i-1}) + T_s\, e_{Me}(t_i) & \text{, if } (e_{Me}(t_i) > 0) \,\&\, (i \geq 1) \\ 0 & \text{, else} \end{cases}$$

where $e_{Me} = M^s_e - M_e$.

Selection criterion 2

To capture the entire operating region the transients should include operating points with low flows and high flows respectively, i.e. low speed and torque and high speed and torque.

Selection criterion 3

It is important to find transients which excite all control modes in (6)–(7). Therefore the third selection criterion is to find transients which excite all control modes in the following control mode signals. The activation times for the different control modes shall be of approximately similar length.

Control modes for the EGR valve:

$$
\text{mode}_{egr} = \begin{cases} 1 & \text{, if } \text{PID}_1(e_{\lambda_O}) \text{ active} \\ 2 & \text{, if } \text{PID}_2(e_{xegr}) \text{ active} \end{cases} \tag{13}
$$

Control modes for the VGT position:

$$
\text{mode}_{vgt} = \begin{cases} 1 & \text{, if } u_{vgt} = 100 \\ 2 & \text{, if } \text{PID}_3(e_{xegr}) \text{ active} \\ 3 & \text{, if } \text{PID}_4(e_{nt}) \text{ active} \end{cases} \tag{14}
$$

Selection criterion 4

If the driving cycle consists of several driving conditions, at least one transient from each driving condition should be included in order to get representative transients for the complete driving cycle.

6   Results from European Transient Cycle simulations

The transient selection method and control tuning method are illustrated and applied, and a simulation study is performed on the European Transient Cycle (ETC). The cycle consists of three parts representing different driving conditions: urban (0-600 s), rural (600-1200 s), and high-way (1200-1800 s) driving.

The closed loop system, consisting of the model in Sec. 3 and the control structure in Sec. 4 (depicted in Fig. 3), is simulated in Matlab/Simulink. The set points for λ_O and x_{egr} are authentic recordings that have been provided by industry. A remark is that an observer is not used in the simulations. Instead a low pass filter is used on all variables assumed to come from an observer in order to model its time constant. This is done in the block "Signals" in Fig. 3. The different signals in the cost function (12) are calculated by simulating the complete system and sampling the signals with a frequency of 100 Hz. Note also that the EGR-valve position is saturated at 80% due to that the EGR-valve does not affect the system if the EGR-valve position is larger than 80%.

Table 1 *Selected transients from the ETC cycle that meet the selection criteria in Sec. 5.3. These transients are used when calculating the cost function* $V(\theta)$ *(12).*

Transient time interval	Characteristics
285-360 s	Urban driving, high torque deficiency, high turbocharger speed, low and high flow.
850-870 s	Rural driving, high EGR error and high torque deficiency.
1680-1720 s	High-way driving, $\mathtt{mode}_{egr} = 2$ and $\mathtt{mode}_{vgt} = 1$ have long activation times.

Table 2 *Activation times for the different control modes in* $\mathtt{mode}_{egr}$ *(13) and in* $\mathtt{mode}_{vgt}$ *(14) expressed in percentages of the total transient time for each selected transient in Tab. 1.*

Transient	$\mathtt{mode}_{egr}$		$\mathtt{mode}_{vgt}$		
	1	2	1	2	3
285-360 s	83	17	22	48	30
850-870 s	81	19	23	51	27
1680-1720 s	36	64	66	34	0

6.1   Transient selection results for the European Transient Cycle

The four criteria in the transient selection method (see Sec. 5.3) are fulfilled for the ETC cycle by selecting the transients manually according to Tab. 1, where the characteristics of each transient are summarized in the right column. More details about the selection are as follows. To apply the selection criteria, the control system is simulated during the complete ETC cycle using the initialized PID parameters according to Sec. 5.2, see Fig. 4. High values for the performance measures, as well as low and high values for both torque and engine speed that are close to each other are found in the first two transients in Tab. 1. Consequently, selection criteria 1 and 2 are fulfilled. Tab. 2 shows the activation times for the different control modes in $\mathtt{mode}_{egr}$ (13) and $\mathtt{mode}_{vgt}$ (14). In the first two transients, $\mathtt{mode}_{egr} = 2$ and $\mathtt{mode}_{vgt} = 1$ have short activation times. In order to get longer activation times for these two modes, the third transient is also used and thereby selection criterion 3 is fulfilled. Selection criterion 4 is fulfilled since the three transients in Tab. 1 are selected from the three driving conditions: urban, rural, and high-way driving.
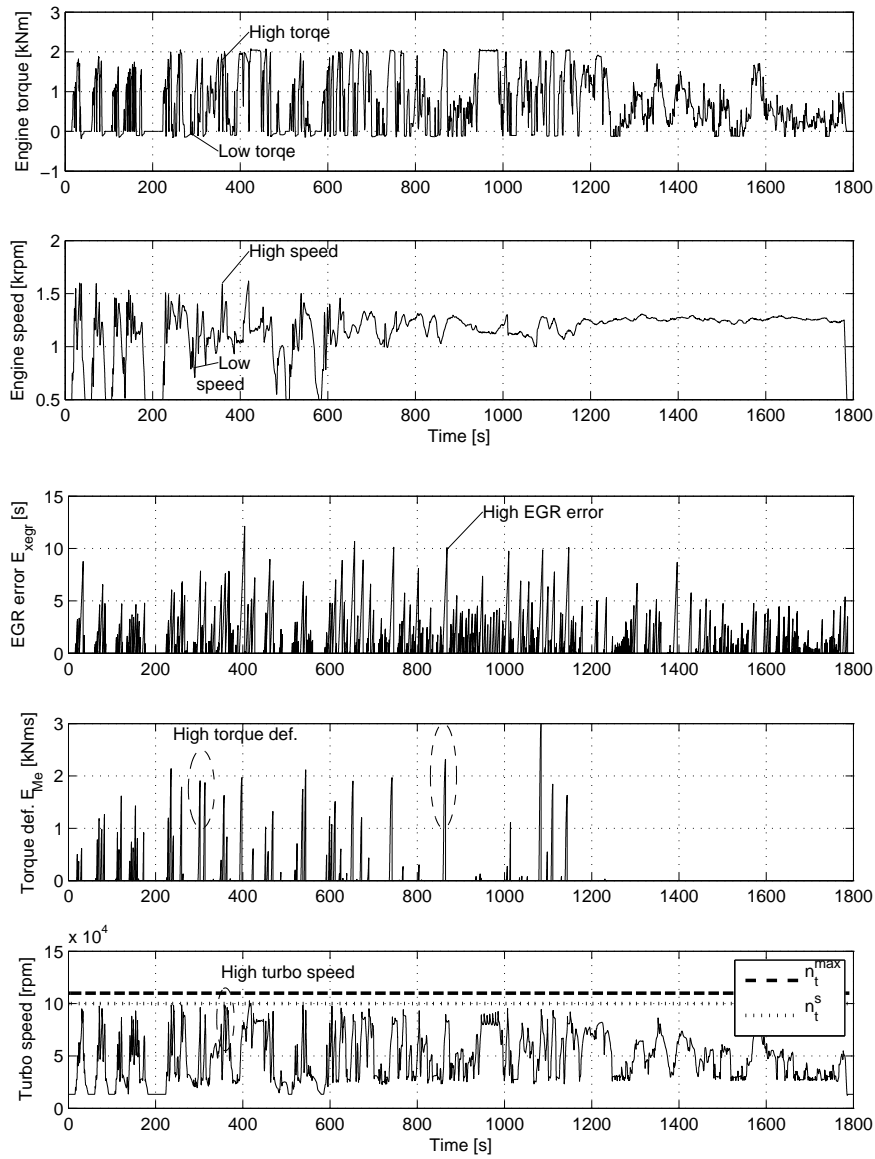
Figure 4 *Simulation of the control system during the complete ETC cycle using the initialized PID parameters according to Sec. 5.2. The goal is to find transients where the EGR error measures* E_{xegr}, *the torque deficiency measures* E_{Me}, *and the turbo speed are high and where the torque and speed are low and high, see Sec. 5.3. The result is the first two transients in Tab. 1, i.e. 285-360 s and 850-870 s.*
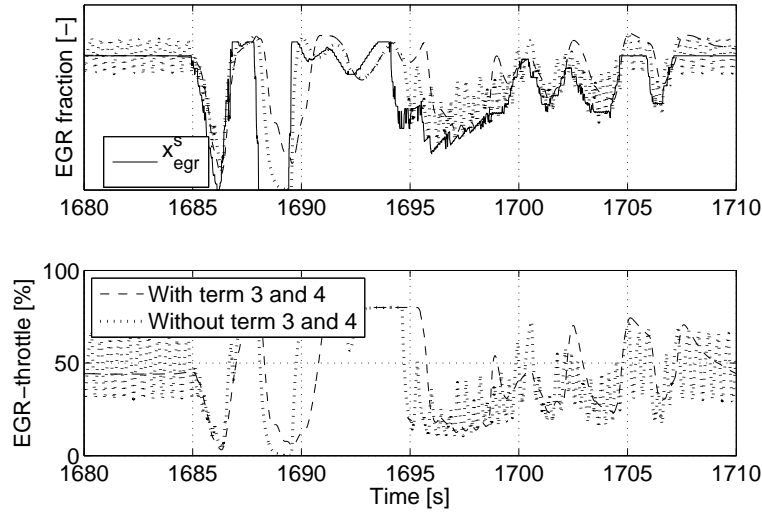
Figure 5 *Comparison in simulation between two sets of PID parameters. The first set of PID parameters is optimized using the cost function (12) and the second is optimized without term 3 and 4. The second set of PID parameters gives oscillations in the control signals. Consequently term 3 and 4 in the cost function are important in order to avoid oscillations.*

6.2 Actuator oscillations

The importance of term 3 and 4 (actuator oscillations) in the cost function is illustrated in Fig. 5, where the control system is simulated with two sets of PID parameters. The first set of PID parameters is optimized using the cost function (12) and the second is optimized without term 3 and 4. The second set of PID parameters gives oscillations in the control signals. Consequently term 3 and 4 in the cost function are important in order to decrease the actuator oscillations. This is also shown in Tab. 3, where the values of term 3 and 4 are lower at the optimized PID parameters than the values at the initialized PID parameters. Further, a tuning rule for avoiding oscillations in the control signals u_{egr} and u_{vgt} is to decrease the sum $\gamma_{Me} + \gamma_{egr}$ until the oscillations in the control signals disappear.

6.3 Balancing control objectives

The weighting factors γ_{Me}, γ_{egr}, and γ_{nt} in the cost function (12) are tuning parameters. When tuning these, trade-offs are made between torque deficiency, EGR error, pumping losses, and turbo over-speed.

A tuning strategy for the relation between γ_{Me} and γ_{egr} is to increase γ_{Me} when a controller tuner wants to decrease the torque deficiency and increase γ_{egr} when a controller tuner wants to decrease the EGR error and the pumping losses.

It is important that the sum $\gamma_{Me} + \gamma_{egr}$ is constant in order to avoid influence of the third and fourth term in the cost function when tuning the first and the second term. In the following sections $\gamma_{Me} + \gamma_{egr} = 2$. A tuning strategy for avoiding turbo over-speeding is to increase γ_{nt} until the fifth term becomes equal to zero.

The effects of the automatic tuning on the dynamic behavior, on the complete cycle, and on the controller parameters are described in the following sections.

Effect of tuning on dynamic behavior

The effect of the automatic tuning on the dynamic behavior is shown in Fig. 6, where the control system is simulated on a significant transient (a part of the first transient in Tab. 1) from the ETC cycle with two sets of weighting factors. The first set is $\gamma_{Me} = 1$ and $\gamma_{egr} = 1$ and the second set is $\gamma_{Me} = 3/2$ and $\gamma_{egr} = 1/2$. The latter set of weighting factors penalizes the torque deficiency more than the first one.

The setting $\gamma_{Me} = 3/2$ and $\gamma_{egr} = 1/2$ gives less torque deficiency but more EGR error and more pumping losses compared to $\gamma_{Me} = 1$ and $\gamma_{egr} = 1$, which is seen in Fig. 6 in the following way. Between 305 and 308 s the engine torque is low which leads to a high λ_O, an open EGR-valve, and that the VGT position controls the EGR-fraction so that the EGR error is low. Thereafter, an increase in engine torque at 308 s leads to a decrease in λ_O and therefore a closing of the EGR-valve. This closing is faster if γ_{Me}/γ_{egr} is increased from 1 to 3 which leads to a lower EGR-fraction (i.e. more EGR error), a more closed VGT position, a faster increase in turbocharger speed, and consequently a lower torque deficiency. Note also that there are more pumping losses at $\gamma_{Me} = 3/2$ and $\gamma_{egr} = 1/2$ due to that the EGR-valve and the VGT position are more closed during the transient.

Effect of tuning on complete cycle

The effect of the automatic tuning on the complete cycle is shown in Tab. 3, where the cost function (12) and its 5 terms together with the mean value of the pumping loss are calculated from simulations of the complete ETC cycle. Note that the relation between the 5 terms and the cost function in Tab. 3 is

$$\begin{aligned} V = &\gamma_{Me}(\text{Term 1}) + \gamma_{egr}(\text{Term 2}) + \\ &(\text{Term 3}) + (\text{Term 4}) + \gamma_{nt}(\text{Term 5}) \end{aligned} \tag{15}$$

Exactly as Fig. 6, Tab. 3 shows that $\gamma_{Me} = 3/2$ and $\gamma_{egr} = 1/2$ give less torque deficiency but more EGR error and more pumping losses compared to $\gamma_{Me} = 1$ and $\gamma_{egr} = 1$. Consequently, the selected transients in Tab. 1 are representative for the complete ETC cycle. Tab. 3 also shows that the turbocharger speed never exceeds its maximum limit during the ETC cycle except for $\gamma_{Me} = 1/2$ and $\gamma_{egr} = 3/2$ where the term 5 has a small positive value.

It is important to note that the pumping loss is minimized in stationary points by the control structure in all 4 cases in Tab. 3. However, in dynamic conditions trade-offs are made between torque deficiency and pumping loss according to Fig. 6.
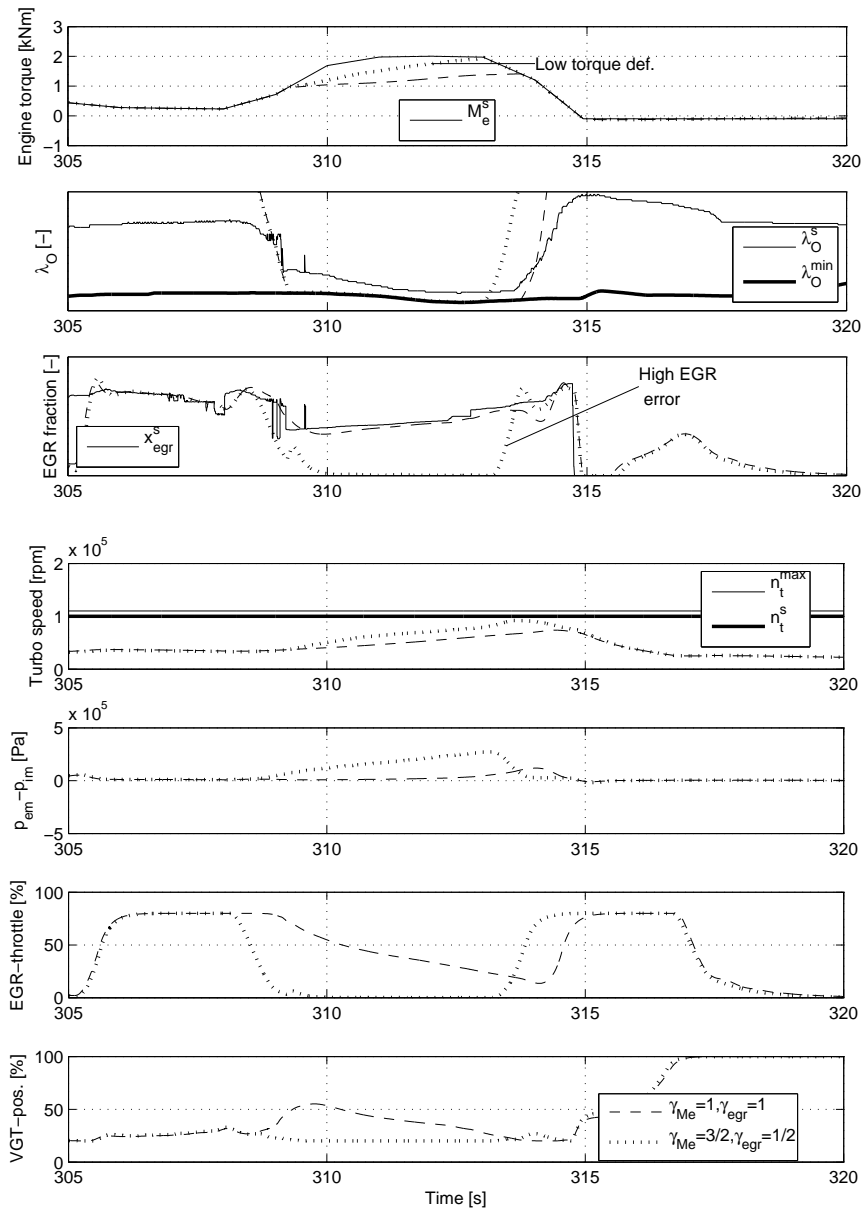
Figure 6 *Comparison between two simulations of the control system using two sets of weighting factors. The first set is $\gamma_{Me} = 1$ and $\gamma_{egr} = 1$ and the second set is $\gamma_{Me} = 3/2$ and $\gamma_{egr} = 1/2$. The latter set of weighting factors gives less torque deficiency but more EGR error and more pumping losses compared to the first set of weighting factors.*

Table 3 *Values of different variables computed from simulations of the complete ETC cycle using initialized and optimized PID parameters for three different sets of weighting factors. The variables are the 5 terms in the cost function (12), the cost function* V, *and the time mean value of the pumping loss. These variables show that the automatic tuning has a significant effect and improves the control performance.*

	θ_{init}	Optimized θ		
γ_{Me}		3/2	1	1/2
γ_{egr}		1/2	1	3/2
Term 1, torque deficiency	0.36	0.25	0.29	0.75
Term 2, EGR error	1.74	1.34	1.10	0.57
Term 3, u_{egr} diff.	0.32	0.17	0.14	0.07
Term 4, u_{vgt} diff.	0.17	0.05	0.04	0.07
Term 5, turbo over-speed	0	0	0	5e-05
V(Optimal θ)		1.27	1.57	1.41
V(Initial θ)		1.90	2.59	3.29
$\frac{1}{T}\int_0^T (p_{em} - p_{im})\, dt$ [bar]	0.27	0.35	0.31	0.22

These trade-offs can also be seen in Tab. 3, where a decrease in pumping loss leads to an increase in torque deficiency.

Using the cost function in Sec. 5.1 for tuning has a significant effect and improves the control performance compared to if only the initialization method in Sec. 5.2 is used. This is seen in Tab. 3, where the optimal values of the cost function V are lower than the initial values of V for all cases. It can also be seen that the values of the 5 terms in the cost function decrease for the optimized PID parameters compared to the values of the terms for the initialized PID parameters, except for the torque deficiency and turbo over-speed at $\gamma_{Me} = 1/2$ and $\gamma_{egr} = 3/2$.

Effect of tuning on controller parameters

The optimization steps in the automatic tuning method in Sec. 5.2 have a significant effect on the controller parameters. This is shown in Fig. 7 where the initialized and optimized PID parameters are calculated. The difference between the initialized and optimized K_4 is about 10^2 and for K_1 and K_3 the differences are about 10^1. Consequently, the initialization is far away from the optimal solution. It can also be seen in Fig. 7 that the optimized gains K_j are decreased compared to the initialized gains (except for K_2 at $\gamma_{Me} = 1$, $\gamma_{egr} = 1$), which means that the optimized PID parameters give a more cautious control compared to the initialized parameters.
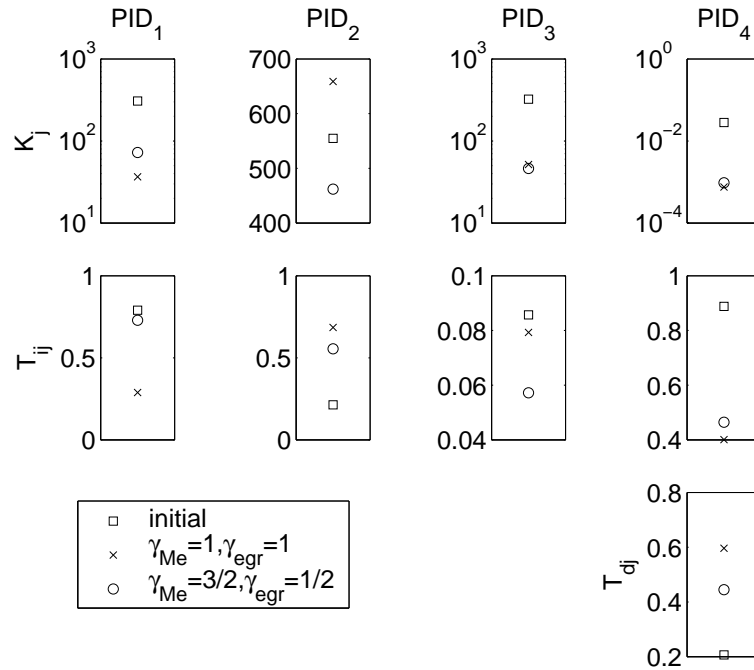
Figure 7 *Comparison between initialized and optimized PID parameters showing that there is a significant difference between them. The optimized PID parameters are calculated for two different sets of weighting factors.*

7   Engine test cell results

The PID parameters, that are obtained off-line in Sec. 6 using the proposed tuning method, are applied on the control structure in Sec. 4 and validated in an engine test cell in two different experiments. The first experiment below investigates if the control structure achieves the control objectives stated in Sec. 2.1. This is done on a ETC cycle transient that was used for optimization in the tuning method. The second experiment below validates the control structure on a transient that was not used for optimization.

The signals needed for the controller are either measured or estimated using observers. The mass flow into the engine W_{ei}, oxygen mass fraction X_{Oim}, λ_O and x_{egr} are estimated using observers [7]. The engine speed (n_e), intake and exhaust manifold pressure (p_{im}, p_{em}) and turbocharger speed (n_t) are measured. The controller runs at 100 Hz and there are no additional sensors necessary compared to the standard controller used by the industry.

7.1   Investigation of the control objectives

This first engine test cell experiment was performed to investigate if the control structure, where the PID parameters are based on the tuning method in Sec. 5, achieves the control objectives in Sec. 2.1. This experiment is shown in Fig. 8 for the second transient in Tab. 1. The set points for λ_O and x_{egr} are given as functions of the operating point and have been provided by industry.

The PID parameters are initially tuned off-line using the weighting factors $\gamma_{Me} = 4/3$ and $\gamma_{egr} = 2/3$. This resulted in actuator oscillations in the engine test cell experiments probably due to model errors and that no gain scheduling is used on the PID parameters. Therefore, the gains K_j in the vector (11) were manually decreased in the engine test cell experiments which gives slower response. However, the values of the parameters T_{dj} and T_{ij} obtained from the tuning method are unchanged, and therefore the relation between the proportional, integral, and derivative part of the PID controllers are preserved. Consequently, the decrease in K_j only effects the total gain of the PID controllers and it does not influence the main goal of evaluating how the control structure achieves the control objectives where the PID parameters have received their basic tuning using the method in Sec. 5.

Control objective 1 is achieved since λ_O is larger than the set-point λ_O^s except when the torque increases rapidly at 851 s and 858 s. To handle this, the controller closes the EGR-throttle at 851 s and the controller closes both the EGR-throttle and the VGT-position at 858 s in order to increase λ_O as fast as possible. Control objective 2 is achieved since λ_O is always larger than or equal to the minimum limit λ_O^{min}. Note that the smoke limiter is active when $\lambda_O = \lambda_O^{min}$. Control objective 3 is achieved since x_{egr} follows its set-point x_{egr}^s if $\lambda_O > \lambda_O^{min}$. At 858 s λ_O is equal to λ_O^{min} and the EGR-throttle is closed in order to increase λ_O, resulting in a high EGR-error. At 854 s the controller closes the EGR-throttle in order to decrease the EGR-error. However, this closing speed is low due to that the gains in the PID-controllers were decreased. Control objective 4 is achieved since M_e follows its set-point M_e^s except when the smoke limiter is active at 858 s. The smoke limiter is also active at 851 s, but the torque deficiency is very small at this point. Control objective 5 is achieved since the turbocharger speed is always smaller than its maximum value n_t^{max}. Finally, control objective 6 is achieved since the EGR-throttle and the VGT position are opened as much as possible when $\lambda_O > \lambda_O^s$, yielding a minimized pumping loss. This can been seen at 853 s where the EGR-throttle is fully open while the VGT controls the EGR-fraction and at 854 s where the VGT is fully open while the EGR-throttle controls the EGR-fraction.

7.2   Results from a non-optimized transient

This second engine test cell experiment was performed to validate the control structure on a transient that was not used for optimization in the tuning method. This experiment is shown in Fig. 9 where the set point for λ_O is constant and the set point for x_{egr} is changed manually. The PID parameters are initially tuned off-line
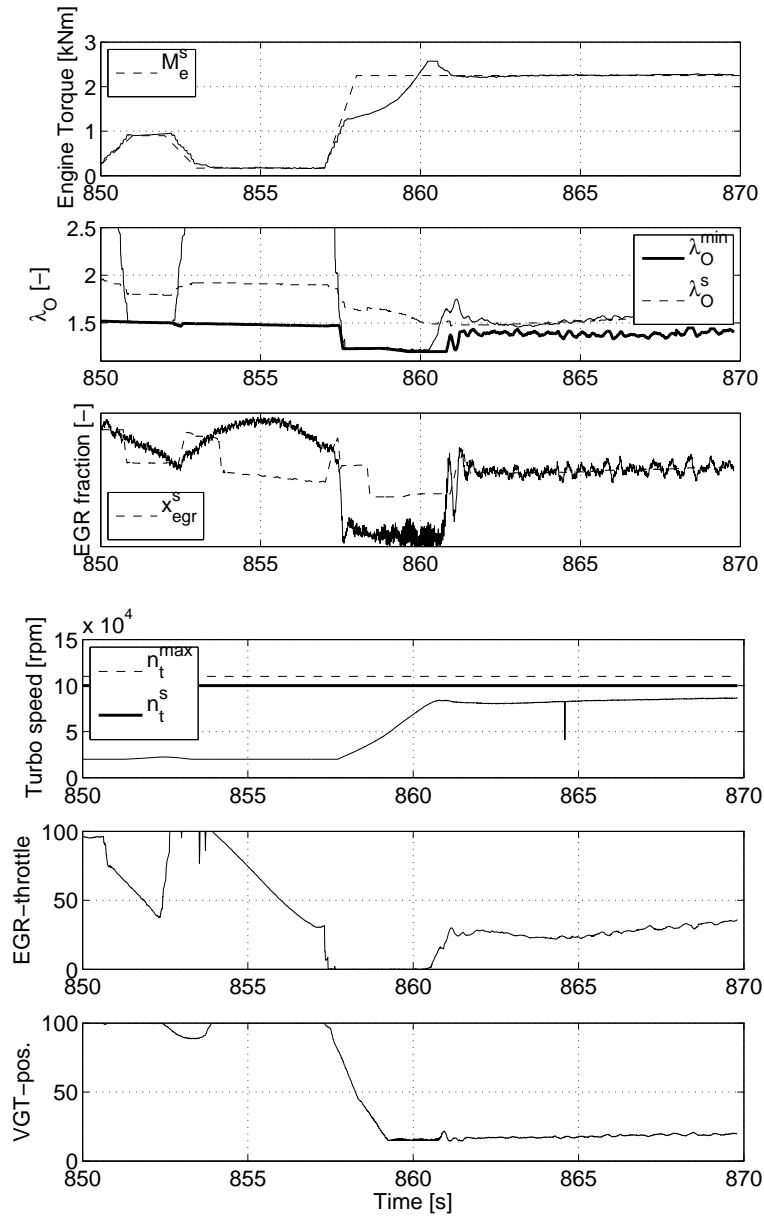
Figure 8 *Validation of the control structure in an engine test cell on a significant transient from the ETC cycle. Here, the PID parameter tuning is based on the method proposed in Sec. 5. The control structure achieves all the control objectives stated in Sec. 2.1.*
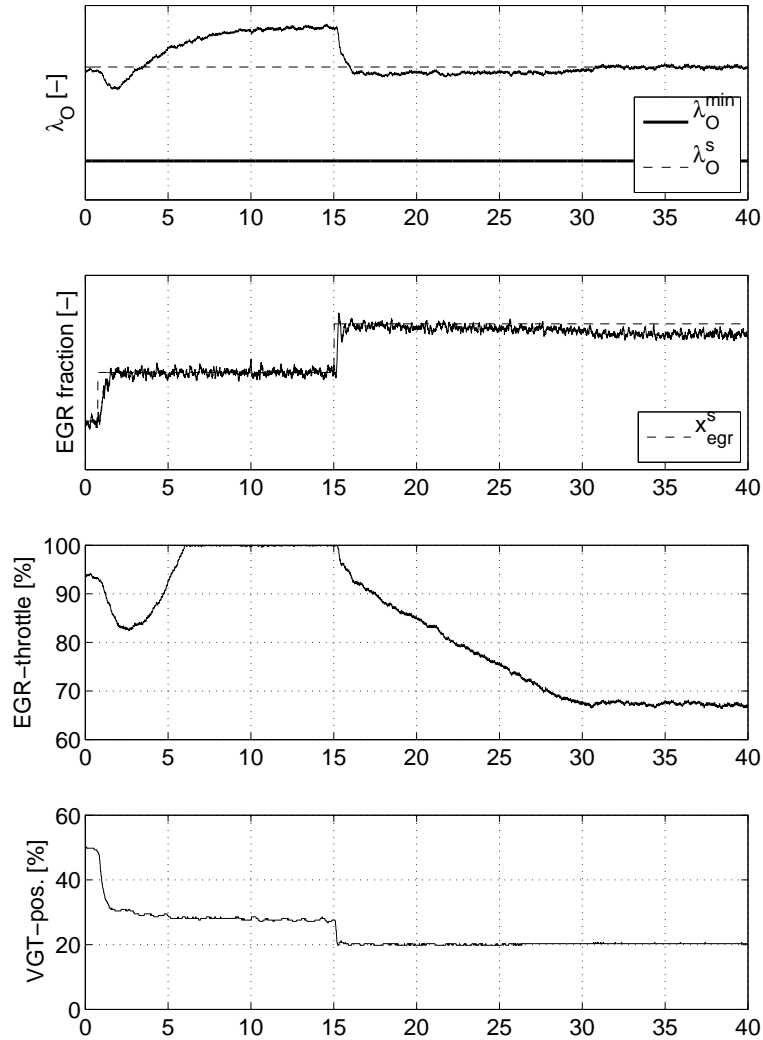
Figure 9 *Validation of the control structure in an engine test cell on a non-optimized transient, showing that the control structure gives priority to λ_O before the EGR-fraction between 30 and 40 s. Here, the PID parameter tuning is based on the method proposed in Sec. 5.*

using the weighting factors $\gamma_{Me} = 3/2$ and $\gamma_{egr} = 1/2$. Then, the PID parameters are manually fine tuned in the engine test cell experiments in order to improve the control performance.

Fig. 9 shows that the controller with the applied tuning method results in a controller that achieves control objectives 1, 2, 3, and 6. In addition it shows that the controller also handles actuator saturation and non reachable set points. The experiment shows that the objectives for λ_O are fulfilled and that the pumping minimization is achieved by opening the EGR-throttle fully when $\lambda_O > \lambda_O^s$. The control objective for EGR is fulfilled as long as the set point is reachable. The set-point commanded at 15 s combines a high λ_O and EGR-fraction and is not reachable with the engine configuration, this is an engine property and does not depend on the controller. After the transients in turbocharger speed and λ_O, due to the set-point change at 15 s, this results in an EGR error after 30 s. At these points the VGT is saturated at 20 % and the EGR-valve controls λ_O. It is worth to note that it is the control structure and not the proposed tuning that gives priority to λ_O before the EGR-fraction, if the set-points for λ_O and EGR-fraction are not reachable at the same time and $\lambda_O \leq \lambda_O^s$.

Furthermore it is seen in both Fig 8 and 9 that actuator saturation is handled well by the controller, i.e. the controller has bumpless transfer between modes when the actuators enter and leave their saturations. The control structure and tuning method thus gives a controller that achieves the control objectives as long as set-points are reachable.

Based on the experimental results shown in Fig 8 and 9, it is seen that the control structure, with parameters based on the proposed tuning method, achieves all the control objectives in Sec. 2.1 in the engine test cell.

8   Conclusions

For efficient calibration a control tuning method was proposed for a control structure with PID controllers and selectors that regulates oxygen/fuel ratio λ_O and intake manifold EGR-fraction. The tuning method is based on control objectives that are captured in a cost function, and the tuning is formulated as a non-linear least squares problem. An important step in obtaining the solution was precautions to avoid ending up in a local minimum in a separate phase. To aid the tuning a systematic method was developed for selecting significant transients that exhibit different challenges for the controller.

The performance was evaluated on the European Transient Cycle. It was demonstrated how the weights in the cost function influence behavior, and that the tuning method is important in order to improve the control performance compared to if only the initialization method is used. Furthermore, it was shown that the control structure with parameters based on the proposed tuning method achieves all the control objectives, and it has been successfully applied in an engine test cell.

Acknowledgments

References

[1] M. Ammann, N.P. Fekete, L. Guzzella, and A.H. Glattfelder. Model-based Control of the VGT and EGR in a Turbocharged Common-Rail Diesel Engine: Theory and Passenger Car Implementation. *SAE Technical paper 2003-01-0357*, January 2003.

[2] A. Amstutz and L. Del Re. EGO sensor based robust output control of EGR in diesel engines. *IEEE Transactions on Control System Technology*, pages 37–48, 1995.

[3] Per Andersson and Lars Eriksson. Mean-value observer for a turbocharged SI-engine. In *IFAC Symposium on Advances in Automotive Control*, 2004.

[4] L. Guzzella and A. Amstutz. Control of diesel engines. *IEEE Control Systems Magazine*, 18:53–71, 1998.

[5] J.B. Heywood. *Internal Combustion Engine Fundamentals*. McGraw-Hill Book Co, 1988.

[6] M. Jankovic, M. Jankovic, and I.V. Kolmanovsky. Robust nonlinear controller for turbocharged diesel engines. In *Proceedings of the American Control Conference*, pages 1389–1394, Philadelphia, Pennsylvania, June 1998.

[7] Andreas Jerhammar and Erik Höckerdal. Gas flow observer for a Scania diesel engine with VGT and EGR. Master's thesis, Linköpings Universitet, SE-581 83 Linköping, 2006.

[8] I.V. Kolmanovsky, A.G. Stefanopoulou, P.E. Moraal, and M. van Nieuwstadt. Issues in modeling and control of intake flow in variable geometry turbocharged engines. In *Proceedings of 18th IFIP Conference on System Modeling and Optimization*, Detroit, July 1997.

[9] I.V. Kolmanovsky, J. Sun, and M. Druzhinina. Charge control for direct injection spark ignition engines with EGR. In *Proceedings of the American Control Conference*, 2000.

[10] Shigeki Nakayama, Takao Fukuma, Akio Matsunaga, Teruhiko Miyake, and Toru Wakimoto. A new dynamic combustion control method based on charge oxygen concentration for diesel engines. In *SAE Technical Paper 2003-01-3181*, 2003. SAE World Congress 2003.

[11] M. Nieuwstadt, P.E. Moraal, I.V. Kolmanovsky, A. Stefanopoulou, P. Wood, and M. Widdle. Decentralized and multivariable designs for EGR–VGT control of a diesel engine. In *IFAC Workshop, Advances in Automotive Control*, 1998.

[12] M.J. Nieuwstadt, I.V. Kolmanovsky, P.E. Moraal, A.G. Stefanopoulou, and M. Jankovic. EGR–VGT control schemes: Experimental comparison for a high-speed diesel engine. *IEEE Control Systems Magazine*, 2000.

[13] R. Rajamani. Control of a variable-geometry turbocharged and wastegated diesel engine. *Proceedings of the I MECH E Part D Journal of Automobile Engineering*, November 2005.

[14] J. Rückert, A. Schloßer, H. Rake, B. Kinoo, M. Krüger, and S. Pischinger. Model based boost pressure and exhaust gas recirculation rate control for a diesel engine with variable turbine geometry. In *IFAC Workshop: Advances in Automotive Control*, 2001.

[15] A.G. Stefanopoulou, I.V. Kolmanovsky, and J.S. Freudenberg. Control of variable geometry turbocharged diesel engines for reduced emissions. *IEEE Transactions on Control Systems Technology*, 8(4), July 2000.

[16] Fredrik Swartling. Gas flow observer for diesel engines with EGR. Master's thesis, Linköpings Universitet, SE-581 83 Linköping, 2005.

[17] Johan Wahlström. Control of EGR and VGT for emission control and pumping work minimization in diesel engines. Licentiate Thesis, Linköping University, 2006.

[18] Johan Wahlström, Lars Eriksson, Lars Nielsen, and Magnus Pettersson. PID controllers and their tuning for EGR and VGT control in diesel engines. In *Preprints of the 16th IFAC World Congress*, Prague, Czech Republic, 2005.

[19] Johan Wahlström and Lars Eriksson. Modeling of a diesel engine with VGT and EGR including oxygen mass fraction. Technical report, Linköping University, 2006.

[20] K. J. Åström and T. Hägglund. *PID Controllers: Theory, Design and Tuning.* Research Triangle Park, Instrument Society of America, 2nd edition, 1995.

Notation

Table 4 *Symbols used in the paper.*

Symbol	Description	Unit
e	Control error	—
E	Performance measures	—
$\mathsf{K_j}$	Gain in a PID	—

Symbol	Description	Unit
M_e	Engine torque	Nm
n_{cyl}	Number of cylinders	—
n_e	Rotational engine speed	rpm
$(O/F)_s$	Stoichiometric oxygen-fuel ratio	—
p	Pressure	Pa
t	Time	s
T_{dj}	Derivative time in a PID	s
T_{ij}	Integral time in a PID	s
T_s	Sample time	s
u_{egr}	EGR control signal. 100:open 0:closed	%
u_{vgt}	VGT control signal. 100:open 0:closed	%
u_δ	Injected amount of fuel	mg/cycle
V	Cost function	—
W	Mass flow	kg/s
x_{egr}	EGR fraction	—
X_O	Oxygen mass fraction	—
γ	Weighting factor	—
θ	PID parameters	—
λ_O	Oxygen-fuel ratio	—
ω	Rotational speed	rad/s

Table 5 *Indices used in the paper.*

Index	Description
c	compressor
egr	EGR
ei	engine cylinder in
em	exhaust manifold
eo	engine cylinder out
im	intake manifold
Norm	normalized
Setp	set-point
t	turbine
vgt	VGT
δ	fuel injection

Non-linear Compensator for handling non-linear Effects in EGR VGT Diesel Engines[1]

Johan Wahlström and Lars Eriksson

Vehicular Systems, Department of Electrical Engineering,
Linköping University, S-581 83 Linköping,
Sweden.

5

Abstract

A non-linear compensator is investigated for handling of non-linear effects in diesel engines. This non-linear compensator is a non-linear state dependent input transformation that is developed by inverting the models for EGR-flow and turbine flow having actuator position as input and flow as output. The non-linear compensator is used in an inner loop in a control structure for coordinated control of EGR-fraction and oxygen/fuel ratio. A stability analysis of the open-loop system with a non-linear compensator shows that it is unstable in a large operating region. This system is stabilized by a control structure that consists of PID controllers and min/max-selectors. The EGR flow and the exhaust manifold pressure are chosen as feedback variables in this structure. Further, the set-points for EGR-fraction and oxygen/fuel ratio are transformed to set-points for the feedback variables. In order to handle model errors in this set-point transformation, an integral action on oxygen/fuel ratio is used in an outer loop. Experimental validations of the proposed control structure show that it handles nonlinear effects, and that it reduces EGR-errors but increases the pumping losses compared to a control structure without non-linear compensator.

1   Introduction

Legislated emission limits for heavy duty trucks are constantly reduced. To fulfill the requirements, technologies like Exhaust Gas Recirculation (EGR) systems and Variable Geometry Turbochargers (VGT) have been introduced. The primary emission reduction mechanisms utilized to control the emissions are that NO_x can be reduced by increasing the intake manifold EGR-fraction x_{egr} and smoke can be reduced by increasing the air/fuel ratio [4]. Note that exhaust gases, present in the intake, also contain oxygen which makes it more suitable to define and use the oxygen/fuel ratio λ_O instead of the traditional air/fuel ratio. The main motive for this is that it is the oxygen contents that is crucial for smoke generation. Besides λ_O it is natural to use EGR-fraction x_{egr} as the other main performance variable, but one could also use the burned gas fraction instead of the EGR-fraction.

The oxygen/fuel ratio λ_O and EGR fraction x_{egr} depend in complicated ways on the EGR and VGT actuation. It is therefore necessary to have coordinated control of the EGR and VGT to reach the legislated emission limits in NO_x and smoke. Various approaches for coordinated control of the EGR and VGT for emission abatement have been published. [3] presents a good overview of different control aspects of diesel engines with EGR and VGT, and in [9] there is a comparison of some control approaches with different selections of performance variables. Other control approaches are described in [2], [8], [12], [1], and [11].

Inspired by an approach in [5], a non-linear compensator is investigated for handling of non-linear effects in diesel engines. This non-linear compensator is a non-linear state dependent input transformation that is developed by inverting the models for EGR-flow and turbine flow having actuator position as input and flow as output. The non-linear compensator is used in an inner loop and a control structure with PID controllers and min/max-selectors similar to [13] is used in an outer loop. The control objectives for the control structure are described in Sec. 1.1. Sec. 2 describes a mean value diesel engine model that is first used for system analysis in Sec. 3 and later used for development and analysis of the non-linear compensator and the proposed control structure. The control structure in [13] is described in Sec. 4. The non-linear compensator is developed and analyzed in Sec. 5, while Sec. 6 describes a control structure with non-linear compensator. The control structure in [13] and the proposed control structure are compared in an engine test cell in Sec. 7.

1.1   Control objectives

The primary variables to be controlled are normalized oxygen/fuel ratio λ_O, intake manifold EGR-fraction x_{egr}, engine torque M_e, and turbocharger speed n_t. The goal is to follow a driving cycle while maintaining low emissions, low fuel consumption, and suitable turbocharger speeds, which gives the following control objectives for the performance variables.

1. λ_O should be greater than a soft limit, a set-point λ_O^s, which enables a trade-off between emission, fuel consumption, and response time.
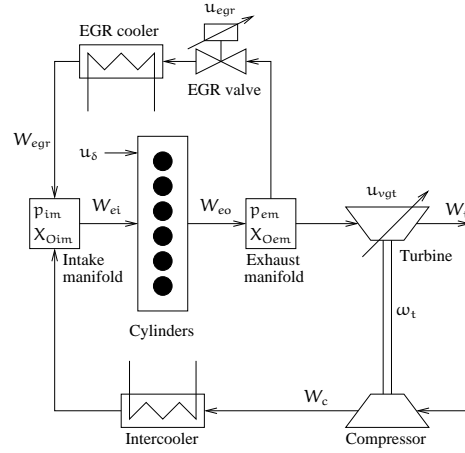
Figure 1 *Sketch of the diesel engine model used for system analysis and control design. It has five states related to the engine (p_{im}, p_{em}, X_{Oim}, X_{Oem}, and ω_t) and three for actuator dynamics.*

2. λ_O is not allowed to go below a hard minimum limit λ_O^{min}, otherwise there will be too much smoke. λ_O^{min} is always smaller than λ_O^s.

3. x_{egr} should follow its set-point x_{egr}^s. There will be more NO_x if the EGR-fraction is too low and there will be more smoke if the EGR-fraction is too high.

4. The engine torque, M_e, should follow the set-point M_e^s from the drivers demand.

5. The turbocharger speed, n_t, is not allowed to exceed a maximum limit n_t^{max}, preventing turbocharger damage.

6. The pumping losses, M_p, should be minimized in stationary points in order to decrease the fuel consumption.

The aim is now to develop a control structure that achieves all these control objectives when the set-points for EGR-fraction and engine torque are reachable.

2   Diesel engine model

A model for a heavy duty diesel engine is used for system analysis and control design. This diesel engine model is focused on the gas flows, see Fig. 1, and it is a mean value model with eight states: intake and exhaust manifold pressures (p_{im} and p_{em}), oxygen mass fraction in the intake and exhaust manifold (X_{Oim} and X_{Oem}), turbocharger speed (ω_t), and three states describing the actuator dynamics for the two control signals (u_{egr} and u_{vgt}) where there are two states for

the EGR-actuator to describe an overshoot. These states are collected in a state vector x

$$x = [p_{im} \quad p_{em} \quad X_{Oim} \quad X_{Oem} \quad \omega_t \quad \tilde{u}_{egr1} \quad \tilde{u}_{egr2} \quad \tilde{u}_{vgt}]^T$$

There are no state equations for the manifold temperatures, since the pressures and the turbocharger speed govern the most important system properties, such as non-minimum phase behaviors, overshoots, and sign reversals, while the temperature states have only minor effects on these system properties.

The resulting model is expressed in state space form as

$$\dot{x} = f(x, u, n_e)$$

where the engine speed n_e is considered as an input to the model, and u is the control input vector

$$u = [u_\delta \quad u_{egr} \quad u_{vgt}]^T$$

which contains mass of injected fuel u_δ, EGR-valve position u_{egr}, and VGT actuator position u_{vgt}.

A detailed description and derivation of the model together with a model tuning and a validation against test cell measurements is given in [15]. The derivatives of the engine state variables are given by (1), the dynamics of the actuators is given by (2)–(5), and the oxygen concentration in the exhaust gas is calculated in (6). Further, the main performance variables are defined by (7), the EGR flow model is given by (8)–(11), and the turbine flow model is given by (12)–(14).

$$\frac{d}{dt} p_{em} = f_1(x, u), \quad \frac{d}{dt} \omega_t = f_2(x, u) \tag{1a}$$

$$\frac{d}{dt} p_{im} = \frac{R_a T_{im}}{V_{im}} (W_c + W_{egr} - W_{ei}) \tag{1b}$$

$$\frac{d}{dt} X_{Oim} = \frac{R_a T_{im}}{p_{im} V_{im}} ((X_{Oem} - X_{Oim}) W_{egr} +$$
$$(X_{Oc} - X_{Oim}) W_c) \tag{1c}$$

$$\frac{d}{dt} X_{Oem} = \frac{R_e T_{em}}{p_{em} V_{em}} (X_{Oe} - X_{Oem}) (W_f + W_{ei}) \tag{1d}$$

$$\tilde{u}_{egr} = K_{egr} \tilde{u}_{egr1} - (K_{egr} - 1) \tilde{u}_{egr2} \tag{2}$$

$$\frac{d}{dt} \tilde{u}_{egr1} = \frac{1}{\tau_{egr1}} (u_{egr}(t - \tau_{degr}) - \tilde{u}_{egr1}) \tag{3}$$

$$\frac{d}{dt} \tilde{u}_{egr2} = \frac{1}{\tau_{egr2}} (u_{egr}(t - \tau_{degr}) - \tilde{u}_{egr2}) \tag{4}$$

$$\frac{d}{dt} \tilde{u}_{vgt} = \frac{1}{\tau_{vgt}} (u_{vgt}(t - \tau_{dvgt}) - \tilde{u}_{vgt}) \tag{5}$$

$$X_{Oe} = \frac{W_{ei}\, X_{Oim} - W_f\, (O/F)_s}{W_f + W_{ei}} \tag{6}$$

$$x_{egr} = \frac{W_{egr}}{W_c + W_{egr}}, \quad \lambda_O = \frac{W_{ei}\, X_{Oim}}{W_f\, (O/F)_s} \tag{7}$$

$$W_{egr} = \frac{A_{egrmax}\, f_{egr}(\tilde{u}_{egr})\, p_{em}\, \Psi_{egr}}{\sqrt{T_{em}\, R_e}} \tag{8}$$

$$\Psi_{egr} = 1 - \left(\frac{1 - \Pi_{egr}}{1 - \Pi_{egropt}} - 1\right)^2 \tag{9}$$

$$\Pi_{egr} = \begin{cases} \Pi_{egropt} & \text{if } \frac{p_{im}}{p_{em}} < \Pi_{egropt} \\[2mm] \frac{p_{im}}{p_{em}} & \text{if } \Pi_{egropt} \le \frac{p_{im}}{p_{em}} \le 1 \\[2mm] 1 & \text{if } 1 < \frac{p_{im}}{p_{em}} \end{cases} \tag{10}$$

$$f_{egr}(\tilde{u}_{egr}) =$$
$$\begin{cases} c_{egr1}\, \tilde{u}_{egr}^2 + c_{egr2}\, \tilde{u}_{egr} + c_{egr3} & \text{if } \tilde{u}_{egr} \le \frac{-c_{egr2}}{2\, c_{egr1}} \\[3mm] c_{egr3} - \frac{c_{egr2}^2}{4\, c_{egr1}} & \text{if } \tilde{u}_{egr} > \frac{-c_{egr2}}{2\, c_{egr1}} \end{cases} \tag{11}$$

$$W_t = \frac{A_{vgtmax}\, p_{em}\, f_{\Pi t}(\Pi_t)\, f_{vgt}(\tilde{u}_{vgt})}{\sqrt{T_{em}\, R_e}} \tag{12}$$

$$f_{\Pi t}(\Pi_t) = \sqrt{1 - \Pi_t^{K_t}}, \quad \Pi_t = \frac{p_{amb}}{p_{em}} \tag{13}$$

$$f_{vgt}(\tilde{u}_{vgt}) = c_{f2} + c_{f1} \sqrt{\max\left(0, 1 - \left(\frac{\tilde{u}_{vgt} - c_{vgt2}}{c_{vgt1}}\right)^2\right)} \tag{14}$$

3 System properties

An analysis of the characteristics and the behavior of a system aims at obtaining insight into the control problem. This is known to be important for a successful design of a EGR and VGT controller due to non-trivial intrinsic properties, see for example [7]. Therefore, a system analysis of the model in Sec. 2 is performed in [16]. The analysis shows that the DC-gains for the channels $u_{vgt} \to \lambda_O$, $u_{egr} \to \lambda_O$, and $u_{vgt} \to p_{em}$ change sign with operating point.

3.1   Mapping of sign reversal

Knowledge about the sign reversal in the entire operating region is important when developing a control structure. Therefore, the sign reversal is mapped in [16] by simulating step responses in the entire operating region. In Fig. 2 the sign reversals in $u_{vgt} \to \lambda_O$, $u_{egr} \to \lambda_O$, and $u_{vgt} \to p_{em}$ are mapped by calculating the DC-gain in the step responses and then plotting the contour line where the DC-gain is equal to zero. The step responses are simulated at 20 different u_{vgt} points, 20 different u_{egr} points, 3 different n_e points, and 3 different u_δ points. The size of the steps in u_{vgt} is 5% of the difference between two adjoining operating points. A system analysis also shows that the engine frequently operates in operating points where the sign reversal occurs for the channels $u_{vgt} \to \lambda_O$ and $u_{vgt} \to p_{em}$ [16]. Consequently, it is important to consider the sign reversal for $u_{vgt} \to \lambda_O$ and $u_{vgt} \to p_{em}$ in the control design.

4   Control structure with PID controllers

A control structure with PID controllers and min/max-selectors is proposed in [13] with the following algorithm

$$u_{egr}(t_i) = \begin{cases} \begin{aligned} &\min\left(-\text{PI}_1(e_{\lambda_O}), \\ &\quad\text{PI}_2(e_{xegr})\right) \end{aligned} & \text{, if } u_{vgt}(t_{i-1}) = 100 \\[2ex] -\text{PI}_1(e_{\lambda_O}) & \text{, else} \end{cases} \tag{15}$$

$$u_{vgt}(t_i) = \begin{cases} 100 & \begin{aligned}&\text{, if } (u_{vgt}(t_{i-1}) = 100) \\ &\quad \&\, (e_{xegr} < 0.01)\end{aligned} \\[2ex] \begin{aligned}&\max\left(-\text{PI}_3(e_{xegr}), \\ &\quad -\text{PID}_4(e_{nt})\right)\end{aligned} & \text{, else} \end{cases} \tag{16}$$

where $e_{\lambda_O} = \lambda_O^s - \lambda_O$, $e_{xegr} = x_{egr}^s - x_{egr}$, and $e_{nt} = n_t^s - n_t$. This structure handles the sign reversal in $u_{vgt} \to \lambda_O$ because u_{egr} is used to control λ_O, and it also minimizes the pumping work by opening the EGR-valve and the VGT as much as possible while achieving the control objectives for λ_O and x_{egr} [13].

4.1   Engine test cell experiments

The control structure (15)–(16) is applied and validated in an engine test cell. The goal is to experimentally verify the control performance during steps in λ_O^s.

An available production observer, similar to the one in [10], is used to estimate the oxygen mass fraction X_{Oim}. Once X_{Oim} is estimated, the mass flow into the engine W_{ei}, λ_O and x_{egr} are calculated. The engine speed (n_e), intake and exhaust manifold pressure (p_{im}, p_{em}) and turbocharger speed (n_t) are measured with production sensors. Due to measurement noise, all measured and observed variables are filtered using low pass filters with a time constant of 0.1 s. The
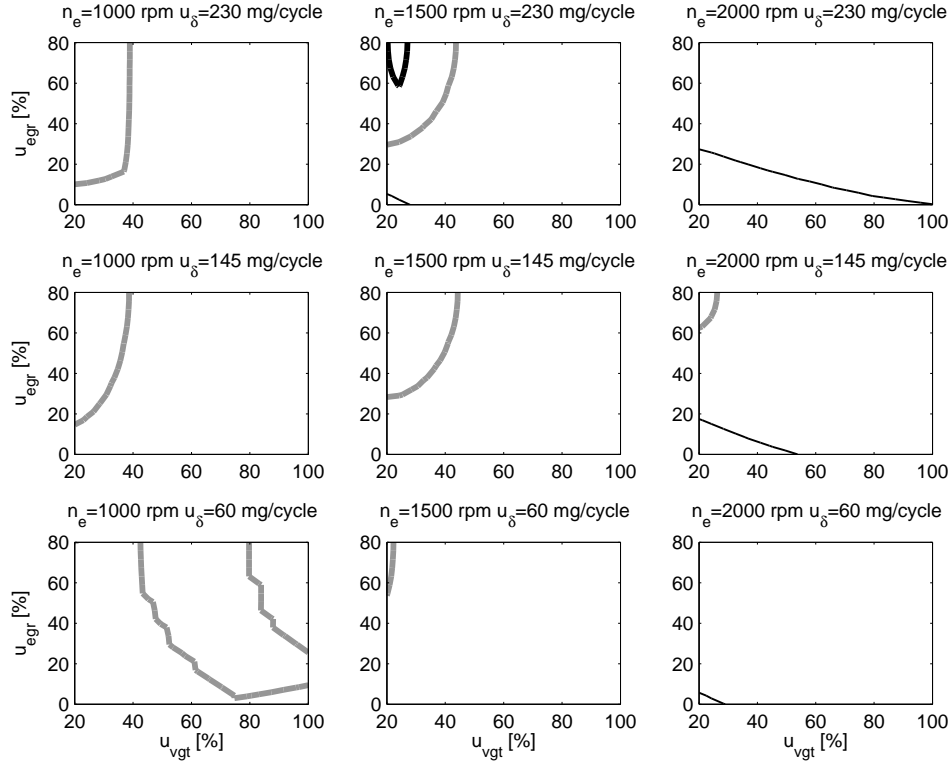
Figure 2 *For the system in Sec. 2, the channel $u_{vgt} \to \lambda_O$ has a sign reversal (thick gray line) that occurs at low to medium engine speed, $u_{egr} \to \lambda_O$ has a sign reversal (thin black line) that occurs at high engine speed, and $u_{vgt} \to p_{em}$ has a sign reversal (thick black line) that occurs at a small region with high load and medium engine speed.*

PID parameters are initially tuned using the method in [14] with $\gamma_{Me} = 3/2$ and $\gamma_{egr} = 1/2$, and are then manually fine tuned in the engine test cell experiments. The experiment in Fig. 3 shows that the control structure (15)–(16) gives slow control at the first step and oscillations at the third step. This is due to that the DC-gains in $u_{egr} \to \lambda_O$ and $u_{vgt} \to x_{egr}$ (the two loops that are used as feedbacks in (15)–(16)) increase when λ_O increases. This could be handled using gain scheduling, but it is time consuming to tune the parameters for each operating point. Instead, these non-linear effects are handled using a non-linear compensator that will be described in the following sections.
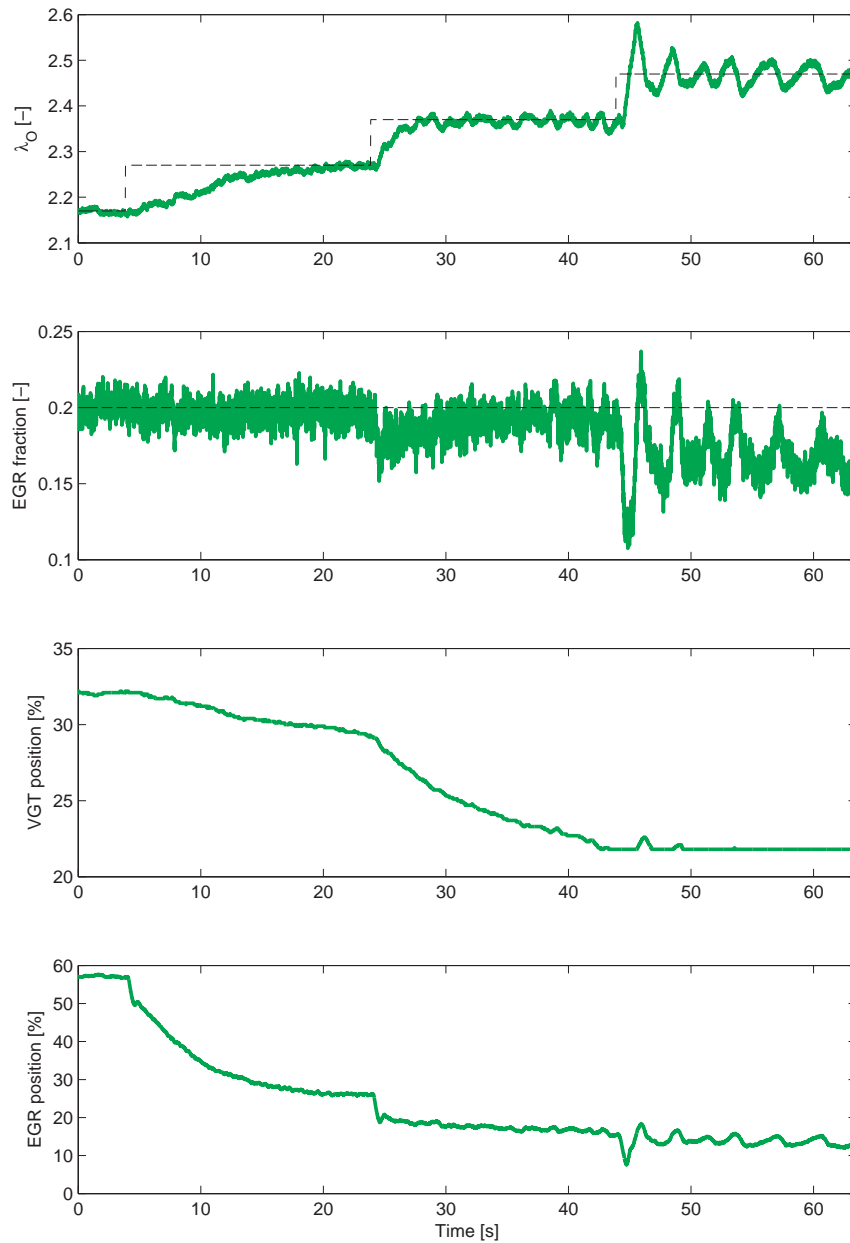
Figure 3 *Step responses for the control structure* (15)–(16) *in an engine test cell showing slow control and oscillations at different steps, i.e. this control structure does not handle non-linear effects in the diesel engine. Operating point:* $n_e = 1200$ *rpm and* $u_\delta = 136$ *mg/cycle.*
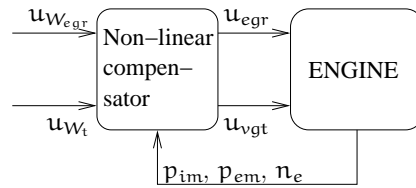
Figure 4 *A block diagram of the system with a non-linear compensator on the EGR and VGT actuator. This non-linear compensator is an inversion of the models for EGR-flow and turbine flow having actuator position as input and flow as output.*
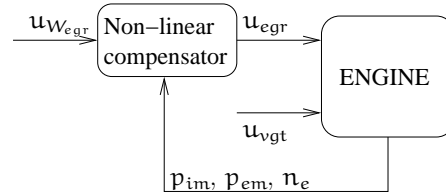

Figure 5 *A block diagram of the system with a non-linear compensator on the EGR actuator. This non-linear compensator is an inversion of the EGR-flow model having actuator position as input and flow as output.*

5   Non-linear compensator

To handle the sign reversal in $u_{vgt} \to \lambda_O$ and $u_{vgt} \to p_{em}$ in Fig. 2 and the non-linear effects in Fig. 3, a non-linear compensator is used according to Fig. 4. This non-linear compensator is a non-linear state dependent input transformation that is developed by inverting the models for EGR-flow and turbine flow having actuator position as input and flow as output. The approach is similar to [5] that performs these inversions on similar models for EGR-flow and turbine flow. These inversions lead to two new control inputs, $u_{W_{egr}}$ and u_{W_t}, which are the EGR-flow W_{egr} and the turbine flow W_t provided there are no model errors in the non-linear compensator.

In the following sections, the non-linear compensator is described and the system properties of the system in Fig. 4 are investigated. In Sec. 5.1 only the non-linear compensator for the EGR-actuator is considered according to Fig. 5 and in Sec. 5.2 the non-linear compensator for both the EGR and VGT-actuator is considered according to Fig. 4.

5.1   Inversion of position to flow model for EGR

The non-linear compensator in Fig. 5 is a static inversion of the EGR-flow model (8) to (11) having actuator position as input and flow as output. This inversion results in the following expressions for u_{egr} with $u_{W_{egr}}$ as a new control input

$$f_{egr} = \frac{u_{W_{egr}} \sqrt{T_{em} R_e}}{A_{egrmax} p_{em} \max(\Psi_{egr}, 0.1)} \tag{17}$$

$$v_{egr} = -\frac{c_{egr2}}{2 c_{egr1}} - \\ \sqrt{\max\left(\left(\frac{c_{egr2}}{2 c_{egr1}}\right)^2 - \frac{c_{egr3}}{c_{erg1}} + \frac{f_{egr}}{c_{egr1}}, 0\right)} \tag{18}$$

$$u_{egr} = \begin{cases} u_{egr}^{max} & \text{if } v_{egr} \geq u_{egr}^{max} \\ v_{egr} & \text{if } u_{egr}^{min} < v_{egr} < u_{egr}^{max} \\ u_{egr}^{min} & \text{if } v_{egr} \leq u_{egr}^{min} \end{cases} \tag{19}$$

where Ψ_{egr} is given by (9) and (10). The exhaust manifold temperature T_{em} is calculated using the model in [15] and [6]

$$T_{em} = T_{amb} + (T_e - T_{amb}) e^{-\frac{h_{tot} \pi d_{pipe} l_{pipe} n_{pipe}}{W_{eo} c_{pe}}} \tag{20}$$

where

$$W_{eo} = W_{ei} + W_f, \quad T_e = T_{im} + \frac{q_{HV} f_{Te}(W_f, n_e)}{c_{pe} W_{eo}} \tag{21}$$

and

$$f_{Te}(W_f, n_e) = c_{fTe1} W_f + c_{fTe2} n_e + c_{fTe3} W_f n_e + c_{fTe4} \tag{22}$$

and $W_{ei} = W_{ei}(p_{im}, n_e)$ and $W_f = W_f(n_e, u_\delta)$. The signals p_{im}, p_{em}, and n_e are measured. Further, in the non-linear compensator it is assumed that the EGR-actuator is ideal, i.e. $\tilde{u}_{egr} = u_{egr}$.

Solving (11) for $\tilde{u}_{egr}$ results only in one solution according to (18) since f_{egr} is saturated in (11) when $\tilde{u}_{egr} > -c_{egr2}/(2 c_{egr1})$. To avoid a complex solution in (18), a max-selector is used inside the square root sign. A max-selector is also used in (17) to avoid a division by zero when $\Psi_{egr} = 0$. Finally, saturation is used in (19).

The goal is now to investigate how the non-linear compensator for the EGR-actuator handles the sign reversals and the non-linear effects in $u_{vgt} \to \lambda_O$ and $u_{vgt} \to p_{em}$. This is done by simulating step responses in u_{vgt} for the system in Fig. 5. The sign reversal in $u_{vgt} \to \lambda_O$ and $u_{vgt} \to p_{em}$ are mapped in Fig. 6 in the same way as in Fig. 2 and the result is that there is no sign reversal in $u_{vgt} \to \lambda_O$ and $u_{vgt} \to p_{em}$ when $u_{egr} < 80\%$. However, when the EGR-valve is

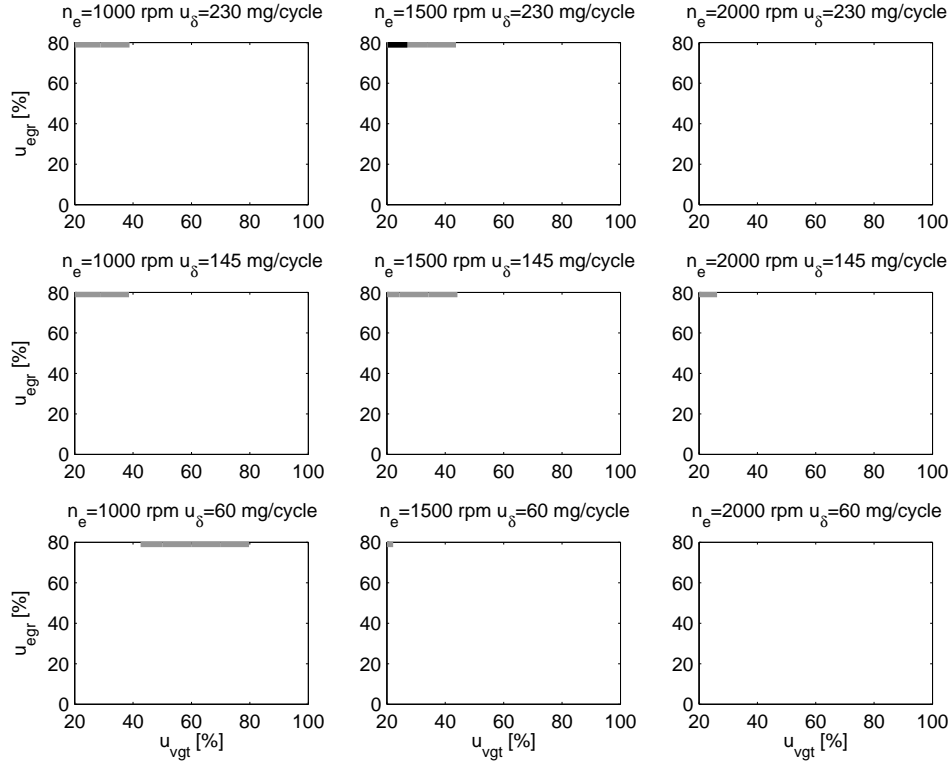**Figure 6** *For the system in Fig. 5, the channel $u_{vgt} \to \lambda_O$ has a sign reversal at the gray line and $u_{vgt} \to p_{em}$ has a sign reversal at the black line. Both these sign reversals only occur when the EGR-valve is saturated.*

saturated at $u_{egr} = 80\%$, there are sign reversals that occur at the same operating points as in Fig. 2 where $u_{egr} = 80\%$.

Further, there are still large non-linear effects in $u_{vgt} \to \lambda_O$ and $u_{vgt} \to p_{em}$ when $u_{egr} < 80$. This is illustrated by calculating the quotient between the maximum and minimum DC-gain for the operating region in Fig. 6 when $u_{egr} < 80$. The result is that

$$\frac{\max(K_{u_{vgt} \to \lambda_O})}{\min(K_{u_{vgt} \to \lambda_O})} = 6.2 \cdot 10^3 \tag{23}$$

$$\frac{\max(K_{u_{vgt} \to p_{em}})}{\min(K_{u_{vgt} \to p_{em}})} = 1.0 \cdot 10^4 \tag{24}$$

where $K_{u_{vgt} \to \lambda_O}$ and $K_{u_{vgt} \to p_{em}}$ are the DC-gains for $u_{vgt} \to \lambda_O$ and $u_{vgt} \to p_{em}$. For linear systems, these quotients are equal to 1, and consequently there are still significant non-linear effects for the system in Fig. 5.

5.2   Inversion of position to flow model for EGR and VGT

To handle the non-linear effects in $u_{vgt} \rightarrow \lambda_O$ and $u_{vgt} \rightarrow p_{em}$ in the quotients (23) and (24), a non-linear compensator for both the EGR and VGT actuator is used according to Fig. 4. The non-linear compensator for the EGR actuator is described in the previous section and the non-linear compensator for the VGT actuator is a static inversion of the turbine flow model (12) to (14) having actuator position as input and flow as output. This inversion results in the following expression for u_{vgt} with u_{W_t} as a new control input

$$f_{vgt} = \frac{u_{W_t}\sqrt{T_{em}\,R_e}}{A_{vgtmax}\,p_{em}\,\max\left(f_{\Pi t},0.1\right)} \tag{25}$$

$$\nu_{vgt} = \\ c_{vgt2} - c_{vgt1}\sqrt{\max\left(1 - \left(\frac{\max\left(f_{vgt} - c_{f2},0\right)}{c_{f1}}\right)^2,0\right)} \tag{26}$$

$$u_{vgt} = \begin{cases} u_{vgt}^{max} & \text{if } \nu_{vgt} \geq u_{vgt}^{max} \\ \nu_{vgt} & \text{if } u_{vgt}^{min} < \nu_{vgt} < u_{vgt}^{max} \\ u_{vgt}^{min} & \text{if } \nu_{vgt} \leq u_{vgt}^{min} \end{cases} \tag{27}$$

where $f_{\Pi t}$ is given by (13) and T_{em} is given by (20)–(22). The pressure p_{em} is measured. Further, it is assumed that the VGT-actuator is ideal, i.e. $\tilde{u}_{vgt} = u_{vgt}$.

The first max-selector in (26) is used to avoid a complex solution and the second max-selector is used so that ν_{vgt} is constant when $f_{vgt} < c_{f2}$. A max-selector is also used in (25) to avoid a division by zero when $f_{\Pi t} = 0$. Finally, saturation is used in (27).

Simulations show that the system in Fig. 5 is stable and that the system in Fig. 4 is unstable. The unstable system in Fig. 4 is stabilized by a controller in Sec. 6. The physical explanation of this instability is as follows. A positive step in u_{W_t} according to Fig. 7 leads to an increase in u_{vgt} and therefore a decrease in p_{em}. Since the output u_{vgt} from the non-linear compensator increases when p_{em} decreases, the non-linear compensator will continue to open up the VGT until it is saturated, and the result is an error between u_{W_t} and the turbine mass flow W_t. This instability is further analyzed in Sec. 5.3 by investigating stability of linearized models of the system in Fig. 4.

To investigate the system in Fig. 4 for non-linear effects in $u_{vgt} \rightarrow \lambda_O$ and $u_{vgt} \rightarrow p_{em}$, the quotients

$$\frac{\max(K_{u_{W_t}\rightarrow\lambda_O})}{\min(K_{u_{W_t}\rightarrow\lambda_O})}, \quad \frac{\max(K_{u_{W_t}\rightarrow p_{em}})}{\min(K_{u_{W_t}\rightarrow p_{em}})}$$

are calculated for the operating region in Fig. 6 when $u_{egr} < 80$. $K_{u_{W_t}\rightarrow\lambda_O}$ and $K_{u_{W_t}\rightarrow p_{em}}$ are the DC-gains for $u_{W_t} \rightarrow \lambda_O$ and $u_{W_t} \rightarrow p_{em}$ between different
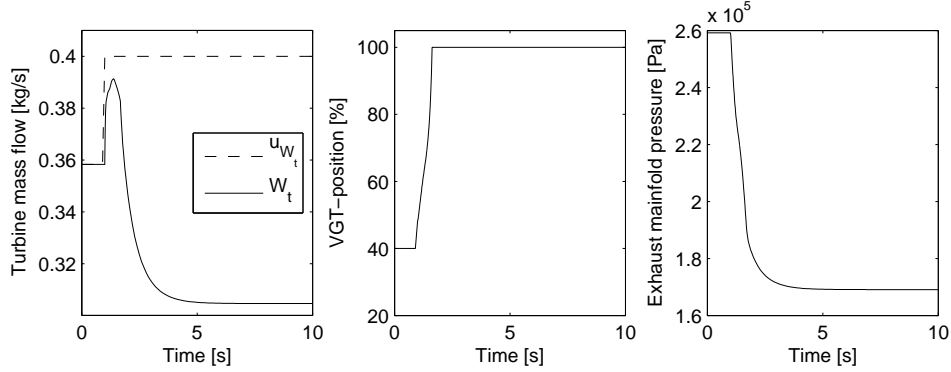
Figure 7 *A step response of the system in Fig. 4 with* $u_{W_{egr}} = 0.04$ *kg/s showing that this system is unstable.*

stationary points. However, these DC-gains can not be calculated directly since the stationary points are unstable for the system in Fig. 4. Therefore, these DC-gains are calculated using the chain rule according to

$$K_{u_{W_t} \to \lambda_O} = \frac{K_{u_{vgt} \to \lambda_O}}{K_{u_{vgt} \to W_t}} \tag{28}$$

$$K_{u_{W_t} \to p_{em}} = \frac{K_{u_{vgt} \to p_{em}}}{K_{u_{vgt} \to W_t}} \tag{29}$$

where the DC-gains $K_{u_{vgt} \to \lambda_O}$, $K_{u_{vgt} \to p_{em}}$, and $K_{u_{vgt} \to W_t}$ are calculated from step responses in u_{vgt} for the system in Fig. 5. The result is that

$$\frac{\max(K_{u_{W_t} \to \lambda_O})}{\min(K_{u_{W_t} \to \lambda_O})} = 77 \tag{30}$$

$$\frac{\max(K_{u_{W_t} \to p_{em}})}{\min(K_{u_{W_t} \to p_{em}})} = 30 \tag{31}$$

Comparing these quotients with (23) and (24), the conclusion is that the system in Fig. 4 has less non-linear effects compared to the system in Fig. 5.

5.3 Stability analysis of the open-loop system

A mapping of poles for linearized models of the system in Fig. 4 is performed in order to analyze the stability of these models. The linear models are constructed by linearizing the non-linear system in Fig. 4 where the block "ENGINE" is the eight-order model in Sec. 2. The linearization is performed in the same operating

points as the operating points in Fig. 2 and 6. The linear models have the form

$$\dot{x} = A_i\, x + B_i\, u$$
$$y = C_i\, x + D_i\, u \tag{32}$$

where i is the operating point number and

$$u = [u_{W_{egr}} \quad u_{W_t}]^T$$
$$x = [p_{im} \quad p_{em} \quad X_{Oim} \quad X_{Oem} \quad \omega_t \quad \tilde{u}_{egr1} \quad \tilde{u}_{egr2} \quad \tilde{u}_{vgt}]^T$$
$$y = [W_{egr} \quad p_{em}]^T$$

The motives for selecting W_{egr} and p_{em} as outputs will be described in Sec. 6.1.

A mapping of the poles for the models (32) are performed in Fig. 8 showing that there is one pole in the right complex half plane for almost the complete operating region except in the black areas and at the thick black lines where all poles are in the left complex half plane. Consequently, the linearized models (32) are stable only in the black areas and at the thick black lines in Fig. 8.

6   Control structure with non-linear compensator

The control design objective is to coordinate $u_{W_{egr}}$ and u_{W_t} in Fig. 4 in order to achieve the control objectives stated in Sec. 1.1. The approach is to build a controller structure using min/max-selectors and PID controllers similar to the structure (15) and (16). The solution is presented step by step in the following sections and a block diagram of the proposed closed-loop system is shown in Fig. 9.

6.1   Main feedback loops

The first step in the control design is to choose outputs and main feedback loops. It is natural to choose the EGR flow W_{egr} and the turbine flow W_t as outputs due to that $u_{W_{egr}} = W_{egr}$ and $u_{W_t} = W_t$ if there are no model errors in the non-linear compensator. However, the system can not be stabilized using these outputs. The reference [5] shows that if W_{egr} and the compressor flow W_c are chosen as outputs in feedback linearization, there will be an unstable zero dynamics in p_{em}. To handle this unstable mode, W_{egr} and p_{em} are chosen as outputs. Therefore, the following main feedback loops are chosen

$$u_{W_{egr}} = PI_1(W_{egr}^s, W_{egr}) \tag{33}$$
$$u_{W_t} = -PI_2(p_{em}^s, p_{em}) \tag{34}$$

These two main feedback loops are selected to handle items 1 and 3 of the control objectives stated in Sec. 1.1 where the set-points λ_O^s and x_{egr}^s are transformed to the set-points W_{egr}^s and p_{em}^s according to the following section.
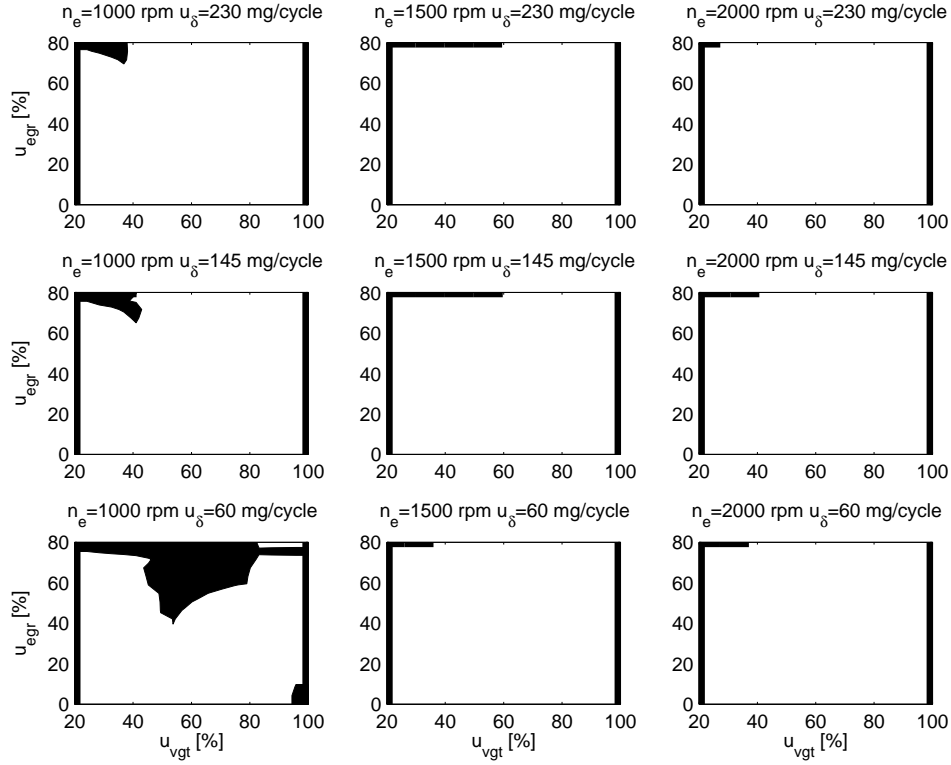
Figure 8 *A mapping of poles for linearized models of the system in Fig. 4 showing that there is one pole in the right complex half plane for almost the complete operating region except in the black areas and at the thick black lines where all poles are in the left complex half plane. In the thin white area in the upper right corner in the left bottom plot, u_{egr} is equal to 80%.*

6.2   Set-point transformation and integral action

The set-points λ_O^s and x_{egr}^s are transformed to the set-points W_{egr}^s and p_{em}^s in two steps. Firstly, the equilibriums for W_c and W_{egr} of the mass balances (1b)–(1d) are calculated from λ_O^s and x_{egr}^s

$$W_c^s = \frac{W_f}{2X_{Oc}}\left(\beta + \sqrt{\beta^2 + 4\lambda_O^s\,(O/F)_s(1 - x_{egr}^s)X_{Oc}}\right) \tag{35}$$

$$W_{egr}^s = \frac{x_{egr}^s}{1 - x_{egr}^s}W_c \tag{36}$$

where

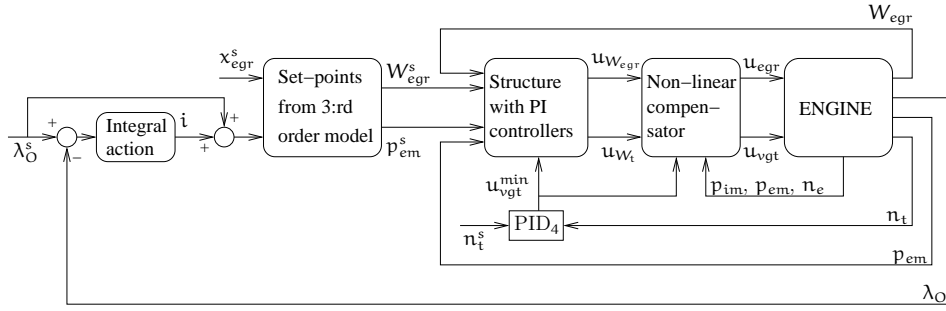$$\beta = (\lambda_O^s\,(O/F)_s - X_{Oc})(1 - x_{egr}^s) + (O/F)_s\,x_{egr}^s,$$

Figure 9 *Block diagram of the closed-loop system, showing; an integral action on λ_O, set-points calculations, a structure with PI controllers, a PID controller for the turbocharger speed n_t, and a non-linear compensator.*

X_{Oc} is the constant oxygen concentration in air passing the compressor, and $(O/F)_s$ is the stoichiometric relation between oxygen and fuel masses. Note that W_c is used instead of W_c^s in (36) in order to get the correct value of W_{egr}^s in stationary points when $W_c > W_c^s$, i.e. when $\lambda_O > \lambda_O^s$ that is allowed in diesel engines. Secondly, the equilibriums for p_{im} and p_{em} of a third-order model are calculated from W_c^s and x_{egr}^s. This third-order model is a simplification of the eighth-order model in Sec. 2 and the three states in the simplified model are p_{im}, p_{em}, and the compressor power P_c. This model is based on the control design model developed in [5]:

$$
\begin{aligned}
\dot{p}_{im} &= k_{im}\,(W_c + u_1 - k_e\,p_{im}) \\
\dot{p}_{em} &= k_{em}\,(k_e\,p_{im} - u_1 - u_2 + W_f) \\
\dot{P}_c &= \frac{1}{\tau}(\eta_m\,P_t - P_c)
\end{aligned}
\tag{37}
$$

$$
\begin{aligned}
W_c &= \frac{\eta_c\,P_c}{T_{amb}\,c_{pa}\,((p_{im}/p_{amb})^{\mu_a} - 1)} \\
P_t &= \eta_t\,c_{pe}\,T_{em}\,(1 - (p_{amb}/p_{em})^{\mu_e})\,u_2
\end{aligned}
$$

The variables $k_{em} = k_{em}(T_{em})$, $W_f = W_f(u_\delta, n_e)$, $k_e = k_e(n_e)$, and η_c are treated as external slowly varying signals and k_{im}, τ, η_m, T_{amb}, c_{pa}, p_{amb}, μ_a, η_t, c_{pe}, and μ_e are constants.

The equilibriums for p_{im} and p_{em} of the third-order model (37) are

$$
p_{im}^s = \frac{W_c^s}{k_e(1 - x_{egr}^s)}
$$

$$
p_{em}^s = p_{amb}\left(1 - \frac{c_{pa}\left(\left(\frac{p_{im}^s}{p_{amb}}\right)^{\mu_a} - 1\right)T_{amb}\,W_c^s}{c_{pe}\,\eta_{cmt}\,T_{em}^s(W_c^s + W_f)}\right)^{-\frac{1}{\mu_e}}
\tag{38}
$$

where $\eta_{cmt} = \eta_c^s \eta_m \eta_t$. The set-point T_{em}^s for the exhaust manifold temperature is calculated using the model in [15] and [6]

$$T_{em}^s = T_{amb} + (T_e - T_{amb})\, e^{-\frac{h_{tot}\, \pi\, d_{pipe}\, l_{pipe}\, n_{pipe}}{W_{eo}^s\, c_{pe}}}$$

where

$$W_{eo}^s = \frac{W_c^s}{1 - x_{egr}^s} + W_f, \quad T_e = T_{im} + \frac{q_{HV}\, f_{Te}(W_f, n_e)}{c_{pe}\, W_{eo}^s}$$

and

$$f_{Te}(W_f, n_e) = c_{fTe1}\, W_f + c_{fTe2}\, n_e + c_{fTe3}\, W_f\, n_e + c_{fTe4}$$

The set-point η_c^s for the compressor efficiency is calculated using the model in [15]

$$\eta_c^s = \eta_{cmax} - \chi^T Q_c \chi$$

χ is a vector which contains the inputs

$$\chi = \left[\begin{array}{c} W_c^s - W_{copt} \\ \pi_c - \pi_{copt} \end{array} \right]$$

where the non-linear transformation for $\frac{p_{im}^s}{p_{amb}}$ is

$$\pi_c = \left(\frac{p_{im}^s}{p_{amb}} - 1 \right)^{c_\pi}$$

and the symmetric and positive definite matrix Q_c consists of three parameters

$$Q_c = \left[\begin{array}{cc} a_1 & a_3 \\ a_3 & a_2 \end{array} \right]$$

The model parameters η_{cmax}, a_1, a_2, and a_3 are tuned according to [15].

Integral action

If the control structure is applied on a higher order model or a real engine, there will be control errors for λ_O. This is due to that the equilibriums (38) for the third order model are not the same as the equilibriums for p_{im} and p_{em} of a higher order model or a real engine due to model errors in the third order model. In order to decrease these control errors, the following integral action is used

$$\frac{di}{dt} = K_{\lambda_O}\, e_{\lambda_O} \tag{39}$$

where $e_{\lambda_O} = \lambda_O^s - \lambda_O$. The state i is fed into W_c^s in (35) according to

$$W_c^s = \frac{W_f}{2\,X_{Oc}} \cdot$$
$$\left(\beta + \sqrt{\beta^2 + 4\,(\lambda_O^s + i)(O/F)_s(1 - x_{egr}^s)X_{Oc}} \right)$$
$$\beta = ((\lambda_O^s + i)(O/F)_s - X_{Oc})(1 - x_{egr}^s) + (O/F)_s\, x_{egr}^s$$

The set-point transformation (36) between x_{egr}^s and W_{egr}^s is based on the definition of x_{egr} in (7) and does not have any model errors and consequently there is no need of using integral action on x_{egr}.

6.3   Saturation levels

The saturation levels for the control inputs $u_{W_{egr}}$ and u_{W_t} are calculated using the models for the EGR-flow (8) and the turbine flow (12) in the following way. The saturation levels for $u_{W_{egr}}$ are calculated as

$$W_{egr}^{min} = \frac{A_{egrmax}\, f_{egr}(u_{egr}^{min})\, p_{em}\, \max(\Psi_{egr}, 0.1)}{\sqrt{T_{em}\, R_e}} \tag{40}$$

$$W_{egr}^{max} = \frac{A_{egrmax}\, f_{egr}(u_{egr}^{max})\, p_{em}\, \max(\Psi_{egr}, 0.1)}{\sqrt{T_{em}\, R_e}} \tag{41}$$

where $f_{egr}(u_{egr}^{min})$ and $f_{egr}(u_{egr}^{max})$ are given by (11), and u_{egr}^{min} and u_{egr}^{max} are the saturations levels for u_{egr}. The saturation levels for u_{W_t} are calculated as

$$W_t^{min} = \frac{A_{vgtmax}\, p_{em}\, \max\left(f_{\Pi t}, 0.1\right)\, f_{vgt}(u_{vgt}^{min})}{\sqrt{T_{em}\, R_e}} \tag{42}$$

$$W_t^{max} = \frac{A_{vgtmax}\, p_{em}\, \max\left(f_{\Pi t}, 0.1\right)\, f_{vgt}(u_{vgt}^{max})}{\sqrt{T_{em}\, R_e}} \tag{43}$$

where $f_{vgt}(u_{vgt}^{min})$ and $f_{vgt}(u_{vgt}^{max})$ are given by (14), and u_{vgt}^{min} and u_{vgt}^{max} are the saturations levels for u_{vgt}. To get the correct values on the saturation levels (40)–(43), the max-selectors in (17) and (25) have to be used in the same way in (40)–(43).

6.4   Additional control modes

In order to achieve the control objectives 3, 5, and 6 stated in Sec. 1.1, additional control modes are added to the main control loops (33)–(34) according to

$$u_{W_{egr}}(t_i) = \begin{cases} W_{egr}^{max} & , \text{if } (u_{W_{egr}}(t_{i-1}) = W_{egr}^{max})\& \\ & \quad (e_{W_{egr}} > -5 \cdot 10^{-3}) \\[2mm] PI_1(W_{egr}^s, W_{egr}) & , \text{else} \end{cases} \tag{44}$$

$$u_{W_t}(t_i) = \begin{cases} \min(-PI_2(p_{em}^s, p_{em}), \\ \quad -PI_3(W_{egr}^s, W_{egr})) & , \text{if } u_{W_{egr}}(t_{i-1}) = W_{egr}^{max} \\[2mm] -PI_2(p_{em}^s, p_{em}) & , \text{else} \end{cases} \tag{45}$$

$$u_{vgt}^{min} = -PID_4(e_{nt}) \tag{46}$$

where $e_{W_{egr}} = W_{egr}^s - W_{egr}$ and $e_{nt} = n_t^s - n_t$. The additional control modes in the structure (44)–(46) are motivated as follows. In operating points with low

engine torque there is too little EGR-flow although $u_{W_{egr}}$ is saturated at W_{egr}^{max}. To achieve control objective 3 also for these operating points, a higher EGR-flow is obtainable by decreasing u_{W_t} when $u_{W_{egr}} = W_{egr}^{max}$ using $PI_3(W_{egr}^s, W_{egr})$ in (45). The appropriate value for u_{W_t} is then the smallest value of the outputs from the two different PI controllers. To achieve control objective 5 and avoid over-speeding of the turbo, the lower saturation level u_{vgt}^{min} for the VGT is influenced by the turbine speed n_t in (46). In this case n_t is controlled with u_{vgt}^{min} to a set-point n_t^s which has a value slightly lower than the maximum limit n_t^{max} in order to avoid that overshoots shall exceed n_t^{max}. This means that u_{vgt}^{min} will open up the VGT, thereby decreasing the input torque to the turbocharger, and thereby keeping its speed within limits. The PID controller in (46) benefits from a derivative parts in order to predict high turbocharger speeds [13]. The other saturation levels for u_{egr} and u_{vgt} are set to $u_{egr}^{min} = 0$, $u_{egr}^{max} = 80$, and $u_{vgt}^{max} = 100$. The saturation levels for PID_4 are set to 22 and 100.

Further, the proposed control structure (44)–(46) gives priority to x_{egr} before λ_O or equivalent it gives priority to W_{egr} before p_{em} during aggressive load transients. This can be seen in the following way. During aggressive load transients, p_{em}^s increases yielding a decrease in u_{W_t}. If p_{em}^s is too large, u_{W_t} is saturated at W_t^{min} and p_{em}^s is not reached while $u_{W_{egr}}$ controls W_{egr}. Consequently, W_{egr} has higher priority than p_{em}.

Pumping minimization and handling of other control objectives

This structure also minimizes the pumping work in stationary points by striving to open the actuators as much as possible. Consequently, control objective 6 is achieved, and this can be understood as follows. The important controller action is coupled to λ_O and p_{em}, and in particular the operating conditions where there is a degree of freedom when $\lambda_O > \lambda_O^s$. For these conditions $p_{em} > p_{em}^s$ since p_{em} and p_{em}^s increases when λ_O and λ_O^s increases for constant x_{egr}. There are two cases to consider for these conditions. In the first case the proposed controller strives to reduce p_{em} by opening the VGT, through the second row in (45). To maintain W_{egr}^s, the second row in (44) forces the EGR-valve to be opened as much as possible. Either p_{em}^s is reached or $PI_2(p_{em}^s, p_{em})$ saturates at W_t^{max}, due to the integral action. In the other case, coupled to the first rows in (44)–(45), the EGR-valve is fully open and it is necessary to increase W_{egr} by closing the VGT to reach W_{egr}^s. In both cases the actuators are thus opened as much as possible while achieving control objectives 1 and 3 and this minimizes the pumping work according to [13].

In case 1 in (44) $u_{W_{egr}}$ is locked to W_{egr}^{max} until $e_{W_{egr}} > -5 \cdot 10^{-3}$ in order to avoid undesirable oscillations between case 1 and 2 in (45). Further, control objective 2 and 4 are achieved using feedforward fuel control and a smoke limiter in the same way as in [13].

6.5   Integral action with anti-windup

The integral action (39) is implemented in discrete form with anti-windup according to Algorithm 1 that is motivated as follows. In operating points where u_{W_t} or $u_{W_{egr}}$ are saturated at their maximum values and $e_{p_{em}} < 0$, p_{em} can not be decreased to get $e_{p_{em}} = 0$ while controlling W_{egr}. Consequently, λ_O can not be decreased to get $e_{\lambda_O} = 0$ leading to that $e_{\lambda_O} < 0$ and $i \to -\infty$. To handle this and affect i so that $i \to 0$ for these operating points, row 2 in Algorithm 1 is executed that is a discrete form of $di/dt = -\delta i$ if $\alpha_1 = i_n$. In order to increase i if $e_{\lambda_O} > 0$, a max-selector between α_1 and α_2 is used in row 4, where $\alpha_2 := i_{n-1} + T_s K_{\lambda_O} e_{\lambda_O}$ in row 3 is a discrete form of (39) if $\alpha_2 = i_n$. Further, due to noise, time delays, and dynamics in the system there are some few operating points where $e_{\lambda_O} \ll 0$, $u_{vgt} \ll 100$, and $u_{egr} < 80$ leading to that $i \to -\infty$ slowly. To handle this, row 2–4 are also executed when $e_{\lambda_O} < -1$ and $u_{vgt} > 50$, otherwise row 6 is executed. Moreover, in operating points where $u_{W_t} = W_t^{min}$ or $p_{em}^s > 10^6$, p_{em} can not reach p_{em}^s leading to that $e_{p_{em}} > 0$ while controlling W_{egr}. This leads to that λ_O can not reach λ_O^s leading to that $e_{\lambda_O} > 0$ and $i \to +\infty$. To handle this and limit i for these operating points, a min-selector between α_3 and i_{n-1} is used in row 9, otherwise row 11 is executed.

Algorithm 1 Integral action with anti-windup

1: **if** $(e_{p_{em}} < 0$ **and** $(u_{W_t} = W_t^{max}$ **or** $u_{W_{egr}} = W_{egr}^{max}))$ **or**
   $(e_{\lambda_O} < -1$ **and** $u_{vgt} > 50)$ **then**
2:     $\alpha_1 := i_{n-1} - T_s \delta i_{n-1}$
3:     $\alpha_2 := i_{n-1} + T_s K_{\lambda_O} e_{\lambda_O}$
4:     $\alpha_3 := \max(\alpha_1, \alpha_2)$
5: **else**
6:     $\alpha_3 := i_{n-1} + T_s K_{\lambda_O} e_{\lambda_O}$
7: **end if**
8: **if** $u_{W_t} = W_t^{min}$ **or** $p_{em}^s > 10^6$ **then**
9:     $i_n := \min(\alpha_3, i_{n-1})$
10: **else**
11:     $i_n := \alpha_3$
12: **end if**

6.6   PID parameterization and implementation

Each PI controller in (44)–(45) has the following parameterization

$$PI_j(y^s, y) = K_j \left(\alpha_j y^s - y + \frac{1}{T_{ij}} \int (y^s - y) \, dt \right) \tag{47}$$

where the index j is the number of the different PI controllers. The PID controller in (46) has the following parameterization

$$\mathrm{PID}_4(e) = \mathsf{K}_4 \left(e + \frac{1}{\mathsf{T}_{i4}} \int e \, \mathrm{dt} + \mathsf{T}_{d4} \frac{\mathrm{de}}{\mathrm{dt}} \right) \qquad (48)$$

that does not benefit from the tuning parameter α_j in (47) due to that the set-point n_t^s in (46) is constant. The PI and PID controllers are implemented in incremental form which leads to anti-windup and bump-less transfer between the different control modes [17].

6.7 Stability analysis of the closed-loop system

To analyze if the proposed control structure (44)–(45) stabilizes the linearized models (32), the control structure is applied to these linearized models and the closed-loop poles are mapped. The control parameters are tuned using the method in [14] with $\gamma_{Me} = 3/2$ and $\gamma_{egr} = 1$. Each control mode in (44)–(45) is analyzed separately resulting in linear closed-loop systems. The poles for these closed-loop systems are mapped in Fig. 10 showing that all poles are in the left complex half plane for almost the complete operating region except in operating points at the thick black line in the left bottom plot where there is one pole in the right complex half plane. Further, the system analysis in [16] shows that the DC-gain from u_{vgt} to x_{egr} has reversed sign (positive sign) in these unstable operating points. The question is what effect this instability and sign reversal have on the control performance. Simulations show that if the system operates in these unstable points in the beginning of a transient and $W_{egr} < W_{egr}^s$, the VGT position decreases until $W_{egr} = W_{egr}^s$ (according to $\mathrm{PI}_3(W_{egr}^s, W_{egr})$) in (45)). Consequently the system will leave the unstable operating points. If the system operates in the unstable points in the beginning of a transient and $W_{egr} > W_{egr}^s$, the VGT position increases until it is fully open, and then $\mathrm{PI}_1(W_{egr}^s, W_{egr})$ in (44) becomes active and closes the EGR-valve until $W_{egr} = W_{egr}^s$. Consequently, the system can not get caught in the unstable region. However, the effect of this instability and sign reversal is that there exist two sets of solutions for the EGR-valve and the VGT-position for the same value of W_{egr}^s depending on if $W_{egr} < W_{egr}^s$ or if $W_{egr} > W_{egr}^s$ in the beginning of a transient. However, the proposed control structure is not extended to handle this, since the maximum profit in pumping work would only be 2.5 mBar, which is an insignificant value.

7 Engine test cell experiments

The control structure proposed in Sec. 6 is applied and validated in an engine test cell. The goal is to compare the following two control structures for the steps in Fig. 3, for an aggressive transient from the European Transient Cycle (ETC), and for the complete ETC cycle.

PID: The control structure without non-linear compensator (15)–(16).
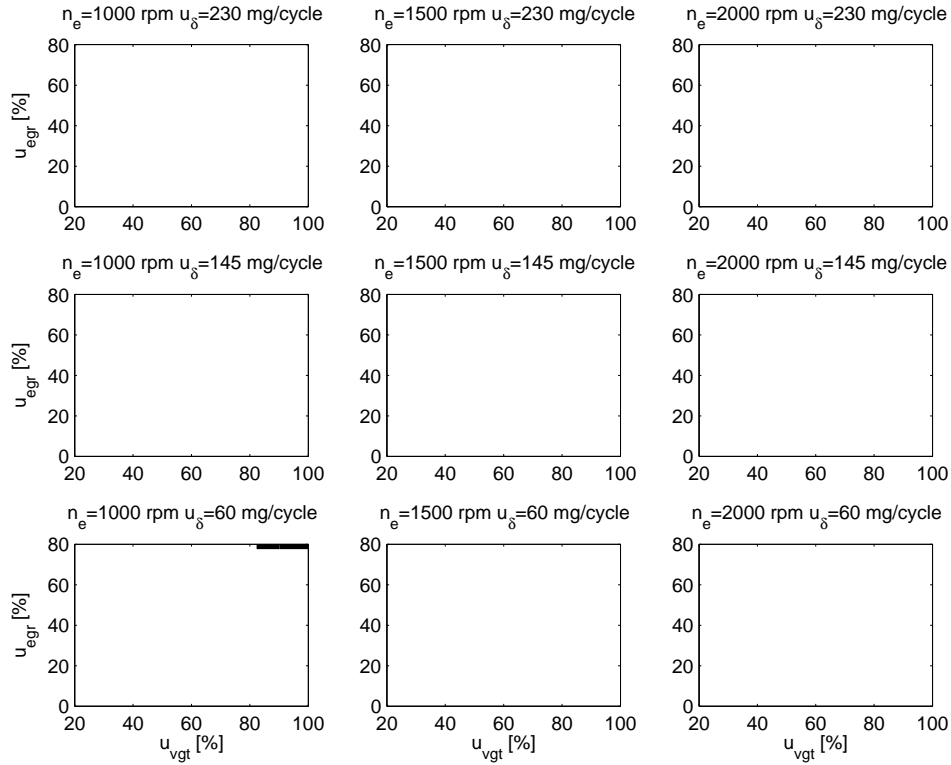
Figure 10 *A mapping of poles for the closed-loop system where the proposed control structure (44)–(45) is applied to the linearized models (32). All poles are in the left complex half plane for almost the complete operating region except in operating points at the thick black line in the left bottom plot where there is one pole in the right complex half plane.*

NLC: The proposed control structure with non-linear compensator as depicted in Fig. 9.

The observer, measured signals, and tuning for PID are explained in Sec. 4. For NLC, the same observer as the one in Sec. 4.1 is used to estimate the oxygen mass fraction X_{Oim}. Once X_{Oim} is estimated, the mass flow into the engine W_{ei}, λ_O and W_{egr} are calculated using the model in Sec. 2. The engine speed (n_e), intake and exhaust manifold pressure (p_{im}, p_{em}), compressor mass flow (W_c), and turbocharger speed (n_t) are measured with production sensors. Due to measurement noise, all measured and observed variables are filtered using low pass filters with a time constant of 0.1 s. The controller parameters are initially tuned using the method in [14] with manual initialization and $\gamma_{Me} = 3/2$ and $\gamma_{egr} = 1$, and are then manually fine tuned in the engine test cell experiments.

7.1 Comparing step responses in oxygen/fuel ratio

PID and NLC are compared in Fig. 11 for the same three steps as in Fig. 3. The result is that NLC gives approximately the same step response in λ_O for all three steps with fast control and less oscillations compared to PID. Consequently, NLC handles nonlinear effects. Further, the internal variables for NLC for this experiment in Fig. 12 show that p_{em} and W_{egr} follow their set-points and that $i_n \neq 0$ in stationary points, i.e. integral action is necessary to handle model errors in the set-point transformation.

7.2 Comparison on an aggressive ETC transient

PID and NLC are compared in Fig. 13–14 on an aggressive ETC transient showing that NLC gives less EGR-error but more λ_O-error when $\lambda_O < \lambda_O^s$. This can be understood as follows. At t=122-124 s, PID closes the VGT in order to increase x_{egr} and it closes the EGR-valve to fully closed in order to increase λ_O, yielding $x_{egr} = 0$ and a high EGR-error. However, NLC closes the VGT in order to increase p_{em} and it opens the EGR-valve in order to increase W_{egr}, yielding less EGR-error compared to PID. However, since PID closes the VGT and the EGR-valve more than NLC, PID gives a faster increase in turbocharger speed and therefore a faster increase in λ_O and less torque deficiency.

Further, at t=127-132 s x_{egr}^s is equal to zero and NLC closes the EGR-valve directly yielding $x_{egr} = 0$. However, PID has to first fully open the VGT, and then the PID can switch control mode and close the EGR-valve. This leads to a later closing of the EGR-valve and more EGR-error compared to NLC. However, since the EGR-valve is more open for PID, PID gives less pumping losses at t=126-131 s.

The differences in EGR-error, λ_O-error, and pumping losses between the two controllers at t=122-125 s are only due to that the tuning of the controllers have different trade-offs between EGR-error and λ_O-error. However, the differences in EGR-error and pumping losses at t=127-132 s are due to the selected control loops and modes in the control structures according to the explanation above. Consequently, the main benefit with NLC is that it reduces the EGR-error at t=127-132 s. However, one drawback with NLC is that it increases the pumping losses at t=126-131 s.
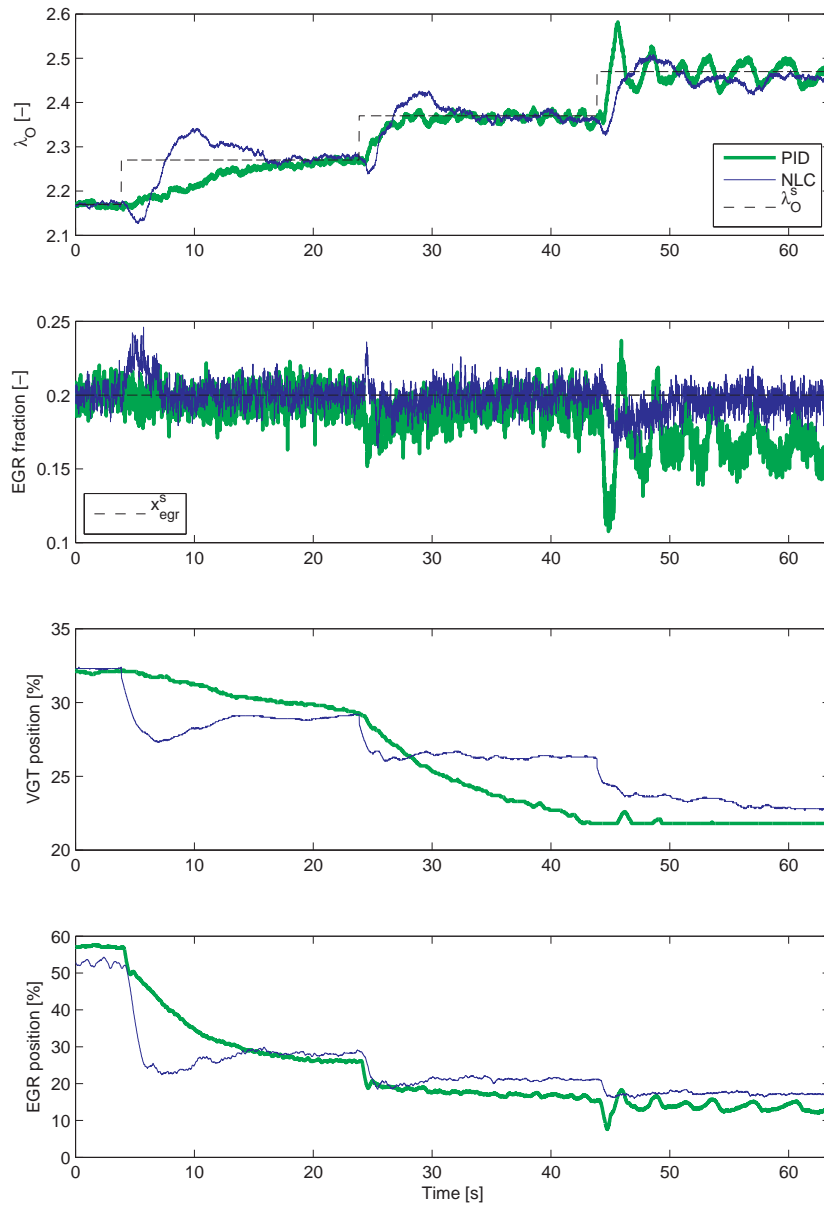
Figure 11 *Comparison between PID and NLC for the same steps in λ_O^s as in Fig. 3. NLC gives approximately the same step response in λ_O for all three steps with fast control and less oscillations compared to PID. Consequently, NLC handles nonlinear effects.*
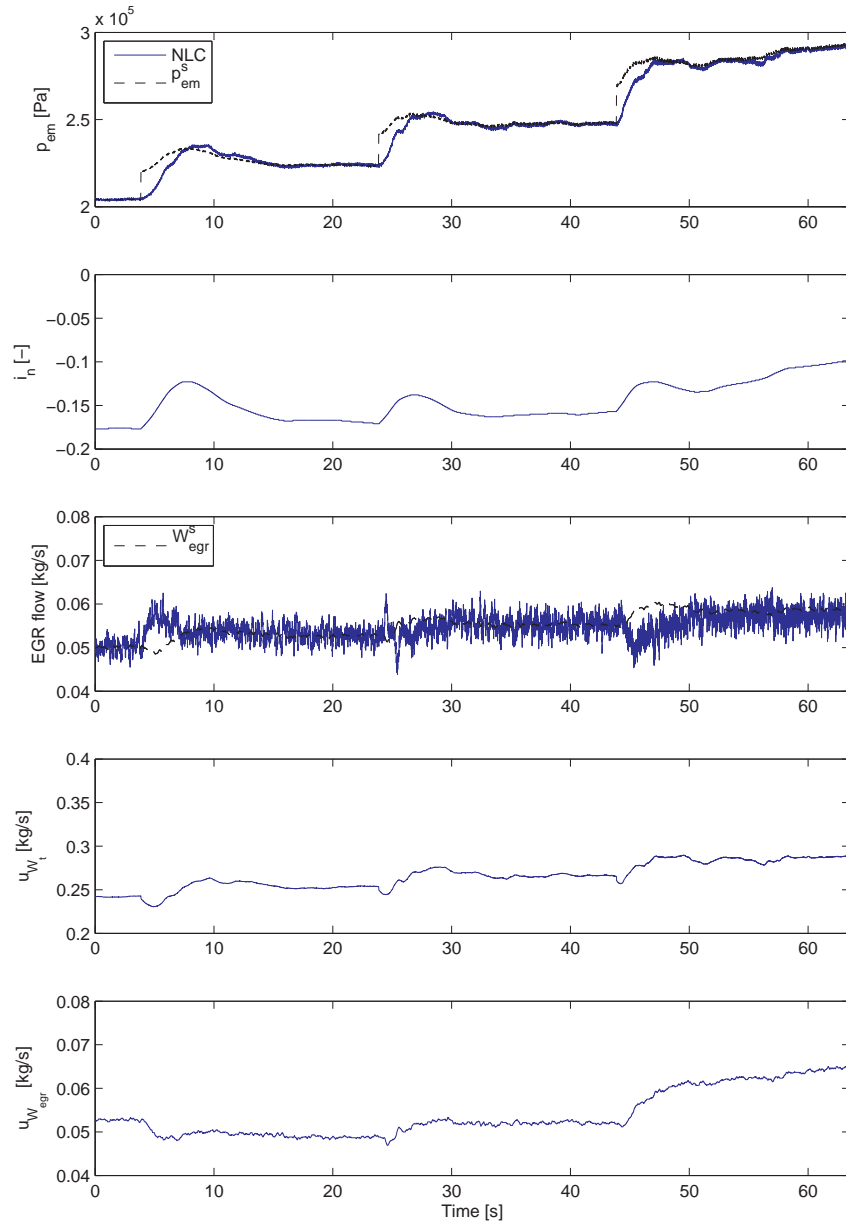
Figure 12 *Validation of the internal variables for NLC for the experiment in Fig. 11 showing that* p_{em} *and* W_{egr} *follow their set-points and that* $i_n \neq 0$ *in stationary points, i.e. integral action is necessary to handle model errors in the set-point transformation.*
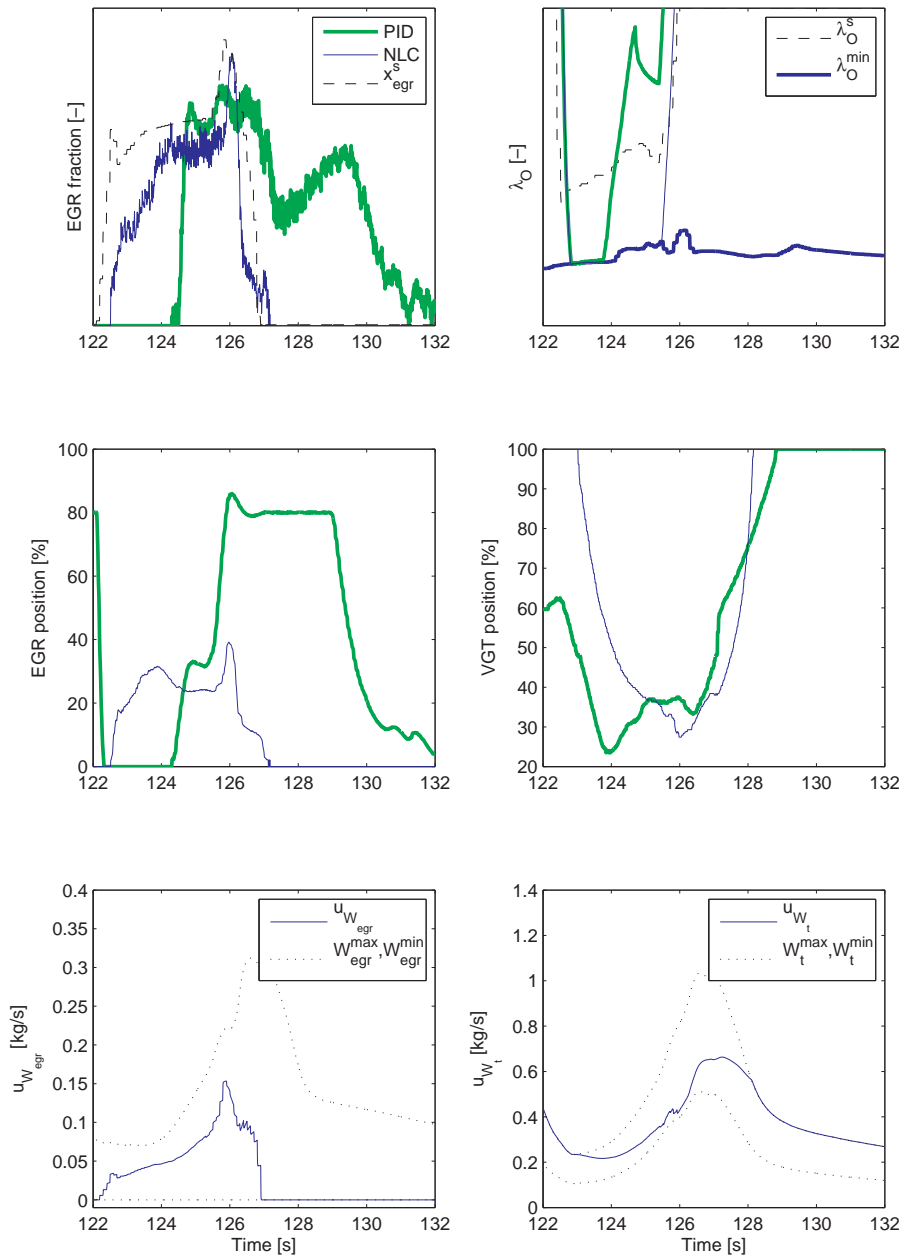
Figure 13 *Comparison between PID and NLC on an aggressive ETC tran-sient. NLC gives less EGR-error but more λ_O-error when $\lambda_O < \lambda_O^s$ compared to PID.*
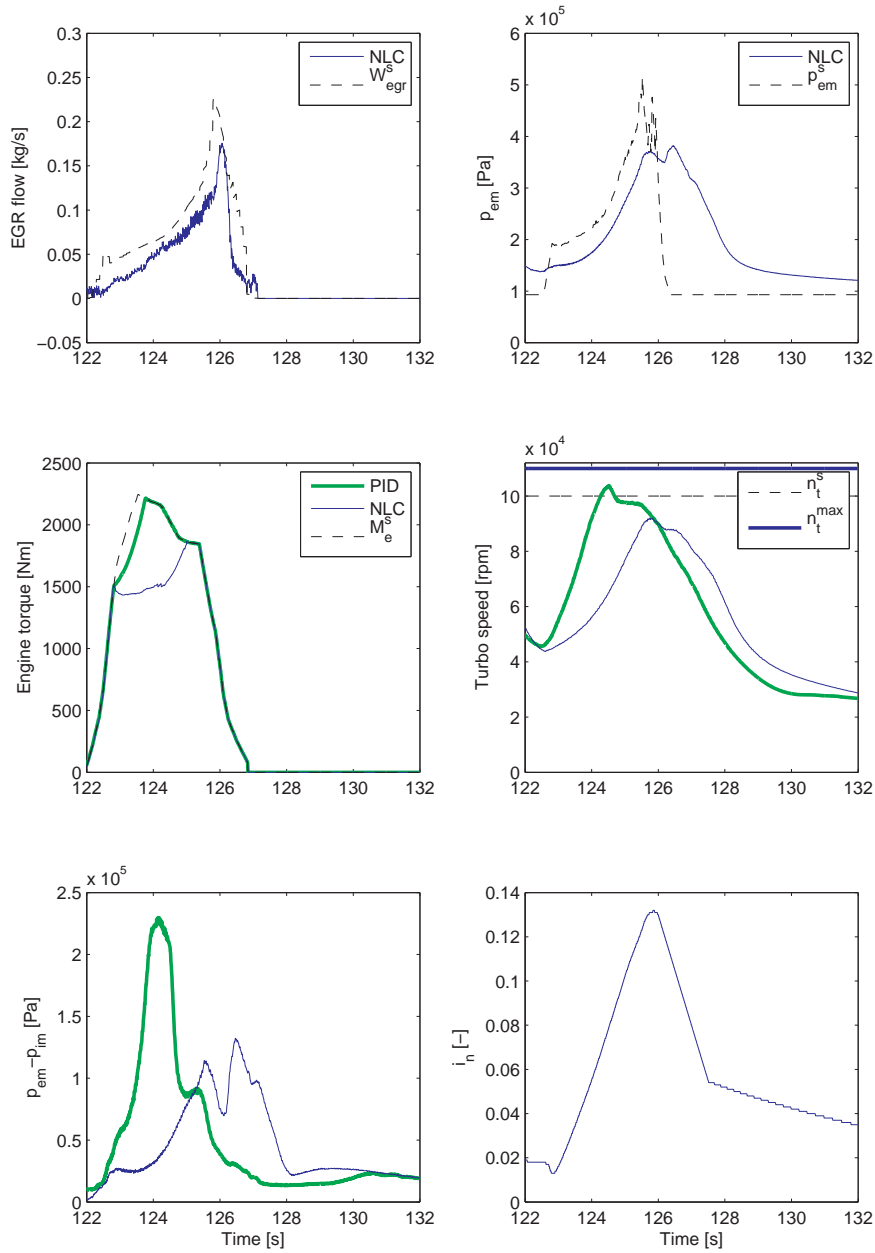
Figure 14 *Comparison between PID and NLC on an aggressive ETC transient. PID gives less torque deficiency and a faster increase in turbo speed compared to NLC.*

7.3   Comparison on the complete ETC cycle

PID and NLC are compared on the complete ETC cycle by comparing λ_O-error, x_{egr}-error, and pumping losses

$$
E_{\lambda_O} = \sum_{i=1}^{N} \max(e_{\lambda_O}(t_i), 0)
$$

$$
E_{x_{egr}} = \sum_{i=1}^{N} |e_{xegr}(t_i)| \tag{49}
$$

$$
PMEP = \sum_{i=1}^{N} (p_{em}(t_i) - p_{im}(t_i))
$$

where t_i is the time at sample number i. The comparison in Tab. 1 shows that PID has 47% higher EGR-error and 13% lower pumping losses. These two differences are due to the selected control loops and modes in the control structures and that the tuning of the controllers have different trade-offs between EGR-error and λ_O-error as explained in Sec. 7.2. However, the difference in λ_O-error is only due to that the tuning of the controllers have different trade-offs.

Table 1 *The measures* (49) *for two different controllers over the ETC cycle. The measures are normalized with respect to NLC.*

Controller	E_{λ_O}	$E_{x_{egr}}$	PMEP
NLC	1.00	1.00	1.00
PID	0.44	1.47	0.87

8   Conclusions

Inspired by an approach in [5], a non-linear compensator has been investigated for handling of non-linear effects in diesel engines. This non-linear compensator is a non-linear state dependent input transformation that was developed by inverting the models for EGR-flow and turbine flow having actuator position as input and flow as output. This leads to two new control inputs: the EGR-flow and turbine flow. A mapping of the sign reversals in $u_{vgt} \rightarrow \lambda_O$ and $u_{vgt} \rightarrow p_{em}$ when the non-linear compensator for the EGR-actuator is used shows that they only occur when the EGR-valve is saturated. Further, a stability analysis of linearized models of the open-loop system with a non-linear compensator shows that these models are unstable in a large operating region. This system is stabilized by a control structure that consists of PID controllers and min/max-selectors. The EGR flow and the exhaust manifold pressure are chosen as feedback variables in this structure. Further, the set-points for λ_O and x_{egr} are transformed to set-points for the feedback variables. In order to handle model errors in this set-point

transformation, an integral action on λ_O is used in an outer loop. Experimental validations of the proposed control structure show that it handles nonlinear effects, and that it reduces EGR-errors but increases the pumping losses compared to a control structure without non-linear compensator.

References

[1] M. Ammann, N.P. Fekete, L. Guzzella, and A.H. Glattfelder. Model-based Control of the VGT and EGR in a Turbocharged Common-Rail Diesel Engine: Theory and Passenger Car Implementation. *SAE Technical paper 2003-01-0357*, January 2003.

[2] A. Amstutz and L. Del Re. EGO sensor based robust output control of EGR in diesel engines. *IEEE Transactions on Control System Technology*, pages 37–48, 1995.

[3] L. Guzzella and A. Amstutz. Control of diesel engines. *IEEE Control Systems Magazine*, 18:53–71, 1998.

[4] J.B. Heywood. *Internal Combustion Engine Fundamentals*. McGraw-Hill Book Co, 1988.

[5] M. Jankovic, M. Jankovic, and I.V. Kolmanovsky. Constructive lyapunov control design for turbocharged diesel engines. *IEEE Transactions on Control Systems Technology*, 2000.

[6] Andreas Jerhammar and Erik Höckerdal. Gas flow observer for a Scania diesel engine with VGT and EGR. Master's thesis, Linköpings Universitet, SE-581 83 Linköping, 2006.

[7] I.V. Kolmanovsky, A.G. Stefanopoulou, P.E. Moraal, and M. van Nieuwstadt. Issues in modeling and control of intake flow in variable geometry turbocharged engines. In *Proceedings of 18th IFIP Conference on System Modeling and Optimization*, Detroit, July 1997.

[8] M. Nieuwstadt, P.E. Moraal, I.V. Kolmanovsky, A. Stefanopoulou, P. Wood, and M. Widdle. Decentralized and multivariable designs for EGR–VGT control of a diesel engine. In *IFAC Workshop, Advances in Automotive Control*, 1998.

[9] M.J. Nieuwstadt, I.V. Kolmanovsky, P.E. Moraal, A.G. Stefanopoulou, and M. Jankovic. EGR–VGT control schemes: Experimental comparison for a high-speed diesel engine. *IEEE Control Systems Magazine*, 2000.

[10] R. Rajamani. Control of a variable-geometry turbocharged and wastegated diesel engine. *Proceedings of the I MECH E Part D Journal of Automobile Engineering*, November 2005.

[11] J. Rückert, A. Schloßer, H. Rake, B. Kinoo, M. Krüger, and S. Pischinger. Model based boost pressure and exhaust gas recirculation rate control for a diesel engine with variable turbine geometry. In *IFAC Workshop: Advances in Automotive Control*, 2001.

[12] A.G. Stefanopoulou, I.V. Kolmanovsky, and J.S. Freudenberg. Control of variable geometry turbocharged diesel engines for reduced emissions. *IEEE Transactions on Control Systems Technology*, 8(4), July 2000.

[13] Johan Wahlström. Control of EGR and VGT for emission control and pumping work minimization in diesel engines. Licentiate Thesis, Linköping University, 2006.

[14] Johan Wahlström, Lars Eriksson, and Lars Nielsen. Controller tuning based on transient selection and optimization for a diesel engine with EGR and VGT. In *Electronic Engine Controls*, number 2008-01-0985 in SAE Technical paper series SP-2159, SAE World Congress, Detroit, USA, 2008.

[15] Johan Wahlström and Lars Eriksson. Modeling of a diesel engine with VGT and EGR capturing sign reversal and non-minimum phase behaviors. Technical report, Linköping University, 2009.

[16] Johan Wahlström, Lars Eriksson, and Lars Nielsen. System analysis of a diesel engine with VGT and EGR. Technical report, Linköping University, 2009.

[17] K. J. Åström and T. Hägglund. *PID Controllers: Theory, Design and Tuning*. Research Triangle Park, Instrument Society of America, 2nd edition, 1995.

Nonlinear EGR and VGT Control with Integral Action for Diesel Engines[1]

Johan Wahlström and Lars Eriksson

Vehicular Systems, Department of Electrical Engineering,
Linköping University, S-581 83 Linköping,
Sweden.

Abstract

A non-linear multivariable control design with integral action is proposed
and investigated for control of EGR valve and VGT position in heavy duty
diesel engines. The main control goal is to regulate oxygen/fuel ratio and
intake manifold EGR-fraction, and they are specified in an outer loop.
These are chosen as main performance variables since they are strongly
coupled to the emissions. An existing non-linear control design based on
feedback linearization is extended with integral action. In particular the
control design method utilizes a control Lyapunov function, inverse optimal
control, and a non-linear compensator. Comparisons between different
control structures are performed in simulations showing the following four
points. Firstly, integral action is necessary to handle model errors so that
the controller can track the performance variables specified in the outer
loop. Secondly, the proposed control design handles the non-linear effects
in the diesel engine that results in less control errors compared to a control
structure with PID controllers. Thirdly, it is important to use the non-
linear compensator and it is sufficient to use a control structure with PID
controllers and a non-linear compensator to handle the non-linear effects.
Fourthly, the proposed control design is sensitive to model errors in the
EGR and turbine flow model while a control structure with PID controllers
and a non-linear compensator handles these model errors.

---

[1]This is an extended version of the paper "Robust Nonlinear EGR and VGT Control with Integral Action for Diesel Engines" by Johan Wahlström and Lars Eriksson, IFAC World Congress, Seoul, Korea, 2008.

1 Introduction

Legislated emission limits for heavy duty trucks are constantly reduced. To fulfill the requirements, technologies like Exhaust Gas Recirculation (EGR) systems and Variable Geometry Turbochargers (VGT) have been introduced. The primary emission reduction mechanisms utilized to control the emissions are that NO_x can be reduced by increasing the intake manifold EGR-fraction x_{egr} and smoke can be reduced by increasing the air/fuel ratio [5]. Note that exhaust gases, present in the intake, also contain oxygen which makes it more suitable to define and use the oxygen/fuel ratio λ_O instead of the traditional air/fuel ratio. The main motive for this is that it is the oxygen contents that is crucial for smoke generation. Besides λ_O it is natural to use EGR-fraction x_{egr} as the other main performance variable, but one could also use the burned gas fraction instead of the EGR-fraction.

The oxygen/fuel ratio λ_O and EGR fraction x_{egr} depend in complicated ways on the EGR and VGT actuation. It is therefore necessary to have coordinated control of the EGR and VGT to reach the legislated emission limits in NO_x and smoke. Various approaches for coordinated control of the EGR and VGT for emission abatement have been published. Reference [4] presents a good overview of different control aspects of diesel engines with EGR and VGT, and in [9] there is a comparison of some control approaches with different selections of performance variables. Other control approaches are described in [2], [8], [12], [1], and [10].

A non-linear multivariable control design is proposed in [6]. This design includes construction of a Lyapunov function, inverse optimal control, and a non-linear compensator which provides a control law that handles interactions and non-linear properties in the system. The compressor mass flow W_c and exhaust manifold pressure p_{em} are chosen as outputs, and therefore the set-points for λ_O and x_{egr} are transformed to set-points for W_c and p_{em}. This transformation is based on a third-order model that describes the most important dynamics in the engine: the pressure dynamics in the intake and exhaust manifolds and the turbocharger dynamics. The third order non-linear model captures the main system properties, such as non-minimum phase behaviors and sign reversals. If the control design is applied to a higher order model or a real engine, there will be control errors for λ_O and x_{egr} due to model errors in the third order model. In order to decrease these control errors, this paper proposes a control design that extends the one in [6] with integral action. It also analyzes the robustness of the structure and compares it with the design in [6] and with two other PID based controllers.

1.1 Outline

A mean value diesel engine model that is used in simulation for tuning and validation of the developed controller is described in Sec. 2. The control design method used in this paper is described in Sec. 3. Sec. 4 describes the proposed control design with integral action. For efficient calibration an automatic controller tuning method is developed in Sec. 5. Finally, Sec. 6 illustrates the advantages with integral action, non-linear control, and a non-linear compensator. It also illustrates
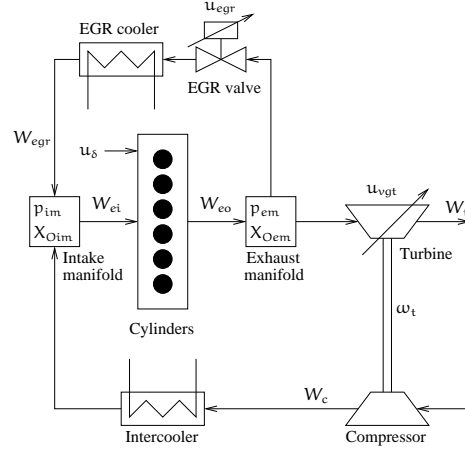
Figure 1 *Sketch of the diesel engine model used for simulation, control design, and tuning. It has five states related to the engine (p_{im}, p_{em}, X_{Oim}, X_{Oem}, and ω_t) and three for actuator dynamics.*

the sensitivity to model uncertainties by comparing the proposed control design with a control structure with PID controllers and a non-linear compensator.

2 Diesel engine model

A model for a heavy duty diesel engine is used in simulation for tuning and validation of the developed controller. This diesel engine model is focused on the gas flows, see Fig. 1, and it is a mean value model with eight states: intake and exhaust manifold pressures (p_{im} and p_{em}), oxygen mass fraction in the intake and exhaust manifold (X_{Oim} and X_{Oem}), turbocharger speed (ω_t), and three states ($\tilde{u}_{egr1}$, $\tilde{u}_{egr2}$, and $\tilde{u}_{vgt}$) describing the actuator dynamics for the two control signals (u_{egr} and u_{vgt}). These states are collected in a state vector x

$$x = [p_{im} \quad p_{em} \quad X_{Oim} \quad X_{Oem} \quad \omega_t \quad \tilde{u}_{egr1} \quad \tilde{u}_{egr2} \quad \tilde{u}_{vgt}]^\mathsf{T}$$

There are no state equations for the manifold temperatures, since the pressures and the turbocharger speed govern the most important system properties, such as non-minimum phase behaviors, overshoots, and sign reversals, while the temperature states only have minor effects on these system properties.

The resulting model is expressed in state space form as

$$\dot{x} = f(x, u, n_e)$$

where the engine speed n_e is considered as an input to the model, and u is the control input vector

$$u = [u_\delta \quad u_{egr} \quad u_{vgt}]^\mathsf{T}$$

which contains mass of injected fuel u_δ, EGR-valve position u_{egr}, and VGT actuator position u_{vgt}.

A detailed description and derivation of the model together with a model tuning and a validation against test cell measurements is given in [15]. The derivatives of the engine state variables are given by (1), and the oxygen concentration in the exhaust gas is calculated in (2). Further, the main performance variables are defined by (3).

$$\frac{d}{dt}\, p_{em} = f_1(x, u), \quad \frac{d}{dt}\, \omega_t = f_2(x, u) \tag{1a}$$

$$\frac{d}{dt}\, p_{im} = \frac{R_a\, T_{im}}{V_{im}} \left(W_c + W_{egr} - W_{ei}\right) \tag{1b}$$

$$\frac{d}{dt}\, X_{Oim} = \frac{R_a\, T_{im}}{p_{im}\, V_{im}} ((X_{Oem} - X_{Oim})\, W_{egr} +$$
$$(X_{Oc} - X_{Oim})\, W_c) \tag{1c}$$

$$\frac{d}{dt}\, X_{Oem} = \frac{R_e\, T_{em}}{p_{em}\, V_{em}} \left(X_{Oe} - X_{Oem}\right) \left(W_f + W_{ei}\right) \tag{1d}$$

$$X_{Oe} = \frac{W_{ei}\, X_{Oim} - W_f\, (O/F)_s}{W_f + W_{ei}} \tag{2}$$

$$x_{egr} = \frac{W_{egr}}{W_c + W_{egr}}, \quad \lambda_O = \frac{W_{ei}\, X_{Oim}}{W_f\, (O/F)_s} \tag{3}$$

3   Robust nonlinear control

The control design method used is based on a non-linear multivariable method proposed in [11] and [7]. It includes construction of a Control Lyapunov Function (CLF) and inverse optimal control that guarantees robustness of optimal controllers. The control design method is briefly reviewed below.

Consider the system

$$\dot{x} = f(x) + g(x)u$$
$$y = h(x) + j(x)u, \quad x \in \mathbb{R}^n, \quad u, y \in \mathbb{R}^m \tag{4}$$

where $u = 0$ render the equilibrium point $x = 0$. As mentioned above, the control design method includes construction of a CLF $V(x)$ that is defined as follows.

Definition 1 (Control Lyapunov Function)
A positive definite, radially unbounded, smooth scalar function $V(x)$ is called a Control Lyapunov Function (CLF) for (4) if there exists a u such that

$$\dot{V}(x) = L_f\, V(x) + L_g\, V(x)u < 0$$

for all $x \neq 0$. The notation $L_q\, V(x)$ denotes the Lie derivate of $V(x)$ along the vector field $q(x)$.

The control design method also includes inverse optimal control, where the goal is to first design a control law and then determine which cost function it minimizes. In order to obtain a simple relation between the control law and the cost function, the cost function is chosen quadratic in u according to

$$\int_0^\infty l(x) + u^\mathsf{T} R(x)\, u\, dt, \quad l(x) > 0, \quad R(x) > 0 \tag{5}$$

In standard optimal control [3], the control law that minimizes (5) is found by solving the Hamilton-Jacobi-Bellman equation

$$0 = \min_u [l(x) + u^\mathsf{T} R(x)\, u + L_f\, V(x) + L_g\, V(x)u] \tag{6}$$

where $V(x)$ is a CLF. Eq. (6) has the solution

$$u(x) = -\frac{1}{2} R^{-1} (L_g\, V)^\mathsf{T}(x) \tag{7}$$

Consequently, the goal is to first design $V(x)$ and the matrix $R(x)$, and then determine $l(x)$ in order to see which cost function the control law (7) minimizes. The function $l(x)$ is found by solving (6) for $l(x)$, with the control law (7) inserted, yielding

$$l(x) = \frac{1}{4} L_g\, V(x) R^{-1} (L_g\, V)^\mathsf{T}(x) - L_f\, V(x) \tag{8}$$

The optimal control law (7) guarantees stability and robustness properties. In particular, if

$$l(x) > 0 \tag{9}$$

and $R(x)$ is diagonal then the control law (7) gives asymptotic stability and it is robust to static input uncertainties and has $(1/2, \infty)$ gain margin [11].

4 Control design with integral action

A control design without integral action of a diesel engine using the method in Sec. 3 is proposed in [6]. This gives an inner loop that handles nonlinearities and decouples the system. However, as will be shown in Sec. 6, integral action is necessary to handle model errors so that the controller can track the performance variables λ_O and x_{egr} specified in an outer loop. Therefore, the proposed design is extended with integral action, resulting in the proposed closed-loop system with integral action shown in Fig. 2.

4.1 Control design model

In order to get a simple control law, the eighth order model in Sec. 2 is simplified to a model with three states: p_{im}, p_{em}, and the compressor power P_c. This model is based on the control design model developed in [6].
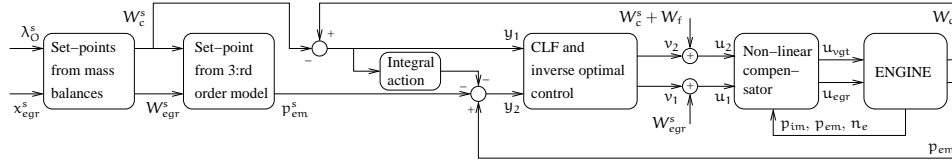
Figure 2 *Block diagram of the closed-loop system, showing; set-points cal-culations, integral action on the flow W_c, non-linear control of the flows u_1 and u_2, and a non-linear compensator that is an inversion of position to flow models.*

The simplifications that lead to this third order model are as follows. First, the states X_{Oim} and X_{Oem} are removed from the eighth order model due to that they do not affect the other states. However, these states affect the performance variable λ_O and it can therefore not be chosen as an output for the third order model in Sec. 4.2. Next, it is assumed that the actuators dynamics are fast and the actuator states are therefore removed. Further, the exhaust manifold temperature T_{em} is treated as an external slowly varying signal, the turbine and compressor efficiencies are assumed to be constant, and the turbocharger dynamics is modeled as a first-order system by using the compressor power P_c as a state. Moreover, the EGR-flow W_{egr} and the turbine flow W_t are treated as control inputs u_1 and u_2. The values for u_{egr} and u_{vgt} are then obtained by using inversion of position to flow models (see Fig. 2). These simplifications lead to the following control design model

$$
\begin{aligned}
\dot{p}_{im} &= k_{im}\left(W_c + u_1 - k_e\,p_{im}\right)\\
\dot{p}_{em} &= k_{em}\left(k_e\,p_{im} - u_1 - u_2 + W_f\right)\\
\dot{P}_c &= \frac{1}{\tau}\left(\eta_m\,P_t - P_c\right)
\end{aligned}
\tag{10}
$$

$$
\begin{aligned}
W_c &= \frac{\eta_c\,P_c}{T_{amb}\,c_{pa}\left(\left(p_{im}/p_{amb}\right)^{\mu_a} - 1\right)}\\
P_t &= \eta_t\,c_{pe}\,T_{em}\left(1 - \left(p_{amb}/p_{em}\right)^{\mu_e}\right)u_2
\end{aligned}
$$

The variables $k_{em} = k_{em}(T_{em})$, $W_f = W_f(u_\delta, n_e)$, and $k_e = k_e(n_e)$ are treated as external slowly varying signals and k_{im}, τ, η_m, η_c, T_{amb}, c_{pa}, p_{amb}, μ_a, η_t, c_{pe}, and μ_e are constants. This model is the same as the control design model developed in [6] if $c_{pa} = c_{pe}$ and $\mu_a = \mu_e$.

A linearization of this model is performed in several operating points covering the complete operating region showing that these linearized models have one pole in the right complex half plane for the complete operating region and are therefore unstable.

4.2 Outputs and set-points

The design objective is to regulate λ_O and x_{egr} to their set-points λ_O^s and x_{egr}^s. However, λ_O can not be calculated from the control design model in Sec. 4.1. Further, p_{em} has to be chosen as one output in order to get stable zero dynamics [6]. Therefore, the following outputs are chosen

$$y_1 = W_c - W_c^s, \quad y_2 = p_{em} - p_{em}^s \tag{11}$$

The set-points λ_O^s and x_{egr}^s are transformed to the set-points W_c^s and p_{em}^s in two steps. Firstly, the equilibriums for W_c and W_{egr} of the mass balances (1b)–(1d) are calculated from λ_O^s and x_{egr}^s

$$
\begin{aligned}
W_c^s &= \frac{W_f}{2\,X_{Oc}} \left(\beta + \sqrt{\beta^2 + 4\,\lambda_O^s\,(O/F)_s(1 - x_{egr}^s)X_{Oc}} \right) \\
W_{egr}^s &= \frac{x_{egr}^s}{1 - x_{egr}^s} W_c^s
\end{aligned}
\tag{12}
$$

where

$$\beta = (\lambda_O^s\,(O/F)_s - X_{Oc})(1 - x_{egr}^s) + (O/F)_s\,x_{egr}^s,$$

where X_{Oc} is the constant oxygen concentration in air passing the compressor, and $(O/F)_s$ is the stoichiometric relation between oxygen and fuel masses. Secondly, the equilibriums for p_{im} and p_{em} of the third-order model in Sec. 4.1 are calculated from W_c^s and W_{egr}^s

$$
\begin{aligned}
p_{im}^s &= \frac{W_c^s + W_{egr}^s}{k_e} \\
p_{em}^s &= p_{amb} \left(1 - \frac{c_{pa} \left(\left(\frac{p_{im}^s}{p_{amb}} \right)^{\mu_a} - 1 \right) T_{amb}\,W_c^s}{c_{pe}\,\eta_{cmt}\,T_{em}(W_c^s + W_f)} \right)^{-\frac{1}{\mu_e}}
\end{aligned}
\tag{13}
$$

where $\eta_{cmt} = \eta_c\,\eta_m\,\eta_t$.

4.3 Integral action

If the control design is applied on a higher order model or a real engine, there will be control errors in (11), yielding errors in λ_O and x_{egr} (this will be illustrated in Fig. 4). This is due to that the equilibriums (13) for the third order model are not the same as the equilibriums for p_{im} and p_{em} of a higher order model or a real engine due to model errors in the third order model. In order to decrease these control errors, the following approximate integral action is used

$$\frac{di}{dt} = -\delta\,i - K(W_c - W_c^s) = -\delta\,i - K\,y_1 \tag{14}$$

where δ is small and positive to ensure stable zero dynamics. The choice of y_1 as input to the integral action ensures that the set-point W_c^s is achieved. Integral

action can not be performed on λ_O since λ_O can not be calculated from the control design model. Further, if integral action is performed on x_{egr}, stable zero dynamics can not be guaranteed.

The next step is then to ensure that W_{egr}^s is achieved and this is done by feeding the state i into p_{em}^s. The set-point p_{em}^s depends nonlinearly on W_c^s and W_{egr}^s it is therefore natural to utilize (13) when determining the gain from i to p_{em}^s. As a result the following set-point for p_{em} is received

$$\tilde{p}_{im}^s(i) = \frac{W_c^s + W_{egr}^s + i}{k_e}$$

$$\tilde{p}_{em}^s(i) = p_{amb} \left(1 - \frac{c_{pa} \left(\left(\frac{\tilde{p}_{im}^s(i)}{p_{amb}} \right)^{\mu_a} - 1 \right) T_{amb} \left(W_c^s + i \right)}{c_{pe} \, \eta_{cmt} \, T_{em} (W_c^s + W_f + i)} \right)^{-\frac{1}{\mu_e}}$$

To simplify the control design, the Taylor expansion of $\tilde{p}_{em}^s(i)$ is used according to

$$\tilde{p}_{em}^s(i) \approx \tilde{p}_{em}^s(0) + \frac{d}{di}\tilde{p}_{em}^s(0)i = p_{em}^s + \frac{d}{di}\tilde{p}_{em}^s(0)i \tag{15}$$

where $\frac{d}{di}\tilde{p}_{em}^s(0) = d_1/d_2$ with

$$d_1 = \left[\mu_a W_c^s (W_c^s + W_f)(W_c^s + W_{egr}^s)^{\mu_a - 1} + \right.$$
$$\left. \left((W_c^s + W_{egr}^s)^{\mu_a} - k_e^{\mu_a} p_{amb}^{\mu_a} \right) W_f \right] c_{pa} (p_{em}^s)^{\mu_e + 1} T_{amb}$$
$$d_2 = c_{pe} \eta_{cmt} k_e^{\mu_a} \mu_e p_{amb}^{\mu_a + \mu_e} T_{em} (W_c^s + W_f)^2$$

Using the set-point (15) for p_{em}, the outputs become

$$y_1 = W_c - W_c^s, \quad y_2 = p_{em} - p_{em}^s - d_1 \, i/d_2 \tag{16}$$

4.4   Feedback linearization

The first step in the control design method is to construct a CLF $V(x)$, which is done using feedback linearization. For the fourth order model (10) and (14), and the outputs (16), the relative degrees become $r_1 = 1$ and $r_2 = 1$. Consequently, $\dot{y}$ can be formulated as

$$\dot{y} = G(y, z)u + F(y, z) \tag{17}$$

where $y = [y_1 \, y_2]^T$, $u = [u_1 \, u_2]^T$, $z = [p_{im}, i]^T$, the matrix

$$G(y, z) = \begin{bmatrix} -a & b \\ -k_{em} & -k_{em} \end{bmatrix}$$

is invertible with

$$a = \frac{k_{im} \, \mu_a \left(\frac{p_{im}}{p_{amb}} \right)^{\mu_a - 1} W_c}{p_{amb} \left(\left(\frac{p_{im}}{p_{amb}} \right)^{\mu_a} - 1 \right)} \tag{18}$$

$$b = \frac{c_{pe}\,\eta_{cmt}\left(1 - \left(\frac{p_{amb}}{p_{em}}\right)^{\mu_e}\right)T_{em}}{c_{pa}\left(\left(\frac{p_{im}}{p_{amb}}\right)^{\mu_a} - 1\right)\tau\,T_{amb}} \tag{19}$$

and where

$$F(y,z) = \begin{bmatrix} a\,k_e\,p_{im} - a\,W_c - \frac{W_c}{\tau} \\ \frac{d_1(\delta\,i + K(W_c - W_c^s))}{d_2} + k_{em}(k_e\,p_{im} + W_f) \end{bmatrix}$$

Note that the set $\Omega = \{(p_{im}, p_{em}, P_c) : p_{im} > p_{amb}, p_{em} > p_{amb}, P_c > 0\}$ is invariant, i.e. every trajectory starting in Ω stays in Ω for all t [6]. This leads to that $a, b > 0$.

Then by applying the feedback and input transformation

$$u = G^{-1}(y,z)(-\alpha\,y - F(y,z) + w) \tag{20}$$

and the change of coordinates $x \to [y, z]$, the system (10) and (14) is transformed into the system

$$\dot{y} = -\alpha\,y + w \tag{21}$$

$$\dot{z} = f_0(y,z) + g_0(y,z)\,w \tag{22}$$

where w is the new input and α is a positive scalar constant.

4.5   Stability of the zero dynamics

When feedback linearization is used it is necessary to investigate the stability of the zero dynamics, that is defined by

$$\dot{z} = f_0(0, z)$$

For (22) the zero dynamics becomes

$$\frac{dp_{im}}{dt} = \frac{q_1(p_{im})}{q_2(p_{im}, i)}\,(p_{im}^{\mu_a} - q_3(i)) \tag{23}$$

$$\frac{di}{dt} = -\delta\,i$$

where

$$q_1(p_{im}) = c_{pa}k_{im}p_{im}T_{amb}W_c^s$$

$$q_2(p_{im}, i) = -c_{pa}k_{im}\mu_a p_{im}{}^{\mu_a}T_{amb}\tau W_c^s -$$

$$c_{pe}\eta_{cmt}p_{amb}{}^{\mu_a}\left(1 - \left(\frac{p_{amb}}{\frac{d_1 i}{d_2} + p_{em}^s}\right)^{\mu_e}\right)p_{im}T_{em}$$

$$q_3(i) = \frac{p_{amb}{}^{\mu_a}}{c_{pa}k_{em}T_{amb}W_c^s}\left(\left(\frac{d_1\delta i}{d_2} + k_{em}(W_c^s + W_f)\right)\cdot\right.$$

$$\left.\left(1 - \left(\frac{p_{amb}}{\frac{d_1 i}{d_2} + p_{em}^s}\right)^{\mu_e}\right)c_{pe}\eta_{cmt}T_{em} + c_{pa}k_{em}T_{amb}W_c^s\right)$$

To analyze the stability of the zero dynamics (23), the Lyapunov function

$$V_z = \frac{1}{2} c_{z1} z_1^2 + \frac{1}{2} c_i i^2$$

is used where $z_1 = p_{im}^{\mu_a} - q_3(i)$. The zero dynamics (23) is asymptotically stable if

$$\dot{V}_z = c_{z1} z_1^2 \left(\mu_a \, p_{im}^{\mu_a - 1} \, \frac{q_1}{q_2} + \frac{\delta \, c_{z1} (q_3'(i))^2}{4 \, c_i} \right) - c_i \, \delta \left(i - \frac{c_{z1}}{2 \, c_i} q_3'(i) z_1 \right)^2 < 0$$

for all $[z_1, i] \neq 0$ which is true if $\delta > 0$ and

$$\frac{c_{z1}}{c_i} < -\frac{4}{\delta (q_3'(i))^2} \mu_a \, p_{im}^{\mu_a - 1} \, \frac{q_1}{q_2}$$

This is possible if $q_1/q_2 < 0$, which is true if $d_1 \, i/d_2 + p_{em}^s \geq p_{amb}$. This relation is achieved by implementing the integral action (14) in discrete form with anti-windup according to

$$\epsilon_n = i_{n-1} - T_s (\delta \, i_{n-1} + K \, y_1)$$

$$i_n = \begin{cases} \epsilon_n & , \text{if } \epsilon_n \geq i_{min} \\ i_{min} & , \text{if } \epsilon_n < i_{min} \end{cases}$$

where T_s is the sample time and

$$i_{min} = -\frac{d_2}{d_1} (p_{em}^s - p_{amb})$$

4.6 Construction of a CLF

In order to obtain a simple control law, a quadratic Lyapunov function

$$V = c_1 \, y_1^2 + c_2 \, y_2^2 \tag{24}$$

is constructed, which is a CLF for the system (21), since

$$\dot{V} = -2 \, c_1 \, \alpha \, y_1^2 - 2 \, c_2 \, \alpha \, y_2^2 < 0$$

for $w = 0$ and all $y \neq 0$.

4.7 Control law

Using the CLF (24), the control law (7) can be applied to the system (21). However, this control law will contain the non-linear cancellation (20) that is sensitive to model errors. In order to obtain a robust control law, this cancellation is avoided by applying the control law (7) to the system (17) instead, using the same Lyapunov function V. Since V is a CLF for the system (21), it is a CLF for (17) since u can be selected according to (20). Note that z is known since p_{im} is measured and i is calculated in the control structure.

   To apply the control law (7), the control inputs are centered at their set-point values

$$v_1 = u_1 - W_{egr}^s, \quad v_2 = u_2 - W_c^s - W_f$$

This leads to that $v = 0$ renders the equilibrium point $y = 0$.

   A simple control law for the system (17) is achieved by choosing $R^{-1} = \text{diag}\{\gamma_1, \gamma_2\}$, yielding

$$\begin{bmatrix} v_1 \\ v_2 \end{bmatrix} = -\frac{1}{2}R^{-1}(L_G V)^\mathsf{T} = \begin{bmatrix} \gamma_1(\quad c_1\, a\, y_1 + c_2\, k_{em}\, y_2) \\ \gamma_2(-c_1\, b\, y_1 + c_2\, k_{em}\, y_2) \end{bmatrix} \qquad (25)$$

The last step is to find $l(x)$ and check the criterion (9). This is done in Proposition 1 in Appendix A showing that there exist no γ_1, γ_2, c_1, c_2, and K such that $l(x) > 0$ for all x and therefore there is no guarantee that the control law (25) gives a globally robust system according to Sec. 3. An analysis of $\dot{V}(x)$ also shows that that there exist no γ_1, γ_2, c_1, c_2, and K such that $\dot{V}(x) < 0$ for all x and therefore there is no guarantee that the control law (25) gives a globally asymptotically stable system. In Appendix B, $l(x)$ and $\dot{V}(x)$ are also analyzed for the control design without integral action proposed in [6] showing that this design does neither guarantee a globally robust nor an asymptotically stable system for all x, even though it is shown in [6] that there exists a constant c such that the design in [6] guarantees an locally asymptotically stable and robust system in the region $L = \{x : V(x) \le c\}$ by selecting γ_1 and γ_2 sufficiently large.

   Even without a control law that gives a globally asymptotically stable and robust system, there is a possibility that the control law (25) handles interactions and non-linear properties in the system since the control law is model based. Therefore, the control performance of the proposed control structure is investigated in the following sections.

5   Automatic controller tuning

In the proposed control design there are five tuning parameters: γ_1, γ_2, c_1, c_2, and K. The tuning objectives are to minimize the error between λ_O and λ_O^s, minimize the error between x_{egr} and x_{egr}^s, and to achieve the inequality (9) for as many x as possible. However, it is difficult to achieve these objectives by manual tuning, especially the last objective. Therefore a method for automatic tuning of the parameters is developed. It is based on the method in [14] but with a modified cost function.

5.1   Cost function for tuning

The automatic tuning method is obtained by formulating a non-linear least squares problem

$$\min V(\theta)$$
$$\theta > 0$$

where θ are the tuning parameters

$$\theta = [\gamma_1, \gamma_2, c_1, c_2, K]^\mathsf{T} \tag{26}$$

The cost function $V(\theta)$ is calculated as

$$
\begin{aligned}
V(\theta) = \sum_{i=1}^{N} & \gamma_{\lambda_O} \left(\frac{e_{\lambda_O}(t_i)}{\lambda_{ONorm}} \right)^2 + \gamma_{egr} \left(\frac{e_{xegr}(t_i)}{x_{egrNorm}} \right)^2 \\
& + \left(\frac{u_{egr}(t_i) - u_{egr}(t_{i-1})}{u_{egrNorm}} \right)^2 + \left(\frac{u_{vgt}(t_i) - u_{vgt}(t_{i-1})}{u_{vgtNorm}} \right)^2 \\
& + \gamma_l \left(\frac{\min\left(l(x(t_i)), 0 \right)}{l_{Norm}} \right)^2
\end{aligned} \tag{27}
$$

where t_i is the time at sample number i. The motives for the different terms in the cost function are:

Term 1: Minimizes λ_O error ($e_{\lambda_O} = \lambda_O^s - \lambda_O$)

Term 2: Minimizes EGR error ($e_{xegr} = x_{egr}^s - x_{egr}$).

Term 3 and 4: Minimize oscillations in the EGR valve and VGT control signals. The terms have equal weight.

Term 5: If the inequality (9) is not satisfied, this term minimizes $l(x)^2$ using a high penalty, $\gamma_l = 100$. However, this does not guarantee that the inequality (9) is satisfied for all operating points. For example, if the tuning method is applied to the transient cycles defined by Tab. 1, $l(x)$ becomes negative in 31 % of the total number samples.

In the tuning method in [14] there is also a term that penalizes high turbocharger speeds to avoid overspeeding. This is important to handle, but it is not the focus in this paper. In this paper the focus is on the control performance for λ_O and x_{egr}, and therefore the investigated operating points in Sec. 6 have no overspeeding of the turbocharger.

As seen in (27) all the terms are normalized in order to get the same order of magnitude for the five terms. The weighting factors γ_{λ_O} and γ_{egr} are set to 3 and 1, and the constant δ in (14) is set to 10^{-6}.

5.2 Optimization

A solver has been developed for the optimization problem stated in the previous section, and it consists of three phases. Firstly, the tuning parameters are initialized manually. Secondly, a globalization heuristic method is used to scan a large region around the initial values in order to avoid ending up in a bad local minimum. Thirdly, a standard non-linear local least squares solver is used. A detailed description of this optimization method is given in [14].

Table 1 *The table defines 4 transient cycles that consist of steps between 17 different operating points. Cycle 1 starts at 1 and ends at 5, cycle 2 starts at 6 and ends at 9, cycle 3 starts at 10 and ends at 12, and cycle 4 starts at 13 and ends at 17. All cycles spend 10 s in each point. These cycles are used for tuning, and they cover a large operating region and capture important system properties such as non-linear effects and sign reversals. The values for λ_O^s and x_{egr}^s are obtained by calculating the stationary points of the eighth order model for the 17 points below. The operating points OP_1 and OP_2 are not used due to that $p_{em} < p_{im}$ in these operating points that might result in back-flow in the EGR-valve in a real engine. Instead, the operating point 8 is used where the EGR-valve is closed. The operating points OP_3 and OP_4 are not used due to that the turbocharger speed is too high in these operating points.*

u_δ [mg/cycle]	u_{egr} [%]	Operating points			
	40	7	OP_1	OP_3	11
230	10	6,9	OP_2	OP_4	10,12
	0		8		
60	40	4	3	14	13,17
	10	1,5	2	15	16
	u_{vgt} [%]	30	60	30	60
	n_e [rpm]	1000		2000	

6 Controller evaluation

The performance of the control system in Fig. 2 is evaluated by comparing four different control systems:

CLF with integral action: The control system in Fig. 2 where the controller tuning method in Sec. 5 is applied to the transient cycles defined by Tab. 1. These transients consist of steps in λ_O^s and x_{egr}^s between 17 different operating points.

CLF without integral action: Same as above, but K is set to zero and removed from θ in (26). Simulations show that there are negligible differences in control performance between "CLF without integral action" and the control design in [6]. In particular, these two controllers becomes equal if $c_{pa} = c_{pe}$ and $\mu_a = \mu_e$ in (18)–(19) and if $c_3 = 0$ in [6].

PID: The control structure with PID controllers and automatic tuning method proposed in [13]. It has the following control structure

$$
u_{egr}(t_i) = \begin{cases} \min\left(-\mathrm{PI}_1(e_{\lambda_O}),\right. \\ \left.\mathrm{PI}_2(e_{xegr})\right) & \text{, if } u_{vgt}(t_{i-1}) = 100 \\ \\ -\mathrm{PI}_1(e_{\lambda_O}) & \text{, else} \end{cases} \tag{28}
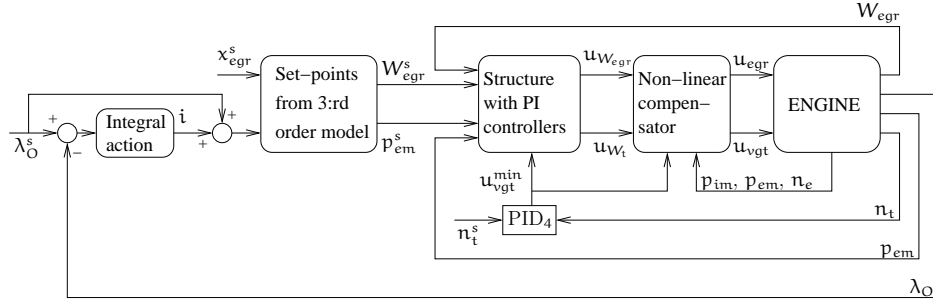$$

Figure 3 *A control design with an integral action on the oxygen/fuel ratio λ_O, set-points calculations, a structure with PI controllers, and a non-linear compensator that is a flow to opening inversion.*

$$u_{vgt}(t_i) = \begin{cases} 100 & \text{, if } (u_{vgt}(t_{i-1}) = 100) \\ & \& (e_{xegr} < 0.01) \\ \max(-\text{PI}_3(e_{xegr}), & \\ -\text{PID}_4(e_{nt})) & \text{, else} \end{cases} \tag{29}$$

where $e_{\lambda_O} = \lambda_O^s - \lambda_O$, $e_{xegr} = x_{egr}^s - x_{egr}$, and $e_{nt} = n_t^s - n_t$.

PID and non-linear compensator: The control structure with PID controllers and a non-linear compensator in Fig. 3 proposed in [16]. The non-linear compensator is the same non-linear compensator as in Fig. 2. The block "Structure with PI controllers" in Fig. 3 consists of the following equations

$$u_{W_{egr}}(t_i) = \begin{cases} W_{egr}^{max} & \text{, if } (u_{W_{egr}}(t_{i-1}) = W_{egr}^{max}) \& \\ & (e_{W_{egr}} > -5 \cdot 10^{-3}) \\ \text{PI}_1(W_{egr}^s, W_{egr}) & \text{, else} \end{cases} \tag{30}$$

$$u_{W_t}(t_i) = \begin{cases} \min(-\text{PI}_2(p_{em}^s, p_{em}), & \\ -\text{PI}_3(W_{egr}^s, W_{egr})) & \text{, if } u_{W_{egr}}(t_{i-1}) = W_{egr}^{max} \\ -\text{PI}_2(p_{em}^s, p_{em}) & \text{, else} \end{cases} \tag{31}$$

where $e_{W_{egr}} = W_{egr}^s - W_{egr}$. The controller parameters are automatically tuned by applying the method in Sec. 5 to the transient cycles in Tab. 1, changing the parameters in (26) to the parameters for the controllers in Fig. 3, and setting the weighting factors to $\gamma_{\lambda_O} = 1/8$, $\gamma_{egr} = 3/8$, and $\gamma_l = 0$.

The full eighth order model, described in Sec. 2, is used as plant model to evaluate the four control systems above. All their control parameters are held constant for the entire operating region, i.e. no gain scheduling is used. In addition, a low pass filter is applied to all variables that are assumed to come from an observer. These variables are λ_O, x_{egr}, W_{egr}, and T_{em}.
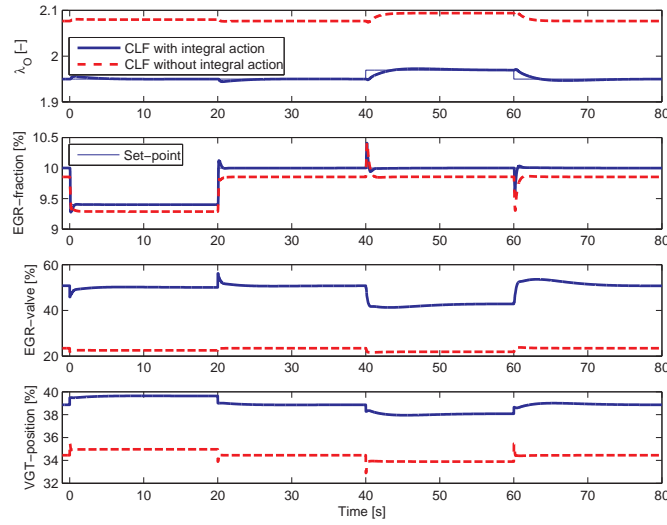
Figure 4 *Illustrative example simulating CLF with and without integral action showing that the stationary control errors in λ_O and x_{egr} are reduced if an integral action is used.*

Sec. 6.1–6.4 discuss various properties of the four controllers with the aid of steps in the set-points for λ_O and x_{egr}. In all cases the operating point is $n_e = 1200$ rpm and $u_\delta = 130$ mg/cycle, that is not used in the four transient cycles in Tab. 1. Then, Sec. 6.5 compares and discusses the four controllers and their performance on all cycles defined by Tab. 1.

6.1 Benefits with integral action

In Fig. 4, advantages with integral action are illustrated by comparing "CLF with integral action" and "CLF without integral action". Steps in λ_O^s and x_{egr}^s are performed and the result is that the stationary control errors in λ_O and x_{egr} are reduced when the integral action is included.

6.2 Benefits with non-linear control and compensator

In Fig. 5 and 6, advantages with non-linear control and a non-linear compensator are illustrated by comparing "CLF with integral action" and PID. In Fig. 5 the same steps in λ_O^s and x_{egr}^s are performed as in Fig. 4. The result from Fig. 5 is that PID gives slower control compared to CLF.

In Fig. 6, "CLF with integral action" and PID are simulated at two other steps in λ_O^s and x_{egr}^s compared to Fig. 5. The operating point in Fig. 6 renders higher DC-gains in $u_{egr} \rightarrow \lambda_O$ and $u_{vgt} \rightarrow x_{egr}$ (that corresponds to the two loops that
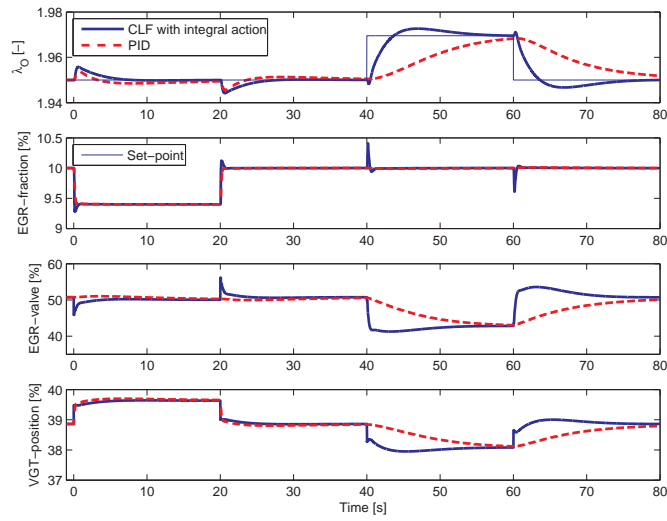
Figure 5 *Illustrative example simulating "CLF with integral action" and PID showing that PID gives slower control compared to CLF.*
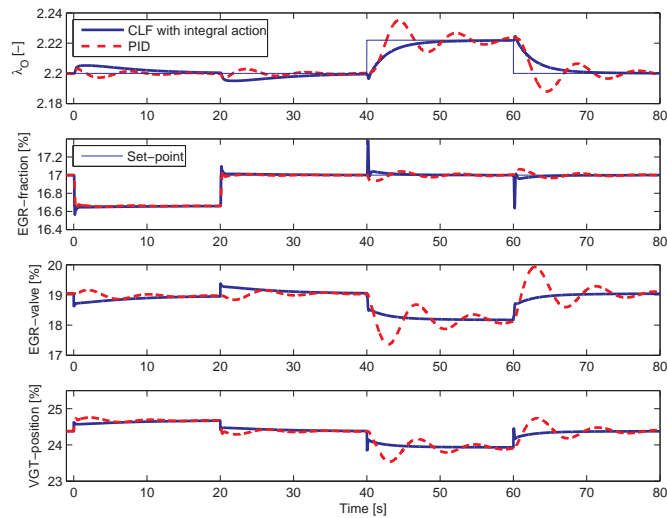

Figure 6 *Illustrative example simulating "CLF with integral action" and PID at two other steps in λ_O^s and x_{egr}^s compared to Fig. 5 showing that PID gives oscillations and CLF gives no oscillations.*

are used for feedback in (28) and (29)) compared to the operating point in Fig. 5. The result is that PID gives oscillations, while CLF gives no oscillations. Since the same control parameters are used in Fig. 5 and 6 for CLF respectively PID, the simulations show that the CLF based design handles the non-linear effects in the diesel engine, such as non-linear gains. Fig. 5 and 6 also show that the proposed design gives a stable system for the investigated operating points and achieves good control performance.

6.3 Importance of the non-linear compensator

The previous section shows that the non-linear control law (25) together with the non-linear compensator handle the non-linear effects in the diesel engine. The question now is: is it important to use both a non-linear control law and a non-linear compensator or is it sufficient to use the PID control structure with a non-linear compensator in Fig. 3 to handle the non-linear effects? To answer this question "CLF with integral action" and "PID and non-linear compensator" are compared in Fig. 7 and 8 on the same steps in λ_O^s and x_{egr}^s as were used in Fig. 5 and 6. Fig. 7 and 8 show that there are only small differences in control performance between these two control systems. "PID and non-linear compensator" gives a little faster response in λ_O while "CLF with integral action" gives a little smaller EGR-error. These differences are only due to that the tuning of the controllers have different trade-offs between λ_O-error and x_{egr}-error. However, both these control systems handle the non-linear effects in the diesel engine. Consequently, it is important to use the non-linear compensator to handle the non-linear effects since both "PID and non-linear compensator" and "CLF with integral action" use the non-linear compensator. Further, it is sufficient to use the control structure in Fig. 3 to handle the non-linear effects since "PID and non-linear compensator" and "CLF with integral action" have approximately the same control performance.

6.4 Drawback with the proposed CLF based control design

In Fig. 9 and 10, disadvantages with the proposed control design are illustrated by comparing "CLF with integral action" and "PID and non-linear compensator". In this comparison two model errors are introduced in the plant model. These errors are 10 % positive errors in the maximum opening areas for the EGR and turbine flow model. The same steps in λ_O^s and x_{egr}^s are investigated as in Fig. 7 and 8. The result is that "CLF with integral action" gives stationary control errors and "PID and non-linear compensator" gives no stationary control errors. Consequently, "PID and non-linear compensator" handles the model errors in the EGR and turbine flow model while "CLF with integral action" is sensitive to these model errors. This is due to that "PID and non-linear compensator" has integral parts in the PID controllers and "CLF with integral action" has no integral parts in the control law (25). The integral action in Fig. 2 only handles model errors in the block "Set-point from 3:rd order model" and the control law (25) only handles model errors in the block "CLF and inverse optimal control".
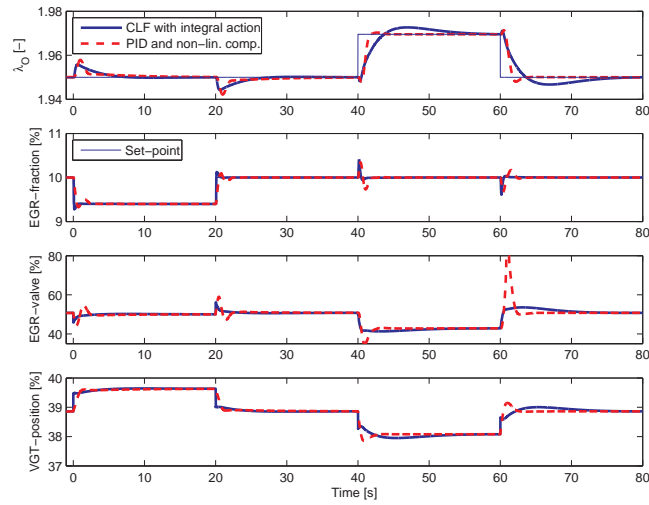
Figure 7 *Illustrative example simulating "CLF with integral action" and "PID and non-linear compensator" showing only small differences in control performance and that these control systems handle the non-linear effects compared to PID in Fig. 5.*

Figure 8 *Illustrative example simulating "CLF with integral action" and "PID and non-linear compensator" showing only small differences in control performance and that these control systems handle the non-linear effects compared to PID in Fig. 6.*
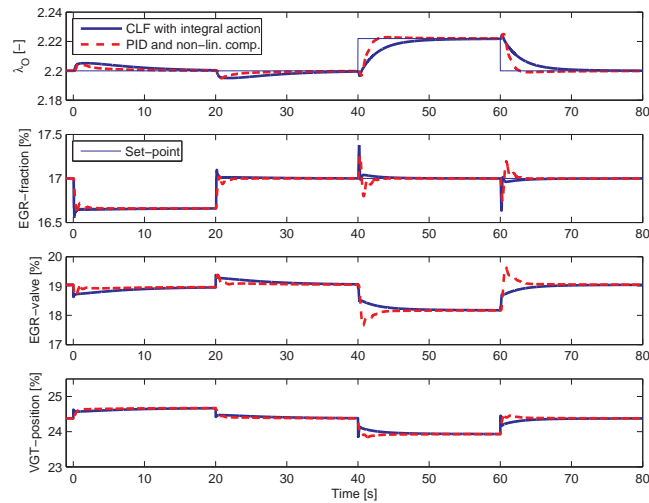
Figure 9 *Illustrative example simulating "CLF with integral action" and "PID and non-linear compensator". In this comparison model errors are introduced in the EGR and turbine flow model for the simulation model showing that "CLF with integral action" gives control errors while "PID and non-linear compensator" gives no control errors.*
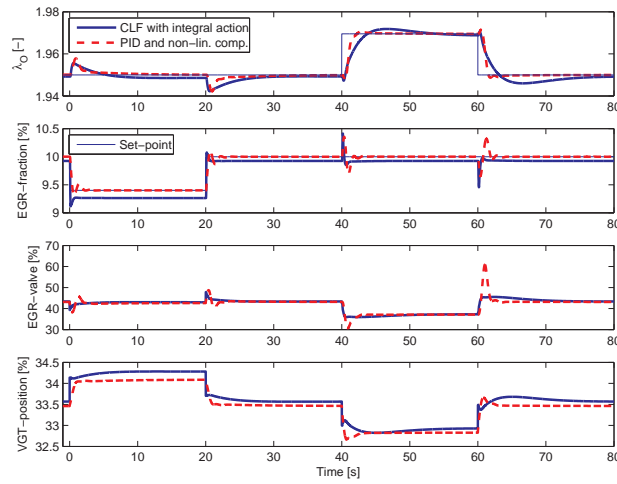

Figure 10 *Illustrative example simulating "CLF with integral action" and "PID and non-linear compensator". In this comparison model errors are introduced in the EGR and turbine flow model for the simulation model showing that "CLF with integral action" gives control errors while "PID and non-linear compensator" gives no control errors.*
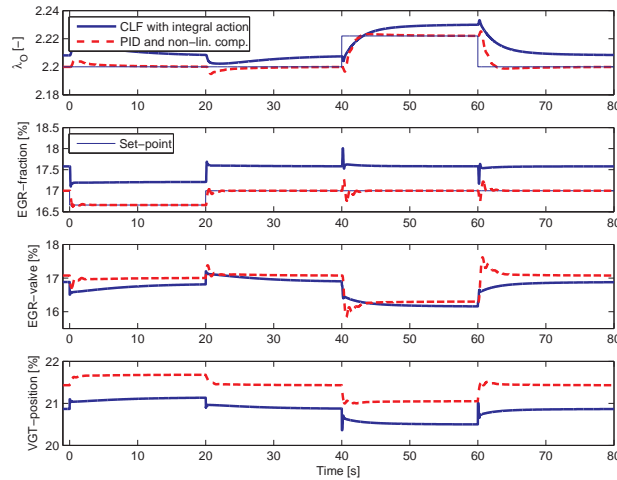
It is natural that the proposed control design in Fig. 2 is sensitive to these model errors, since the non-linear compensator is developed by using feedback linearization on the EGR and turbine flow model, i.e. by inverting these models. To handle these model errors, it is important to use integrators that directly affect the inputs to the non-linear compensator according to the structure in Fig. 3. Such integrators with feedback from p_{em} and/or W_{egr} could be added to the structure in Fig. 2 to handle these model errors. However, this has not been investigated.

6.5   Comparison on the four transient cycles

The four control structures are compared on the four transient cycles defined in Tab. 1 by comparing λ_O-error and x_{egr}-error

$$E_{\lambda_O} = \sum_{i=1}^{N} e_{\lambda_O}^2(t_i)$$

$$E_{x_{egr}} = \sum_{i=1}^{N} e_{xegr}^2(t_i)$$

$$(32)$$

where t_i is the time at sample number i. Each control structure is simulated on two different simulation models. Simulation model A is the model in Sec. 2 and simulation model B is the same model except that the maximum opening areas are increased with 20 % for the EGR and turbine flow models in the plant model. These model errors are larger than the model errors in Sec. 6.4 in order to get large effects on the control errors in Tab. 2. The model errors in Sec. 6.4 are set to 10 % to avoid saturations in the actuators.

The goal is to investigate if the results in Sec. 6.1–6.4 are valid also for the four transient cycles. Tab. 2 shows that "CLF with integral action" reduces the errors compared to "CLF without integral action". Consequently, integral action reduces control errors and the result from Sec. 6.1 is valid. PID has higher errors than the

Table 2 *The measures (32) for four different controllers over the cycles defined in Tab. 1. Two different simulation models are used. Simulation model A is the model in Sec. 2 and simulation model B is the same model except that 20 % positive model errors are introduced in the maximum opening areas for the EGR and turbine flow model. The measures are normalized with respect to PID for simulation model A.*

Simulation model	A		B	
Measure	E_{λ_O}	$E_{x_{egr}}$	E_{λ_O}	$E_{x_{egr}}$
PID	1.00	1.00	0.79	0.84
PID and non-linear compensator	0.17	0.92	0.16	0.86
CLF with integral action	0.27	0.37	0.49	1.23
CLF without integral action	0.38	0.66	1.57	6.14

other three controllers for simulation model A. Consequently, non-linear control improves the control performance which confirms the result from Sec. 6.2. "PID and non-linear compensator" and "CLF with integral action" have approximately the same control performance for simulation model A. The differences in E_{λ_O} and $E_{x_{egr}}$ between these two controllers for simulation model A are only due to that the tuning of the controllers have different trade-offs between the λ_O and x_{egr}-errors. Consequently, it is important to use the non-linear compensator and it is sufficient to use "PID and non-linear compensator" to reduce the control errors compared to PID which confirms the result from Sec. 6.3. Finally, "PID and non-linear compensator" has lower errors compared to "CLF with integral action" for simulation model B which confirms the result from Sec. 6.4 that "PID and non-linear compensator" handles model errors in the EGR and turbine flow model while "CLF with integral action" is sensitive to these model errors.

7 Conclusions

A non-linear multivariable control design is proposed in [6] for control of EGR and VGT in diesel engines. This design includes construction of a Lyapunov function, inverse optimal control, and a non-linear compensator which provides a control law that handles interactions and non-linear properties in the system. This design is extended with integral action on the compressor mass flow to handle model errors so that the controller can track the performance variables specified in the outer loop. The design in [6] is locally asymptotic stable and robust, but it is shown that neither the here proposed design nor the one in [6] guarantee a globally asymptotically stable and robust system.

Comparisons between different control structures have been performed in simulations showing the following four points. Firstly, stationary control errors are reduced when integral action is used in the proposed design compared to a control design without integral action. Secondly, the proposed control design handles the non-linear effects in the diesel engine that results in less control errors compared to a control structure with PID controllers. Thirdly, it is important to use the non-linear compensator and it is sufficient to use a control structure with PID controllers and a non-linear compensator to handle the non-linear effects. Fourthly, the proposed control design is sensitive to model errors in the EGR and turbine flow model while a control structure with PID controllers and a non-linear compensator handle these model errors.

Acknowledgments

A   Analysis of stability and robustness properties for the proposed design with integral action

An analysis of the robustness properties for the proposed design with integral action is performed. This is done by checking the criteria (9) in the following proposition.

Proposition 1

For the system (17), the outputs (16), the CLF (24), and $\mathsf{R}^{-1} = diag\{\gamma_1, \gamma_2\}$ there exist $\mathsf{x} = [y_1 \ y_2 \ p_{im} \ i]^\mathsf{T}$ such that $l(x)$ in (8) is negative for any positive γ_1, γ_2, c_1, c_2, and K.

Proof

The function $l(x)$ becomes

$$l(x) = a_1\, y_1 + a_2\, y_2 + a_3\, y_1\, y_2 + a_4\, y_1^2 + a_5\, y_2^2$$

where

$$a_1 = -2\, c_1 \left(-\frac{W_c}{\tau} - a(-k_e\, p_{im} + W_c + W_{egr}^s) + b(W_c^s + W_f) \right)$$

$$a_2 = -2\, c_2 \left(\frac{d_1\, (\delta\, i + K\, y_1)}{d_2} - k_{em}(-k_e\, p_{im} + W_c^s + W_{egr}^s) \right)$$

$$a_3 = 2\, a\, c_1\, c_2\, k_{em}\, \gamma_1 - 2\, b\, c_1\, c_2\, k_{em}\, \gamma_2$$

$$a_4 = c_1^2(a^2\, \gamma_1 + b^2\, \gamma_2) > 0$$

$$a_5 = c_2^2\, k_{em}^2(\gamma_1 + \gamma_2) > 0$$

Completing the squares in $l(x)$ gives

$$l(x) = a_4 \left(y_1 + \frac{a_3}{2\, a_4}y_2 + \frac{a_1}{2\, a_4} \right)^2 + b_1 \left(y_2 + \frac{b_2}{2\, b_1} \right)^2 - \frac{b_2^2}{4\, b_1} - \frac{a_1^2}{4\, a_4}$$

where

$$b_1 = a_5 - \frac{a_3^2}{4\, a_4} = \frac{(a+b)^2\, c_2^2\, k_{em}^2\, \gamma_1\, \gamma_2}{\gamma_1\, a^2 + \gamma_2\, b^2} > 0$$

$$b_2 = a_2 - \frac{a_3\, a_1}{2\, a_4}$$

There exist x such that

$$y_2 = -\frac{b_2}{2\, b_1}, \quad y_1 = -\frac{a_3}{2\, a_4}y_2 - \frac{a_1}{2\, a_4} \tag{33}$$

$$a_1 \neq 0 \tag{34}$$

since y_1 and y_2 can be selected to satisfy (33) and p_{im} can be selected to satisfy (34). For these x, it holds that

$$l(x) = -\frac{b_2^2}{4\,b_1} - \frac{a_1^2}{4\,a_4} < 0$$

for any positive γ_1, γ_2, c_1, c_2, and K. □

Consequently, there exist no γ_1, γ_2, c_1, c_2, and K such that $l(x) > 0$ for all x and therefore there is no guarantee that the control law (25) gives a globally robust system according to Sec. 3. $\dot{V}(x)$ is analyzed in the same way as the analysis of $l(x)$ above, showing that there exist no γ_1, γ_2, c_1, c_2, and K such that $\dot{V}(x) < 0$ for all x and therefore there is no guarantee that the control law (25) gives a globally asymptotically stable system.

B Analysis of stability and robustness properties for the design without integral action

An analysis of the robustness properties for the design without integral action in [6] is performed. This is done by checking the criteria (9) in the same way as the analysis in Appendix A and this is done in the following proposition.

Proposition 2
For the design in [6], i.e. for the system (10), the outputs (11), the CLF

$$V = c_1\,y_1^2 + c_2\,y_2^2 + c_3\,z_2^2 \tag{35}$$

where $z_2 = (p_{im}/p_{amb})^{\mu_a} - (p_{im}^s/p_{amb})^{\mu_a}$, and $R^{-1} = \text{diag}\{\gamma_1, \gamma_2\}$ there exist $x = [y_1\ y_2\ z_2]^T$ such that $l(x)$ in (8) is negative for any positive γ_1, γ_2, c_1, c_2, and c_3.

Proof

The function $l(x)$ becomes

$$\begin{aligned}
l(x) =\,& a_1\,y_1 + a_2\,y_2 + a_3\,y_1\,y_2 + a_4\,y_1^2 + a_5\,y_2^2 + \\
& a_6\,y_1\,z_2 + a_7\,y_2\,z_2 + a_8\,z_2^2 + a_9\,z_2
\end{aligned}$$

where

$$a_1 = -2\, c_1 \left(-\frac{W_c}{\tau} - a(-k_e\, p_{im} + W_c + W_{egr}^s) + b(W_c^s + W_f) \right)$$

$$a_2 = 2\, c_2\, k_{em}(W_c^s + W_{egr}^s - k_e\, p_{im})$$

$$a_3 = 2\, a\, c_1\, c_2\, k_{em}\, \gamma_1 - 2\, b\, c_1\, c_2\, k_{em}\, \gamma_2$$

$$a_4 = c_1^2(a^2\, \gamma_1 + b^2\, \gamma_2) > 0$$

$$a_5 = c_2^2\, k_{em}^2(\gamma_1 + \gamma_2) > 0$$

$$a_6 = -2\, a\, c_1\, c_3\, k_{im}\, \mu_a\, p_{amb}^{-\mu_a}\, p_{im}^{\mu_a-1}\, \gamma_1 < 0$$

$$a_7 = -2\, c_2\, c_3\, k_{em}\, k_{im}\, \mu_a\, p_{amb}^{-\mu_a}\, p_{im}^{\mu_a-1}\, \gamma_1 < 0$$

$$a_8 = c_3^2\, k_{im}^2\, \mu_a^2\, p_{amb}^{-2\mu_a}\, p_{im}^{2\mu_a-2}\, \gamma_1 > 0$$

$$a_9 = -2\, c_3\, k_{im}\, \mu_a\, p_{amb}^{-\mu_a}\, p_{im}^{\mu_a-1}\, (-k_e\, p_{im} + W_c + W_{egr}^s)$$

Completing the squares in $l(x)$ *gives*

$$l(x) = a_4 \left(y_1 + \frac{a_3}{2\, a_4}y_2 + \frac{a_6}{2\, a_4}z_2 + \frac{a_1}{2\, a_4} \right)^2 +$$

$$b_1 \left(y_2 + \frac{b_4}{2\, b_1}z_2 + \frac{b_2}{2\, b_1} \right)^2 - \frac{b_2^2}{4\, b_1} - \frac{a_1^2}{4\, a_4} + b_3\, z_2$$

where

$$b_1 = a_5 - \frac{a_3^2}{4\, a_4} = \frac{(a + b)^2\, c_2^2\, k_{em}^2\, \gamma_1\, \gamma_2}{\gamma_1\, a^2 + \gamma_2\, b^2} > 0$$

$$b_2 = a_2 - \frac{a_3\, a_1}{2\, a_4}$$

$$b_4 = a_7 - \frac{a_3\, a_6}{2\, a_4}$$

$$b_3 = a_9 - \frac{a_6\, a_1}{2\, a_4} - \frac{b_2\, b_4}{2\, b_1} = -\frac{2\, c_3\, k_{im}\, \mu_a\, ((b\, \tau - 1)W_c + b\, \tau\, W_f)}{p_{amb}^{\mu_a}\, p_{im}^{1-\mu_a}\, (a + b)\tau}$$

There exist x *such that*

$$y_2 = -\frac{b_4}{2\, b_1}z_2 - \frac{b_2}{2\, b_1}, \quad y_1 = -\frac{a_3}{2\, a_4}y_2 - \frac{a_6}{2\, a_4}z_2 - \frac{a_1}{2\, a_4} \tag{36}$$

$$b_3\, z_2 < 0 \tag{37}$$

since y_1 *and* y_2 *can be selected to satisfy* (36) *and* z_2 *can be selected to satisfy* (37). *Note that* $b_3 \neq 0$ *since* $x \neq 0$ *for these* x. *The* x *that satisfy* (36)–(37) *gives*

$$l(x) = -\frac{b_2^2}{4\, b_1} - \frac{a_1^2}{4\, a_4} + b_3\, z_2 < 0$$

for any positive $\gamma_1,\ \gamma_2,\ c_1,\ c_2,$ *and* c_3. $\qquad\qquad\square$

Consequently, there exist no γ_1, γ_2, c_1, c_2, and c_3 such that $l(x) > 0$ for all x and therefore there is no guarantee that the design in [6] gives a globally robust system according to Sec. 3. $\dot{V}(x)$ is analyzed in the same way as the analysis of $l(x)$ above, showing that there exist no γ_1, γ_2, c_1, c_2, and c_3 such that $\dot{V}(x) < 0$ for all x and therefore there is no guarantee that the design in [6] gives a globally asymptotically stable system.

References

[1] M. Ammann, N.P. Fekete, L. Guzzella, and A.H. Glattfelder. Model-based Control of the VGT and EGR in a Turbocharged Common-Rail Diesel Engine: Theory and Passenger Car Implementation. *SAE Technical paper 2003-01-0357*, January 2003.

[2] A. Amstutz and L. Del Re. EGO sensor based robust output control of EGR in diesel engines. *IEEE Transactions on Control System Technology*, pages 37–48, 1995.

[3] Arthur E. Bryson and Yu-Chi Ho. *Applied Optimal Control*. Taylor and Franchis, 1975.

[4] L. Guzzella and A. Amstutz. Control of diesel engines. *IEEE Control Systems Magazine*, 18:53–71, 1998.

[5] J.B. Heywood. *Internal Combustion Engine Fundamentals*. McGraw-Hill Book Co, 1988.

[6] M. Jankovic, M. Jankovic, and I.V. Kolmanovsky. Constructive lyapunov control design for turbocharged diesel engines. *IEEE Transactions on Control Systems Technology*, 2000.

[7] Mrdjan Jankovic, Rodolphe Sepulchre, and Petar Kokotovic. CLF based designs with robustness to dynamic input uncertainties. *Systems and Control Letters*, 1999.

[8] M. Nieuwstadt, P.E. Moraal, I.V. Kolmanovsky, A. Stefanopoulou, P. Wood, and M. Widdle. Decentralized and multivariable designs for EGR–VGT control of a diesel engine. In *IFAC Workshop, Advances in Automotive Control*, 1998.

[9] M.J. Nieuwstadt, I.V. Kolmanovsky, P.E. Moraal, A.G. Stefanopoulou, and M. Jankovic. EGR–VGT control schemes: Experimental comparison for a high-speed diesel engine. *IEEE Control Systems Magazine*, 2000.

[10] J. Rückert, A. Schloßer, H. Rake, B. Kinoo, M. Krüger, and S. Pischinger. Model based boost pressure and exhaust gas recirculation rate control for a diesel engine with variable turbine geometry. In *IFAC Workshop: Advances in Automotive Control*, 2001.

[11] Rodolphe Sepulchre, Mrdjan Jankovic, and Petar Kokotovic. *Constructive Nonlinear Control.* Springer-Verlag, 1997.

[12] A.G. Stefanopoulou, I.V. Kolmanovsky, and J.S. Freudenberg. Control of variable geometry turbocharged diesel engines for reduced emissions. *IEEE Transactions on Control Systems Technology*, 8(4), July 2000.

[13] Johan Wahlström. Control of EGR and VGT for emission control and pumping work minimization in diesel engines. Licentiate Thesis, Linköping University, 2006.

[14] Johan Wahlström, Lars Eriksson, and Lars Nielsen. Controller tuning based on transient selection and optimization for a diesel engine with EGR and VGT. In *Electronic Engine Controls*, number 2008-01-0985 in SAE Technical paper series SP-2159, SAE World Congress, Detroit, USA, 2008.

[15] Johan Wahlström and Lars Eriksson. Modeling of a diesel engine with VGT and EGR capturing sign reversal and non-minimum phase behaviors. Technical report, Linköping University, 2009.

[16] Johan Wahlström and Lars Eriksson. Non-linear compensator for handling non-linear effects in EGR VGT diesel engines. Technical report, Linköping University, 2009.

Linköpings Studies in Science and Technology
Department of Electrical Engineering
Dissertations, Vehicular Systems

No. 10 *Efficient Simulation and Optimal Control for Vehicle Propulsion*
Anders Fröberg, Disseration No. 1180, 2008

No. 9 *Single-Zone Cylinder Pressure Modeling and Estimation for Heat Release Analysis of SI Engines*
Markus Klein, Disseration No. 1124, 2007

No. 8 *Modelling for Fuel Optimal Control of a Variable Compression Engine*
Ylva Nilsson, Disseration No. 1119, 2007

No. 7 *Fault Isolation in Distributed Embedded Systems*
Jonas Biteus, Disseration No. 1074, 2007

No. 6 *Design and Analysis of Diagnosis Systems Using Structural Mehods*
Mattias Krysander, Dissertation No. 1033, 2006

No. 5 *Air charge Estimation in Turbocharged Spark Ignition Engines*
Per Andersson, Dissertation No. 989, 2005

No. 4 *Residual Generation for Fault Diagnosis*
Erik Frisk, Dissertation No. 716, 2001

No. 3 *Model Based Fault Diagnosis: Methods, Theory, and Automotive Engine Applications*, Mattias Nyberg, Disseration No. 591, 1999

No. 2 *Spark Advance Modeling and Control*
Lars Eriksson, Dissertation No 580, 1999

No. 1 *Driveline Modeling and Control*
Magnus Pettersson, Dissertation No. 484, 1997